NUMERICAL AND EXPERIMENTAL INVESTIGATION OF UNIFORM COOLING TECHNIQUES FOR PHOTOVOLTAIC PANELS

BY

AHMER ALI BOZDAR BALOCH

A Thesis Presented to the

DEANSHIP OF GRADUATE STUDIES

KING FAHD UNIVERSITY OF PETROLEUM & MINERALS

DHAHRAN, SAUDI ARABIA

In Partial Fulfillment of the
Requirements for the Degree of

MASTER OF SCIENCE

In

MECHANICAL ENGINEERING

DECEMBER, 2014

KING FAHD UNIVERSITY OF PETROLEUM & MINERALS

DHAHRAN, SAUDI ARABIA

DEANSHIP OF GRADUATE STUDIES

This thesis, written by **Ahmer Ali Bozdar Baloch** under the direction of his thesis advisor and approved by his thesis committee, has been presented to and accepted by the Dean of Graduate Studies, in partial fulfillment of the requirements for the degree of **MASTER OF SCIENCE in MECHANICAL ENGINEERING**.

Thesis Committee

Thesis Advisor

Dr. Haitham M.S. Bahaidarah

Member

Dr. Palanichamy Gandhidasan

Department Chairman

Dr. Zuhair Mattoug Gasem

Member

Dr. Fahad A. Al Sulaiman

15/4/15

Dean of Graduate Studies

Prof. Salam A. Zummo

Dedicated to

My Beloved Ami and Abu

and

My brother and sister

ACKNOWLEDGEMENTS

In the Name of Allah, the Most Beneficent, the Most Merciful.

"…This is by the Grace of my Lord to test me whether I am grateful or ungrateful! And whoever is grateful, truly, his gratitude is for (the good of) his own self, and whoever is ungrateful, (he is ungrateful only for the loss of his own self). Certainly! My Lord is Rich (Free of all wants), Bountiful."

Surat An-Naml: Verse 40

I begin with the name of Allah, the most beneficent, the most merciful. May Allah bestow peace on our beloved Prophet Mohammed (*peace and blessings of Allah be upon him*), his pure family, his noble companions, and all those who follow them with righteousness until the Day of Judgment. I would never have been able to finish my research without the guidance of Allah who endowed me with health, aptitude and patience.

I would like to pay my deepest respect and gratitude to my beloved parents who have been a constant source of motivation, appreciation and prayers throughout my life. No amount of "thank you" can suffice for the hardships they had to bear to make me a person I am today. I can never thank them enough and can only pray to God to bless them in this dunya and akhirah. If only my words can convey the emotions, I would just like to say I love you both very much and I dedicate my lifelong achievements to you. Special thanks to my brother and sister for their unconditional support and prayers.

Acknowledgements are due to *King Fahd University of Petroleum and Minerals* which gave me the opportunity to pursue a graduate degree and also for all the support I

received in carrying out this research. I am also grateful to the *King Abdul-Aziz city for Science and Technology (KACST)* for its support through the project No. 0667-11-A-L.

I would like to express my deepest gratitude to my thesis advisor, Dr. Haitham M.S. Bahaidarah, for his excellent guidance, caring, patience, and providing me with an excellent atmosphere for doing research. His patience and support helped me overcome many crisis situations and finish this thesis. I am also very grateful to my thesis committee members Dr. Palanichamy Gandhidasan and Dr. Fahad A. Al-Sulaiman for their involvement and encouragement. Their insightful comments and constructive criticisms at different stages of my research were thought-provoking and they helped me focus my ideas.

I would also like to thank all my colleagues, friends and seniors at KFUPM for providing the moral support and a pleasant atmosphere. Special thanks to my friends Furqan Tahir, Haider Ali, Yasir Jamil, Maimoon Atif, Waqas Ahmed, Muhammad Waqar and Ayyaz Mustafa for making my time at KFUPM memorable.

TABLE OF CONTENTS

LIST OF TABLES

LIST OF FIGURES

ABSTRACT (ENGLISH)

NAME: Ahmer Ali Bozdar Baloch

TITLE: Numerical And Experimental Investigation Of Uniform Cooling Techniques For Photovoltaic Panel.

MAJOR FIELD: MECHANICAL ENGINEERING

DATE OF DEGREE: DECEMBER 2014

Cooling of PV systems is one of the key parameters to optimize the cell efficiency. The main design considerations for the cooling systems are low and uniform cell temperatures. The need for uniform cooling of PV panels arises due to the uneven solar flux distribution and temperature variations across the cell. Moreover conventional cooling mechanism does not address the issue of temperature variations. The objective of the current work is to model and experimentally validate the effect of uniform cooling techniques applied to the parameters of PV panels. For uniform cooling of PV panels, design of jet impingement configuration and a converging channel is proposed to eliminate non-uniform heat transfer across the surface of the PV Panel. Also to examine the effect of non-uniformity, a rectangular channel is studied with an uncooled PV panel. This research is achieved by modeling and experimentation of four configurations for PV systems with and without uniform cooling. Computational Fluid Dynamics (CFD) is used for thermal modeling of converging channel. Thermal model for PV panel with impingement cooling is developed to notice the effect on thermal characteristics of the panel using different average heat transfer correlations. For converging channel, optimum and practically feasible geometric parameters are found for maintaining uniform cell temperature. For all the configurations thermal modeling is developed using energy balance approach on the PV cell. Isotropic sky radiation model is used to calculate the

absorbed radiation whereas investigation of electrical parameters is carried out using seven parameters electrical model for PV. Experimental setup for cooling systems are manufactured and installed at the test facility with all the necessary equipment for data collection and analysis. Finally a comprehensive comparative analysis and experimental validation is carried out for the cases of uncooled, cooled and uniformly cooled PV strings for the climate of June and December. For an uncooled PV string, maximum temperature of 83˚C was recorded. In comparison to this, cooling the PV string by converging channel resulted in maximum temperature of 47˚C whereas for rectangular channel heat exchanger resulted in maximum temperature of 47.5˚C. For jet cooled PV string, maximum temperature of 35.8˚C was recorded with an efficiency of 15.7%. Cooling the PV string by converging channel and rectangular channel heat exchanger resulted in maximum efficiency of 12.5% and 12.7%, respectively. By using jet, PV string was cooled effectively and power produced was increased by 81% when compared with the performance of an uncooled PV whereas for converging and rectangular channel, percentage improvement in power was 57% and 60 %, respectively. Converging channel cooling and rectangular channel cooling showed similar results for the configurations and conditions analyzed but since converging channel can result in a better thermal profile over PV surface, it is suggested for employment for PV cooling and future research for CPV cells. Results revealed that uniform cooling by jet impingement did not only perform better in terms of power output and conversion efficiency but also reduced the cell temperature significantly while keeping it constant for each cell.

ABSTRACT (ARABIC)

ملخص الرسالة

الاسم الكامل : أحمر علي بوزدار بالوش

عنوان الرسالة : دراسة تحليلية وتجريبية لطرق التبريد المنتظم للخلايا الضوئية

التخصص : الهندسة الميكانيكية

تاريخ الدرجة العلمية : جمادى الأول 1436 هـ

يعتبر تبريد الخلايا الضوئية مفتاحا رئيسيا للوصول للأداء الأمثل للخلايا الضوئية. درجة الحرارة المنخفضة والمنتظمة من أهم الاعتبارات الرئيسية في تصميم نظام التبريد لهذه الخلايا. تأتي الحاجة لنظام تبريد يوفر توزيع حرارة منتظم بسبب عدم التوزيع المنتظم لدفق الحرارة الشمسي مما يسبب تباين في درجات حرارة الخلايا الضوئية. هذه المشكلة –عدم الانتظام في درجات الحرارة– لم يتم اعتباره في طرق التبريد التقليدية. الهدف الأساسي من هذه الدراسة هو تطبيق نموذج رياضي للتبريد المنتظم للخلايا الضوئية والتحقق من النتائج بالتجارب المعملية. للتخلص من تأثر التوزيع الغير منتظم للإشعاع الشمسي الساقط تمت دراسة نظاميّ التبريد بواسطة النفث الصدمي والقناة المتقاربة (اللامة). أيضا، للمقارنة ولتوضيح تأثير عدم الانتظام في درجات الحرارة تمت دراسة الخلايا من غير نظام للتبريد. تم استخدام طرقة حوسبة الموائع في النمذجة الحرارية لنظام التبريد بواسطة القناة المتقاربة. النموذج الحرارة للنظام بواسطة التبريد بالنفث الصدمي تم تطويره لرصد التأثير على الخصائص الحرارية للخلايا باستخدام معادلات تجريبية لحساب متوسط معامل نقل الحرارة. تم إيجاد القيم المثلى والعملية للأبعاد الهندسية لنظام التبريد بالقناة المتقاربة للوصول

للتوزيع المنتظم لدرجات الحرارة. لكل التوليفات المختلفة لنظم التبريد قيد الدراسة، تم تطوير النموذج الحراري بتطبيق قانون حفظ الطاقة. لحساب كمية الإشعاع التي تم امتصاصه بواسط الخلايا تم استخدام نموذج خواص السماء الإشعاعي، بينما تم استخدام نموذج السبعة-أبعاد للتنبؤ بالأداء الكهربي للخلايا الضوئية. تم تركيب وتجهيز التجارب المعملية بكل الأدوات المطلوبة للحصول على القراءات المعملية ولتحليلها. أخيرا، تم عرض مقارنة تحليليه لجميع نظم التبريد قيد الدراسة، والتي تم تأكيد صحتها معمليا، تحت الظروف الجوية لشهري يونيو وديسمبر. أعلى درجة حرارة تم تسجيلها للخلايا غير المبردة هي 83 درجة مئوية. مقارنة بذلك، فانه قد نتج عن تبريد الخلايا بواسطة القناة اللاّمة أن أعلى درجة حرارة للخلايا تم تسجيلها هي 47 درجة، بينما أدى استخدام القناة ذات المقطع المستطيل الى أن تكون أعلى درجة حرارة للخلايا 47.5 درجة. بالنسبة للخلايا المبردة بنظام النفث الصدمي، فان أعلى درجة حرارة تم تسجيلها هي 35.8 درجة بكفاءة 15.7%. تبريد الخلايا بواسطة القناة اللاّمة والقناة ذات المقطع المستطيل نتج عنه كفاءات كهربيه 12.5% و12.7%، على التوالي. التبريد باستخدام النفث الصدمي أدى الى زيادة بمقدار 81% في القدرة المنتجة مقارنة بالخلايا غير المبردة، بينما كانت الزيادة في القدرة نتيجة لاستخدام لقناة اللاّمة والقناة ذات المقطع المستطيل 57% و60% على التوالي. من ذلك يتضح أن التبريد بنظام لقناة اللاّمة والقناة ذات المقطع لهما نتائج متقاربة، لكن بالرغم من ذلك فان نظام القناة اللاّمة أدى الى الحصول على توزيع للحرارة أكثر انتظاما ولذلك فانه ينصح باستخدامه في أنظمة الخلايا المعرضة للإشعاع الشمسي المركز. أظهرت الدراسة أن التبريد بواسطة النفث الصدمي له الأداء الأفضل مقارنة بالنظم الأخرى للتبريد من ناحية القوة الكهربية المولّدة وكفاءة التحويل، كما ساعد في تقليل درجات الحرارة بصوره ملحوظه وكبيره.

CHAPTER 1

INTRODUCTION

A growing demand for energy, the security of supply of fossil resources and international agreements to climate changes are the key issues to modern society. These developments drastically increase the necessity of large scale implementation of renewable energy technologies over the past two decades and will continue to do so in the near future[1]. The reliance of energy and power on human beings has increased exponentially in the last century. This growing trend of energy usage and production with earths depleting fossil reserves demands an in-depth investigation by scientists and researchers into the feasibility of opting renewable energy alternatives. In the present time, the need for producing efficient renewable energy system is the one of the primary concerns of the researchers. The main reason lies under the unsustainable exploitation of natural resources like oil and natural gas for the industrial and domestic purposes. This harnessing of oil and gas has not only left the world with limited reserves of energy but has also increased the threats for the ecosystem. The issue of global warming is mainly caused by burning fossil fuels to generate energy for industrial or residential usage as

shown by Fig 1.1. Saudi Arabia is amongst top consumers of fossil fuels which makes it a key player to encounter the energy crisis. With an increasing energy demand and urbanization, the quest for alternative green energy resource has increased. Globally, every country depending on its economic and environmental constraints is contributing towards achieving the goal of harnessing renewable and reducing the dependency on fossil fuels. Figure 1.2 shows the global outlook of energy supplies till year 2100 with solar energy as the main method[2].

Figure 1.1 Per capita oil usage (tons) [2]

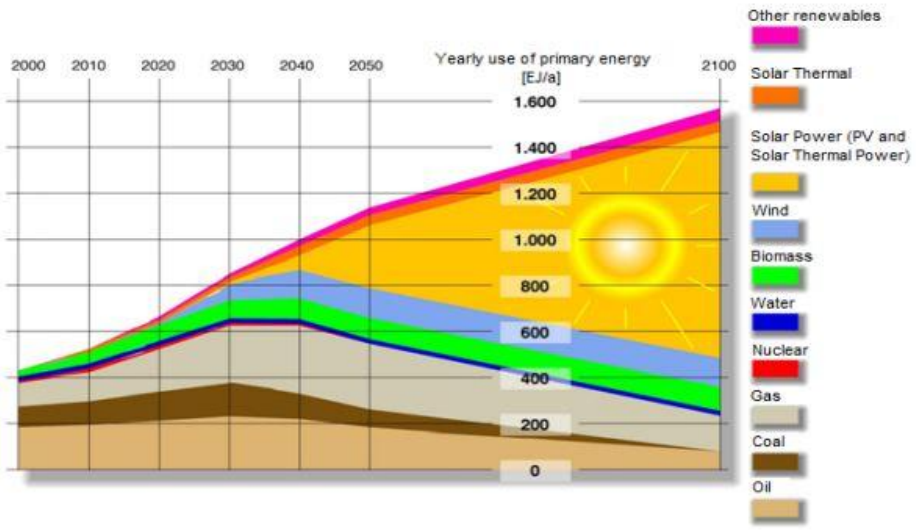

Figure 1.2 Global energy supply till 2100[2]

The primary renewable energy resources are solar, wind, geothermal, tidal, ocean etc. Solar energy, with its high irradiation and abundance in the Middle East, provides one such option and demonstrates all these desirable characteristics to fulfill future's energy demands. Saudi Arabia, being located in the so called "sun belt" region, is a prime candidate for adopting the solar energy. Considering the need for energy production and the exhaustion of oil reserves, Saudi Arabia has taken major steps to achieve low reliance on oil usage by adopting alternative energy options. The major aim is to provide solar energy based plants which will utilize the vast space of the Kingdom with its abundant incident radiation. The importance given by this region on solar energy as illustrated in Fig 1.3 shows that it aims at a strong local solar industry for local economic progress in this increasing polluted atmosphere. The in-depth research and availability of cost

effective solar power will produce low cost and low environmental impact energy especially for solar PV plants.

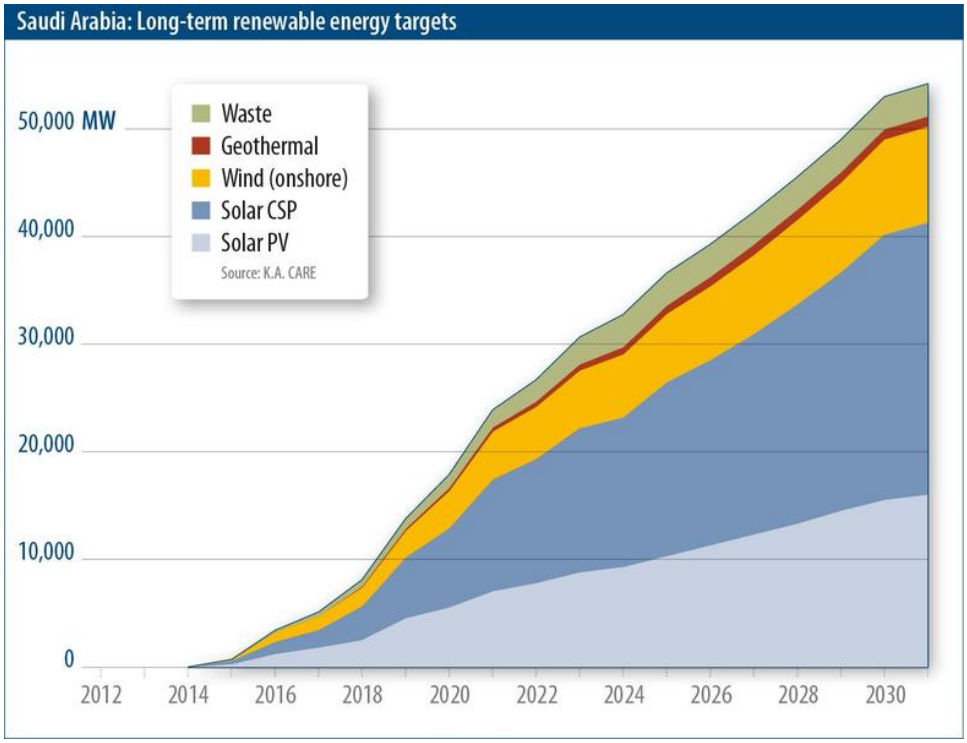

Figure 1.3 Renewable energy goals for Saudi Arabia

1.1 THE ROLE OF PHOTOVOLTAICS

With fossil fuel depletion and global warming, there is a need to find out alternative renewable energy sources. One of the most promising sources is the solar energy. Solar energy is utilized for producing power in two basic methods - one by the employment of photovoltaic (PV) technology and the other by the use of solar thermal technologies. PV converters are semiconductor devices that convert part of the incident solar radiation

directly into electrical energy. The use of PV cells to produce electricity has increased in the last decade and keeps growing as their manufacturing cost decreases and as the world becomes more concerned about energy use. They are relatively simple to use. They can be used for large electricity production, such as centralized electrical power plants or decentralized electrical power plants. Further, they can be installed directly in the house or in remote areas where there is no electricity transmission lines. Therefore, any improvement in the photovoltaic cell performance will have significant impact. There are two predominate PV systems on the market: crystalline silicon (~ 200 μm) and thin film (~ 5 μm). The main reason for the high cost of present PV modules is the high cost of the base material. Si solar cells, which contribute 94 % to the world market, are made from wafer-based mono-crystalline and multi-crystalline silicon .

Saudi Arabia has an area of about 2.3 million km^2 and has many remote villages and settlements. The Kingdom is blessed with solar energy in abundant measure of about 2.11 kWh/m^2 annually and has enormous potential for exploiting solar energy as shown in Fig 1.4. Photovoltaic (PV) power systems are highly suitable for producing small amounts of clean and renewable electricity generation in remote areas.

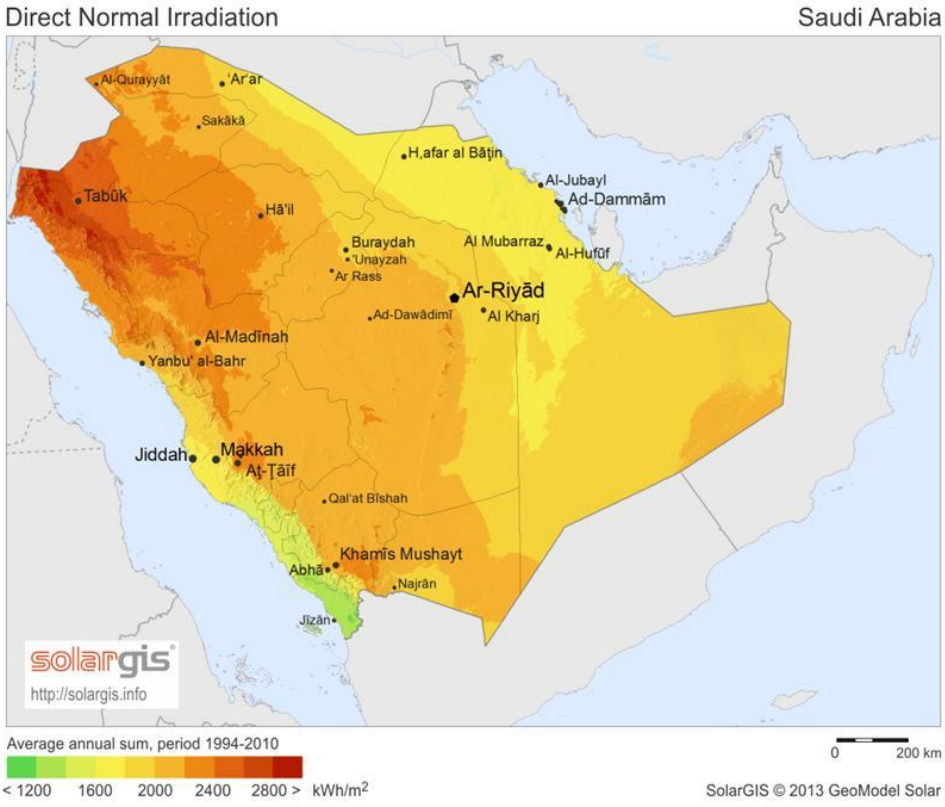

Figure 1.4 Average annual solar radiation on Saudi Arabia.

1.2 PV PERFORMANCE PARAMETERS

The performance of PV panels depends upon certain input parameters. The main effect on the performance of PV arises from the incoming solar radiation, ambient conditions and cell temperature. Photovoltaic cells are semiconductor devices that work on the principle of photoelectric effect. It converts photon energy of the sunlight directly into electricity. The efficiency of solar cells is inherently limited because of the

absorption of sunlight from the solar spectrum based on the band gap of the material .The photons with higher energy than the band gap excites the electron to higher state which when calms back to the conduction state results in the process called thermalization thereby increasing thermal energy in the cell and reducing conversion efficiency.

1.2.1 Effect of radiation

Photovoltaic output power is affected by incident irradiation. PV module short circuit current (I_{sc}) is linearly proportional to the irradiation, while open circuit voltage (V_{oc}) increases exponentially to the maximum value with increasing the incident irradiation, and it varies slightly with the light intensity [3]. Figure 1.5 describes the relation between Photovoltaic voltage and current with the incident irradiation.

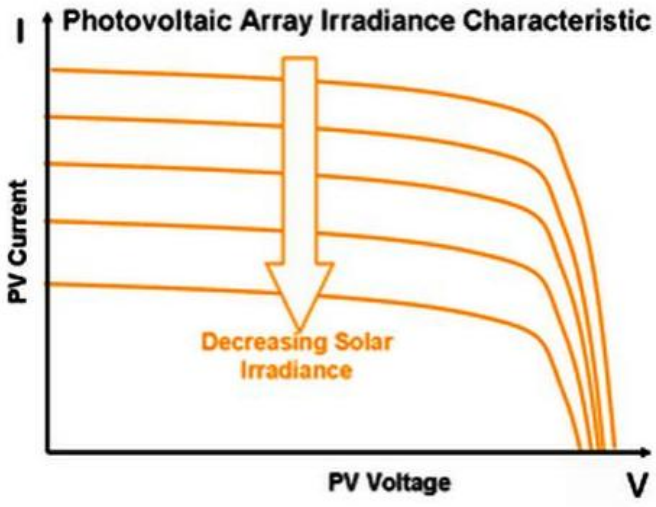

Figure 1.5 Effect of radiation on PV performance [3]

1.2.2 Effect of Temperature

Module temperature is highly affected by ambient temperature. Short circuit current increases slightly when the PV module temperature increases more than the Standard Test Condition (STC) temperature, which is 25˚C. However, open circuit voltage is enormously affected when the module temperature exceeds 25˚C. In other words the increasing current is proportionally lower than the decreasing voltage. Therefore, the output power of the PV module is reduced [3]. Figure 1.6 explains the relation between module temperature with voltage and current.

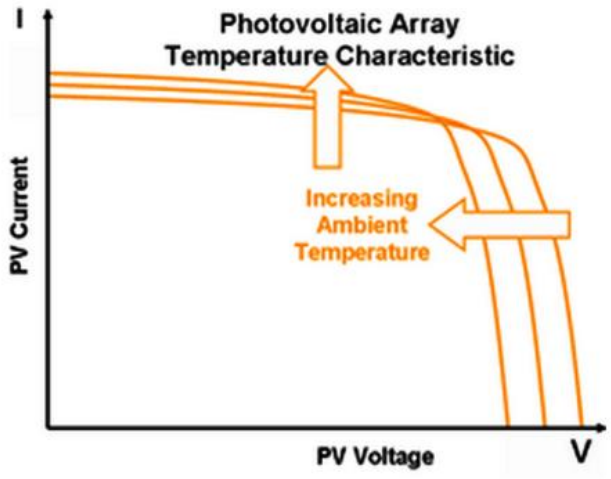

Figure 1.6 Effect of temperature on PV performance [3]

1.2.3 Maximum power point (MPP)

Maximum electrical power of the PV module is equal to the current at maximum power point (IMP) multiplied by the voltage at maximum power point (VMP), which is the maximum possible power at Standard Test Condition (STC). Referring to Figure 1.7, the "knee" of the I-V curve represents the maximum power point (PMPP) of the PV module/system. At this point the maximum electrical power is generated at STC [4] . The usable electrical output power depends on the PV module efficiency which is related to the module technology and manufacture.

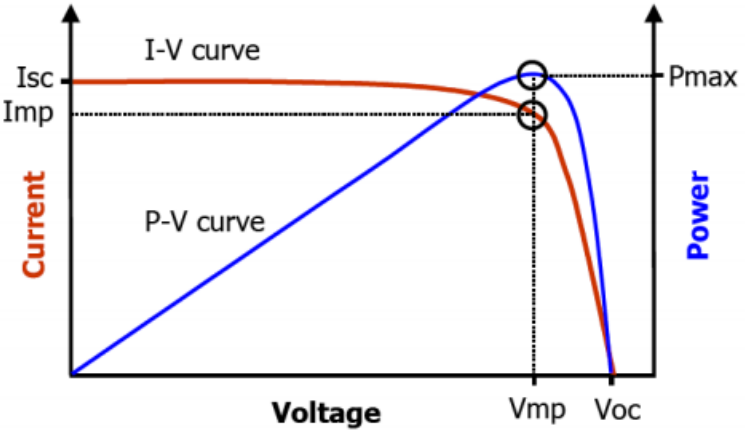

Figure 1.7 I-V curve of PV cell showing maximum power point [4]

1.3 MOTIVATION BEHIND PRESENT WORK

Thermal management of photovoltaic (PV) systems plays a key role for low and high concentration systems. The overall performance of solar panels is strongly dependant by the affect of PV cells' operating temperature. Typically the efficiency of solar cells is around 15 %. The remaining component of radiation absorbed in the cell transforms into thermal energy which causes the temperature of the cell to be increased. This further causes the panel efficiency to decrease as the open circuit voltage and fill factor is reduced with rising temperature [5]–[15]. The power output from the PV cells is controlled by the amount of incident solar radiation, cell temperature, orientation of the panel, and its size, among others. The intensity of light affects mainly the quantity of current generated whereas the temperature of the solar cell determines the voltage generated by PV. As the cell temperature increases, the current produced remains the same but the voltage is reduced, reducing the output power. Therefore, the power generated in summer does not necessarily increase even if the irradiance increases. The drop in efficiency due to these reasons decreases the global system performance and leads to an increase in cost per unit power. To achieve optimum and better solar cell performance, innovative cooling techniques for maintaining the solar cell temperature at operating conditions are required.

In addition to cell temperature, non-uniform temperature and non-uniform illumination across the cells has been found to affect the cell efficiency and overall system performance in a negative way [16]–[21]. Series connected PV cells faces greater

damage as current directly varies with light, so the current in an array of series of identical PV cells will be restricted by the solar cell with the minimum irradiation. This failure is called as the ‘current matching problem’. This issue can be solved by using bypass diodes or by keeping a uniform temperature across each series connection[13,18]. The uniform temperature across PV can be achieved by using conventional and non-conventional cooling mechanisms with novel designs for high heat dissipation. Low solar cell temperature and high temperature uniformity are one of the most important characteristics affecting the overall performance of PV systems [13]. Non-uniformity in temperature distribution affects the PV system performance in two ways: (1) Cells experience efficiency loss due to loss in power output; (2) Temperature variation induces thermal fatigue because of large amount of thermal cycles and stresses. This further cause the irreversible damage to solar cell due to excess localized heating across the region and reduces the reliability of the system [13].The cooling method should be such that it keeps the average cell temperature at its minimum with a uniform distribution. This will help in the appropriate design of CPV systems and for proper calculation of the global PV performance.

1.4 OBJECTIVES OF CURRENT STUDY

The overall objectives of this research are to model and experimentally validate the effect of uniform cooling techniques applied to the parameters of PV panels. For the investigation of PV panels subjected to uniform cooling, following configurations will be compared with meteorological data of Dhahran, both experimentally and numerically. Experimental setup for each configuration will be developed and comparison with modeling results will be carried out.

- Configuration 1. PV string without Cooling
- Configuration 2. PV string with Cooling
- Configuration 3. PV string with Converging Channel
- Configuration 4. PV string with Jet Impingement Cooling

The specific objectives for modeling are to develop:

- Radiation and Optical Modeling for PV string
- Thermal Modeling for Rectangular Channel Heat Exchanger Cooling
- Thermal Modeling for Converging Channel Cooling
- Thermal Modeling for Jet Impingement Cooling
- Development of Jet Cooling Model
- Electrical Modeling using seven parameters model

CHAPTER 2

LITERATURE REVIEW

This chapter discusses the need for uniform cooling of PV panels for low and high concentrated system by exploring the possible causes and effects of non-uniformity in PV systems. To address this issue, cooling methods which can cater the requirement for high heat flux and uniform cooling has been reviewed from literature and discussed. Finally potential cooling techniques that could be utilized for decreasing temperature non-uniformity has been analyzed for improvement in the overall performance of the PV systems. To understand the behavior of impingement cooling system, literature survey on jet has also been carried out and discussed in the chapter.

2.1 THE NEED FOR UNIFORM COOLING

This section highlights the importance of uniform cooling of PV panels by discussing the most notable causes and effects of non-uniformity on the solar cell. The solar cell under concentration undergoes a series of losses based on the concentrator geometry, optical losses, reflection losses, tracking losses and non-uniform illumination [21,22]. All these losses occurring in the system tends to increase the temperature of the cell and

series resistance which lowers the overall efficiency. In the case of concentrated systems, due to errors induced by geometry, there is an uneven distribution of radiation flux and non-uniform temperature across the surface of PV panel. Non-uniformity has a major impact on the performance of PV system and directly effects cell temperature, series resistance and efficiency. Non-uniformity results in:

- Increase in cell temperature and series resistance
- Decrease in fill factor and conversion efficiency

Broadly classifying the need for cooling PV panel uniformly arises due to:

- Non-uniform and high radiation flux distribution
- Non-uniformity in temperature
- Effect on cell parameters from non-uniformity

Moreover conventional cooling mechanism results in temperature variation. Also due to these non-uniform distribution current mismatching problem and hot spots occurs on the cell resulting in either reduction of efficiency (short term loss) or permanent structural damage due to thermal stresses (long term effect). Figure 2.1 shows typical behavior of solar cell with increasing temperature. As the cell temperature increases, electrical efficiency of the solar cell decreases [23].

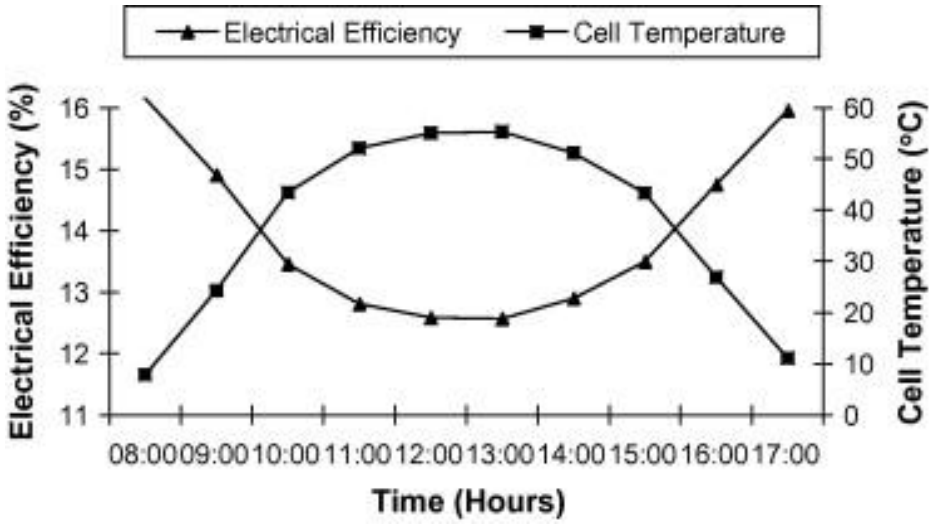

Figure 2.1 Hourly variation of cell temperature and cell efficiency for a typical day of summer [23].

2.1.1 Non-uniform and high radiation flux distribution

Baig et al. [21] has reviewed the causes and effects of non-uniform flux distribution on the solar cell. The main reasons discussed in the paper for this issue are the PV cell material, geometry of the concentrator, optical properties of concentrators, design, and manufacturing method. Reduction in electrical efficiency was found to be the main effect resulting in increasing the overall cost per unit power of the PV system. This drop in cell efficiency was explained by the reduction in fill factor and open circuit voltage which was shown to affect all concentrated PV systems. Based on the analysis, it was reported that a result of non-uniform illumination almost 40 % of energy is lost when compared to an ideal concentrated PV system

Luque et al. [16] calculated the outcome of non-homogeneity of radiation flux on concentration based cells. Their experimental setup included linear CPV system. They

concluded non-uniform radiation flux distribution takes place on cell which will cause inhomogeneous distribution of temperature across the cell.

Coventry [24] performed an investigation on concentrating parabolic trough system pertaining to flux intensity. They concluded that with concentration ratio of 30X for the system, the flux intensity reached as high as 100X at the localized region of the center of cell showing non-homogenous flux. In a review by Royne et al. [17] , it was shown that in the case of non-uniform illumination at the receiver, the peak flux at the center is higher than the average flux therefore resulting in a need for cooling mechanism that has the capability to cool high peak radiation areas as well as to maintain the temperature uniformity. This could be achieved by high heat extraction cooling mechanisms.

For multi-junction solar cells such as (GaInP/GaAs/Ge) I–VIII–V, the temperature of the cell raises to the value of 1300˚C [25]. These multi-junction cells generally utilize 37% of the absorbed energy to generate electrical power whereas the rest of 63 % is dissipated in the form of heat. The variation in uniform illumination also increases the ohmic losses in the high concentration zones which results in the working of solar cell at lower efficiency point. Non-uniform illumination causes the intensities at center of the cell higher than the cell bus-bar which increases the power losses at solar cell's front grid and front face diffused zones of planar solar strings [26].The geometry and optics of the concentration systems also plays a vital role in determining the profile for incident flux. Improper design of the concentrator can lead to misdistribution of incident flux thereby

reducing the conversion efficiency. Figure 2.2 shows the effect of non-uniform illumination on the length of concentrated PV systems [27].

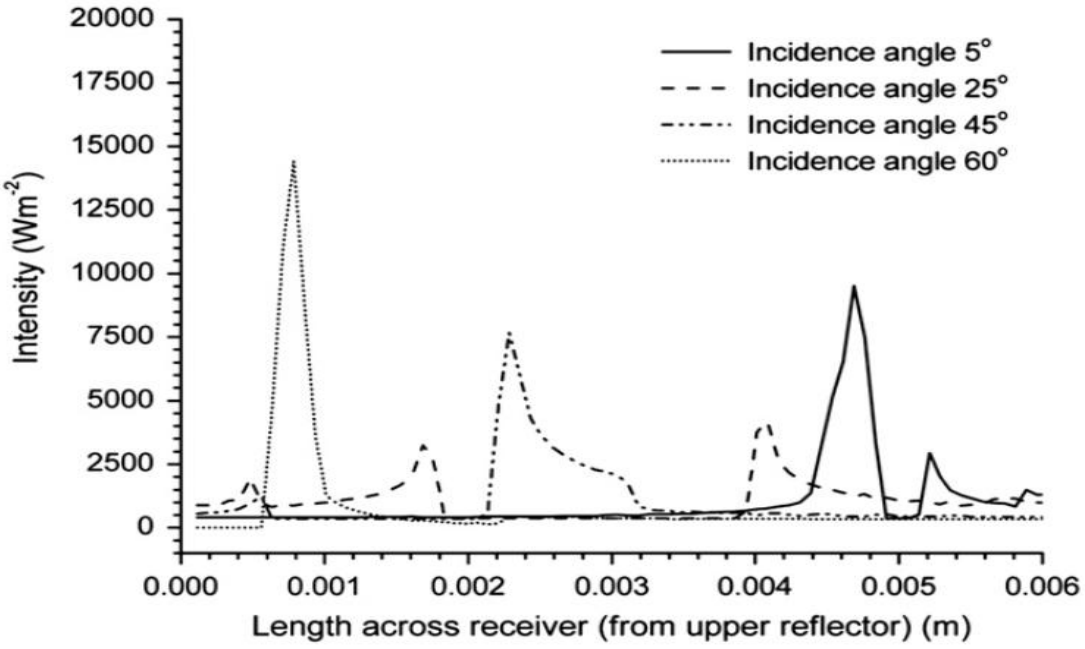

Figure 2.2 Distribution of incident radiation on concentrated system [27]

2.1.2 Non-uniformity in temperature

The non-uniformity in temperature on the surface of concentrated or non-concentrated PV system arises mostly from non-uniform illumination causing degradation and excessive wear of solar cells. Concentrator solar cells receive high amount of solar radiation which makes it necessary to employ cooling mechanism for proper thermal regulation [26]. The major disadvantage of non-uniform flux on solar cell is the increment of local temperature and hot spots. The performance of solar cell is mainly related to the series resistance of its components [28]. This effect causes the

efficiency of the PV panel to drop. Luque et al. [16] developed a model to predict the distribution of temperature on a solar cell. Their analysis substantiated the hypothesis that temperature gradients arises in the panel, and observed a localized temperature drop of 36.4 ˚C due to hot spots.

Coventry and Franklin [29] analyzed the temperature variation for a separate domestic arrangement of PV system. The temperature variation was analyzed using finite element based method. Temperature distribution over the cell showed a variation of 14 ˚C between the middle and edge of cell.

The inhomogeneous illumination of light throughout the module strongly affects temperature distribution on PV panels. The current and voltage distribution also gets changed which requires further addition in the I-V curves. Furthermore, series joined PV cells will face greater damage as current directly varies with light, so the current in an array of series of identical PV cells will be restricted by the solar cell with the minimum irradiation

The effect of non-uniform distribution can be studied for single cells subjected to hotspots or cells connected in series, each being irradiated differently. Non-uniformity should be studied distinctively for each case, single cell or complete module system [30]. For single cell, there is extra illumination over some parts of the solar cells while others are rarely illuminated. Current is generated from these illuminated regions and in the process the region gets heated resulting in decreased electrical output from cell. In the

case of linear concentrators this problem gets affected by the mismatch of current as the cells are usually connected in series.

2.1.3 Effect on cell parameters from non-uniform illumination and temperature

Non-uniform flux resulting from the use of concentrator, error in tracking, receiver support, mirror optical imperfections, spaces between modules, and the assembly of the module has a drastic effect on temperature distribution in PV panel [17]. These irregularities in the distribution of illumination have significant impact on various cell parameters, such as short circuit current, open circuit voltage, fill factor and overall efficiency of the collector. It is shown in the literature that the cell efficiency decreases as the mean temperature of the solar cell increases [31]–[33]. This is due to the decrease in the fill factor and open circuit voltage. It has been reported that reduction in efficiency of solar cell is of the order 0.45% per ˚C [34].

The main electrical parameters getting affected and reducing the overall performances of solar cells are [21]:

- Short circuit current
- Overall photocurrent
- Open circuit voltage
- Fill factor
- Electrical efficiency
- Average illumination power

The presence of non-uniform illumination causes the solar cell to produce higher ohmic losses because of the functioning of cell locally at higher level of radiation [16].It has been shown that in a solar cell under non-uniform conditions, the internal current flows even in an open circuit condition. This internal current acts in direct relation with level of non-uniformity and radiation [35].

Nishioka et al. [36] studied the dependence of temperature on electrical parameters of solar cells i.e. coefficient of temperature for fill factor, short circuit current, open circuit voltage and efficiency. Temperature coefficient for open circuit voltage was found to have a significant impact on the temperature dependence of efficiency. Cell efficiency was found to increase with the increase in concentration ratio whereas with the rise in cell temperature, there was reduction in efficiency. Figure 2.3 shows the changes in the electrical parameters due to temperature and concentration level.

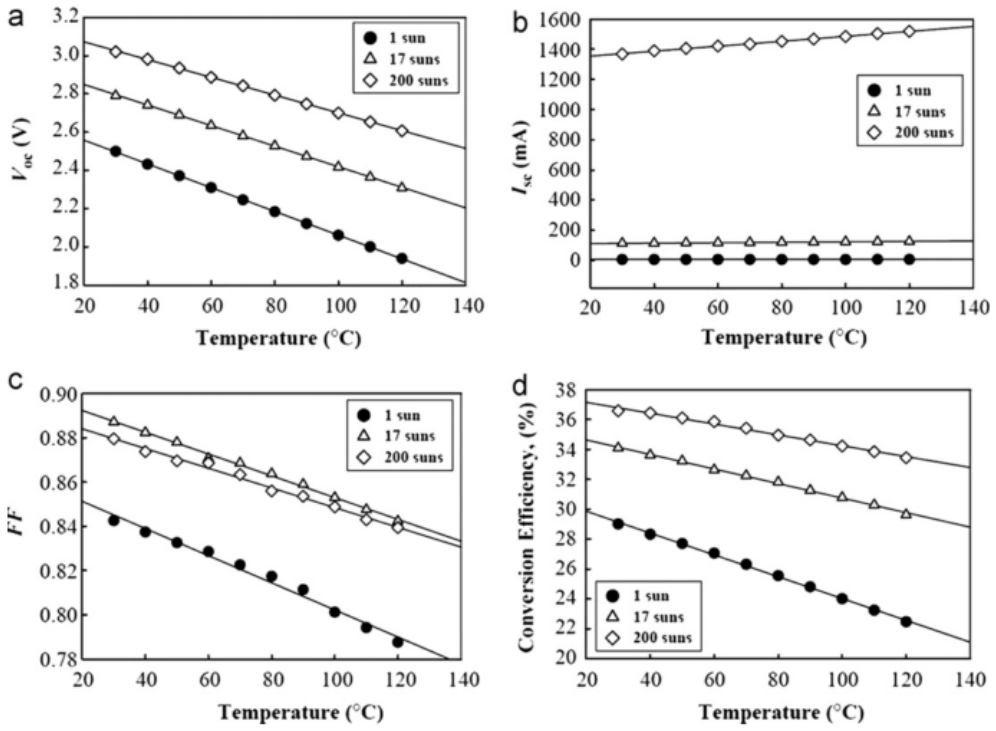

Figure 2.3 Electrical characteristics with temperature and concentration for triple junction solar cell.[36]

Meneses-Rodriguez et al. [37] did a theoretical study on the performance of PV panels at elevated temperatures. They affirmed that the fill factor and open-circuit voltage drops with increasing temperature and found that the basic cause for this efficiency decrement is the decrease of fill factor and open circuit voltage. The distribution of illumination flux concentration on different cell parameters was also studied at 300 X and found that the increase in short circuit current with the level of concentration is very steep than the open circuit voltage's increment. As the concentration level increased, efficiency was also found to increase. The paper concluded that well set combination of concentration and temperature should be chosen for effective performance of solar cell.

In addition, the literature shows as the concentration ratio increases, the open-circuit voltage, short circuit current, and efficiency increases; however, according to the literature reviewed there is no consensus and agreement between their values calculated [20,33–35]. The significance of non-uniform flux distribution is not studied in detail; and, this research core demands in-depth analysis particularly the relation of non-uniform illumination on cell parameters and temperature non-uniformity. These research studies affirms the requirement for research for effective uniform cooling especially in the case of low and high levels of concentration in which high cell temperature causes the cell efficiency to decrease.

2.2 COOLING TECHNIQUES

Cooling of PV panels is a vital factor in the design and operation of solar cell. The cooling method should be such that it keeps the cell temperature at its minimum with a uniform distribution [17].The simple design should keep pumping power to minimum while working at optimum conditions. As the idea of uniform cooling is novel, little literature is available in this area. However based on high heat transfer coefficient and heat extraction capability, uniform cooling techniques reported in literature and reviewed for cooling of photovoltaic and electronics are : jet impingement, microchannels, improved heat exchanger designs, heat pipes, combined microchannel-jet impingement, heat sinks and spreader, phase change material for cooling and dielectric cooling by direct immersion. Figure 2.4 shows the breakdown of cooling techniques reviewed in this study.

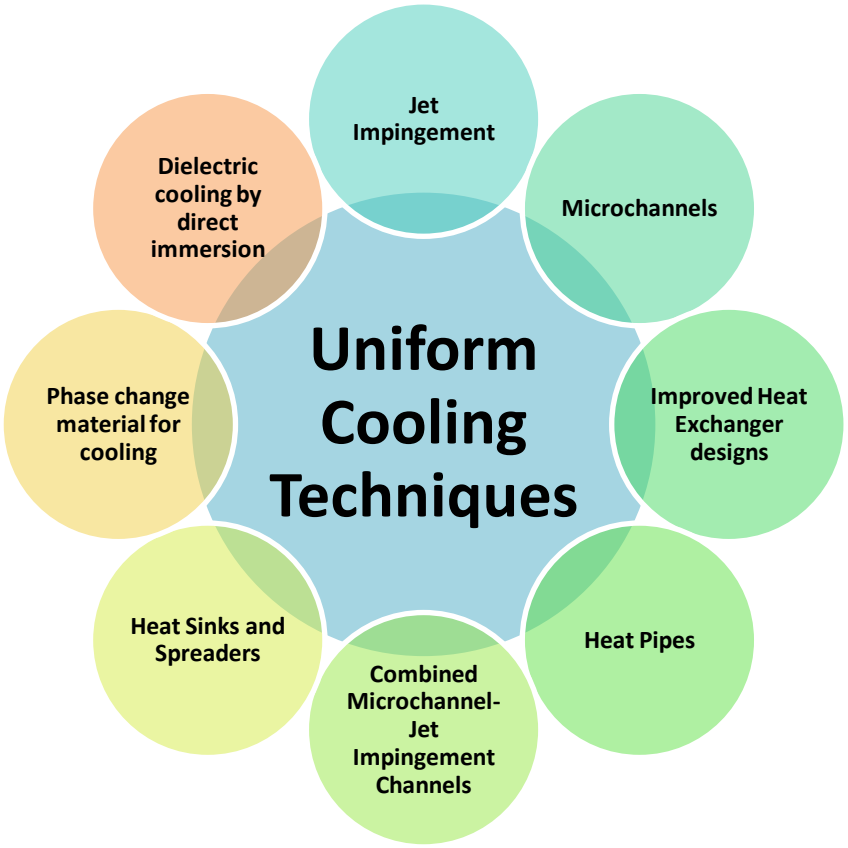

Figure 2.4 Breakdown of uniform cooling techniques reviewed in this literature survey

2.2.1 Heat Pipe Cooling

The development of reliable heat dissipation systems in miniaturized components to maintain their temperature has always been challenging for researchers. The transient and steady- state behavior of flat- type heat pipes has been investigated experimentally [37,38] and some theoretical and numerical models are presented in the literature related to flat heat types and loop heat pipes.[36], [39–41].These model showed that 110 W/cm^2 power can be dissipated without heat transfer restrictions by using heat pipes. Due to their ability to effectively transfer heat with minimal loss, heat pipes have received much attention in thermal managements of microelectronic components [42]. Heat pipes are

high heat flux transformation devices. They can absorb heat from high flux surfaces (rear surface of PV cell) and discharge to a low heat flux sink. Since heat pipes works nearly isothermally, heat sinks surface can also be very useful for flat plate heat pipes [43–45].

Tarabsheh et al. [46] studied analytically the effect of temperature variation on the performance of PV modules with heat pipe cooling and modeled the effect of non-uniform cooling .Three different configuration for PV module cooling were modeled by selection of different heat exchanger passes design to observe the impact of temperature on electrical output of PV system. They concluded that applying cooling pipes beneath each PV string enhances the performance of the PV module. In their results however they only showed the effect on efficiency for temperature not the temperature profile itself. Based on the results of Odeh and Behnia [47] , they showed that the minimum level of temperature non-uniformity is in the case of single string with the change in efficiency of about 0.5 % for the case of design “B” as shown in Figs. 2.5 and 2.6. The worst performance was of design “A” when compared with design “B” and “C” as shown in Figs. 5 and 6 with the maximum variation in cell efficiency across the cooling length. The cooling pipe with lowest length i.e. Design B achieved lowest average cell temperature with highest efficiency. An increase in V_{oc} by 11 %, FF by 4.7 % and efficiency by 17.15 % was observed for an optimum design.

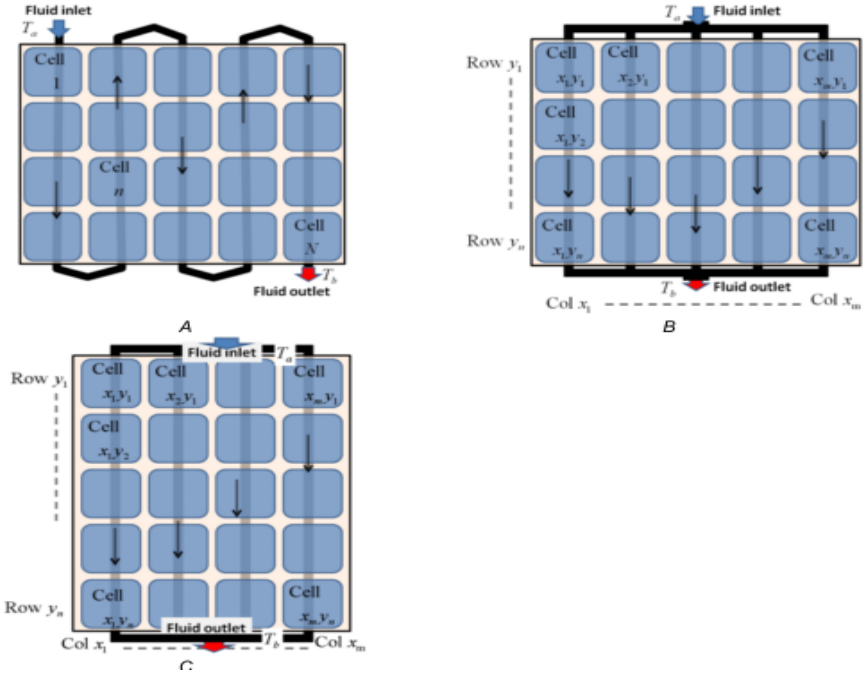

Figure 2.5 Different designs for heat pipe for the study of non-uniform heat transfer [46].

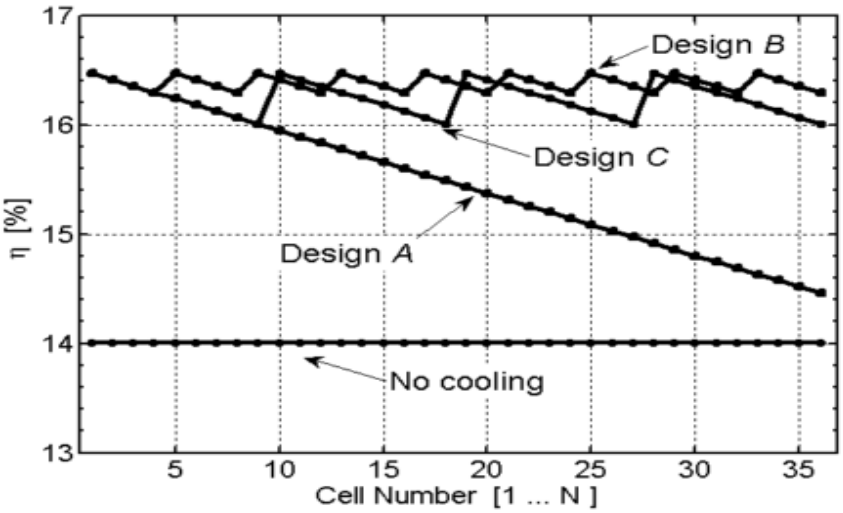

Figure 2.6 Different cases of heat pipe cooling model results [46].

A novel design of heat pipe cooling system was proposed by Russell [48] in which liquid with refractive index is used to concentrate the solar radiation on an photovoltaic cell array that is immersed on it. PV string was used with linear Fresnel lens where single lens directs the sunlight onto each cell. A number of pipes were attached all along the heat pipe of round section to form a panel as shown in Fig. 2.7.By ensuring the uniform temperature across the pipe and string, heat was dissipated by circulating coolant.

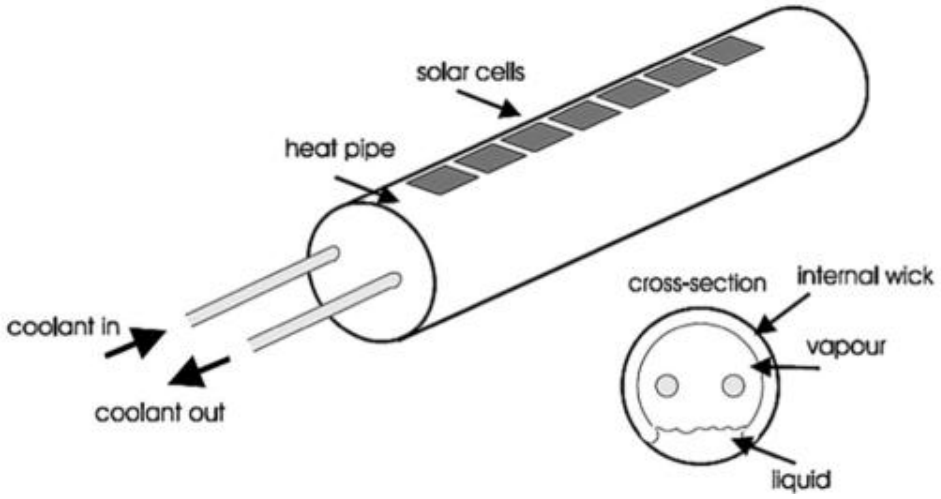

Figure 2.7 Uniform temperature heat pipe [48].

Akbarzadeh and Wadowski [49] experimentally investigated the performance of a heat pipe cooling system for photovoltaic cells subjected to high solar concentration for 4h. The CPV cooling system consisted of fins with heat pipes to cool at concentration ratio of 20 X. The results showed that the solar cell temperature dropped from 84˚C to 46˚C when the heat pipe cooling system is used resulting in 94% increase on the output power. The temperature on the surface of PV string reached as high as 84˚C without

cooling from heat pipes. Figure 2.8 shows the schematic of heat pipe for concentrates system used in their research.

Anderson et al. [50] investigated the utilization of copper heat pipe, with water as a working fluid, for CPV system. A number of fins are attached to the condensing side of the heat pipe to reject the heat flux of 40 W/cm^2 from the PV cells by natural convection to the ambient. In the aim to find the best configuration, a series of CFD analysis was then conducted to optimize the fin design and spacing between fins. The temperature difference between the cell and the ambient conditions was around 40˚C as shown in figure 2.9.

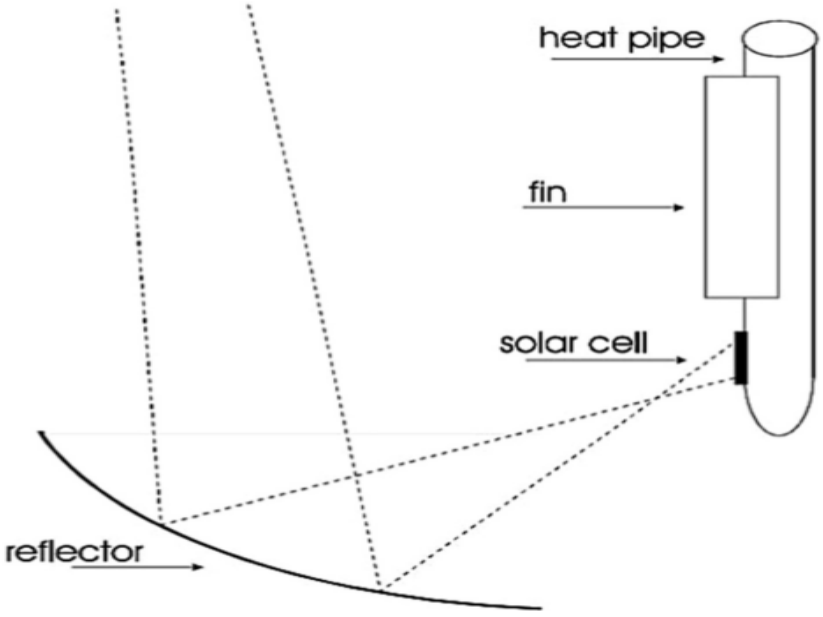

Figure 2.8 Schematic of the CPV heat pipe [49]

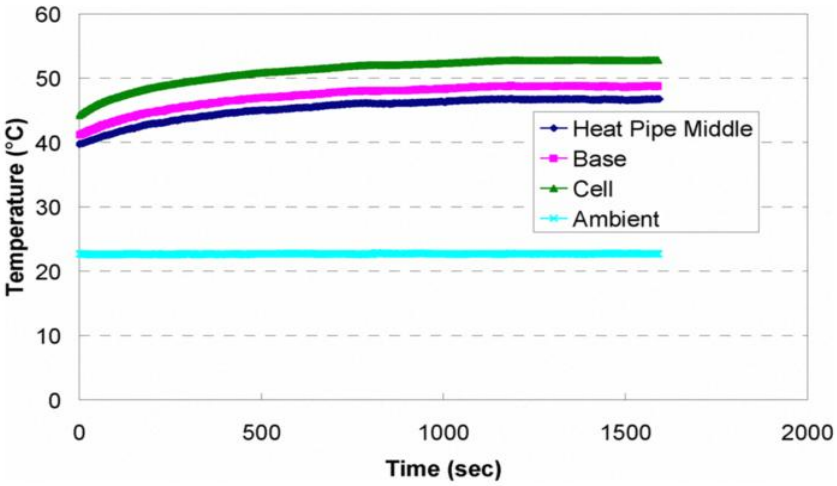

Figure 2.9 Variation of temperature profile with time [50]

Huang et al. [51] proposed and examined the performance of a novel hybrid-structure heat pipe composed from sintered capillary and coronary-stent-like supporting structure for concentrated photovoltaic systems. About 65% reduction in the thermal resistance has been realized compared to the design without supporting structure. Moreover, the electrical efficiency of CPV is enhanced by 3.1% in comparison with aluminum substrate.

Qifen et al. [52] investigated a heat pipe radiator to eliminate non-uniform heat transfer across the surface of CPV panel. They conducted a comparative analysis between small fin design, rectangular fin design and heat pipe (no additional radiator). Based on the preliminary results, optimized design was proposed with heat pipe and fins to keep the cell temperature at its minimum with uniformity in temperature. For a single cell, temperature was reduced to 305 K with a temperature variation across cell of 3 K as

shown in Fig. 2.10. Temperature uniformity was better for the results of heat pipe but the overall cooling effect was found to be best for small fins. Based on the analysis, they proposed a combined heat pipe and small fin design

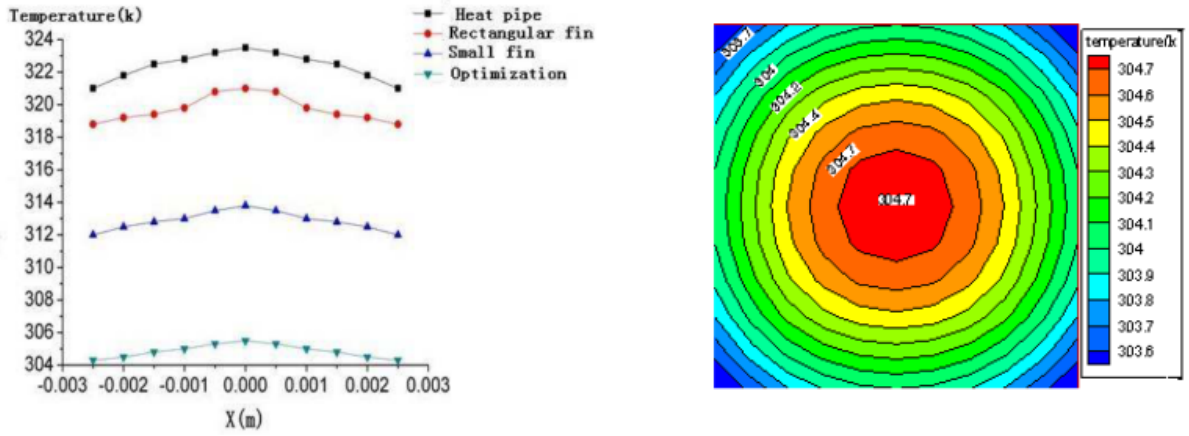

Figure 2.10 Comparison of cell surface temperature with an optimized heat pipe with fins design [52]

2.2.2 Microchannels

Microchannel cooling used for PV panels employs high heat carrying capacity and have been reviewed extensively in literature for the purpose of electronic and PV cooling. Garimella and Sobhan [53] published a detailed literature survey on the microchannels. In their review theoretical and experimental findings from literature has been discussed along with the application of microchannels for electronic and other applications. Phillips et al. [54] showed that heat load as high as 1000 W/cm^2 can be dissipated by the use of microchannel cooling system.

A recent overview on the thermal and fluid characteristics of microchannels using conventional fluids and nanofluids has been provided by Salman et al. [55]. In another

review by Adham et al. [56], hydrodynamic and thermal analysis of microchannel sinks were compared from literature. It was shown the flow characteristics in most microchannel studies are laminar and usage of liquid coolant was preferred amongst scientists and researchers.

Xu et al. [57] performed an experiment with a heat sink of microchannels and separated the whole flow field into several zones. Figure 2.11 shows the schematic of microchannel system used in this research. The microchannels were developed from silicon and thin films of platinum were deposited, which provided uniform heat flux. It had several parallel, longitudinal and transverse microchannels to increase the number of zones. Ten channels had a width of 4.35 mm with hydraulic diameter of 155 μm. Increase in 26.4 % Nusselt Number was found in contrast with a conventional microchannel design, while the pressure drop was decreased up to 27 % in the novel design proposed in the study.

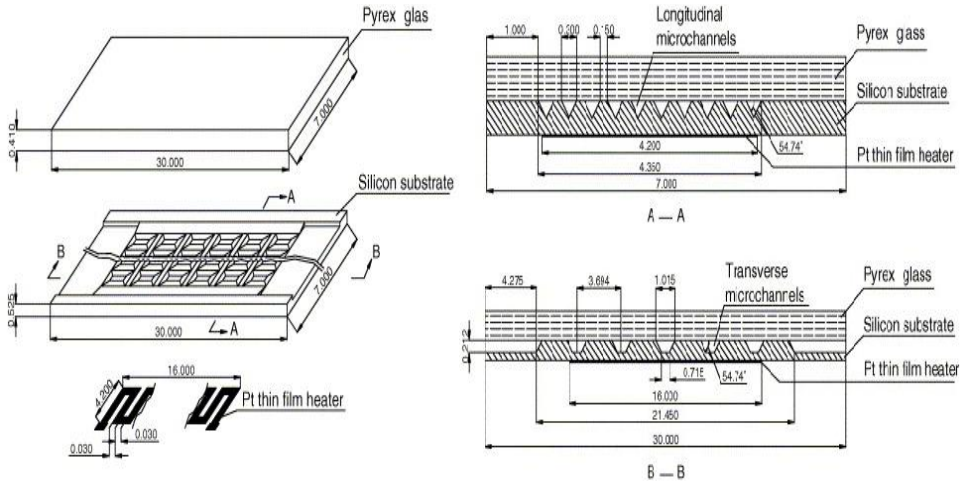

Figure 2.11 Microchannel system by Xu etal [57]

Wang and Ding [58] in an experiment obtained a uniform temperature distribution over the heating area by using microchannels cooling. They used parallel and longitudinal microchannels with silicon substrate and transverse microchannels. Nickel was used as heater and integrated in copper device for spreading. The de-ionized (DI) water was used as working fluid. Infra red thermograph technique was used to measure the steady state temperature. They concluded that the addition of transverse microchannels enhances the cooling capability than conventional channel and this method could be used for high heat flux application like electronics and CPV systems.

Wang and Ding [59] also simulated numerically the similar transverse microchannels configuration and concluded that the highest heat flux input of this novel micro heat sink was greater than 75% of conventional heat sinks. They found an average heat transfer coefficient of wall of around 3.2 kW/ m^2K with the flow rate of 6.7 ml/min and heat flux of 20.3 kW/m^2.

Altering the direction of flow is one technique in microchannels where temperature gradient across the flow length is reduced. Missaggia and Walpole [60] in their study proposed single layer counter flow method. Their design consisted of microchannels etched onto silicon wafers in which flow runs in alternate direction through channels. Their result indicated the thermal resistance of very low $1.1x10^{-5}$ W/m^2K was achievable by using this methodology. In another study by Vafai and Zhu [61], two layers of opposite flow microchannels was suggested. The numerical output showed that the

temperature gradient streamwise is decreased as compared to one layer structure thus giving more uniform profile of temperature

Ryu et al. [62] modeled and simulated a novel two layered microchannels heat sink to decrease the temperature gradient and drop in pressure. This design is called manifold microchannels heat sink in which the fluid flows in an alternate fashion in a direction perpendicular to the sink as depicted in Fig. 2.12. With this configuration the uniform temperature distribution across the cooled surface is obtained as the fluid now has shorter duration to be in contact with base. By using this design thermal resistance was lowered more than 50 % relative to conventional heat sinks, while significantly reducing the gradient of temperature on the base.

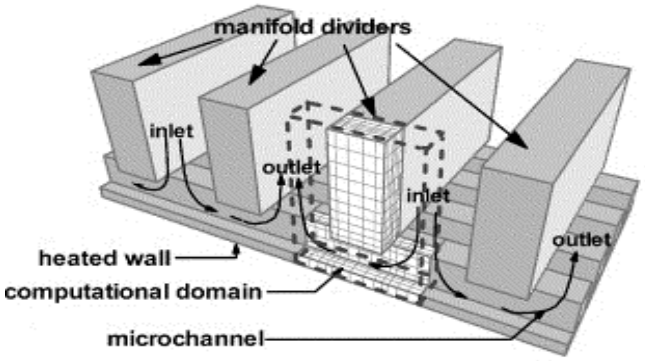

Figure 2.12 Schematic of manifold microchannel [62]

2.2.3 Liquid Immersion Cooling

Liquid immersion cooling involves immersion of solar cells directly into the circulating liquid. In this method the heat is absorbed by the circulating coolant form both the front and back surface of the PV string as compared to other conventional active

cooling methods. In an area of immersion cooling, Russell [63] proposed and patented an elongated tube filled with liquid having non-conductive properties to work as optical concentrator as well as cooling system for the PV string as shown in Fig. 2.13. The refractive index of the immersion liquid was selected such that it will be fitting to concentrate the solar radiation onto the PV cells. Solar cells were installed in the cylinder and immersed in non-conductive liquid.

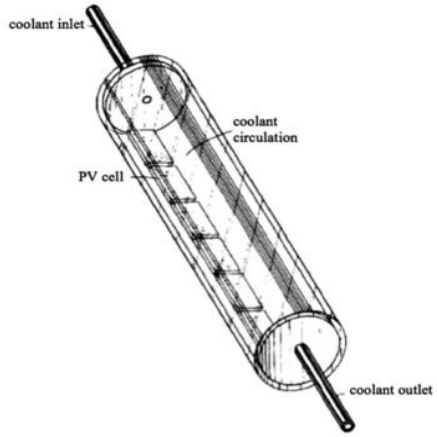

Figure 2.13 A view of optical concentrator for immersion cooling[63]

An idea similar to dielectric cooling for the solar cells under concentration was proposed by Liu et al. [64]. They suggested that the excess heat should be removed from both the back and front of the panel by direct immersion of the module in a dielectric fluid. The main advantage of this method is the direct thermal contact transfer of heat results in higher dissipation of heat and higher efficiencies. Cooling capacity of the system was tested under the standard insolation of 50 and 70 kW/m^2 in which xenon lamp was employed as the sun simulator and dimethyl-silicon oil as dielectric liquid. The

experimental work showed that in turbulent regime, the temperature distribution of the panel in the direction of flow field is approximately uniform with variation of about 3˚C. With this method temperature of cell can be cooled down to 30˚C with heat transfer coefficient of about 1000 W/m^2K. It was also concluded that the inlet temperature of liquid does not significantly alter the temperature distribution of module.

Koehler [65] has also patented a design for the cooling of concentrated modules. His concept involves submerging the cells into a coolant liquid which is continuously circulated, whereby heat transfer takes place between two cells rather than one. This configuration allows the coolant to work as filter by absorbing part of the incoming solar radiation before it reaches the panel. Dielectric coolant liquid is used and with proper combination of coolant and pressure, uniform temperature distribution across the cell surface and a higher heat transfer coefficient can be obtained.

Zhu et al. [66] in a field of immersion cooling investigated the dielectric immersion technique of cooling for concentrating system. A dish with a concentration ratio of 250 with dual axis tracker was used to examine a new CPV system with DI water for cooling as shown in Fig. 2.14. Transient distributions of temperature of the PV module were measured while making a record of I-V curves. They showed that at an insolation level of 940 W/m^2, the PV module temperature was decreased up to 45˚C with inlet water temperature of 30˚C. It was found that the temperature distribution is uniform of the module with maximum temperature variation at the surface being less than 4˚C. The calculated amount of heat transfer coefficient was found to be around 6000 $W/m^2.K$

which showed the capability of extracting high heat by the employment of immersion cooling. They concluded that the performance of the cell electrically degrades because of constant immersion of cells in the DI liquid. This finding has been validated by Han et al. [67] by long term immersion test of 100 days, which showed the degradation of electrical performance was because of consistent interaction of cells with DI water.

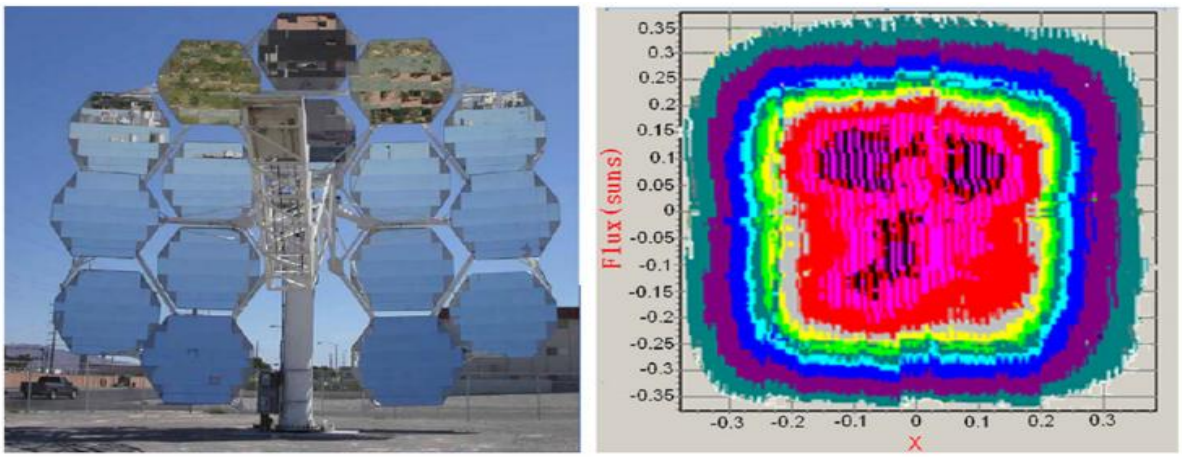

Figure 2.14 Mirror facets and flux profile of dish concentrator [66].

Han et al. [68] analyzed the thermal and electrical characteristics of CPV system using dielectric immersion cooling. Comparison between four different types of liquids namely de-ionized (DI) water, dimethyl silicon oil, ethyl acetate, and isopropyl alcohol (IPA) were carried out. The results from simulation showed that this cooling technique can maintain low and uniform solar cell temperature. It was also found that the thermopyhysical properties, flow mode and the inlet velocity of coolant plays a vital role in the cell temperature. At the inlet condition of 298 K and 1.11 l/s, temperature

distributions are shown in Figs. 2.15 and 2.16 for all the cases. It can be seen that solar cell temperature increases along the length of channel which depended upon the properties of coolant used. The maximum temperature non-uniformity for cooling as function of flow rate across the length are about 4˚C, 17˚C, 12˚C and 32˚C for DI water, IPA, ethyl acetate and dimethyl silicon oil, respectively. It is clear that the use of these liquids for immersion cooling under certain operating conditions resulted in low and uniform temperature profile leading to an increase in output power of CPV systems.

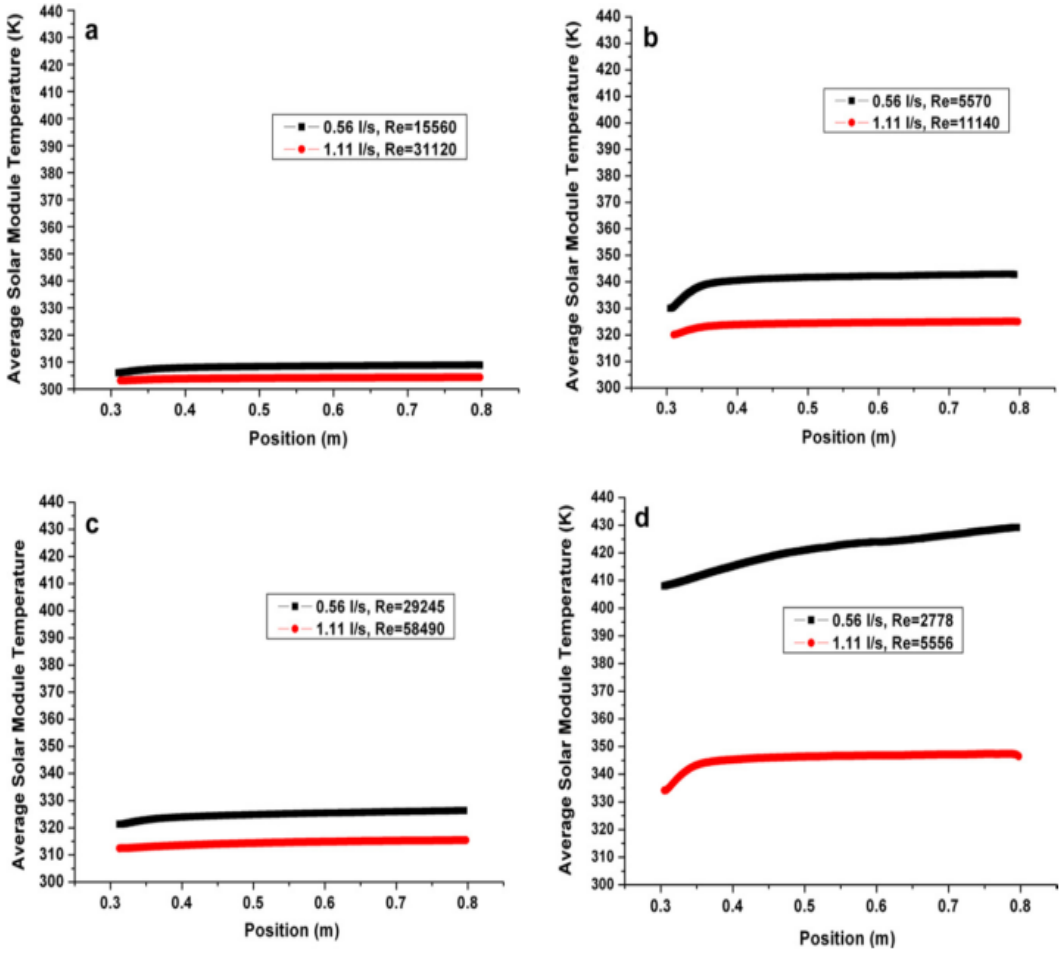

Figure 2.15 Temperature plots over the length of an array of concentrated solar cell for a) de-ionized (DI) water, b) isopropyl alcohol (IPA) , c) ethyl acetate, and d) dimethyl silicon oil [68].

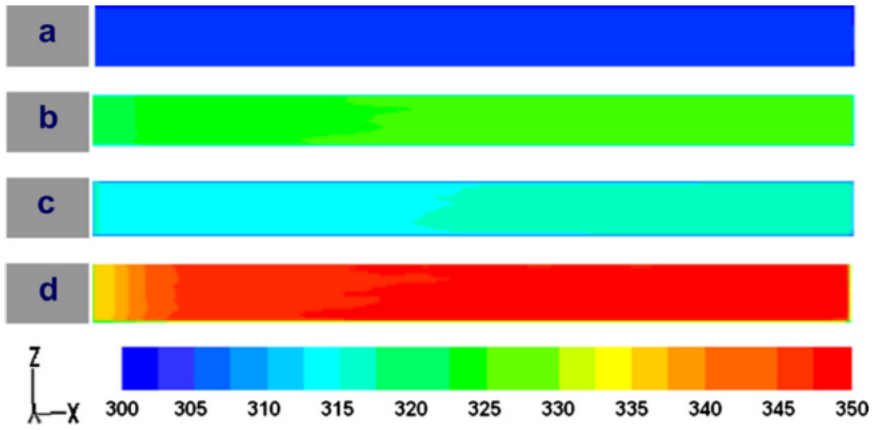

Figure 2.16 Fig. 16 Temperature contours of concentrated solar cell for a) de-ionized (DI) water, b) isopropyl alcohol (IPA) , c) ethyl acetate, and d) dimethyl silicon oil[68].

Xiang et al. [69] performed a three dimensional numerical study on the cylindrical liquid receiver for immersion cooling. They compared the heat transfer performance of bare structural module and finned structural module for 250X CPV systems under actual climatic conditions of the solar intensity of 1000 W/m^2, 25˚C and 15 % conversion efficiency. It was shown that the inlet velocity and the number of fins were the primary factors for cooling. They found that the inclusion of more number of fins reduced the average temperature to 8–10 ˚C. Moreover the temperature non-uniformity was reduced from 15˚C to 10˚C. An optimum design configuration of 11 fins and height 4mm was found to yield better thermal performance as shown in Figs. 2.17 and 2.18. The maximum temperature reached for this case was 47 ˚C while maintaining the surface uniform with temperature variation of around 14-15 ˚C. Simulation results revealed that as the fluid velocity increases, lower temperature with more uniformity is achieved but with an

additional cost of pressure drop and pump power. The simulated results showed promising results for the case of liquid immersion cooling for CPV systems.

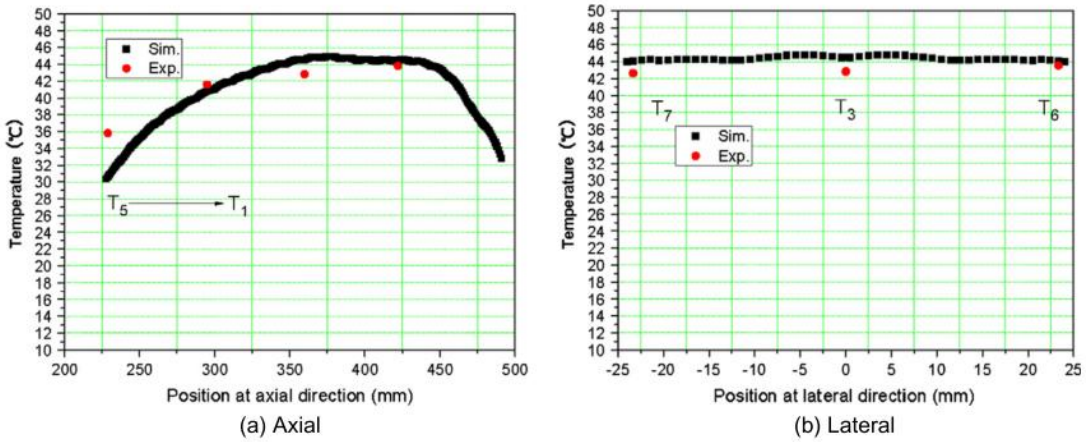

Figure 2.17 Thermocouple readings showing temperature distribution across PV length [69].

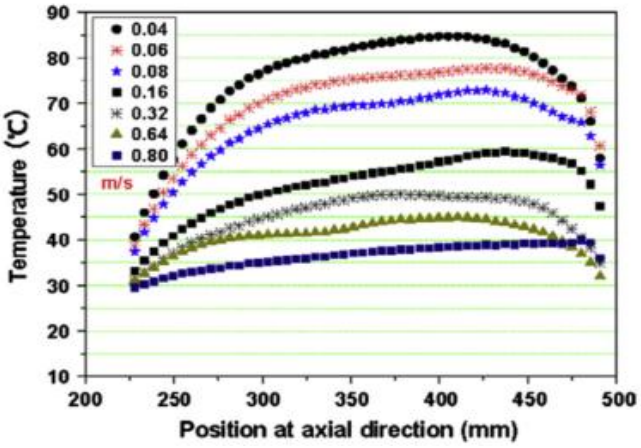

Figure 2.18 Fig. 18 Variation of solar cell temperature along curve length as function of inlet velocity [69].

Sun et al. [70] investigated the performance of direct liquid immersion of concentrator solar cells for linear CPV systems. A narrow rectangular channel receiver

was designed to reduce liquid holdup and its thermal characteristics were investigated under energy flux of 9.1 suns. Di-methyl silicon was used for heat dissipation and real time weather conditions were utilized for testing. Experimental results showed that the cell temperature is controllable to the range of 20-31˚C with the use of this technique under the conditions of 910 W/m^2 direct normal incident (DNI) radiation, silicon oil temperature of 12˚C, and reynolds number in the range of 2720 to 13,602. It was shown that the cell temperature increases linearly with the temperature of silicon oil in the limit of 0-35˚C. The variation in temperature was found to be less than 3˚C alongside axial and lateral direction, hence resulting in a uniform temperature distribution across cell array. Also it was demonstrated that this configuration showed stable results even after 270 days of exposure in real time conditions. Figure 2.19 shows the axial and lateral temperature measurements for different Reynolds numbers.

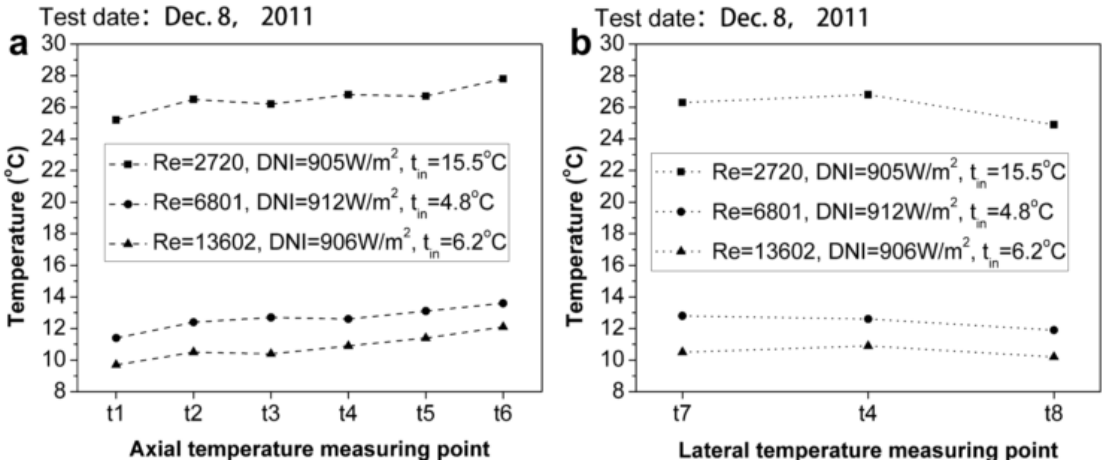

Figure 2.19 Cell array temperature distribution for axial and lateral directions under different Reynolds numbers [70].

Similar configuration utilizing dielectric liquid for immersion cooling for solar cells have been investigated by Abrahamyan et al. [71], Tanaka [72] and Han et al. [67]. The main result shown in these literatures is an enhanced conversion efficiency of the solar cells operating in dielectric medium. In a study by Abrahamyan et al. [71], it was shown that the efficiency of solar cells increases by 40–60% by employing dielectric liquid thin-film whereas Han et al. [67] concluded that by using 1.5 mm thick layer of dielectric liquid over the cell surface, the efficiency of solar cells increased by 8.5–15.2%. This increment in conversion efficiency was reported because of two physical mechanisms; first is the increase in output current due to lesser surface carrier recombination, and the second is the improved collection of light because of refraction and inner reflection of light inside the dielectric medium.

2.2.4 Improved Heat Exchangers

Baek et al. [73] in their numerical study for the uniform cooling of Polymer Electrolyte Membrane Fuel Cell (PEMFC), studied the effect of constant heat flux in the design of heat exchanger for fuel cells. Detailed heat transfer and fluid flow calculations were simulated in CFD using large scale plates of 18 cm x 18 cm. Based on simulation results, evaluation of different flow field designs were done for temperature uniformity, maximum temperature, and pressure drop characteristics. Figure 2.21 shows the boundary conditions and schematic of the serpentine heat exchanger used for numerical analysis. The results showed that multi-pass serpentine flow field (MPSFF) type design could drastically improve distribution of temperature uniformity in a cooling plate

relative to conventional serpentine type flow designs, while keeping the fluid pressure drop same as shown in the contours of Fig. 2.20.

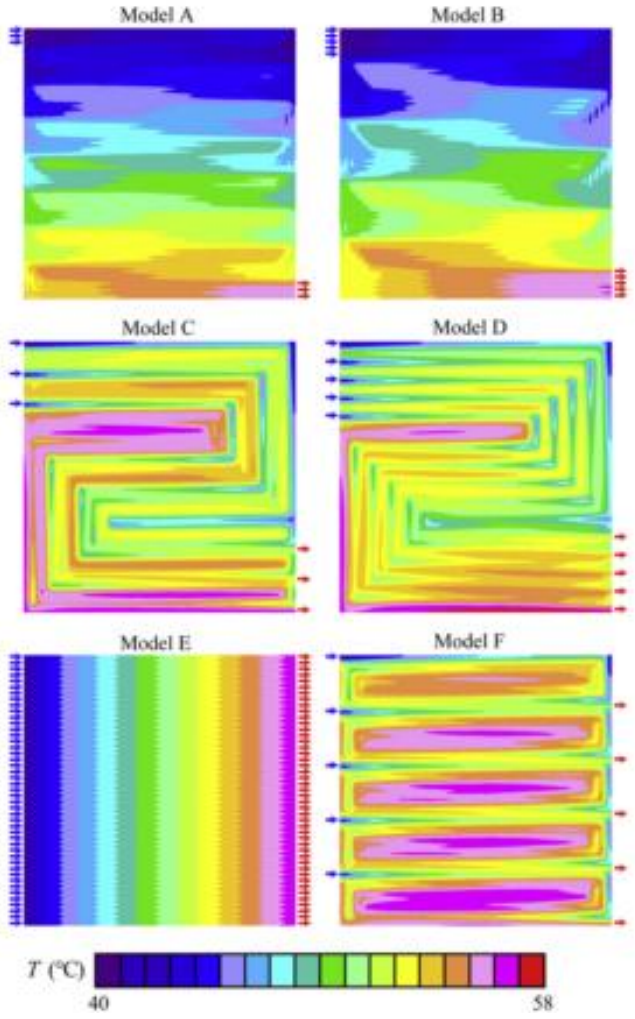

Figure 2.20 Surface temperature distributions in cooling plates with six coolant flow field designs [73].

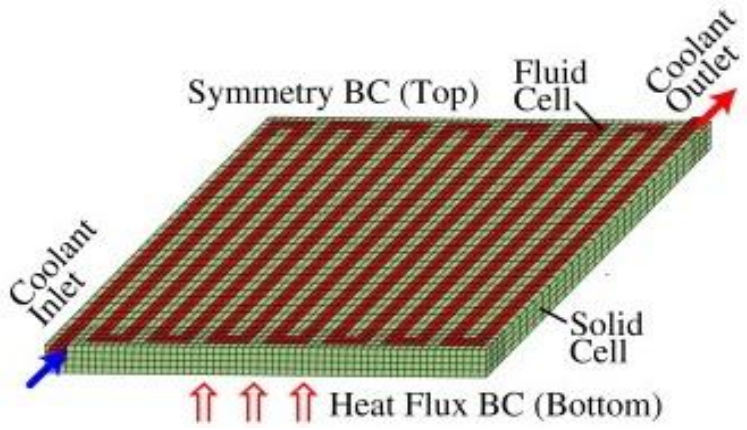

Figure 2.21 Serpentine Type uniform cooling design [73]

In another area of heat dissipation technique, Lasich [74] made a patent of a cooling water circuitry for CPV systems. The design was intended to dissipate heat up to 500 kW/m^2 and to maintain the temperature of cell at 40°C for NOCT conditions. The idea is based upon the flow of water through parallel small channels contacting cells thermally. This patent [74] was used commercially for uniform cooling of the parabolic dish systems [75]. It has been reported to achieve 38.5˚C as an average cell temperature with a cell efficiency of 24 % using concentrated parabolic systems.

2.2.5 Heat sinks

Heat sinks have also been studied in literature for the uniform cooling of electronic devices. In the field of electronics the best results that have been presented for cooling was by Hetsroni [76]. He experimentally investigated the performance of uniform temperature heat sink for electronic cooling. This study involved two phase cooling with dielectric liquid that boils at lower temperature. Comparison was made with dielectric

liquid and water cooling. Figure 2.22 shows the temperature distribution for heat sink. It was found that the maximum temperature difference in the case of dielectric liquid was 4-5˚C and 20˚C for water cooling, respectively. Also the temperature gradient in stream wise and transverse directions was reduced.

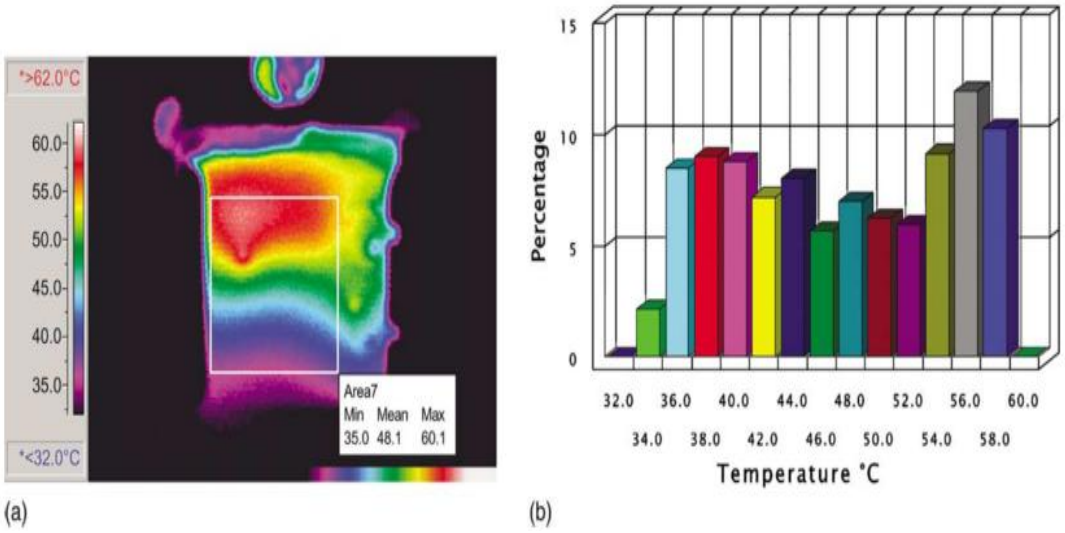

Figure 2.22 Electronic cooling showing (a) infrared image of the heater; (b) histogram of temperature distribution [76].

In an area of passive cooling, promising results have been reported for the case of heat spreader and heat sinks by Araki et al. [77] and Min et al. [78]. Araki et al. [77] analyzed a module geometry as shown in Fig. 2.23 comprising of copper heat spreader mounted on aluminum plate. The cooling technique was used for CPV system and was fabricated using printed thermally conductive epoxy. The aluminum sheet with 3 mm width and heat spreader with high heat spreading coefficient were found to yield lower temperature rise. Real time experiment conducted with non-imaging Fresnel lens

revealed only 21˚C temperature increase which is promising considering a natural convection process.

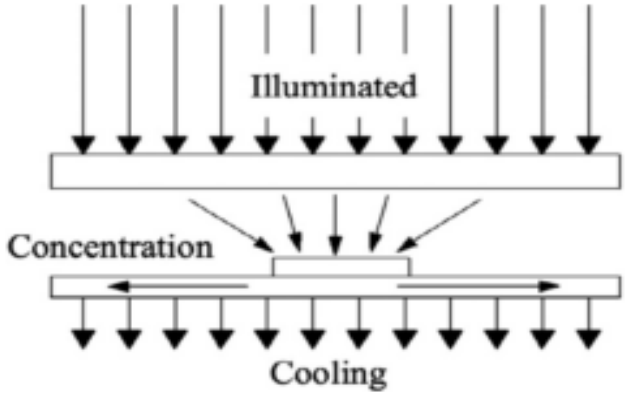

Figure 2.23 Heat spreading concept for concentrator module [77].

Considering the similar cooling scheme as proposed in [77], Min et al. [78] studied metal heat sinks for 400 X PV system and performed an experiment in outdoor environment. The main focus of the study was to investigate the dependence of temperature on cell areas with various concentration ratios. They concluded that for a stable average temperature of 37˚C, area of heat sink was required to be 700 times more than the area of solar cell. Moreover it was also reported that temperature of the cell reduces with an increase in the area of heat sink. It was shown that for the temperature of the cell to remain constant, the heat sink area has to be increased linearly with the concentration ratio. Figure 2.24 shows the profile of cell temperature from this cooling which looks uniform but the problem with these passive designs is the huge size of spreader which makes them less realistic and attractive as cooling alternative.

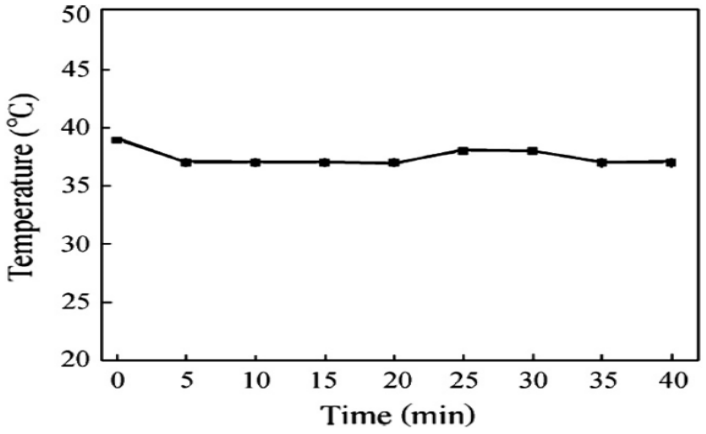

Figure 2.24 Temperature profile of the outdoor test for 400X concentrator PV [78]

Theristis et al. [79] designed and performed numerical analysis for passive cooling of HCPV using MATLAB and COMSOL Multi Physics. Thermal model was developed to examine the effect of heating on PV output and different scenarios pertaining to passive type cooling was applied for 500 X concentration solar cell. It was revealed that for high ambient temperatures, passive cooling technique for HCPV with concentration ratio of 500 is viable to keep the cell temperature below 80°C. It was agreed that passively cooling CPV is insufficient for dissipation of heat even when a large heat sink is used relative to cell size.

2.2.6 Impingement Jet Cooling

One major cooling technique that has been used extensively in several industrial fields is the method of heat extraction by impinging jets. Thermal resistance as low as 10^{-5} to 10^{-6} m^2K/W [80] can be obtained by the use of impinging liquid jet. Impingement jets are capable of extracting large quantity of heat. This is due to existence of thin

thermal boundary layer present at the stagnation zone under the impingement however the heat transfer coefficient decreases radial outwards from the jet. The cooling of plates depends largely on the number of nozzles used. The main concern when design an impingement cooling device is to model the disturbance arising from the interaction of fountain of jet to another jet. In this regard fluid velocity, plate to diameter spacing, nozzle pitch and number of nozzles should be found such that an optimum solution is found.

In a comparative study between microchannels and impingement jets for cooling purpose by Lee and Vafai [81], it was proposed that for cooling of plates greater than 7 cm x 7 cm jet impingement is a superior solution than microchannels given that the spent flow or drainage problem is addressed. Comparative analysis was not done on the basis of pumping power but was addressed on individual optimum conditions for microchannels and jet impingement. The reason is jet cooling requires large flow rate of coolant with small pressure drop whereas the microchannels cooling results in high pressure drop with low flow rate.

Webb and Ma [82] in their review of single phase jet impingement has provided comprehensive study on jet flow. Submerged and free jets are discussed in this paper along with the optimum conditions required for the operation. Also comparative study has been given for planar and axi-symmetric jets along with different correlations for heat transfer.

Womac et al. [83] did an experimental work on impingement jets. They studied heat transfer coefficient of different types of jets with an square array of 2 x 2 and 3 x 3 without considering the issue of spent flow. The impact of nozzle to plate distance was studied and concluded it to be inconsiderable for free jet flow, however it had an impact on submerged jets. Different correlations for the coefficient of heat transfer of free and submerged jet were presented.

Royne and Dey [84] designed an impingement jet device for the cooling of densely packed PV panels. In their study, an experimental setup was designed in which fluid had drainage in direction perpendicular to flow. Submerged jet with four and nine jet with side drainage was analyzed for local and average heat transfer coefficient. Two models based on single and multiple nozzles correlations by Martin [85] and Huber et al. [86] were developed along with net power generated by the PV system. It concluded that the higher number of nozzles will perform better than lower number of nozzles. Optimum diameter for nozzle was also suggested along with pumping power required. General graphs and trends were shown for the cell temperature, PV power output and net PV power generated as highlighted in Fig. 2.25 (difference of PV array power and pump power required). Concentration ratios of 200X and 500 X were considered for the analysis. It was concluded that for 200 X, the cell temperature decreases approximately to the value of 30˚C from 60˚C whereas for 500 X, cell temperature dropped from 110˚C to 40˚C at maximum power point. Average heat transfer coefficient in the range of 10^5 W/m^2K was achieved for the four nozzle array.

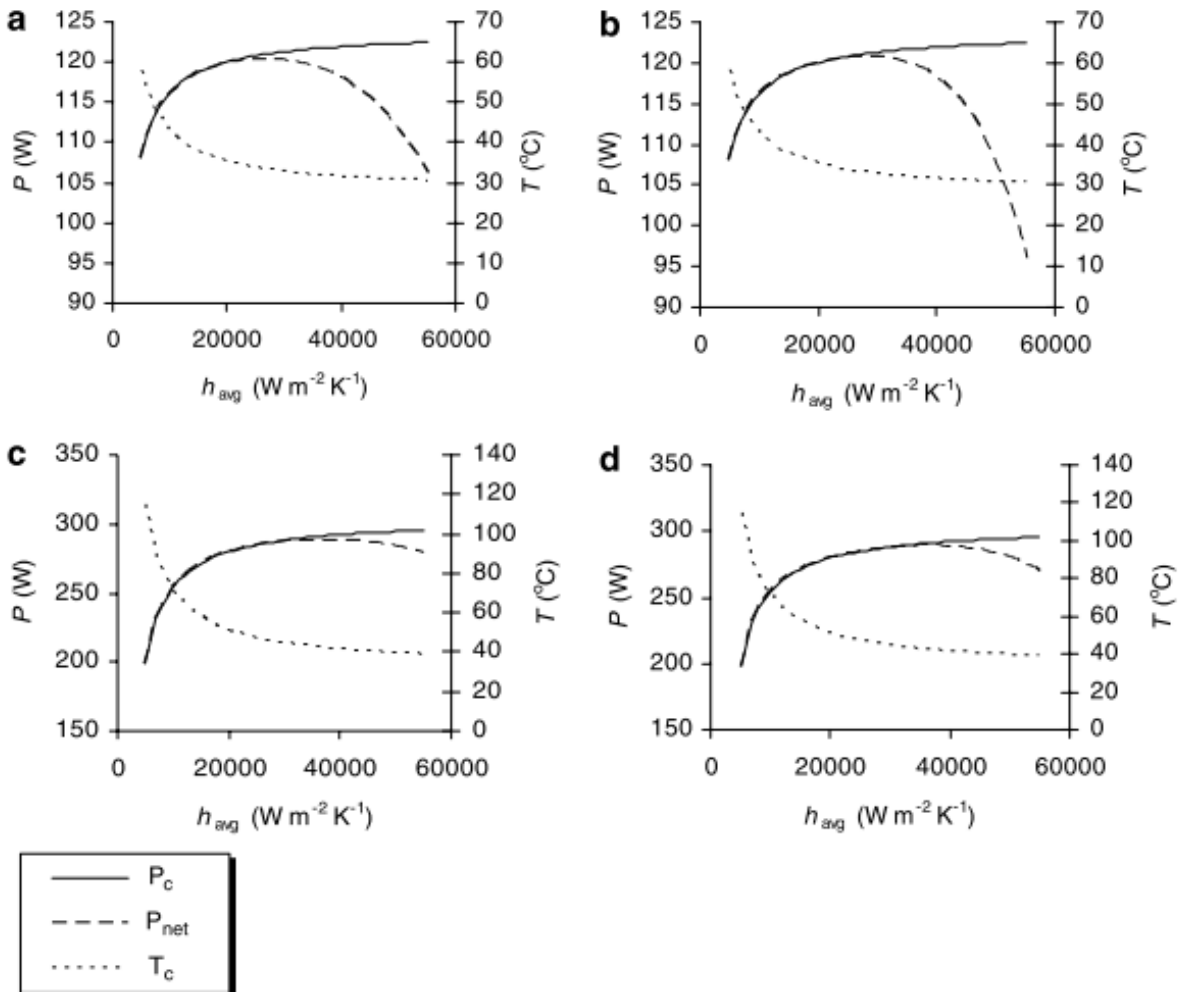

Figure 2.25 Cell temperature and output power shown for two models and concentration ratios: (a) 200 X, Martin model; (b) 200 X, Huber model; (c) 500 X, Martin model; (d) 500 X, Huber Model [84]

Jeong et al. [87] did a study recently on the enhancement of jet design for solar PV power applications. They used a device called Hydraulic Jet Scanner (HJS) for cleaning and cooling of PV panel and compared the performance with rotor sprinklers. Three cases

were investigated namely PV cooling, PV cleaning, and PV combined cooling and cleaning. It was found that HJS could enhance the performance up to 22% conversion efficiency by cooling solar modules with water. Also 2.3% maximum efficiency can be achieved through cleaning the dust accumulation over panel surface whereas up to 19% conversion efficiency can be resulted from the combined action of cleaning and cooling of panels.

2.2.7 Hybrid Microchannels and Impingement Jet Cooling

Barrau et al. [88] used a scheme for combined jet impingement and microchannels for the purpose of uniformity of temperature in cooling applications for electronic and power systems. They used CFD for the purpose of numerical analysis under turbulent model and validated the simulations with experimental results. They concluded that based on the local heat removal capacity and cooling requirement, temperature distribution can be changed using different configurations as shown in Fig. 2.26. Also it was found that as the Reynolds number increases, the pressure losses increases more rapidly than the heat transfer coefficient.

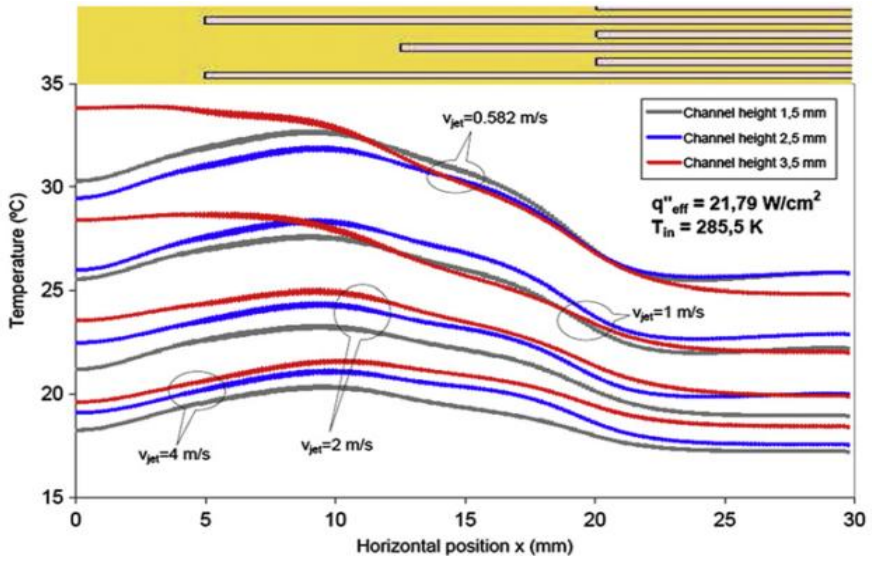

Figure 2.26 Fig. 26 Temperature profile for different cases. The longitudinal arrangement is shown on the upper part of the graph. [88]

In another study by Barrau et al. [89], an in-depth analysis was performed for combined jet and microchannel cooling for PV panels working under high concentration ratios. The cooling mechanism combined slot jet cooling along with microchannels. Main parameters studied in their analysis were temperature non-uniformity on the PV surface and net power generated by PV system. It was found that the hybrid system provided thermal resistance as low as 2.18 x 10^{-5} m^2K/W which is even lower than the required resistance given by Royne and Dey [84] for densely packed cells. The pressure drop in this new system was found to be lower than the microchannels individually which is the main problem generally arising from microchannels cooling. Net power generated by PV system was found to be higher for the combined cooling scheme when compared with microchannels cooling. For temperature non-uniformity effect, three different geometries

for microchannel heat sinks were compared. Typical plots for various heat sink designs showing temperature variations are shown in Fig. 2.27.Temperature variation of 2˚C was obtained for micro-channel heat sink whereas for hybrid cooling standard deviation of 0.4˚C was obtained.

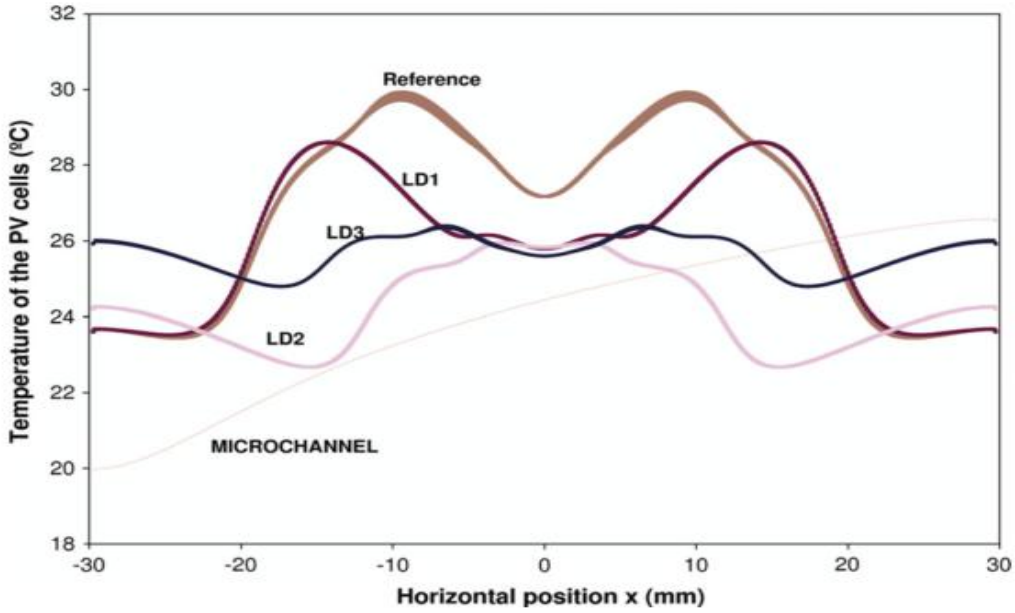

Figure 2.27 Temperature profiles by several microchannel arrangements [89]

2.2.8 Phase Change Material Systems

It is likely that the efficiency of energy conversion by PV modules can be improved with better thermal management by maintaining operating cell temperature below 25 °C. In order to lower the operating temperature, two approaches implemented to restrict temperature increase in PV panels; one involves back panel cooling by natural or forced convection, and the other one utilizes phase change materials (PCMs) to cut the detrimental heat by adopting PV/PCM architecture. PCMs has the unique ability to

absorb excess heat during melting change in phase from solid to liquid at a stable transition temperature and thus can be used for temperature regulation. PCMs also called latent heat storage devices remains at constant temperature during the phase change process which can result in the PV surface to be remained at uniform temperature. Many researchers considering PCMs, as most suitable option to absorb dissipated heat during energy conversion process, have adopted different approaches ranging from single and multiple PCM to novel heat sink design and hybrid solution involving solar thermal for maintaining efficiency of PV panels [90].

Huang et al. [91] found that at solar intensity of 1000W/m^2 insolation and ambient temperature of 20 °C, front surface of PV panel was maintained at constant temperature of 36.4 °C using PCM. Further incorporating actual atmospheric conditions for one day, the electrical conversion efficiency showed improvement as the cell temperature was controlled below 34 °C. Biwole et al. [92] showed similar results where the PCM incorporated PV panel's temperature remained below 40 °C for 80 minutes under solar radiation equivalent to 1000 W/m^2 as shown in Fig. 2.28.

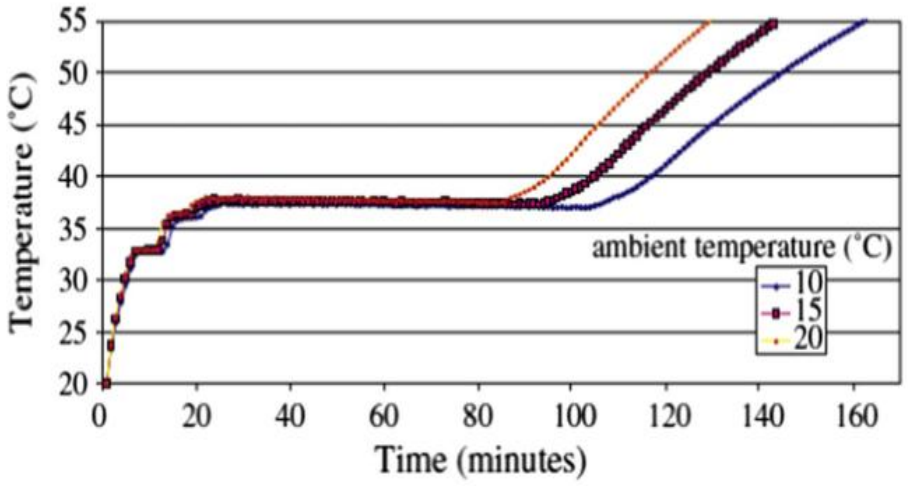

Figure 2.28 Average temperature at front surface of PV/PCM system with an irradiation level of 1000 W/m2 [91]

Hasan et al. [90] evaluated five PCMs under three insolation levels and studied their impact on the PV panels thermal performance. The best results were obtained to provide 18°C and 10°C reduction in front surface temperature. Figure 2.29 shows the average cell temperature for three insolation levels by using PV/PCM cooling. Maiti et al. [93] made use of Paraffin wax having 56-58 °C melting range as PCM to restrict the temperature increase of PV panel in V-trough at 60-65°C for 180 minutes when aluminum turnings in a matrix were added to wax for increasing its thermal conductivity. Also, in the outdoor test, panel's temperature was reduced by 20% and output power was increased by 55% compared to a conventional system without any PCM.

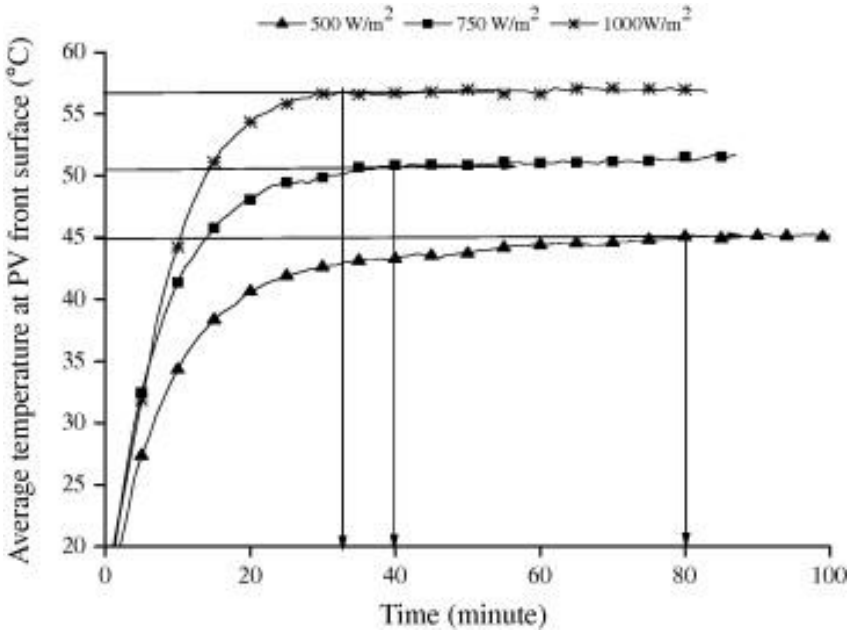

Figure 2.29 Front surface temperature profile for three insolation levels [90]

Tanuwijava et al. [94] found out that PV panels incorporated with micro-encapsulated phase change material (MEPCM) has the potential to reduce the increase in PV cell temperature and consequently, increase the conversion efficiency. They also showed that varying the aspect ratio of MEPCM affected the power output and thermal regulation of the cell. However, they observed that MEPCM with different melting point did not return significant temperature reduction.

Due to lesser thermal conductivity of PCMs, Huang et al. [95] conducted a series of experiments for temperature control of three PV/PCM system configuration having metallic internal fins. They observed best temperature control, and more importantly, a uniform temperature distribution, when the spacing within the matrix was reduced.

Figures 2.30 and 2.31 show the structures and comparison between three PCM configurations for photovoltaic systems.

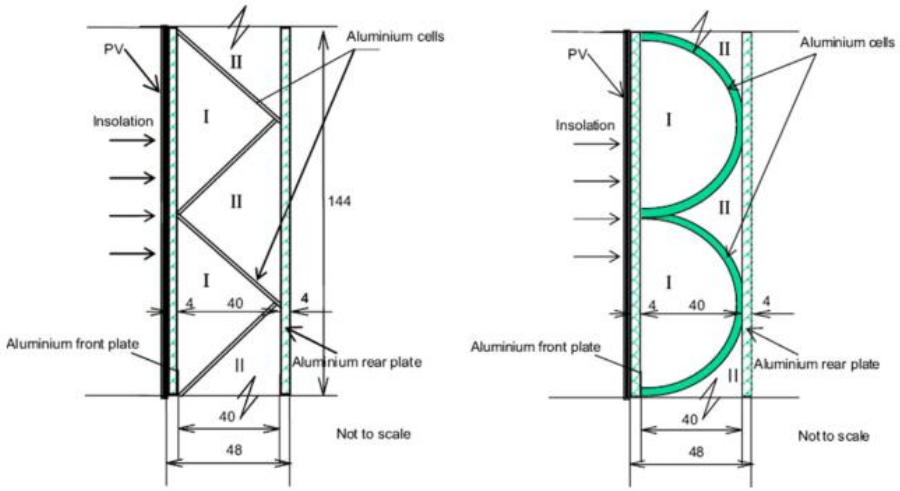

Figure 2.30 Structure of double layer PV/PCM designs [95]

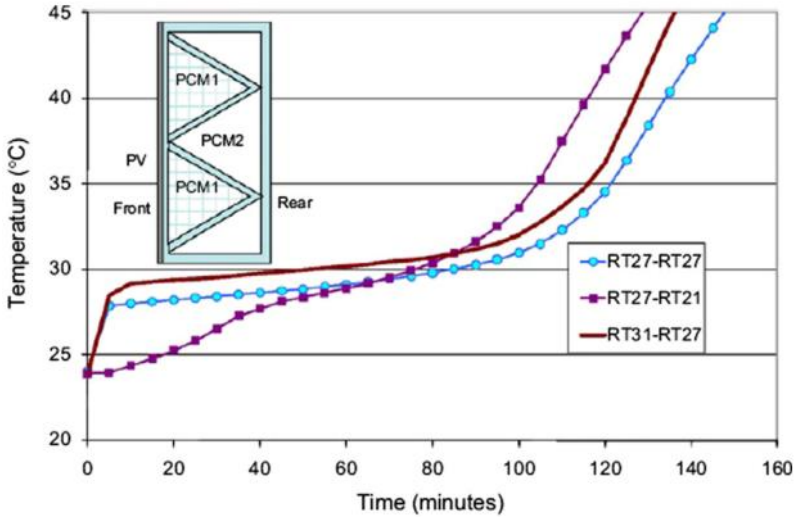

Figure 2.31 Temperature distribution of three configurations of PV/PCM systems with triangle cells [95]

2.3 DISCUSSION AND CONCLUSION ON COOLING TECHNIQUES

This section highlighted the need for uniform cooling of photovoltaic panels by discussing the causes and effect of non-uniformity in PV systems. Based on literature survey, cooling techniques with low average cell temperature and uniform temperature distribution were analyzed and discussed. The presence of non-uniformity on the PV systems was found to increase the cell temperature, increase variable temperature distribution, decrease fill factor, decrease open circuit voltage, decrease overall efficiency, and consequently leading to an increase cost per unit watt of PV power output. The impact of non-uniformity was found to be significant in all PV systems however the effect is more pronounced in the cases of CPV systems.

Table 2.1 shows the summary of uniform cooling techniques reviewed in this paper. The literature shows various types of uniform cooling mechanisms based on the application of solar PV panels. Immersion cooling, heat pipes, microchannels, impingements jet, phase change material cooling, heat sinks and improved heat exchanger designs were found to yield uniform temperature in most of the PV installations. Essentially they are formed by active and passive cooling system build on the basis of geometry and concentration level of the PV system. A comprehensive summary of reviewed cooling techniques is provided in Table 2.1. Heat pipe cooling with its high heat flux dissipation capability was shown to be effective for PV cooling especially with the aid of fins. Cell temperature was found to be in the range of 32-46˚C with the best case temperature non-uniformity of 3˚C for concentrated systems. It is a low

cost system based on its passive cooling. Heat sinks and heat spreader are another passive cooling techniques reported in literature. These systems are capable of reducing the cell temperature to as low as 37˚C even for high concentration levels. The main drawback of these dissipation techniques however is that to keep the cell temperature maintained, heat sink area directly increases with the concentration ratio. As a result a very large heat sink is required to release heat from concentrated PV systems making them less realistic and attractive for cooling. The viability of passive system economic wise is not suitable since it involves large quantity of material fins/planes.

In the field of active cooling, optimization to obtain uniform temperature distribution has been achieved by improved heat exchanger designs. Multipass serpentine field heat exchanger was shown to be operating with less temperature variation. Also the use of variable flow rate of coolant can increase temperature uniformity across the surface of the PV panel. Immersion cooling in dielectric liquid is a promising option which can attain a large amount of heat removal rates. They were reported to cool the temperature of PV panels in the range of 20 - 45˚C for concentrated systems. Shallow immersion in dielectric liquid, addition of fins to the cooling setup and utilizing de-ionized water was also found to be effective in increasing the efficiency and lowering the temperature. Furthermore temperature variation across PV surface was reduced to 3-10˚C by applying immersion cooling. Stable performance of PV strings under dielectric is a challenging assignment for the future researchers as the maximum stable performance that has been reported in literature was 270 days.

Passive cooling by phase change materials provided better thermal management solution for PV systems. The main advantage of using PCM is the ability to regulate temperature based on its latent heat which can result in uniform temperature cooling. However this technique is still in the growing phase and seldom has been used for concentrated systems. The thickness, melting temperature and PCM material can determine the amount of time a PV temperature can be sustained with stability. Cell temperature was controlled in the limits of 28-65˚C using one kind or multiple kinds of PCM materials. The limitation of incorporating PCMs arises from the fact that some of them are toxic and corrosive. Another issue is in regard with fire safety and disposal problem after the completion of life cycle

In contrast, the use of hydraulic jet impingement cooling and microchannels provides high heat dissipation for concentrated systems and may be directly employed in the cooling system. Microchannel heat sinks can efficiently achieve low device temperature and uniform temperature distribution. The use of traverse channel in the microchannel for cooling was reported to enhance cooling capability and provide low uniform cell module temperature. Impingement cooling with its high extraction capability and low thermal resistance is also a promising alternative for PV cooling. PV Impingement cooling is reported to achieve average heat transfer coefficient of the order of 10^5 along with reduction in temperature up to 30˚C for 200 X concentration system. Microchannels requires huge amount of power because of large pressure drop for the coolant to flow and manufacturing costs are higher. The feasibility of incorporating impingement jet directly onto the solar power system makes it a viable option for the cooling of PV panel with its

attractive heat extracting quality. Hybrid impingement and microchannels may prove to be the best solution for uniform cooling of PV panels based on the non-uniformity and low average cell temperature reported in survey. For hybrid cooling standard deviation of 0.46˚C PV surface temperature for high concentrated system was obtained along with thermal resistance as low as 2.18 x 10-5 $W/m^2.K$. Microchannel with jet impingement region was shown to enhance the temperature uniformity. It was also observed temperature distribution can be regulated depending upon cooling requirements which makes it an attractive option for uniform cooling. Very few papers in the literature were found to analyze the net power gained by the cooled PV system and the focus of study was more inclined towards the overall system performance rather than the effect of cooling characteristics on PV system. Each of the cooling system has its own applications and cooling performance of the system varies in different systems. To comprehensively understand the effect of non-uniformity and the application of uniform cooling techniques, detailed theoretical and experimental research is still needed as it can make substantial impact on CPV systems. The review in this paper may provide a good background for further research.

Table 2.1 Summary of uniform cooling techniques reviewed

Researcher	Type of Cooling System	Nature of work	Type of PV system	Coolant Type	Cell Temperature Characteristics	PV Cell Electrical Parameters	Key Findings	General Outcome
Tarabsheh et al.	Cooling Pipe (Heat Exchanger)	Analytical	---	Water	Uniform Cooling using optimized design.	Increase in V_{oc} by 11% Increase in FF by 4.7% Increase in η by 17.15 %	The cooling pipe with lowest length achieved lowest average cell temperature with highest efficiency.	Plots, Correlation
Baek et al.	Improved Heat Exchanger for fuel cell	Numerical	---	Water	Uniform Surface temperature cooling. Temperature gradient around 13˚C using best configuration and variable flow rate.	---	Non-uniform flow rate distribution can increase the surface temperature uniformity.	Plots, Contours
Russell	Heat Pipe cooling	Experimental	CPV	Water	Uniform temperature	---	Uniform temperature across cells were achieved.	Patent
Akbarzadeh and Wadowski	Heat Pipe cooling	Experimental	CPV 20 X	---	46˚C temperature after cooling	Increase in output power by 94 %	Increase in power output. Drop in temperature from 84 ˚C to46˚C.	Numeric data
Anderson et al.	Heat Pipe cooling with fins	Numerical Experimental	CPV	---	40˚C temperature higher than ambient temperature. Temperature profile uniform.	---	Heat flux of 40 W/cm2 was dissipated. Temperature change of 40˚C with heat pipe.	Plots, Contours
Huang et al.	Hybrid structure heat pipe	Experimental	CPV	---	72 % reduction in thermal resistance	Increase in electrical efficiency by 3.1 %	Comparison between aluminum, copper and hybrid design HCPV system efficiency increase by 3.1 %	Plots

Researcher	Type of Cooling System	Nature of work	Type of PV system	Coolant Type	Cell Temperature Characteristics	PV Cell Electrical Parameters	Key Findings	General Outcome
Qifen et al.	Heat Pipe cooling with fins	Numerical	CPV	---	Temperature reduced to 32˚C. Maximum temperature non-uniformity across cell was 3˚C.	---	Comparison between fins and heat pipe Fins with heat pipe resulted in uniform cooling	Plots, Contours
Liu et al.	Immersion Cooling	Experimental	CPV	Dielectric Liquid	Cell temperature 30˚C. Uniform Temperature variation of 3˚C.	---	With heat transfer coefficient of 1000W/m2.K, 30˚C cell temperature achieved.	Plots
Zhu et al.	Immersion Cooling	Experimental	CPV 250 X	Dielectric Liquid	Temperature reduced to 45˚C. Maximum temperature non-uniformity across cell was about 5˚C.	VOC drops 0.3 % /˚C for immersed module Isc increased with light intensity	Conversion efficiency depends on temperature and velocity of medium , 6000 W/m2K of average heat transfer coefficient was achieved.	Plots, Contours
Han et al.	Immersion Cooling	Numerical	CPV	Dielectric Liquid	Solar cell temperature reduced to 29˚C using DI liquid Maximum temperature variation for Deionized water was 4˚C.	Output power increased	Comparison between four different liquids showed DI water under applied conditions performs best.	Plots, Contours
Xiang et al.	Immersion Cooling with fins	Numerical	CPV 250 X	Dielectric Liquid	For optimum design, maximum cell temperature was 40˚C. Temperature non-uniformity reduced from 15˚C to 10˚C.	---	Addition of fins reduced average cell temperature and non-uniformity.	Plots, Contours

Researcher	Type of Cooling System	Nature of work	Type of PV system	Coolant Type	Cell Temperature Characteristics	PV Cell Electrical Parameters	Key Findings	General Outcome
Sun et al.	Immersion Cooling	Experimental	CPV 9.1 X	Dielectric Liquid	Cell temperature controllable from 20˚C to 31˚C. Variation in temperature was less than 3˚C.	---	Cell temperature increased linearly with coolant for 0-35˚C. Uniform temperature distribution and Stable performance after 270 days of exposure.	Plots, Contours, Correlations
Abrahamyan et al.	Immersion Cooling	Experimental	CPV	Dielectric Liquid	---	Efficiency of cells increased by 40-60 %.	Increase in Isc, Voc and efficiency was observed.	Plots
Han et al.	Immersion Cooling	Experimental	CPV 10-30 X	Dielectric Liquid	Temperature controlled to 25˚C.	Increase in efficiency by 8.5 -15.2 %	At 10 X, 20X, and 30 X electrical performances of solar cell was improved by shallow liquid immersion.	Plots
Hetsroni et al.	Heat Sink	Experimental	---	Dielectric Liquid Two phase cooling	Temperature maintained in the range of 50-60 ˚C. Maximum surface temperature difference of 4-5˚C for dielectric and 20˚C for water.	---	Uniform temperature heat sink was achieved for electronic cooling.	Plots
Araki et al.	Heat Spreader	Experimental	CPV 500X	---	Temperature rise from ambient was less than 20˚C.	---	Only 2 % overall loss by temperature.	Plots

Researcher	Type of Cooling System	Nature of work	Type of PV system	Coolant Type	Cell Temperature Characteristics	PV Cell Electrical Parameters	Key Findings	General Outcome
Min et al.	Heat Sink	Experimental	CPV 400X	---	Average cell temperature of 37˚C measured. Almost uniform temperature profile.	---	Heat sink area directly proportional to concentration ratio for constant cell temperature. Large heat sink of 700 times the area of cell needed.	Plots
Huang et al.	Phase Change Material cooling	Analytical	Non-CPV	---	Temperature maintained in the range of 33-36.4˚C Uniform temperature distribution.	Improvement in electrical conversion efficiency	Addition of fins reduced average cell temperature and non-uniformity.	Plots, Contours
Hasan et al.	Phase Change Material cooling	Experimental	Non-CPV	---	18˚C temperature reduction on front surface.	---	Comparison between five different PCM. At most insolation levels, salt hydrate achieved maximum reduction in temperature.	Plots
Maiti et al.	Phase Change Material cooling	Experimental	Non-CPV	---	Panels temperature reduced by 20 % For outdoor condition,62 ˚C whereas 65˚C for indoor was achieved	Output power increased by 55 % in outdoor test	V-trough Paraffin melta-wax matrix resulted in increase in output power.	Plots
Huang et al.	Phase Change Material cooling	Experimental	Non-CPV	---	Temperature controlled to 28˚C. More than 30 °C temperature reduction.	---	Best temperature control and temperature uniformity achieved when spacing between matrix becomes less	Plots, Contours

Researcher	Type of Cooling System	Nature of work	Type of PV system	Coolant Type	Cell Temperature Characteristics	PV Cell Electrical Parameters	Key Findings	General Outcome
Xu et al.	Microchannels Heat Sink	Experimental	---	---	---	---	When compared with conventional microchannels. Increase in nusselt number by 26.4 % and decrease in pressure drop by 27 %.	Plots, Contours
Wang et al.	Microchannels Cooling	Experimental	---	Deionized water	Uniform temperature distribution.	---	Addition of transverse channels enhances cooling capability.	Plots, Contours
Wang et al.	Microchannels Cooling	Numerical	---	---	Maintained at working temperature of 80˚C.	---	Highest heat flux input was 75 % higher than conventional channels. Average heat transfer coefficient 3186.8 W/m2.K was found.	Plots, Contours
Ryu et al.	Microchannels Cooling	Numerical	---	Water	Temperature uniformity on the heated wall increased 10 times	---	Thermal resistance decreased by more than 50 %. Temperature uniformity on the heated wall increased 10 times.	Plots, Contours

Researcher	Type of Cooling System	Nature of work	Type of PV system	Coolant Type	Cell Temperature Characteristics	PV Cell Electrical Parameters	Key Findings	General Outcome
Royne and Christopher	Hydraulic Impingement Cooling	Analytical	CPV 200 X and 500X	Water	For 200 X, cell temperature decreased from 60 to 30˚C. For 500 X, cell temperature decreased from 110 to 40˚C.	Increase in power output	Increase in power output along with reduction in temperature. Average heat transfer coefficient of 10^5 was achieved.	Plots, Numeric data
Jeong et al.	Hydraulic Impingement Cooling	Experimental	Non-CPV	Water	Maintained at working temperature of 25˚C.	Conversion efficiency of 22 % using jets for cooling	Combined cooling and cleaning resulted in 19 % conversion efficiency.	Plots, Numeric data
Barrau et al.	Hybrid Microchannels-Impingement	Numerical	---	Water	Approximate uniform distribution with hybrid cooling.	---	Microchannel with jet impingement region enhances the temperature uniformity. Also temperature distribution can be varied depending upon cooling requirements.	Plots, Contours
Barrau et al.	Hybrid Microchannels-Impingement	Experimental	CPV 1905 X	---	-Temperature variation of 2.01˚C was obtained for micro-channel heat sink -For hybrid cooling standard deviation of 0.46˚C was obtained.	Net power was found to higher than conventional designs	-Thermal resistance of 10-5 m2.K/W was achieved -Uniform surface temperature distribution with LD3 design	Plots, Contours

2.4 LITERATURE ON JET IMPINGEMENT HEAT TRANSFER

This section contains a literature review of jet impingement and correlations for the heat transfer subjected to impingement cooling. Jet impingement cooling is one of the most promising cooling methods for high heat flux applications. Its main applications include gas turbine blades, food cooling, power electronics etc. Since it has been currently used as an effective technique to dissipate heat from densely packed electronics, it is a viable cooling method for PV panels. The main advantage lies in the fact that jet impingement is capable of extracting large amount of heat. Thermal resistance as low as 10^{-5} to 10^{-6} [80] can be obtained by the use of impinging liquid jet. This is due to existence of thin thermal boundary layer present at the stagnation zone under the impingement region however the heat transfer coefficient decreases radial outwards from the jet. The cooling of plates depends largely on the number of nozzles used. The main concern when design an impingement cooling device is to model the disturbance arising from the interaction of fountain of jet to another jet. It is in this regard fluid velocity, plate to diameter spacing, nozzle pitch, nozzle diameter, drainage flow and no of nozzles should be found such that an optimum solution is found.

Jets coming from nozzle can be characterized into flow configuration into axi-symmetric and planar jets. The word axi-symmetric implies to jets coming by circular profiles or holes, in contrasting to planar jets coming by slots. It has been established that arrays of axisymmetric jets produces higher total heat transfer per unit flow rate than

planar jets [96]. The term ‘submerged’ refers to jets issuing into a pool of the same fluid, while free-surface jets impinge into a less dense medium such as water into air.

Submerged liquid jets yield a higher overall heat transfer than free-surface liquid jets [83,97]. One of the most important parameters for jet flow behavior is the ratio of nozzle-to-plate spacing z, to nozzle diameter, d.

Relatively small ratios ($z/d < 6$, sometimes referred to as confined) should be considered because the heat transfer deteriorates significantly beyond this spacing. For arrays with multiple jets there’s an issue of cross flow because of which fountain and interaction of multiple jets takes place.

2.4.1 Flow Regions of Impinging Jets

Figure 2.32 shows the typical flow regimes of a single impinging jet. As the jet issues from the nozzle, the outer layer of the jet, called the mixing region, interacts with the surrounding liquid. The centre of the jet called as the potential core stays uninterrupted for a regime of approximately 3 - 8 nozzle diameters below the exit of jet

The correct measure of the potential core depends on the jet Reynolds number and nozzle configuration [97,98]. Interaction with the surrounding liquid causes the jet velocity to fall off proportionally with the vertical distance below the tip of the potential core. As the jet approaches the impingement plate, it is deflected and slowed down. The deflection region is found to extend 1.2 – 2 nozzle diameters from the impingement plate surface [99]. Due to jet deceleration and the resulting increase in pressure, hydrodynamic

and thermal boundary layers are formed in the impingement zone directly beneath the jet, which may only be a few micrometers thick [82]. The thin thermal boundary layer is what causes the high heat transfer capabilities of impinging jets. The region of flow parallel to the impingement surface is often referred to as the wall jet. In this region, the jet velocity rises rapidly to a maximum before it falls off radially away from the impingement zone. For some configurations, there is a transition from laminar to turbulent flow close to the stagnation point. The thermal and velocity boundary layers grow thicker with radial distance from the jet axis until they encompass the full thickness of the jet flow.

Figure 2.32 depicts the following regions with the nomenclature mentioned for single jet.

1: Potential Core;

2: Mixing Region;

3: Deflection Region;

4: Wall Jet;

5: Stagnation Point.

The nozzle diameter, orifice plate thickness and nozzle-to-plate distance are denoted by d, l, and z, respectively

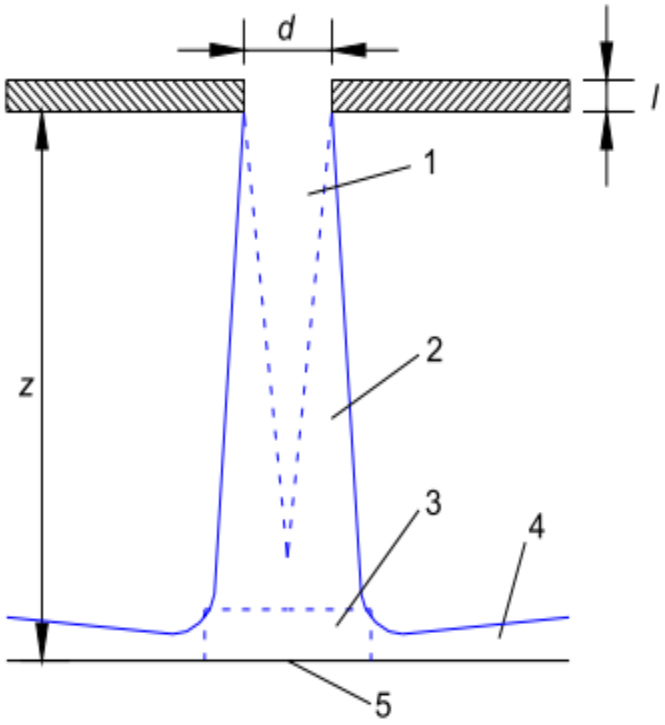

Figure. 2.32 Flow regions of an impinging jet adopted from Jambunathan et al [96]

2.4.2 Effect of Radial Boundaries and Nozzle-Plate Spacing on Heat Transfer

The local heat transfer under an impinging jet is strongly dependent on r/d, which is the ratio of radial distance away from the stag nation point to the nozzle diameter. Figure 2.33 shows the typical radial variation of Nusselt number under a single jet for nozzle-to-plate spacing to diameter ratios of $2 \leq z/d \leq 24$ [99]. The distributions for all spacing are characterized by high heat transfer close to the stag nation point (r/d = 0), followed by a rapid decrease in heat transfer in the wall jet region. For $z/d \leq 6$, the distributions tend to converge, apart from local variations which are explained below. This is because these

spacing are within the length of the potential core, where the jet velocity remains unchanged from the nozzle exit. The heat transfer remains relatively unchanged for spacing within the potential core, the overall magnitude increases slightly with z/d due to increased turbulence. For higher nozzle to plate spacings, the overall heat transfer is drastically reduced because of interaction with the surrounding liquid. For r/d > 7, the Nusselt number distributions for all z/d start to converge. This is because flow deflection and interaction with the surrounding liquid has completely reshaped the initial flow structure.

At low z/d, two peaks appear in the Nusselt number distribution. The inner peak at r/d ~0.5 occurs partly because of acceleration of the fluid out of the stagnation region, which decreases the thickness of the thermal boundary layer, and also because of the influence of shear layer generated turbulence. The inner secondary peak has been found to become less pronounced as the Reynolds number is decreased and the nozzle-to-plate distance is increased [100]. The outer peak at r/d ~ 2 is caused by the transition from laminar to turbulent flow. The location of this peak has been found to move away from the stagnation point as Re or z/d is increased. For z/d beyond the length of the potential core (z/d ~ 6), the maximum Nusselt number is found at the stagnation point and there are no secondary maximums.

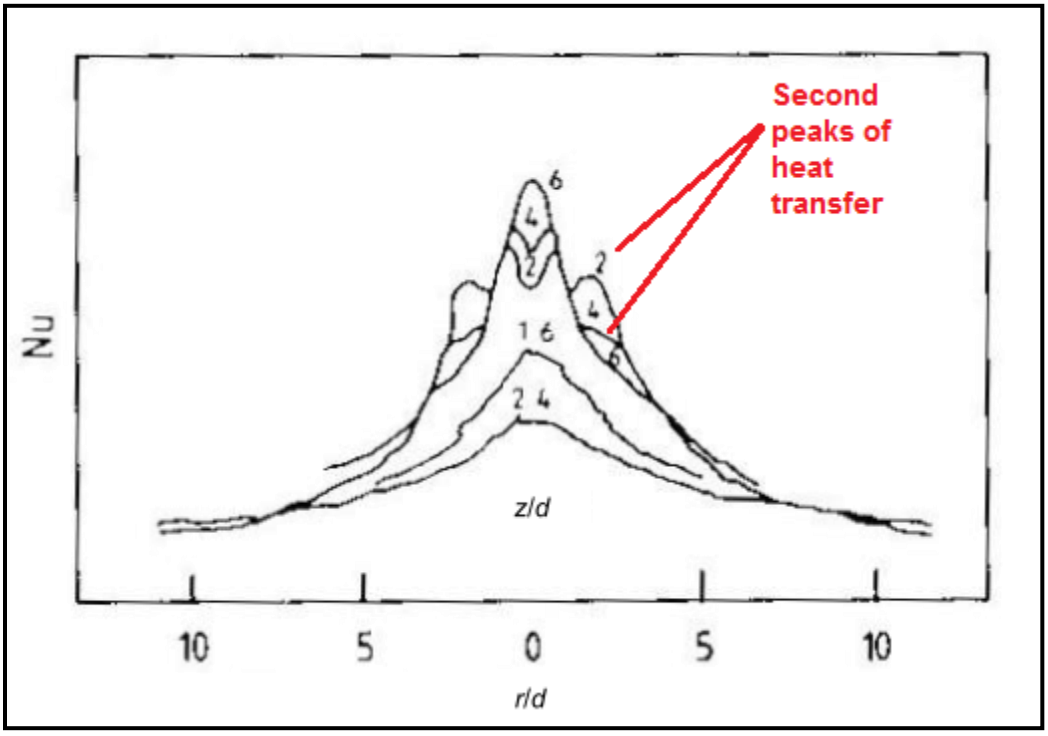

Figure 2.33 Radial variation of heat transfer and the effect of z/d adopted from [101]

The studies of Womac et al. [101] and Garimella and Rice [97] suggest that the optimal nozzle-to-plate spacing for single jets is found at z/d ~ 3-4.Womac et al. [101] studied nozzle-to-plate separations of $1 \leq z/d \leq 14.5$ for a variety of nozzle diameters and Reynolds numbers, and found that the average heat transfer coefficient was relatively insensitive to separation distance at low Reynolds numbers ($Re \leq 4000$). For higher Re, the average heat transfer remained undisturbed or increased slightly with increasing z/d for $1 \leq z/d \leq 4$ and dropped off as the separation distance was further increased. This was used to determine that the length of the potential core was approximately four nozzle diameters. Garimella and Rice [97] studied the local heat transfer under submerged jets

with square-edged orifices over a range of nozzle-to-plate spacings ($1 \leq z/d \leq 14$). The working fluid was FC-77 which is a dielectric liquid with Pr ~ 25. The stagnation point heat transfer coefficient was found to be almost constant up to z/d = 4, but to decrease from z/d = 5, which corresponded with the length of the potential core for this configuration. For z/d < 5, secondary peaks appeared at r/d ~ 2. The magnitudes of these peaks were found to increase with increasing Reynolds number. The local and average Nusselt number was highest for all nozzles at z/d ~ 3. The stagnation point heat transfer coefficient is generally highest at the very end of the potential core. This was shown by, among others, Webb and Ma [82] who found that the stagnation point heat transfer reached a maximum at z/d ~ 5. However, lower z/d tends to shift the Nusselt number peak outwards from the stagnation point, so that the region of high heat transfer occupies a relatively larger area. The highest average heat transfer is thus generally found slightly below the end of the potential core. It is therefore recommended to keep the target plate close to jet nozzle so that maximum heat transfer can take place.

2.4.3 Effect of Nozzle Shape

The heat transfer coefficient is highly sensitive to the level of turbulence in the flow, which in turn is determined by the nozzle configuration. Orifice nozzles have generally been found to introduce a higher level of turbulence and thereby a higher heat transfer coefficient than pipe-like nozzles [102]. Figure 2.34 shows an overview of commonly used orifice nozzle configurations.

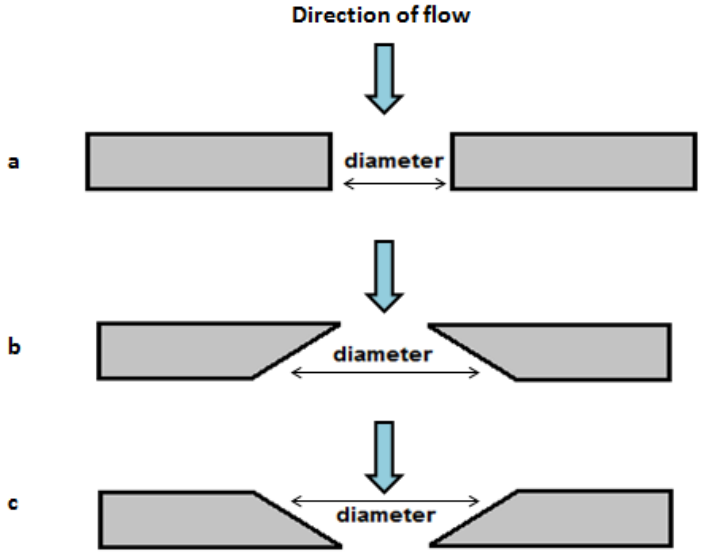

Figure 2.34 Representation of different nozzle configurations: a) square-edged, b) sharp-edged, c) Counter sunk nozzle.

The heat transfer characteristics of sharp, square and an intermediate case of nozzles were compared by Lee and Lee [103] for air jets for 5000 < Re < 30 000. The sharp-edged nozzle showed promising results based on its high heat transfer capabilities and turbulent behavior. It also shows a stronger Reynolds number dependence than the

straight and intermediate nozzles. The impact of nozzle pattern was shown to be higher at small z/d, which ranged from 2 to 10 in this study. This research was substantiated and affirmed by Garimella and Nenaydykh [99], and explained this behavior by the fact that contact with surrounding fluid from the jet exit reduces out differences in the actual flow configuration.

When designing an optimum jet impingement device, it is generally relevant to optimize the system for a given pump power instead of a given flow rate. The pump power is in direct relation to flow rate and pressure drop across the device. Most studies of the effect of nozzle configuration do not take the pressure drop into account, which make them incomplete as a tool for designers. Brignoni and Garimella [102] performed a comparative study between countersunk nozzles and square edged nozzles. Heat transfer and pressure drop characteristics of both configurations were investigated. They found that by countersinking the nozzle pressure drop is reduced significantly while there is only a small relative drop in heat transfer. It was shown that at an angle of 30˚ from normal axis results in highest pressure drop and performance whereas increasing the angle further increased the pressure drop as it resembled more like a sharp edged nozzle.

Lee et al. [104] stated that the diameter of nozzle had an affect on the heat transfer c efficient in the zone of impingement until r/d ~ 0.5. In this zone, the local heat transfer coefficient was shown to increase by approximately 10% from the smallest to the longest nozzle. Long pipe nozzles were used to ensure fully developed flow at the nozzle exit. The length of the potential core (in units of nozzle diameter) was shown to increase with

increasing nozzle diameter. This indicates that for the same z/d, large nozzles create a higher mean velocity. The turbulence level was also higher for the larger nozzles. The higher velocity and turbulence intensity would account for the increased heat transfer under the larger nozzles. Only large nozzles of d = 13.6 to 34.0 mm and Re = 23000 were used in this study. Garimella and Rice [97] also showed there is a relation between stagnation region Nusselt number and nozzle diameter.

2.4.4 Heat Transfer Correlations for Single Jet:

The field of impinging jets with its complex flow field structure and thermal characteristics makes its modeling difficult analytically. However based on experimental result and physics of the impinging jets, several average heat transfer correlations are available in literature. These semi empirical or empirical correlations are shown below in Eq 2.1. Generally the correlations for stagnation point nusselt number are in the form of:

$$Nu_0 = C.\mathrm{Re}^m.\mathrm{Pr}^n \tag{2.1}$$

The Reynolds number dependence, m, is normally determined experimentally and found to lie in the range $0.4 \leq m \leq 0.7$, and is strongly dependent upon nozzle configuration. Because most studies looks only at one liquid at one temperature, the Prandtl number dependence n is most commonly assumed. Most correlations use n ~ 0.4. Li and Garimella [105] performed a study using different Prandtl number liquids to obtain the Pr dependence as a part of the curve-fitting process.

The correlations for average Nusselt number under single jets are generally based on area averaged heat transfer coefficients over either round or square heated areas with the jet centered on the heater. Round heaters are characterized by their radius in units of r/d while square heaters have side lengths L_{heat}.

- **Martin's Correlation :**

For single nozzle system Martin [85] correlation is

$$F = 2 \cdot Re^{0.5} \cdot \left(1 + \left(\frac{Re^{0.55}}{200}\right)\right)^{0.5} \tag{2.2}$$

$$Nu\#_{avg,martin} = \left(\frac{\left(1 - 1.1 \cdot (d/r)\right)}{1 + 0.1 \cdot \left((z/d) - 6\right) \cdot (d/r)}\right) \cdot (d/r) \cdot F \cdot Pr^{0.42} \tag{2.3}$$

$$h_{avg,martin} = Nu\#_{avg,martin} \cdot k/d \tag{2.4}$$

The experimental limits for their work is from, Re=2000-400000, Z/d: 2-12, r/d:2.5-7.5.(z/d) opt=5.3 was found to be an optimum nozzle to plate spacing. The fluid used was air with various nozzle configurations which make it suitable for any nozzle type.

- **Tawfek's correlation** [98]**:**

He used tapered nozzle with air as fluid. The experimental limits for their work are from, Re=3400-41000, z/d: 6-58, r/d:2-30,d=3-7mm

$$Nu\#_{avg,tawfek} = 0.453 \cdot \left(Pr^{0.333}\right) \cdot \left(Re^{0.691}\right) \cdot \left(r/d\right)^{-0.38} \cdot \left(z/d\right)^{-0.22} \quad (2.5)$$

- **Li and Garimella correlation** [105]

They employed square edged nozzle for their setup and compared different fluid for the overall performance. The experimental limits for their work are from, Re=4000-23000, z/d: 1-5, l/d:0.25-12,d=1.59-25.2 mm, Pr=0.7-25.2, D_e= 11.28-22.56 mm.

$$Nu\#_{avg,li} = \left(1.179 \cdot \left(Pr^{0.441}\right) \cdot \left(Re^{0.504}\right) \cdot \left(l/d\right)^{-0.071} \cdot \left(D_e/d\right)^{-0.282} \cdot \left(A_r\right)\right) + \left(1.211 \cdot \left(Pr^{0.441}\right) \cdot \left(Re^{0.637}\right) \cdot \left(D_e/d\right)^{-1.062} \cdot \left(1-A_r\right)\right) \quad (2.6)$$

$$D_e = \left(4 \cdot A_n/\pi\right)^{0.5} \quad (2.7)$$

$$A_r = \left(1.9 \cdot d/D_e\right)^2 \quad (2.8)$$

- **Pressure drop correlation for nozzle:**

  Pressure drop across the jet nozzle can be calculated using the following formulation [106]

$$\Delta P = \left(\frac{8 \cdot \rho \cdot Q^2}{\left(3.142 \cdot N \cdot C_d \cdot d^2\right)^2}\right) \quad (2.9)$$

$$Re = \frac{4 \cdot Q}{\pi \cdot N \cdot d \cdot \nu} \quad (2.10)$$

where,

Q= flow rate

d = diameter of nozzle

r=equivalent radius of the cooled plate" “r/d from 2 to 30"

N = Number of nozzles

z/d=dimensionless nozzle to plate spacing

"z/d varies from 2 to 8,optimum 5.3 by martin [85]"

2.4.5 Heat Transfer Correlations for Multiple Jets

- **Martin** [85] **and Lindeman** [107] **Model for multiple jets:**

For multiple nozzles Martin model [85] is used;

$$f = \frac{3.142 \cdot d^2}{4 \cdot s^2} \tag{2.11}$$

$$G = 2 \cdot \sqrt{f} \cdot \frac{1 - 2.2 \cdot \sqrt{(f)}}{\left(1 + 0.2 \cdot \left((z/d) - 6\right) \cdot \sqrt{(f)}\right)} \tag{2.12}$$

$$K = \left(\left(1 + \left((z/d) \cdot \frac{\sqrt{f}}{0.6}\right)^{0.6}\right)\right)^{-0.05} \tag{2.13}$$

$$Nu\#_{avg,martin} = 0.5 \cdot K_{martin} \cdot G_{martin} \cdot Pr^{0.42} \cdot Re^{0.666} \tag{2.14}$$

The limits for using this correlation is from Re=2000-100000, z/d:2-12 and s/d:4.3-14. For optimum jet pitch (s/d), Lindeman [107] model is coupled with the model [85]

$$\left(s/d\right)_{uniform} = \frac{\frac{\sqrt{A_h}}{d}}{\sqrt{\left(N\right)}+1} \tag{2.15}$$

$$\left(s/d\right)_{optimum} = 1.617 \cdot \left(s/d\right)_{uniform} \cdot N^{-0.1026} \tag{2.16}$$

The schematic diagram shows the arrangement for different number of nozzles. Generally more number of nozzles results in higher average heat transfer coefficient as there is an increased number of stagnation regions but at the same time due to jet interference with neighboring jets becomes significant. Hence there needs to be trade off when selecting number of nozzles.

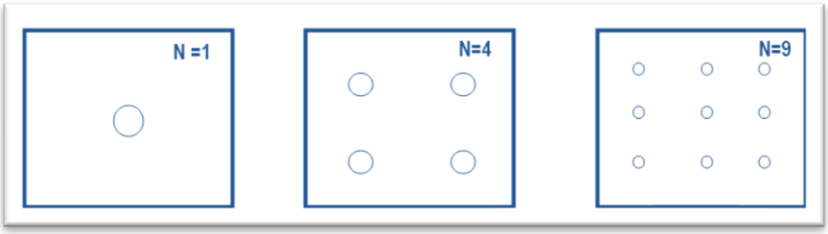

Figure 2.35 Single and multiple nozzle square arrangement

- **Huber and Viskanta** [86]**Correlation for multiple jets:**

$$Nu\#_{avg,viskanta} = 0.285 \cdot \left(Pr^{0.333}\right) \cdot \left(Re^{0.710}\right) \cdot \left(s/d\right)^{-0.725} \cdot \left(z/d\right)^{-0.123} \tag{2.17}$$

Experiments performed for: s/d 4-8, z/d 0.25-6, l/d 1.5, d =6.35 mm

- **Womac** [83] **Correlation for multiple jets:**

$$Nu\#_{avg,womac} = \left(0.509 \cdot \left(Re^{0.5}\right) \cdot \left(l_{heat} / d\right) \cdot \left(A_{r,w}\right)\right) + \left(0.363 \cdot \left(Re_{womac}{}^{0.8}\right) \cdot \left(l_{heat} / l_{womac}\right) \cdot \left(1 - A_{r,w}\right)\right) \quad (2.18)$$

$$l_{womac} = \frac{\left(0.5 \cdot \sqrt{2} \cdot s - 1.9 \cdot d\right) + \left(0.5 \cdot s - 1.9 \cdot d\right)}{2} \quad (2.19)$$

$$Re_{womac} = \frac{Q \cdot l_{womac} \cdot 4}{N \cdot 3.142 \cdot d^2 \cdot \nu} \quad (2.20)$$

$$A_{r,w} = \frac{N \cdot \pi \cdot \left(d\right)^2}{l_{heat}{}^2} \quad (2.21)$$

The experimental limits are: Re = 500-20000,s/d 5-10 , z/d 2-4, l/d 4.69-9.32, d =0.513-1.02 mm. Also If $A_{r,w}$ >1, it has to be set to 1.Where, l_{heat} = length of heated/cooled plate.

CHAPTER 3

PV PERFORMANCE MODELING

All the relevant models are reviewed from literature and a specific model incorporating optical, radiation, thermal, jet cooling and electrical model is developed for the present study. An analysis was carried out to find the optimum parameters suitable for the design of PV cooling systems. The details of the modeling for the four configurations are given in this section.

3.1 DESIGN FOR COOLING SYSTEMS

To design and analyze the performance of the PV systems with different cooling techniques we need to couple all the following sub-models. They are required to find out the I-V curve of any specified cell at any solar radiation, wind speed, solar panel temperature, and environmental conditions.

- Radiation and Optical Modeling
- Thermal Modeling
- Electrical Modeling
- Jet Cooling Modeling

For the investigation of PV panels subjected to uniform cooling, following configurations were compared with meteorological data of Dhahran.

- Configuration 1. PV panel without Cooling
- Configuration 2. PV panel with Rectangular Channel Heat Exchanger
- Configuration 3. PV panel with Converging Channel
- Configuration 4. PV panel with Jet Impingement Cooling

3.1.1 Design Methodology for PV Cooling System

The complete cooling model for PV string incorporates optical, radiation, thermal, electrical and cooling model for the overall performance analysis of the PV cooling system. Following models have been developed and coupled to obtain the performance curves of PV systems considered.

- Radiation Modeling for PV string
- Optical Modeling for PV string
- Thermal Modeling for Non-uniform Cooling
- Thermal Modeling for Uniform Cooling Converging Channel
- Thermal Modeling for Jet Impingement Cooling
- Development of Jet Cooling Model
- Electrical Modeling using seven parameters model

Jet impingement based on its heat extraction capability and retrofitting or application of it to any PV cell independently has been selected as the cooling mechanism for the investigation of uniform cooling of photovoltaic strings. This is because each cell will be exposed to jet separately to avoid the consequence of temperature non uniformity which arises from conventional cooling mechanisms. For the purpose of comparison non-uniformly cooled PV system with rectangular channel heat exchanger has been selected. Also converging channel based on CFD design has been developed to compare its performance with jet cooling and rectangular channel configuration. The general flow chart for modeling is shown in Fig 3.1.

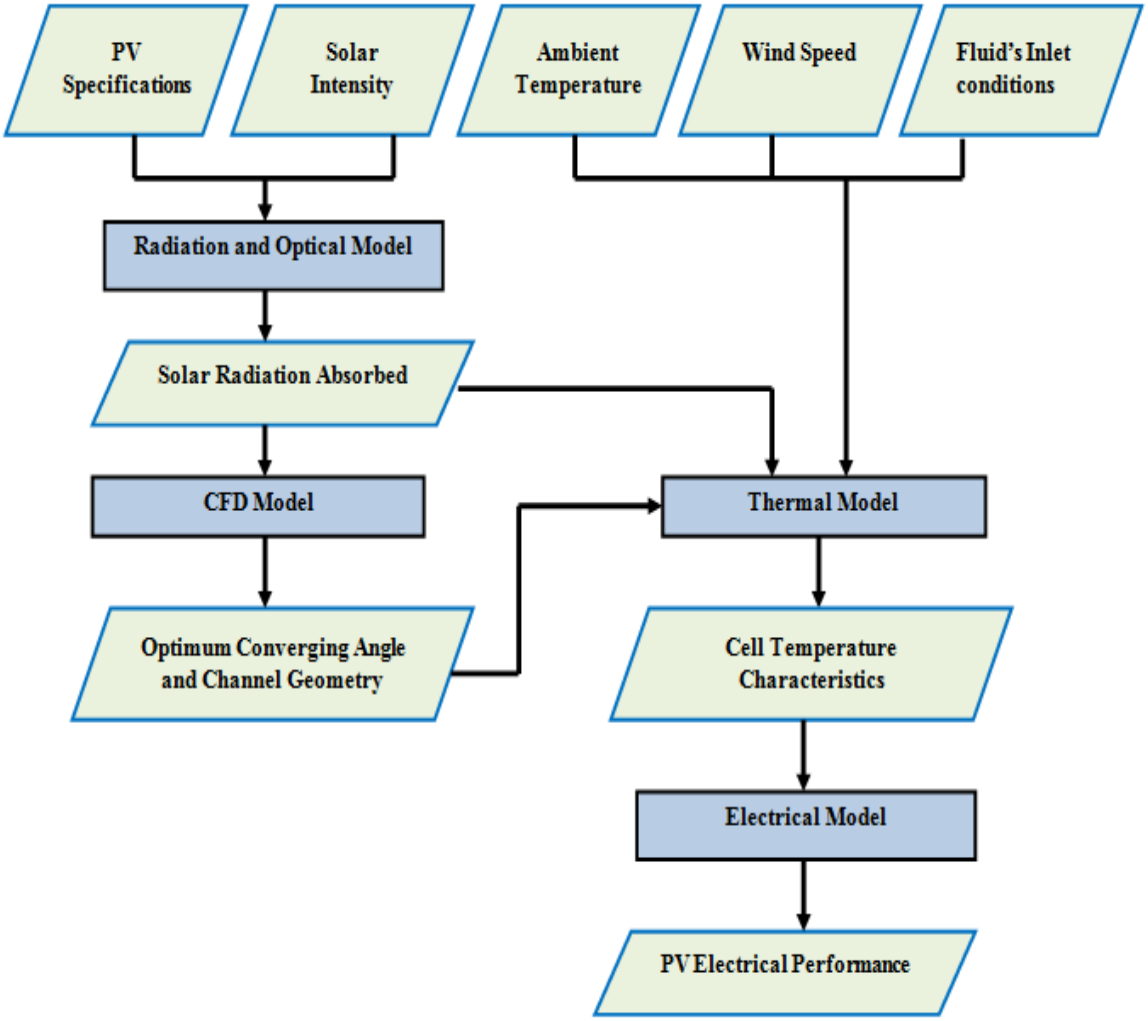

Figure 3.1 Schematic chart for performance evaluation of PV system

3.1.2 Design Schematics of Selected Configurations

Figure 3.2-3.5 shows the schematics of all the four cases to be investigated in this research for the study of uniform and non uniform cooling techniques.

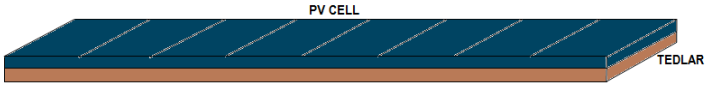

Figure 3.2 Case 1: PV panel without Cooling

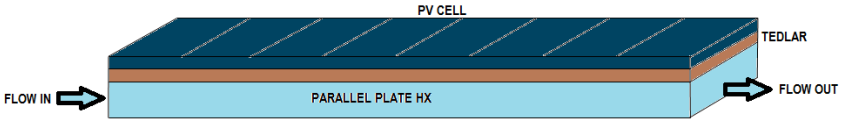

Figure 3.3 Case 2: PV panel with Rectangular Channel Heat Exchanger

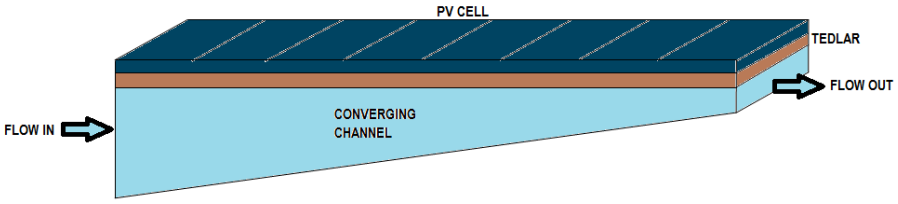

Figure 3.4 Case 3: PV panel with Converging Channel

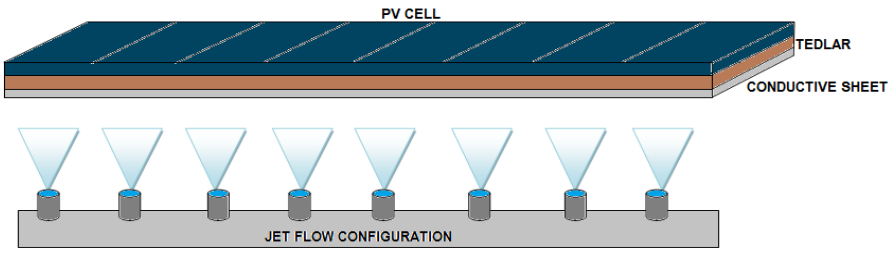

Figure 3.5 Case 4: PV panel with Jet Impingement Cooling

3.2 RADIATION AND OPTICAL MODELING

For precise prediction of the performance of the PV system, the most important input parameter is the absorbed solar radiation. There are several radiation models [108]–[111] available in literature to calculate solar radiation incident on the surface of the PV panels or modules .These radiation models are then coupled with optical model [112] to estimate the absorbed solar radiation. All the radiation models treat direct beam radiation in the similar manner and the only difference between them is the treatment for diffuse radiation. Figure 3.6 shows different components of diffuse radiation.

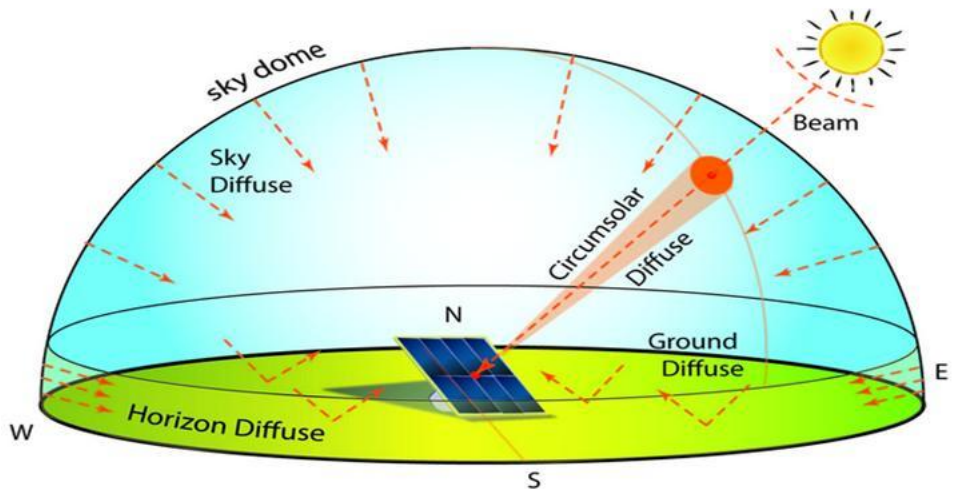

Figure 3.6 Diagram of the multiple components of the clear sky.

The basic model of radiation, the isotropic radiation model [108] considers only the isotropic part. All of these model differ in the way they treat diffuse radiation .The Hay & Davies formulation [111] considers isotropic and circumsolar. Also Perez formulation

[110] and the Hay Davies-Klutcher-Reindl formulation (HDKR) [109] considers the horizon brightening part of insolation.

In a comparative investigation, Mondol et al. [113] evaluated performance of different radiation models using an input of horizontal radiation. They reported that based on the analysis all of the four models showed accurate results for summer than winter. For the case of winter season, the isotropic sky model was reported to be the most correct.

Radiation model employed for analysis is the isotropic sky model which considers all three components of radiation for calculating the incident radiation on tilted plane whereas optical model is used for calculating the solar radiation absorbed in PV cell. The absorbed radiation calculated from radiation and optical model is then used in the electrical model and thermal model to calculate the electrical output and cell temperature.

Optical model for PV cell used is given by Duffie and Beckman [112].

$$\tau\alpha(\theta) = e^{-(KL/\cos\theta_r)}\left[1-\frac{1}{2}\left(\frac{\sin^2(\theta_r-\theta)}{\sin^2(\theta_r+\theta)}+\frac{\tan^2(\theta_r-\theta)}{\tan^2(\theta_r+\theta)}\right)\right] \tag{3.1}$$

$$K_{\tau\alpha}(\theta) = \frac{\tau\alpha(\theta)}{\tau\alpha(0)} \tag{3.2}$$

Absorbed radiation based on isotropic model used in this research is given by:

$$\frac{S_{PV}}{S_{ref}} = M\frac{G_b}{G_{ref}}R_{beam}K_{\tau\alpha,b} + M\frac{G_d}{G_{ref}}K_{\tau\alpha,d}\frac{1+\cos\beta}{2} + M\frac{G}{G_{ref}}\rho K_{\tau\alpha,g}\frac{1-\cos\beta}{2} \quad (3.3)$$

R_{beam} is the geometric factor and subscript ref denotes reference conditions.While determining the ($\boldsymbol{\tau\alpha}$)product, internal reflection losses are also incorporated which occur in the different layers of the solar cell.

Liu and Jordan [108] developed the radiation model of isotropic sky. This model is developed on an assumption that the entire sky dome is surround by diffused radiation which is isotropic. This model deals the beam, diffused and ground reflected radiation on an individual level and consider their effect separately. The model is given by Eq. (3.3). Now to estimate the amount of energy absorbed, we need to determine the contribution of diffuse, ground reflected and beam component in the total absorbed radiation.($\boldsymbol{\tau\alpha}$)is the product of transmittance absorbance product of solar cell which is calculated separately for beam, diffuse and ground reflected radiation

Hay & Davies model [111] is an enhanced form of isotropic model as there's an addition of circumsolar diffuse radiation to the basic model. In this formulation, the direction of beam radiation and circumsolar radiation is considered to be same. The formula is shown by Eq. (3.4).The factor A_i is the Anisotropy term and is represented by Eq. (3.5)

$$\frac{S_{PV}}{S_{ref}} = M\,\frac{G_b + A_i G_d}{G_{ref}} R_{beam} K_{\tau\alpha,b} + M\,\frac{(1-A_i)G_d}{G_{ref}} K_{\tau\alpha,d}\,\frac{1+\cos\beta}{2} + M\,\frac{G}{G_{ref}}\rho K_{\tau\alpha,g}\,\frac{1-\cos\beta}{2} \tag{3.4}$$

$$A_i = \frac{G_b}{G_o} \tag{3.5}$$

Reindl et al. [109] incorporated the horizon brightening diffuse radiation and improved Hays and Davies model. Hay-Davies-Reindl-Klutcher (*HDKR*) model is developed on assumption that the direction of isotropic diffuse is the same as horizon brightening component. The model is shown by Eq. (3.6)

$$\frac{S_{PV}}{S_{ref}} = M\,\frac{G_b + A_i G_d}{G_{ref}} R_{beam} K_{\tau\alpha,b} + M\,\frac{(1-A_i)G_d}{G_{ref}} K_{\tau\alpha,d}\left(\frac{1+\cos\beta}{2}\right)\left(1+ f\sin^3\left(\frac{\beta}{2}\right)\right) + M\,\frac{G}{G_{ref}}\rho K_{\tau\alpha,g}\left(\frac{1-\cos\beta}{2}\right) \tag{3.6}$$

$$f = \sqrt{\frac{G_b}{G}} \tag{3.7}$$

3.3 THERMAL MODEL

Thermal effects on the surface of the PV panel significantly affect its performance. The increment in cell temperature causes the module efficiency to decrease due to reduction in fill factor and open circuit voltage. Also if there is non-uniformity of heat transfer and temperature across the panel, PV cell also experiences loss in conversion efficiency because of the effect of current mismatch problem. Skoplaki et al [114] reviewed and discussed in their paper the dependence of operating temperature on electrical performance of PV systems. They reported a variety of correlations for the cell efficiency and the power output of the PV panels based on operating temperatures. The temperature distribution in PV panels depends on the PV cell material, PV cell type, the panel configuration, the existing ambient state and for the purpose cooling, the characteristics of the heat dissipation technique.

For PV panels operating in hot climate, the need for cooling system becomes larger. For the case of PV panel under extreme conditions, the problems with PV panel becomes two fold; first the drop in cell efficiency because of increasing temperature and secondly structural defects may occur due to long term thermal stresses.

For thermal modeling of PV panel with and without cooling, and to estimate the cell temperature a variety of approaches have been used in literature. Jones et al [115] worked on transient model based on analytical method for the determination of cell temperature. They focused their study on PV system without cooling. For the modeling uniform

temperature in the PV module was assumed. Moreover convection and radiation modes of heat transfer to the surroundings were used along with PV panel output energy as a load to the system.

For PV panel with cooling, Sarhaddi et al [116] proposed a detailed model based on energy balance approach. They improved the conventional PV cooling model by incorporating electrical circuit model instead of correlations for the calculation of cell temperature. Also they used detailed formulations for estimating the thermal resistances within the network and the system. Validation of their model was done to the air PV/T system fabricated by Joshi et al. [117]. They reported improved results with more agreement than the model formulated by Joshi et al for the experimental readings.

Thermal modeling for impingement cooling is developed using an energy balance approach [118] and by applying thermal resistances at the nodes of different layers of PV string and cooling setup. For the case of an uncooled PV panel, modeling is carried out using the thermal network diagram [118]. Thermal modeling for the converging channel cooled PV string has been implemented in CFD software by using the two dimensional geometry previously described in section 3.1. Thermal modeling is used for monitoring the effect of cell temperature and distribution on the overall performance of the PV system. Precise prediction for temperature for PV modeling becomes more important when exposed to the extreme ambient conditions like in the “Sun Belt” region. Temperature characteristics on the PV surface are affected by cooling technique, solar intensity, radiation absorbed, convection losses by wind, radiation losses, wind speed,

type of material and length of the layer of material. The absorbed radiation (S_{PV}) calculated along with cell parameters and PV site information is thus given as an input to the thermal model to calculate the cell temperature. Uniform temperature distribution is important for the efficient working for the PV cells. The PV cells usually work more efficiently under lower temperatures. And the temperature difference of the cells is another main effect on efficiency. When the PV cells work under different temperatures, the arrays with lower efficiency deteriorates the overall performance of the PV cells.

For the optimum converging channel heat exchanger configurations, temperature of the cell is calculated using CFD analysis. Temperature distribution is studied and compared with an experimental performance and average cell temperature is then provided to the electrical model for the overall electrical performance characteristics. The boundary conditions used for the thermal model for CFD are taken from the actual meteorological data for the days of June and December. Water is used as a cooling fluid in the channel. For uncooled PV panel, thermal model is developed using a thermal network approach by[11], [118]. Table 3.1 shows the properties of the material used in the modeling and simulation of cooled and uncooled system

Table 3.1Properties of materials used for PV string in thermal analysis

PV System Layer	Material	Conductivity (W/mK)	Specific Heat (J/kgK)	Density (kg/m^3)
Solar Cell	Silicon	148	677	2330
Enscapsulent	Ethyl Vinyl Acetate	0.311	2090	950
Back sheet	Tedlar	0.033	1250	1200
Heat Exchanger	Aluminum	270	903	2702

In order to compare performance of the four mentioned configurations and to obtain the cell temperature, four different models are necessary pertinent to the cooling mechanism selected. These four different thermal models are discussed for the design of cooling system are mentioned and discussed below.

3.3.1 Thermal Model for PV Panel Without Cooling

Thermal model for PV panel without cooling is developed using the thermal network diagram [118]. By applying energy balance approach on the PV system and solving equation at the nodes, temperature characteristics of PV string was obtained. Figure 3.7 shows the cross sectional schematic of an uncooled PV string.

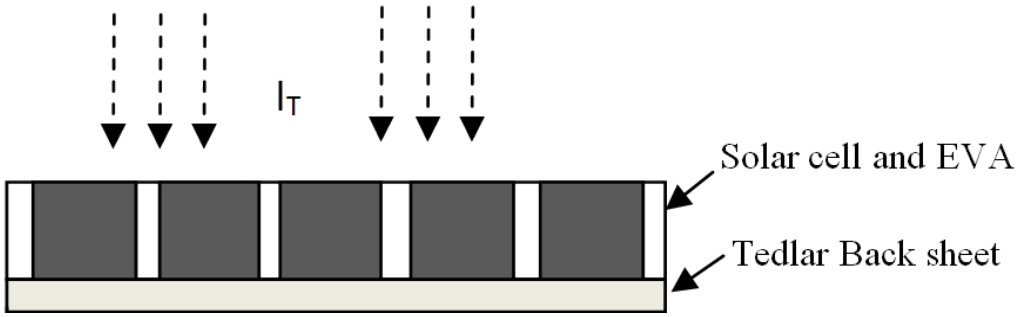

Figure 3.7 Cross sectional view of an uncooled PV string

Figure 3.8 shows the thermal network diagram of an uncooled PV string comprising on the layers of solar cell and encapsulent material (EVA) and tedlar back sheet.

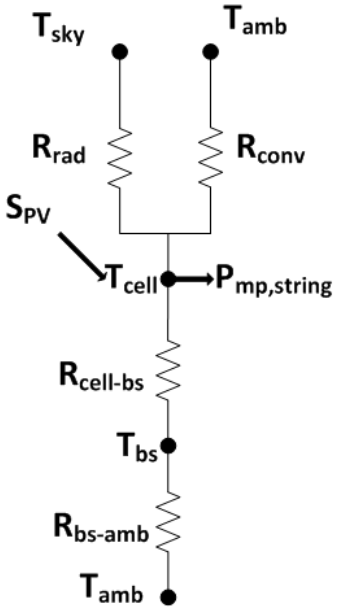

Figure 3.8 Thermal resistance network diagram for an uncooled PV string

By energy balance approach on the layers shown in Fig 3.8 of PV system and analyzing thermal network, following equations are simultaneously solved to obtain the temperature characteristics of PV string.

For the thermal modeling of uncooled PV, Engineering Equation Solver (EES) software has been used and following equations have been solved.

$$q_{loss} = S_{PV} - P_{mp} \tag{3.8}$$

$$q_{loss} = q_{bottom} + q_{top} \tag{3.9}$$

where q_{loss} is the total heat loss, S_{PV} is the absorbed energy by PV and P_{mp} shows the power extracted at maximum power point

$$q_{top} = \frac{T_{cell} - T_{amb}}{R_{top}} \tag{3.10}$$

Where q_{top} is the total heat loss from top of the cell to ambient, T_{cell} is the cell temperature and T_{amb} is the ambient temperature, R_{top} is the total top thermal resistance consisting of convection and radiation losses. It should be noted that R= k/W (thermal resistance per watt)

$$q_{bottom} = \frac{T_{cell} - T_{amb}}{R_{bottom}} \tag{3.11}$$

$$R_{bottom} = R_{bs} + R_{cell} \tag{3.12}$$

Where q_{bottom} is the total heat loss from top of the cell to ambient from bottom side, T_{cell} is the cell temperature and T_{amb} is the ambient temperature, R_{bottom} is the total bottom thermal resistance consisting of individual resistance from back sheet (tedlar) and solar cell.

3.3.2 Thermal Model for PV Panel with Rectangular Channel Heat Exchanger

Thermal model for PV panel with conventional heat exchanger cooling is adopted from Sarhaddi et al [116] by changing the thermopyhysical properties of water coolant used. Energy balance approach was used for PV/T system as described in section 3.3.1 with an additional resistance of heat exchanger fluid and expressions for cell temperature, back sheet temperature and mean fluid temperature was obtained as shown in Eqn (3.13)-(3.16).

$$T_{cell} = \frac{(\tau\alpha)_{eff} G + U_t T_{amb} + U_T T_{bs}}{U_t + U_T} \tag{3.13}$$

$$T_{bs} = \frac{h_{p1}(\tau\alpha)_{eff} G + U_{tT} T_{amb} + h_f \bar{T}_f}{U_{tT} + h_f} \tag{3.14}$$

$$\begin{aligned} \bar{T}_f = {} & \left[T_{amb} + \frac{h_{p1} h_{p2} (\tau\alpha)_{eff} G}{U_L} \right] \left[1 - \left(\exp\left(\frac{-WU_L L}{\dot{m} C_p} \right) \right) \Big/ \left(\frac{WU_L L}{\dot{m} C_p} \right) \right] \\ & + T_{f,in} \left(1 - \left(\exp\left(\frac{-WU_L L}{\dot{m} C_p} \right) \right) \Big/ \left(\frac{WU_L L}{\dot{m} C_p} \right) \right) \end{aligned} \tag{3.15}$$

$$\bar{T}_f = \left[T_{amb} + \frac{h_{p1} h_{p2} (\tau\alpha)_{eff} G}{U_L} \right] \left[1 - \left(\exp\left(\frac{-WU_L L}{\dot{m} C_p} \right) \right) \Big/ \left(\frac{WU_L L}{\dot{m} C_p} \right) \right] \quad (3.16)$$
$$+ T_{f,in} \left(1 - \left(\exp\left(\frac{-WU_L L}{\dot{m} C_p} \right) \right) \Big/ \left(\frac{WU_L L}{\dot{m} C_p} \right) \right)$$

3.3.3 Thermal Model for PV Panel with Converging Channel Heat Exchanger

Thermal model for PV panel with converging channel heat exchanger has been developed using Computational Fluid Dynamics (CFD) tool FLUENT. The main advantage of using FLUENT in this analysis lies in the fact that simulations can yield in the optimum geometry and heat transfer calculations for the converging channel heat exchanger to provide uniform profile of temperature across the surface of the PV panel.

CFD modeling has been carried out to fulfill two purposes. Firstly, the optimum geometrical parameter at which there is uniform distribution of temperature on the PV surface is found. Secondly, thermal modeling on the final geometry is carried out using this numerical technique and applying the data for the month of June and December. CFD numerical simulation has been proved to be effective and promising in predicting fluid characteristics in heat exchanger. In this work, the numerical simulations are performed with the commercial CFD software – FLUENT primarily to obtain the temperature profiles for different boundary conditions. The main advantage of using CFD in this analysis lies in the fact that simulations can yield optimum geometry and heat transfer calculations for the converging channel heat exchanger by providing uniform profile of temperature across the surface of the PV panel.

3.3.3.1 Physical Problem and Governing Equations

A laminar flow of cooling water flowing inside converging channel heat exchanger placed at the bottom of PV string has been considered in this analysis. The converging angle (Ø) is varied from 0˚-10˚ to observe the behavior of temperature characteristics on the surface of PV panel. The top surface of the PV string, modeled as silicon, is exposed to real time ambient data of solar intensity, wind speed and ambient temperature. A schematic diagram for the converging channel heat exchanger is shown in Fig. 3.9. A 2D geometry of converging channel and PV cell is created for the modeling.

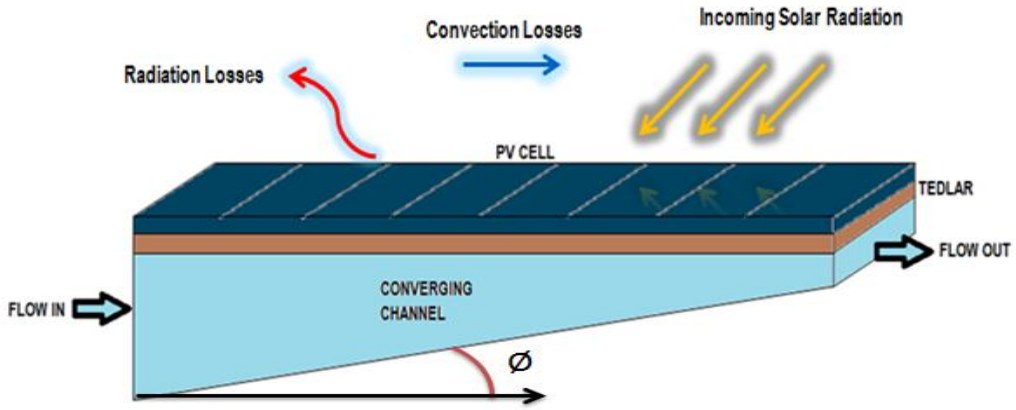

Figure 3.9 Schematic of converging channel heat exchanger with heat transfer modes.

PV cell and tedlar are modeled as solid domain whereas the interior of heat exchanger is modeled as fluid domain with water. For the present study, heat transfer is conjugated conduction and convection in the whole geometry. Flow is considered to be incompressible, steady and laminar in the converging channel heat exchanger. Based on the above mentioned assumptions, the Navier-Stokes equations are reduced as following:

Continuity equation:

$$\nabla(\rho\vec{V}) = 0 \tag{3.17}$$

where ρ is the density of the fluid; $\vec{V}$ is the velocity vector.

Momentum equation:

$$\vec{V}.\nabla(\rho\vec{V}) = -\nabla\vec{P} + .\nabla(\mu\nabla V) \tag{3.18}$$

where P is the pressure; μ is the viscosity of the fluid.

Energy equations:

$$\vec{V}.\nabla(\rho C_p T_f) = \nabla(K_f T_f) + .\nabla(\mu\nabla V) \text{ (in liquid)} \tag{3.19}$$

$$K_w\nabla^2(T_w) = 0 \text{ (in solid)} \tag{3.20}$$

where C_p is the thermal capacity; K_f and K_w are thermal conductivity of fluid and solid respectively; T_f and T_w are the temperature of the fluid and solid wall respectively.

Structured mesh system was used for all the geometries. The grid was made such that the fine mesh was employed near the wall for boundary layer region. Mesh dependency test was carried out to optimize the computational cost and accuracy. It was found that using approximately 10000 elements of cells yielded in precise results when compared with finer mesh. Figure 3.10 shows the results from mesh dependency test.

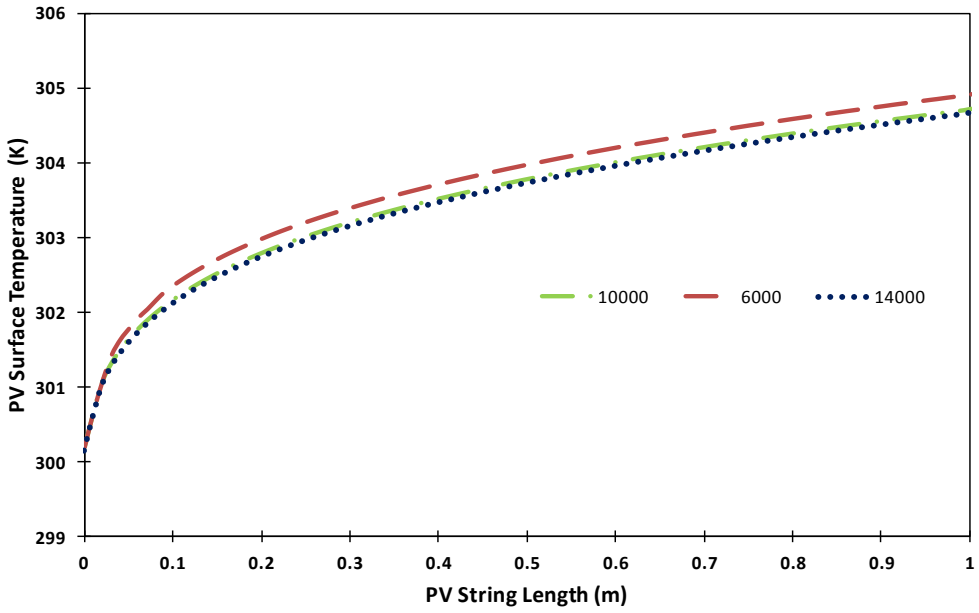

Figure 3.10 Mesh dependency test with 6000, 10000, 14000 cells

3.3.3.2 Boundary Conditions and Numerical Procedure

Table 3.2 shows the seven different configurations and associated boundary conditions used for the analysis of converging angle and its effect on thermal performance. These geometric parameters were used in the simulation and the models were developed using Gambit software. It should be noted that the outlet of the heat exchanger was fixed for all the converging angles and the inlet dimensions were varied. Water is used as a heat transfer fluid.

Table 3.2 Different configurations and associated boundary conditions

S #	Converging Angle (Ø)	Inlet Height (mm)
1	0	20.0
2	1	37.4
3	2	54.9
4	3	72.4
5	4	89.9
6	5	107.5
7	10	196.3

For all the cases, flow rate is kept constant as shown in table 3.2. The inlet condition is set as velocity inlet with temperature of the water at 27˚C. The temperature at the inlet was same for all the cases. Constant velocity is applied to the fluid at the inlet and the direction of the velocity is normal to boundary. The typical ambient conditions for the site location were taken as 37˚C ambient temperature with incident radiation of 2.2 MJ/m^2. The outlet boundary condition is pressure outlet with a gauge pressure of zero. Water is used as coolant whose properties are dependent of the temperature. Flow is single-phase and laminar in the channels. No-slip boundary condition exists at inner walls of the heat exchanger. The top surface is supplied with heat generation source and is assumed to be open to losses.

For the thermal model of converging channel, the incoming solar radiation is calculated using optical and radiation model shown in section 3.1, and then it is applied as an input with a source term addition in the energy equation in FLUENT. This internal heat generation, left after the absorbed energy and losses, is calculated using Eq. 3.21 as

described in [119] where η_{mp} is the conversion factor of the string, A_{string} is the pv string area and the V_{pv} is the volume of the PV cells in the string.

$$q = \frac{(1-\eta_{mp}) \text{ x } S_{PV} \text{ x } A_c}{V_{pvcell}} \tag{3.21}$$

For the case of heat losses convection and radiation boundary conditions were applied for the top surface of PV string. Wind heat transfer correlation is given as input for radiation boundary condition whereas ambient temperature is given for surrounding. Wind heat transfer is calculated using Eq. 3.22 [120]

$$h_w = 5.7 + 3.8V_w \tag{3.22}$$

The Semi-Implicit Method for Pressure Linked Equations (SIMPLE) scheme is used for the computation of pressure-velocity coupling. The second order-upwind scheme is used for the momentum and energy conservation equations. The pressure conservation equation is calculated under standard scheme. For the under-relaxation factors, default values are used. The absolute convergence criterion is 10^{-6} for continuity and momentum equations, and 10^{-9} for energy equation.

3.3.4 Thermal Model for PV Panel with Jet Impingement Cooling

Thermal model for PV panel with jet cooling is developed to assess the effect of temperature on the panel using average heat transfer correlations under single and

multiple jets. In addition, design optimization of the jet parameters is outlined based on the pumping power.

Thermal model for PV panel with impingement cooling is developed using energy balance approach as described in [106].For thermal modeling of jet impingement, energy balance approach on the different components of the PV system (glass cover, cell, back sheet and aluminum substrate for jet cooling) has been applied.

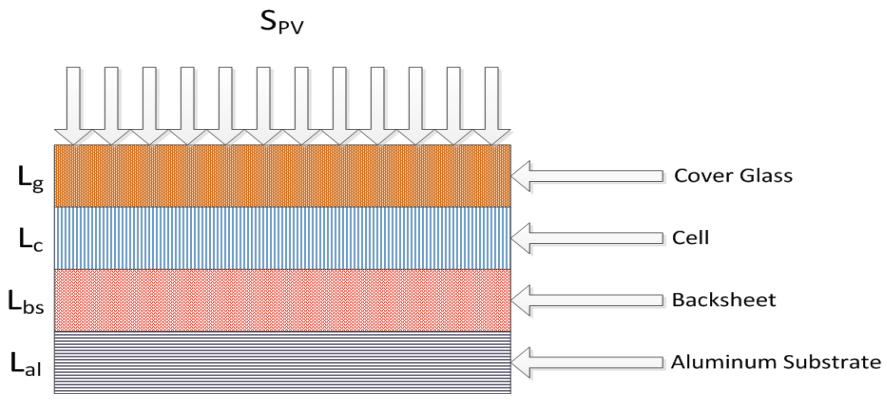

Figure 3.11 Schematic of PV Cell with layers and respective thickness

Where,

L_c = length of silicon solar cell

L_g = length of glass

L_{bs}= length of tedlar back sheet

L_{al}= length of aluminum substrate for jet impingement

S_{PV} = Absorbed radiation by PV

The cell temperature is estimated by calculating resistances of the thermal network as shown in Fig 3.12. By using the energy balance method, various resistances are calculated by the mode of heat transfer between the nodes and the resulted equations are simultaneously solved.

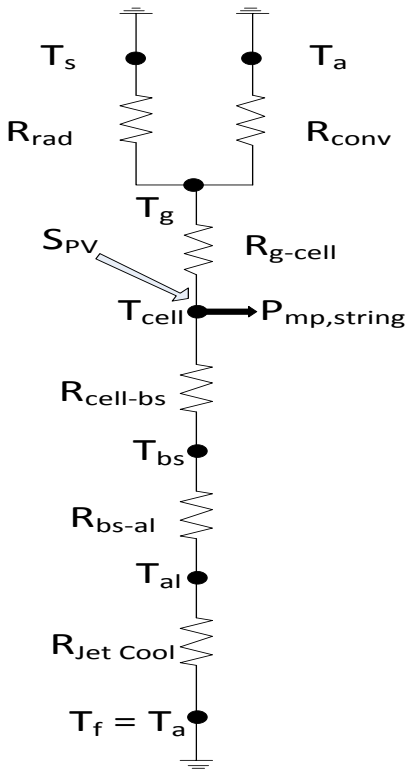

Figure 3.12 Network diagram of PV Cell with layers and respective thermal resistances

To make the system mathematically solvable, following assumptions are used:

- The thermal model developed is based on 1-D analysis.
- System is in quasi steady state.
- The working fluid is water.
- Thermopyhysical properties used are independent of temperature.
- There is no dust and dirt effect on the collector.
- Thermal contact resistances are neglected.
- Temperature variation along the thickness is negligible for each layer.
- Pumping Power is based on pressure drop in the orifice of nozzle.
- For single and multiple nozzles uniform flow of water is assumed at each nozzle inlet.

Based on above assumptions and energy balance approach, a thermal model is developed to predict the heating and electrical characteristics of the PV panel.

Absorbed radiation estimated is employed to evaluate the thermal model for the temperature distribution within the layers of the impingement cooled PV system. For jet cooling system, optimization has been carried out on the basis of pumping power so that the optimum parameters could be used for PV panel modeling.

Energy balance equations for the case of jet impingement PV system are written as follows:

$$q_{loss} = S_{PV} - P_{mp} \tag{3.22}$$

$$q_{loss} = q_{bottom} + q_{top} \tag{3.23}$$

$$q_{top} = \frac{T_{cell} - T_{amb}}{R_{top}} \tag{3.24}$$

$$q_{bottom} = \frac{T_{cell} - T_{amb}}{R_{bottom}} \tag{3.25}$$

$$R_{bottom} = R_{jet} + R_{bs} + R_{cell} \tag{3.26}$$

$$q_{bottom,1} = \frac{T_{cell} - T_{bs}}{R_{cell-bs}} \tag{3.27}$$

$$q_{bottom,2} = \frac{T_{bs} - T_{al}}{R_{bs-al}} \tag{3.28}$$

$$q_{bottom,3} = \frac{T_{al} - T_{a}}{R_{JetCool}} \tag{3.29}$$

$$q_{bottom} = q_{bottom,1} = q_{bottom,2} = q_{bottom,3} \tag{3.30}$$

$$q_{top} = \frac{T_{cell} - T_{g}}{R_{cell-g}} = q_{rad} + q_{conv} \tag{3.31}$$

$$q_{top} = \varepsilon\sigma A_{rad}(T_g^{\,4} - T_s^{\,4}) + h_{conv}A_{conv}(T_g - T_{amb}) \tag{3.32}$$

$$R_{conv} = \frac{1}{h_{conv}A_{conv}} \tag{3.33}$$

$$\frac{(T_g - T_a)}{R_{rad}} = \varepsilon\sigma A_r (T_g{}^4 - T_s{}^4) \tag{3.34}$$

$$\frac{1}{\mathrm{R}_{eq'}} = \frac{1}{R_{rad}} + \frac{1}{R_{conv}} \tag{3.35}$$

$$R_t = R_{g-cell} + \mathrm{R}_{eq'} \tag{3.36}$$

$$\frac{1}{\mathrm{R}_{tot}} = \frac{1}{R_t} + \frac{1}{R_b} \tag{3.37}$$

$$U_L = \frac{1}{R_{tot}} \tag{3.38}$$

Wind heat transfer correlation is given as input for radiation boundary condition whereas ambient temperature is given for surrounding. Wind heat transfer is calculated using Eq. 7 [120]

$$h_w = 5.7 + 3.8V_w \tag{3.39}$$

When designing a jet impingement device, it is not only the flow rate which is important, but also the pressure drop through the device. The preferred cooling system will in many cases be the one that delivers the highest rate of cooling at a given pumping power. The total pumping power is proportional to the product of flow rate and pressure drop.

The only pressure drop considered in this study is the pressure drop across nozzle based on the order of magnitude analysis. It should be noted that the pressure drop in the main jet header although significant is not taken into consideration as the main concern of

this study is the effect of jet nozzle on pv string and its heat transfer performance along with temperature effects.

Pressure drop across jet nozzles can be found using relation [106] and then calculating net power developed by the system utilizing pump power.

$$\Delta P = \frac{8 \cdot \rho \cdot Q^2}{\left(\pi \cdot C_d \cdot d^2\right)^2} \tag{3.40}$$

$$P_{pump} = \Delta P \cdot Q \tag{3.41}$$

$$P_{mp} = I_{mp} \cdot V_{mp} \tag{3.42}$$

$$P_{net} = P_{mp} - P_{pump} \tag{3.43}$$

The other pressure drops occurring the jet impingement system are at least two orders of magnitude small then the pressure drop at the orifice, hence they can neglected. These relatively small pressure drops could arise from the jet system. It may include contraction and expansion losses from the supply and inlet pipe. Also deflection losses at impingement plate may contribute.. It is also assumed that all of the kinetic energy in the jet is dissipated and lost by frictional effects after the jet hits the wall and mixes, so that the pressure after the nozzle does not increase back to the original free stream value.

3.4 ELECTRICAL MODEL

The main objective in modeling the PV device is that the model should be able to regenerate the output characteristics of the PV panel at different ambient condition with high precision. For this study electrical circuit modeling has been selected for the estimation of output parameters like power, current and voltage. The simple diode model of PV consists of five parameters. The electrical model used in this analysis is a seven parameter PV equivalent model presented by Siddiqui et al [121] .This model gives highly accurate and precise result while using data from the module sheet provide by the manufacturer. Siddiqui et al [121] performed the sensitivity analysis on these five parameters by varying the input conditions. The equivalent circuit, shown in Fig. 3.13, comprises of a light dependent current source, a p-n junction diode and two resistances. It should be noted that the equivalent circuit of Fig. 3.13 is based on the physics of crystalline silicon cell. Based on the sensitivity analysis; two translating equations were developed for ideality factor and short circuit current. In the thermal analysis the presence of electrical efficiency makes the thermal analysis dependent on electrical model.

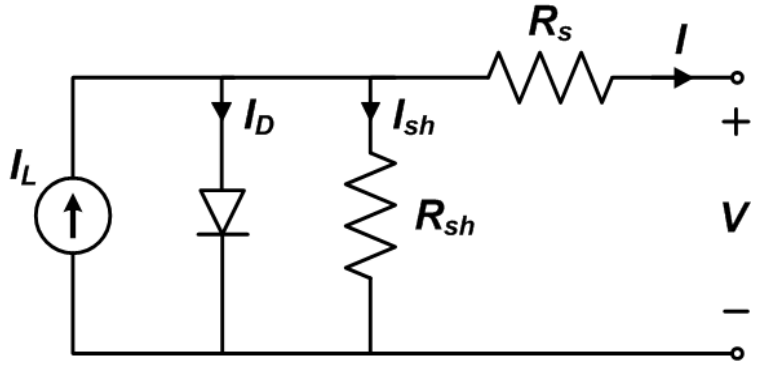

Figure 3.13 Equivalent Circuit model of PV showing basic parameters

The estimation of the model parameters for the single diode model equivalent model of PV systems requires complex techniques because of the extremely nonlinear character of the current voltage relationship.

The estimation of the model parameters for the single diode model equivalent model of PV systems requires complex techniques because of the extremely nonlinear character of the current voltage relationship. The seven parameters model is solved using optimization techniques based on the minimization of errors at high temperature and low intensity module data points. The basic five parameters shown in Fig. 3.13 that governs the IV characteristics of the PV panel are light current "I_L", reverse saturation diode current "I_o", ideality factor "*a"*, series resistance "R_s" and shunt resistance "R_{sh}".

$$I = I_L - I_o \cdot \left(exp\left(\frac{V + I \cdot R_s}{a} \right) - 1 \right) - \frac{V + I \cdot R_s}{R_{sh}} \tag{3.44}$$

where I and V are current and voltage at given load.

The two new introduced variables in seven parameters model are modified translating parameters "m"&"n" to convert reference conditions to operating conditions as shown by Eqs. 3.50 and 3.51.

The following conditions are used to estimate the five reference parameters:

At short circuit	$[dI/dV]_{sc}=-1/R_{sh,ref}$
At open circuit voltage	$V=V_{oc,ref}$, $I=0$
At short circuit current	$V=0, I=I_{sc,ref}$,
At the maximum power point	$V=V_{mp,ref}$, $I=I_{mp,ref}$
At the maximum power point	$[dI/dV]_{mp}=0$

Using the above conditions into the Eq. (3.46) the following equations are obtained:

$$I_{sc,ref} = I_{L,ref} - I_{o,ref}\left[exp\left(\frac{V_{oc,ref}}{a_{ref}} - 1\right)\right] - \frac{I_{sc,ref}R_{s,ref}}{R_{sh,ref}} \tag{3.46}$$

$$I_{L,ref} = I_{o,ref}\left[exp\left(\frac{V_{oc,ref}}{a_{ref}} - 1\right)\right] + V_{oc,ref} \,/\, R_{sh,ref} \tag{3.47}$$

$$I_{mp} = I_L - I_0\left[exp\left(\frac{V_{mp} + I_{mp}R_s}{a}\right) - 1\right] - \left[\frac{V_{mp} + I_{mp}R_s}{R_{sh}}\right] \tag{3.48}$$

$$\frac{I_{mp}}{V_{mp}} = \frac{\frac{I_0}{a}\left[exp\left(\frac{V_{mp}+I_{mp}R_s}{a}\right)\right]+\frac{1}{R_{sh}}}{1+I_0\frac{R_s}{a}\left[exp\left(\frac{V_{mp}+I_{mp}R_s}{a}\right)\right]+\frac{R_s}{R_{sh}}} \tag{3.49}$$

Where V_{mp} ,I_{mp},V_{oc},I_{sc} are maximum power point voltage, maximum power point current, open circuit voltage, and short circuit current, respectively

After obtaining five parameters, remaining two variables are found using:

$$a = a_{ref}\cdot\left(T_{cell}/T_{ref}\right)^n \tag{3.50}$$

$$I_L = \left(S_{PV}/S_{ref}\right)^m\cdot\left(I_{L,ref}+\mu_{isc}\cdot\left(T_{cell}-T_{ref}\right)\right) \tag{3.51}$$

$$error = \sqrt{\left(P_m-P_e\right)^2}\Big|_{Low\,Irradiance} + \sqrt{\left(P_m-P_e\right)^2}\Big|_{High\,Temeperature} \tag{3.52}$$

The objective function shown with Eq. 3.52 is used for error minimization and was calculated using power at low irradiance and high temperature using MATLAB software. In this present study EES is used to evaluate these five parameters at reference conditions $T_{cell,ref}$ = 25^{o}C, I_{ref} = 1000 W/m^2.

The five basic unknown parameters are found using EES version 9.4 by applying the conditions described in [112]. The other two variables are solved using optimization technique in MATLAB R2013a edition. The I_{mp} ,V_{mp}, P_{mp} and electrical efficiency can be obtained at any operating conditions.

$$P_{mp} = I_{mp} V_{mp} \tag{3.53}$$

$$\eta_{mp} = \frac{P_{mp}}{A_c \cdot I_T} \tag{3.54}$$

Where A_c is the area of the PV string and I_T is the amount of incident radiation on the PV string.

3.5 JET IMPINGEMENT COOLING MODEL

The aim of jet modeling is to find the optimum jet parameters to ensure low temperature of solar cell with the requirement of low pumping power. This will result in the maximum possible net power output by the jet cooled PV panels.

The correlations for average Nusselt number under single jets are generally based on area averaged heat transfer coefficients over either round or square heated areas with the jet centered on the heater. Round heaters are characterized by their radius in units of r/d while square heaters have side lengths L_{heat}.

The main parameters governing in the jet impingement cooling are shown in the Figure 3.14 for single and multiple jets.

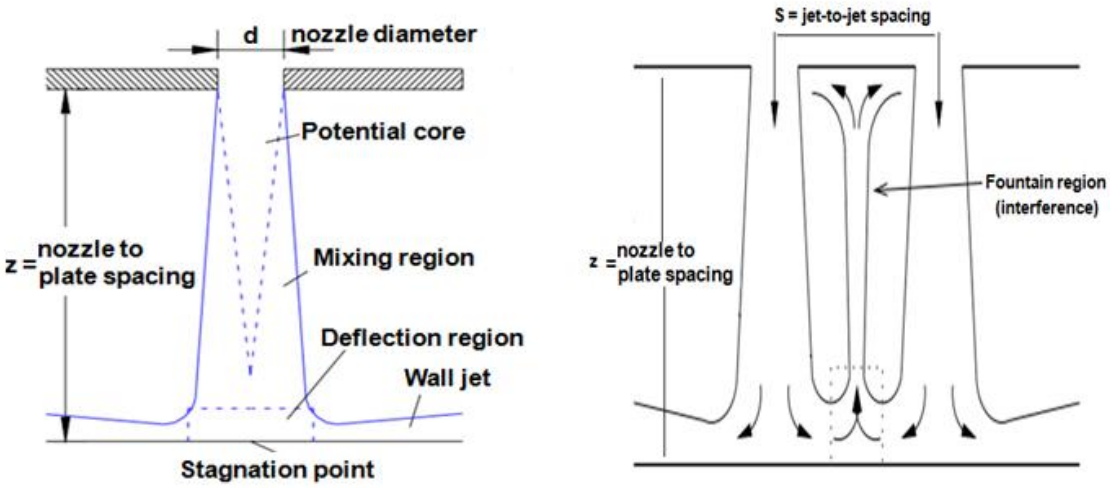

Figure 3.14 Nomenclature shown for single (left) and multiple (right) jets[96]

3.5.1 Jet Modeling for Single Jet (N=1)

For single nozzle system Martin [85] model is employed by changing the thermopyhysical properties of coolant.

$$F = 2 \cdot Re^{0.5} \cdot \left(1 + \left(\frac{Re^{0.55}}{200}\right)\right)^{0.5} \tag{3.55}$$

$$Nu\#_{avg,martin} = \left(\frac{\left(1 - 1.1 \cdot (d/r)\right)}{1 + 0.1 \cdot \left((z/d) - 6\right) \cdot (d/r)}\right) \cdot (d/r) \cdot F \cdot Pr^{0.42} \tag{3.56}$$

$$h_{avg,martin} = Nu\#_{avg,martin} \cdot k/d \tag{3.57}$$

The experimental limits for their work is from, Re=2000-400000, Z/d: 2-12, r/d: 2.5-7.5.(z/d) opt=5.3 was found to be an optimum nozzle to plate spacing

3.5.2 Jet Modeling Based on Multiple Jets (N=4, 9)

For multiple nozzles Martin [85] model is used;

$$f = \frac{3.142 \cdot d^2}{4 \cdot s^2} \tag{3.58}$$

$$G = 2 \cdot \sqrt{f} \cdot \frac{1 - 2.2 \cdot \sqrt{(f)}}{\left(1 + 0.2 \cdot \left((z/d) - 6\right) \cdot \sqrt{(f)}\right)} \tag{3.59}$$

$$K = \left(\left(1 + \left((z/d) \cdot \frac{\sqrt{f}}{0.6}\right)^{0.6}\right)\right)^{-0.05} \tag{3.60}$$

$$Nu\#_{avg,martin} = 0.5 \cdot K_{martin} \cdot G_{martin} \cdot Pr^{0.42} \cdot Re^{0.666} \tag{3.61}$$

$$h_{avg,martin} = k \cdot Nu\#_{avg,martin} / d \tag{3.62}$$

The limits for using this correlation is from Re=2000-100000, z/d:2-12 and s/d:4.3-14.For optimum jet pitch (s/d), Lindeman et al [107] model is coupled with the model in [85].

$$(s/d)_{uniform} = \frac{\frac{\sqrt{A_n}}{d}}{\sqrt{(N)} + 1} \tag{3.63}$$

$$(s/d)_{optimum} = 1.617 \cdot (s/d)_{uniform} \cdot N^{-0.1026} \quad (3.64)$$

Generally more number of nozzles results in higher average heat transfer coefficient as there is an increased number of stagnation regions but at the same time due to jet interference with neighboring jets becomes significant. Hence there needs to be trade off when selecting number of nozzles. For this study square jet configurations with single and multiple jets are investigated. Pipe nozzle has been selected for the research undertaken as fully develop flow takes place resulting in high heat transfer and the ease of manufacturing. Also based on Martin [85] , z/d (dimensionless nozzle to plate spacing) will be taken as approximately 5.3-6.0

3.6 COOLING DESIGN MODEL RESULTS AND DISCUSSION

The correlations developed by Martin [85] were applied for the analysis of jet cooling model. Since it is an empirical correlation based on experimental data, first the validation was carried out with original data to check the curve fitting and then it was applied to the model subsequently.

3.6.1 Validation for Single Jet Model (N=1)

The graph shows validation of experimental data by varying Reynolds number. The experimental data points extracted were from Martin [85]

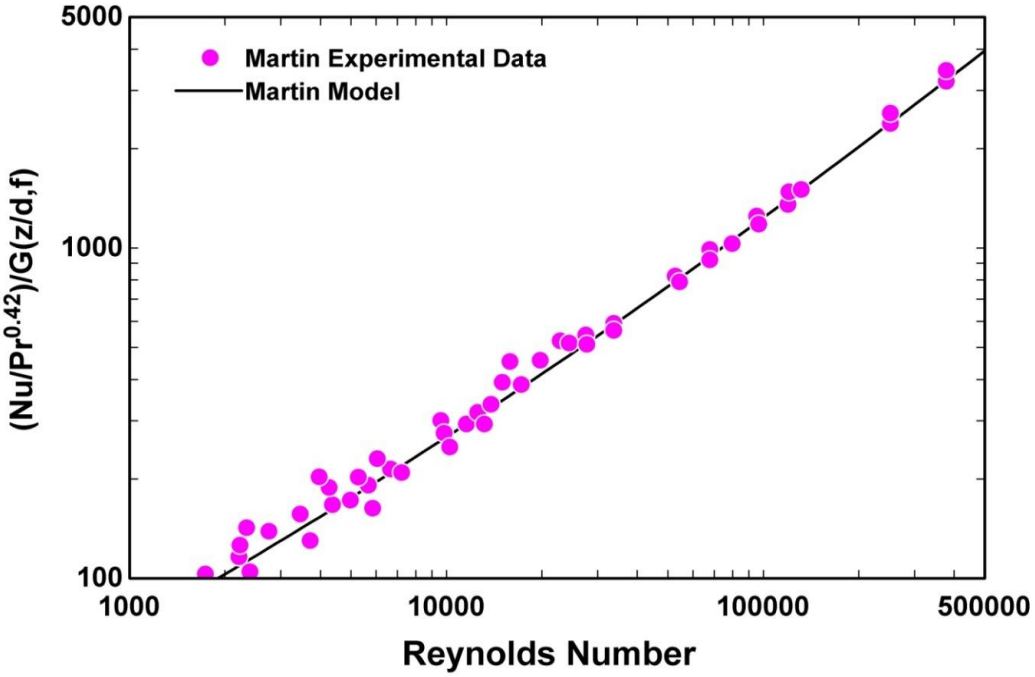

Figure 3.15 Validation plots single nozzle model.

3.6.2 Validation for Multiple Jets Model (N=4, 9)

The graph shows validation of multiple nozzles data by varying Reynolds number. The experimental data points extracted were from Martin [85].

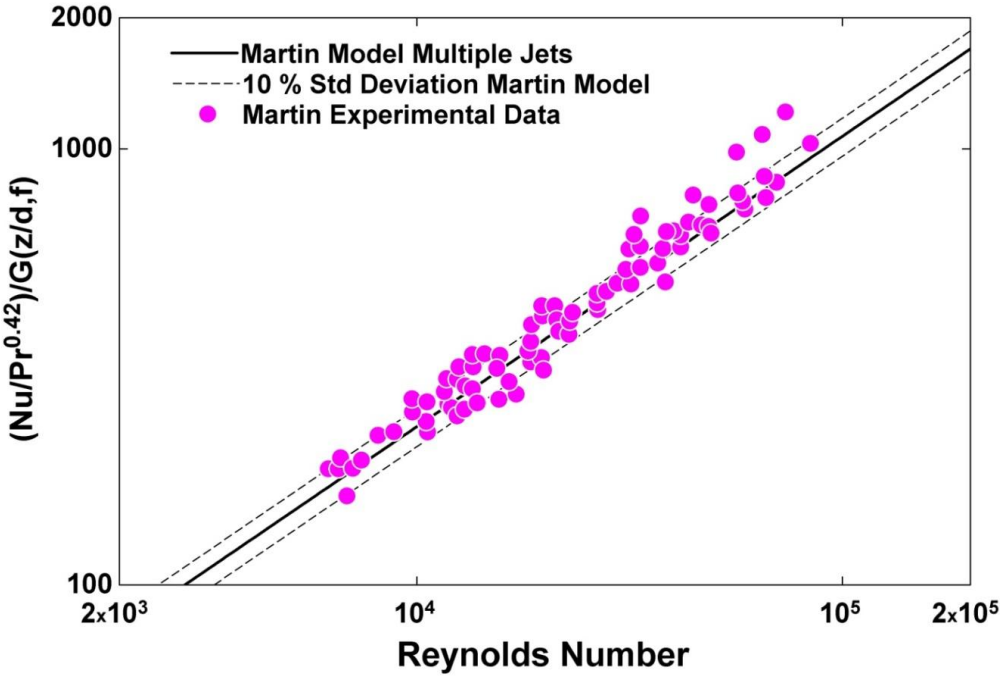

Figure 3.16 Validation plots for multiple nozzles model.

CHAPTER 4

EXPERIMENTAL STUDY

In this chapter the description of manufacturing of apparatus, experimental setup, testing procedures and data collection methods will be discussed for various parameters which determine the overall performance of cooling systems.

4.1 DESCRIPTION OF THE COOLING SYSTEMS

Experimental setup was designed and manufactured to investigate the thermal and electrical performance of PV system. This setup has been built on the open space of building 26 at King Fahad University of Petroleum and Minerals. The present setup is designed to investigate the performance of electrical efficiency and power output from the PV strings during operation.

Following are the schematics of all the four cases to be investigated in this research for the study of uniform and non uniform cooling techniques.

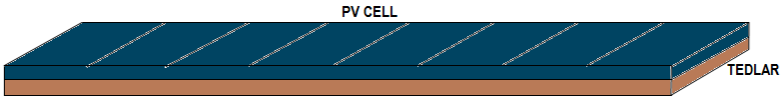

Figure 4.1 Case 1: PV panel without Cooling

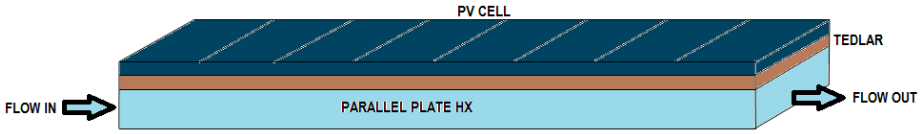

Figure 4.2 Case 2: PV panel with Rectangular Channel Heat Exchanger

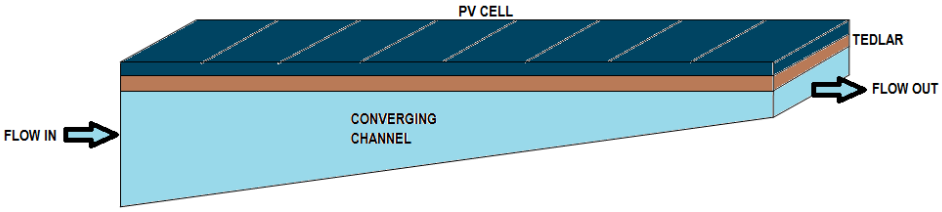

Figure 4.3 Case 3: PV panel with Converging Channel

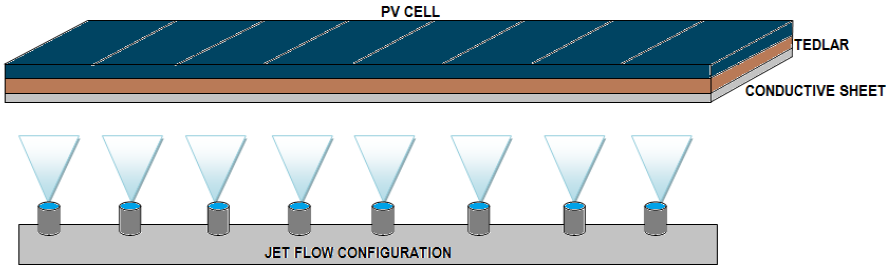

Figure 4.4 Case 4: PV panel with Jet Impingement Cooling

A PV string is fabricated by connecting eight C60 monocrystalline silicon solar cells in series with bottom contacts as shown in Fig. 4.5. In the present setup there are four PV strings which are simultaneously tested under different conditions. The specification of single C60 monocrystalline silicon solar cell is given in Table 1. The schematic diagram all configurations considered is shown in Figs. 4.1-4.4.

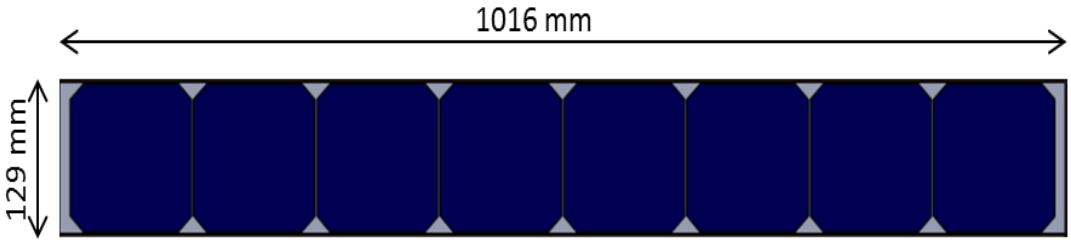

Figure 4.5 Monocrystalline Silicon Cells connected in series

4.1.1 PV String with Rectangular Channel Cooling

In order to compare the performance of PV strings under non uniform cooling, a method of rectangular channel cooling heat exchanger has been designed and fabricated. This is because in the case of rectangular channel heat exchanger, there are continuous temperature variations across the surface of the PV panel.

For lowering the operating temperature of the module, a rectangular channel heat exchanger was placed at the bottom of the cells. The schematic diagram for the rectangular heat exchanger is shown in Fig 4.6. A Pump and bypass system was used in order to maintain the pressure of water supplied to the heat exchanger. The generated electricity by the solar strings was stored in batteries of 12 V.

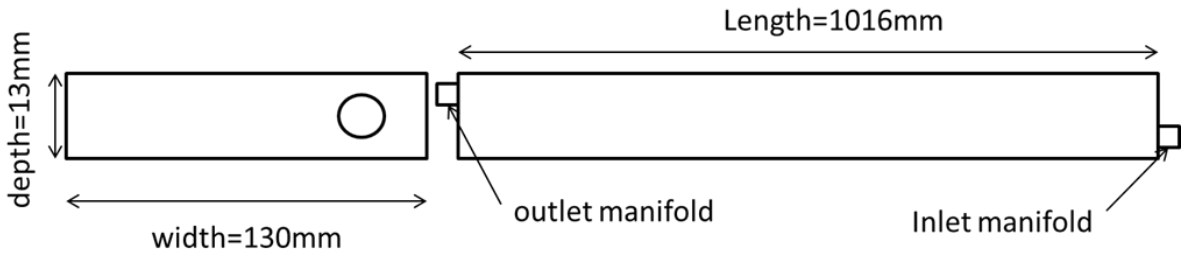

Figure 4.6: Schematic diagram for rectangular channel heat exchanger

4.1.2 PV String with Converging Channel Cooling

This experimental test facility has been designed to investigate the effect of temperature on the performance of PV systems. The effect of temperature on the power output and efficiency is studied. The proposed system consists of converging channel type heat exchanger for PV string to minimize temperature variation across the surface and to cool the panel. The experiments have been conducted in an open compound at King Fahd University of Petroleum and Minerals, Dhahran.

For lowering the operating temperature of the module in a uniform way, a converging channel heat exchanger is placed at the bottom of the cells. The schematic diagram for the converging channel heat exchanger is shown in Fig 4.7. The active area of a single solar cell is 125 mm x 125 mm. Maximum Power Point Tracker (MPPT) device is used during operating conditions to extract maximum current and maximum voltage. The electrical energy generated by the module is stored in 12V batteries. In order to measure the temperature on the PV surface, eight Type K calibrated thermocouples were used and temperature profiles were recorded using data acquisition system. Moreover,

thermocouples at inlet and outlet of the heat exchanger were employed. Figure 4.8 shows the eight points for the extraction of temperature measurements across PV surface.

For uniform cooling of PV strings, converging channel was designed and fabricated. Based on the CFD calculations, converging channel was designed with an angle of 2˚. CFD results showed that with this optimum angle PV top surface will provide almost uniform cooling with the converging channel.

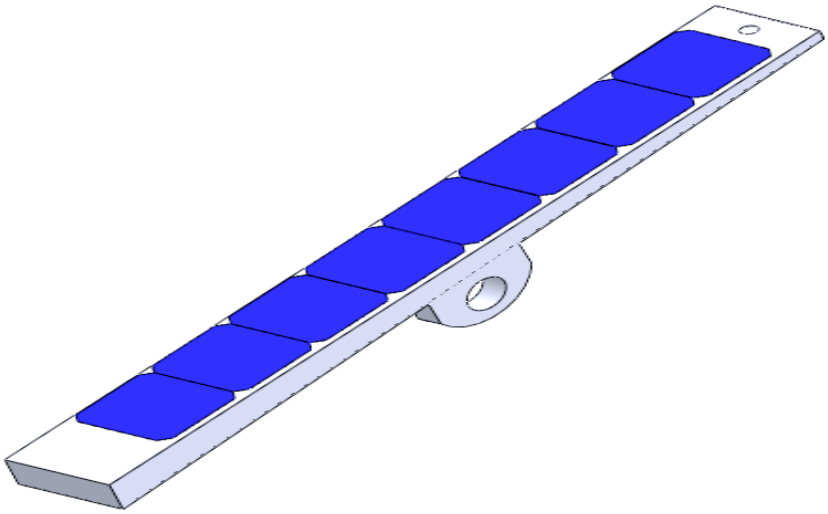

Figure 4.7 A 3D drawing of the heat exchanger with solar cells attached on its top.

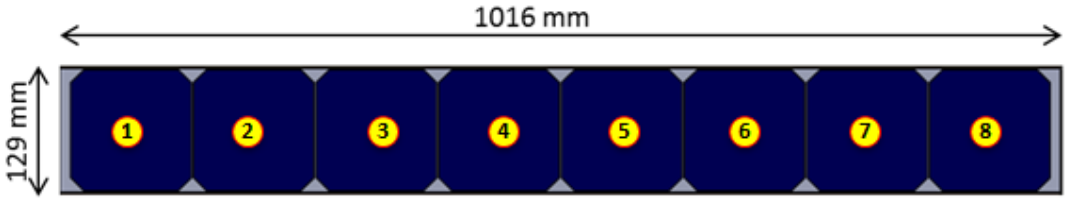

Figure 4.8 PV string with eight solar cells with thermocouples position

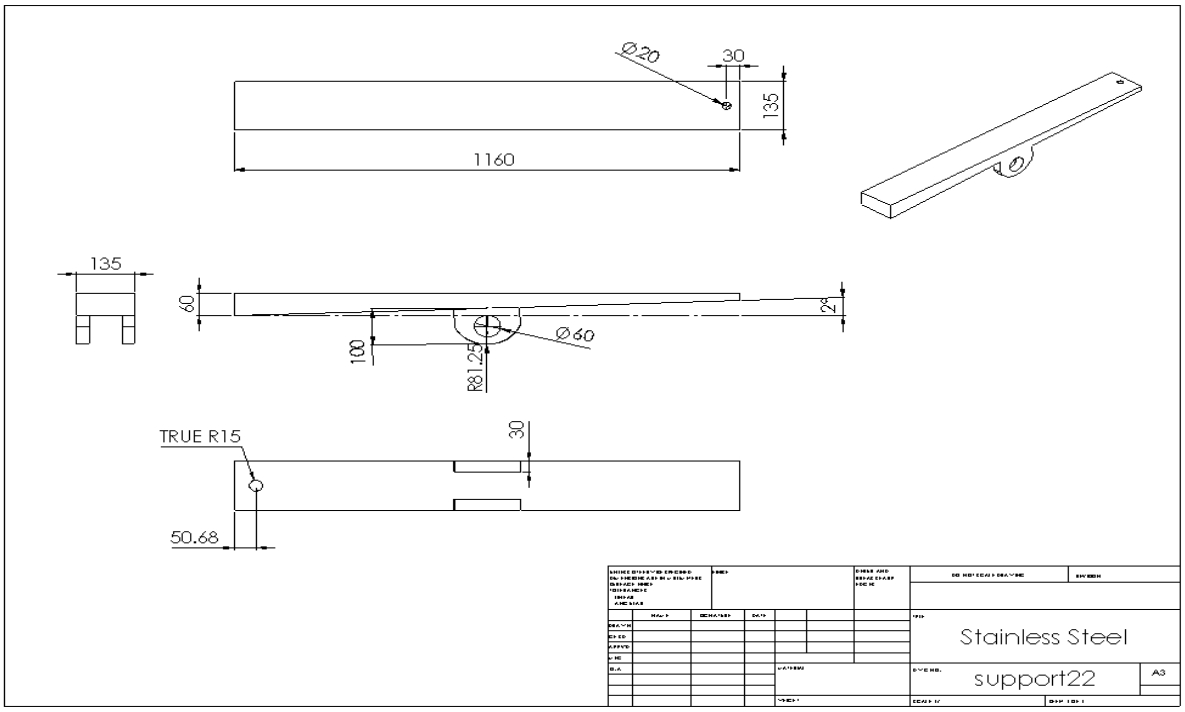

Figure 4.9 Technical drawing of the heat exchanger final design.

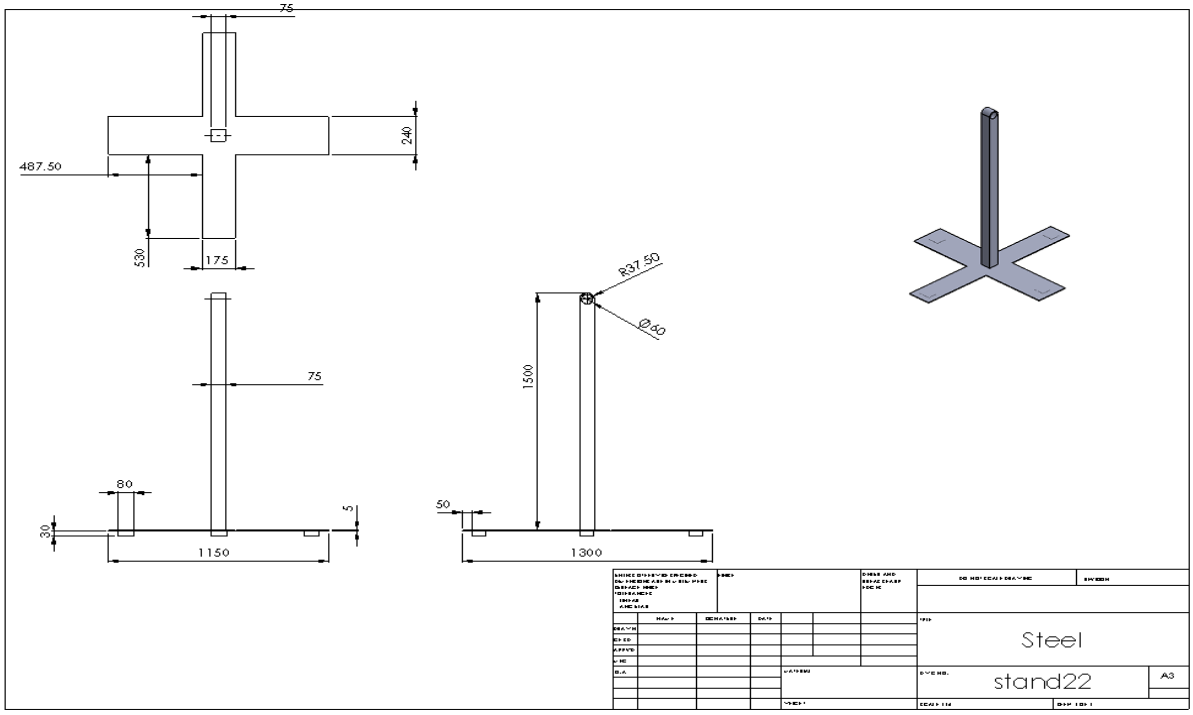

Figure 4.10 Technical drawing of the heat exchanger stand.

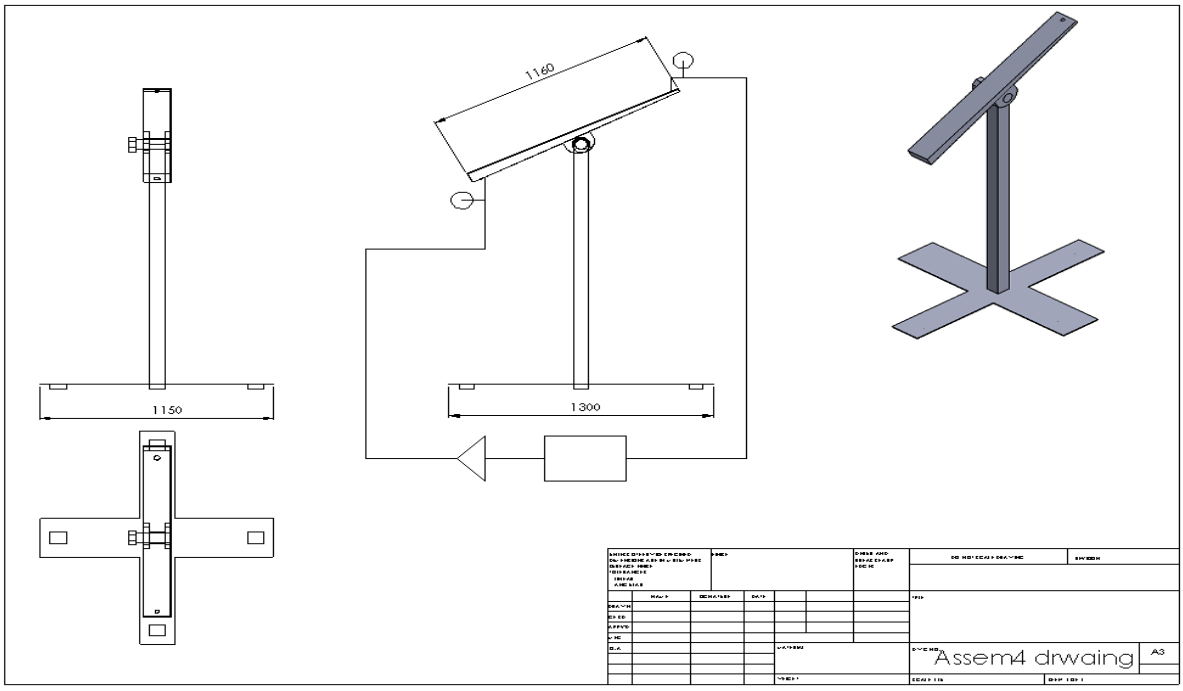

Figure 4.11 Technical drawing of the cooling system assembly.

The material of the heat exchanger used was aluminum because of its high heat conductivity , light weight and corrosion resistance whereas the adjustable stand material was selected to be stainless steel. Technical drawings used for manufactruign are shown in Figs 4.9-4.11. To make sure the complete filling of the heat exchanger, the inlet was kept at the lower side and the outlet of the fluid at the upper side. Heat is disspated from the backside of PV string and is absorbed by the cooling medium i.e. water. Glasswool insulation was used to reduce convection and radiation heat losses from the back side of the heat exchanger in the final assembly. Figures 4.12 -4.18 shows the system during manufacturing progress.

Figure 4.12 Converging channel heat exchanger after manufacturing

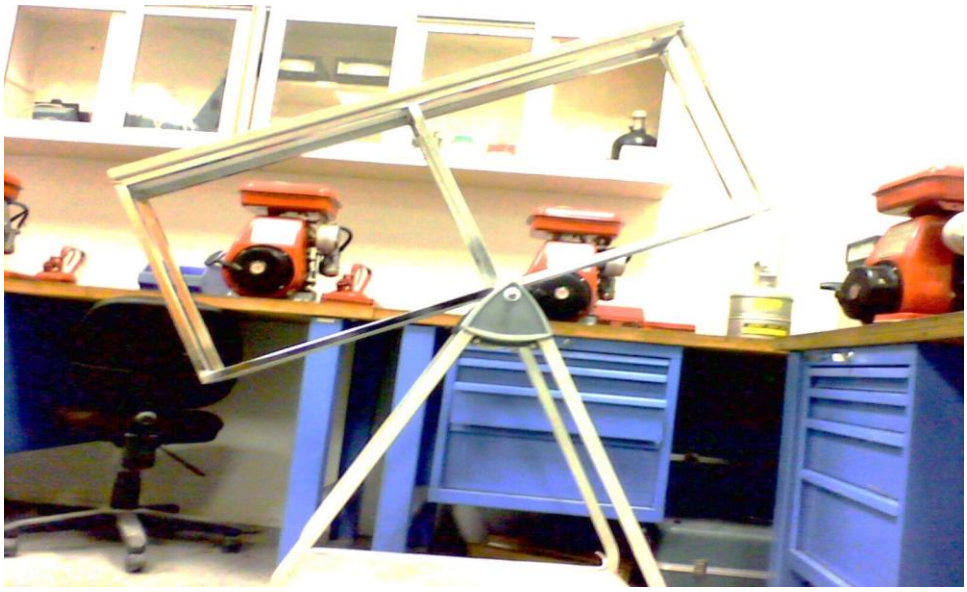

Figure 4.13 The heat exchanger stand after manufacturing.

Figure 4.14 Glasswool insulation for heat exchanger.

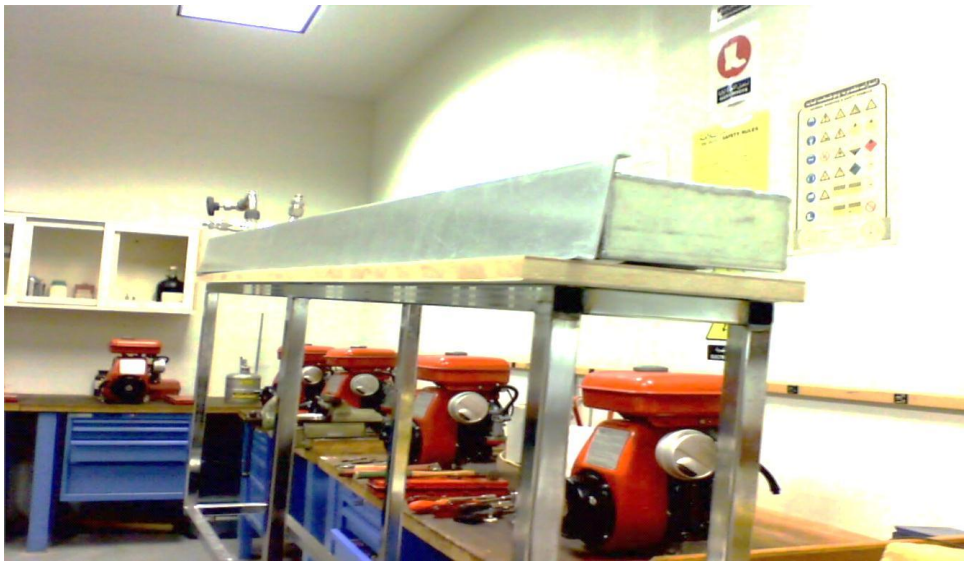

Figure 4.15 Side supports used to hold the exchanger and the string in place.

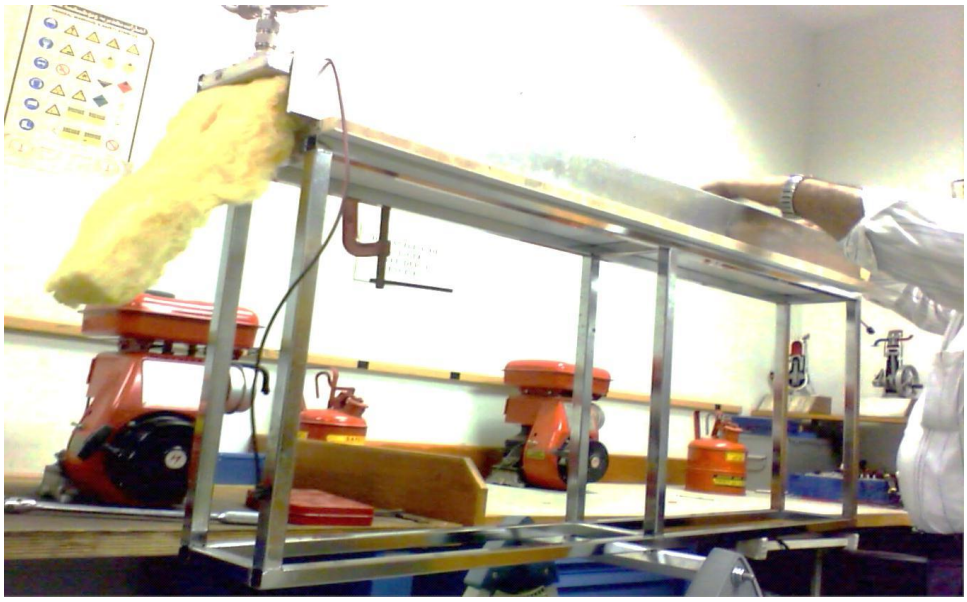

Figure 4.16 Support and insulation assembled.

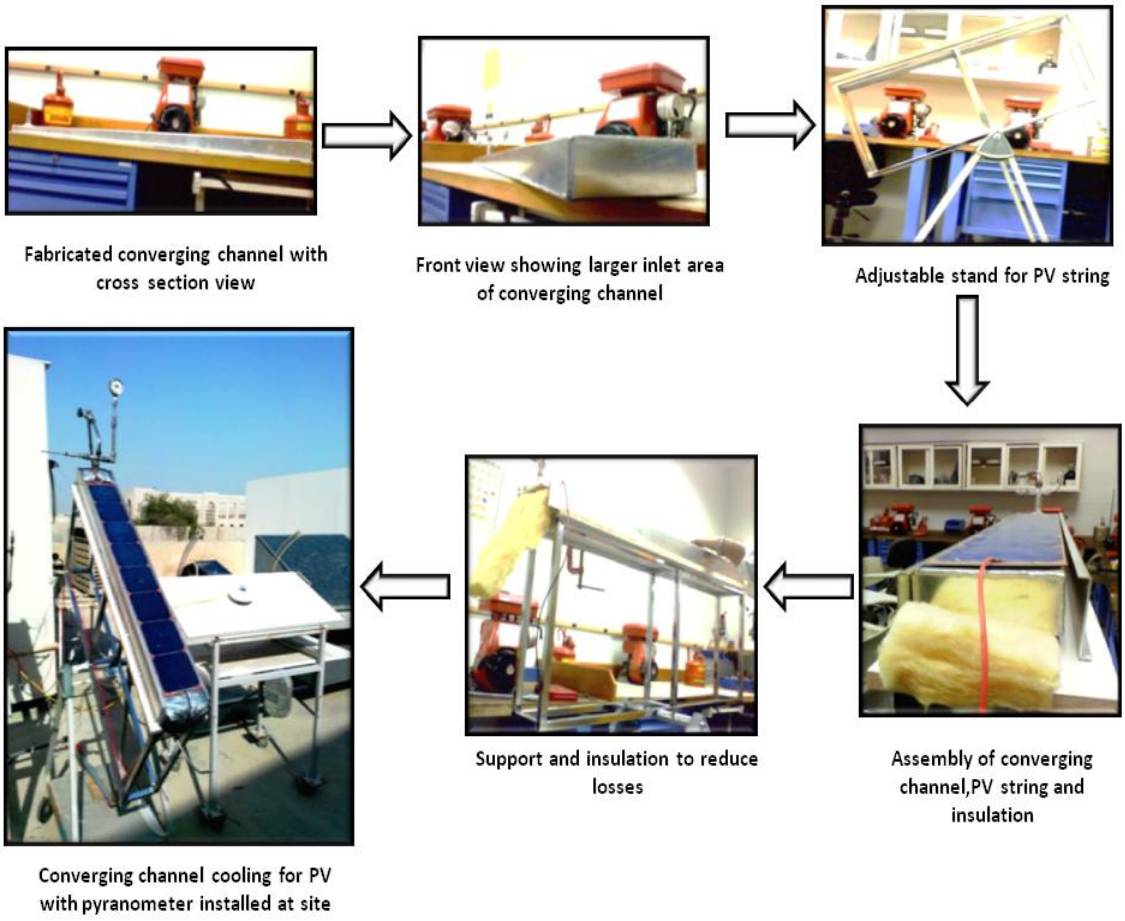

Figure 4.17 Stages of manufacturing process for converging channel

4.1.3 PV String with Jet Impingement Cooling

Jet impingement cooling has been selected as the main configuration for the investigation of uniform cooling. The design and fabrication of the stand alone jet impingement rig was first completed for the pilot study then the main laboratory scale setup was fabricated.

The jet was impinged on aluminum substrate of thickness 1 mm. The solar cell string was of Sun power C60. The general configuration for jet cooling is shown in fig 4.19 with layers of different materials.

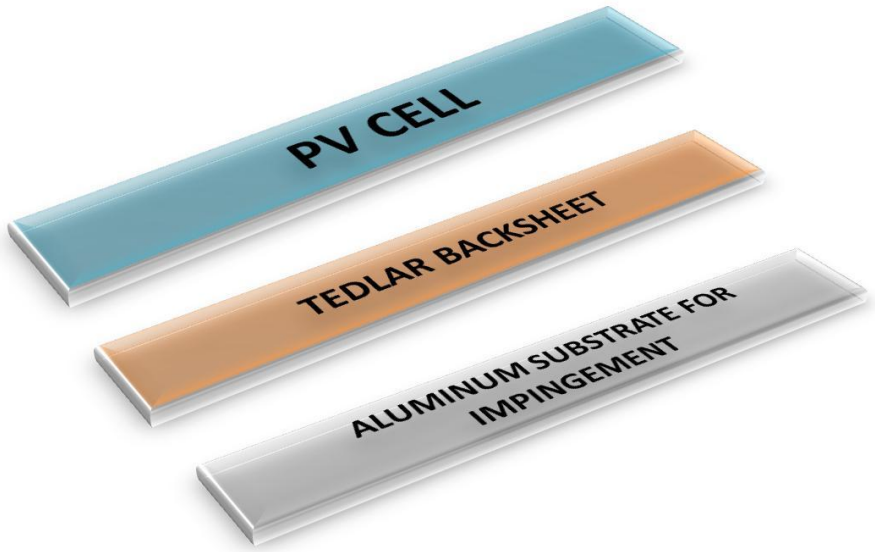

Figure 4.18 Schematic showing different layers for jet cooling.

Circular pipe nozzle was used edge based on the analysis and ease of fabrication with the single jet configuration for each cell. The chamber or the plenum was made of Plexiglass to observe the physics of jet impingement system with the stand made up of

stainless steel inclined at latitude angle of Dhahran. Figure 4.20 shows the preliminary design for the jet cooling with the adjustable stand to control z/d ratio i.e. nozzle to plate spacing with the PV string. Drainage was designed below the jet main header that was placed inside the cavity. The main purpose of this preliminary jet impingement setup was to investigate the real time characteristics of jet position, jet angle, jet to nozzle spacing and the jet nozzle type on the uniform cooling of solar cell. Temperature contours were recorded for the various configurations and the optimum uniform cooling configuration of pipe type nozzle, specific flow rate, jet to nozzle spacing and nozzle angle was selected for the actual test rig. The main objectives for this test were to check the uniformity of cooling and select the optimum values for the flow rate and the nozzle diameter. Thermocouples were attached on the aluminum substrate to examine the thermal characteristics on the surface as shown in Fig 4.20.

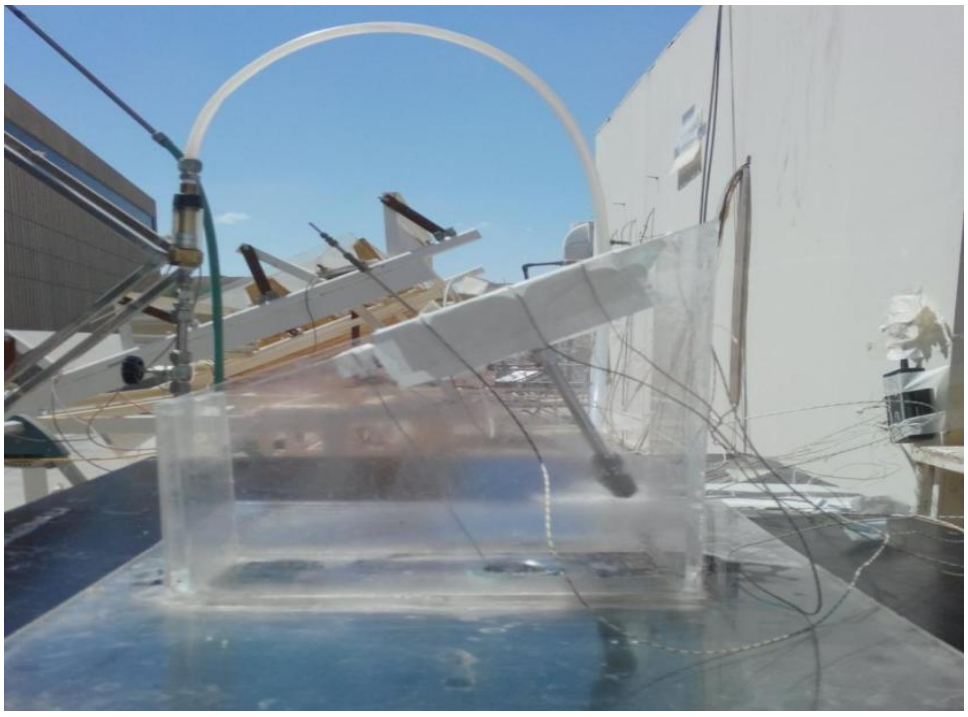

Figure 4.19 Side view showing jet angle, flow meter and drainage arrangement

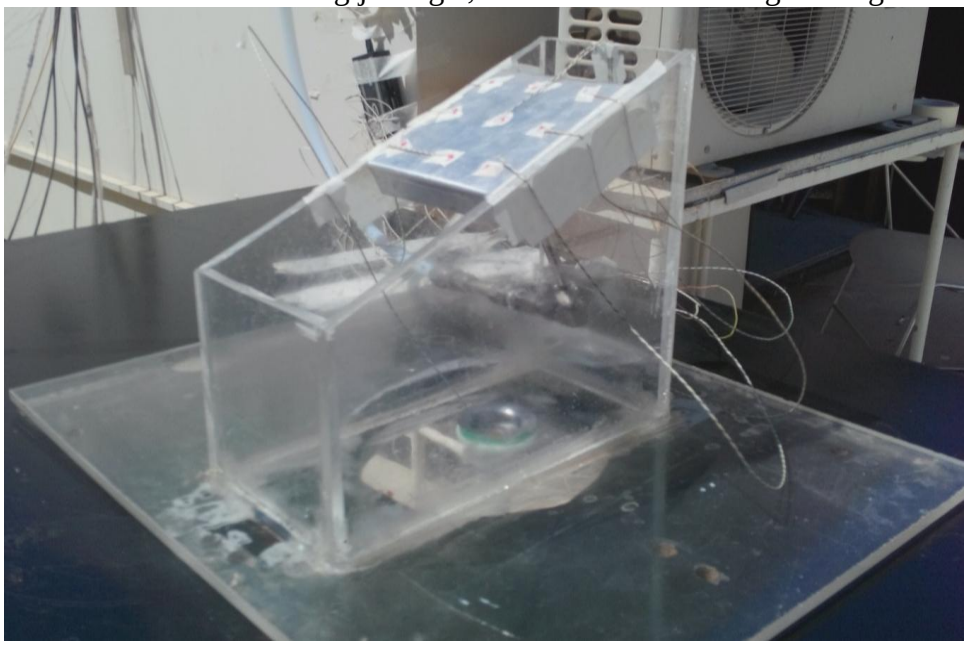

Figure 4.20 Location of thermocouples installed for jet cooling

4.1.3.1 Jet Initial Tests (Single Nozzle Setup)

Jet impingement test rig was manufactured based on the simulation and experiments from initial test rig as shown in the Fig. 4.21.The initial test rig of jet assisted in the fabrication by exploring different jet parameters and its effect on cooling. Positioning of jet, its angle, nozzle diameter, nozzle to plate spacing and flow rate of water was fixed by utilizing this setup.

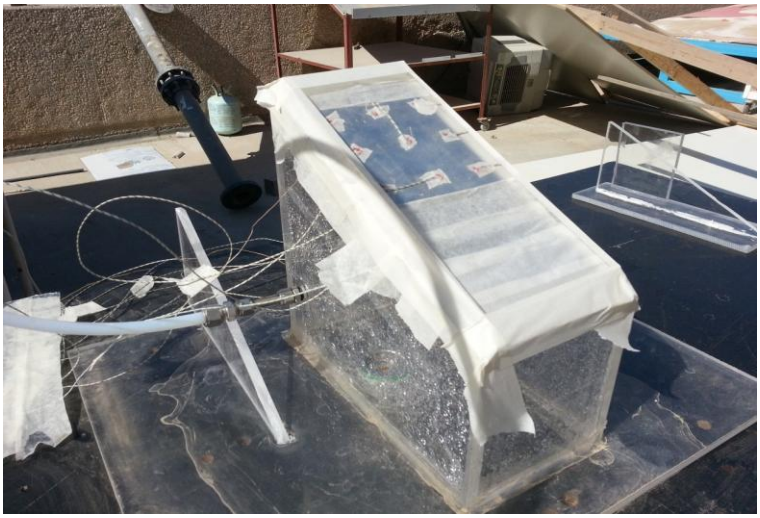

Figure 4.21 Jet test rig for selection of optimum parameters

The test setup was aimed to observe the temperature contours and uniformity on the aluminum substrate which had to be used later for PV cooling. Thermocouples were attached at different locations to observe temperature uniformity.

Table 4.1 shows the chosen parameters for initiating the experiment.

Table 4.1Parameters for initial jet test experiments

Parameters	Value
Flow rate	1-2 l/min
Initial Plate temperature	41 °C - 43 °C
Water Temperature	Approx. 25 ^{0}C
Nozzle Diameter	5 mm
Distance between nozzle and plate	25 mm
Tilt Angle	26.50°

Figure 4.22 shows results experimentally obtained after exposure of 60 mins with different intervals. Readings of five thermocouples placed on aluminum substrate, of equal dimension of single solar cell, were recorded for jet in perpendicular direction with real time environment conditions. Figure 4.22 shows that with even with single impingement jet, uniform cooling can be easily achieved. After only 60 minutes of exposure, entire plate became almost uniform temperature with maximum variation of approximately 1.8 degrees for one cell at that time instant. Figure 4.23 shows the variation of cell temperature at different points on the solar cell. It should be noted after a transient phase, cell temperature achieves steady state condition resulting in overall uniform thermal zone.

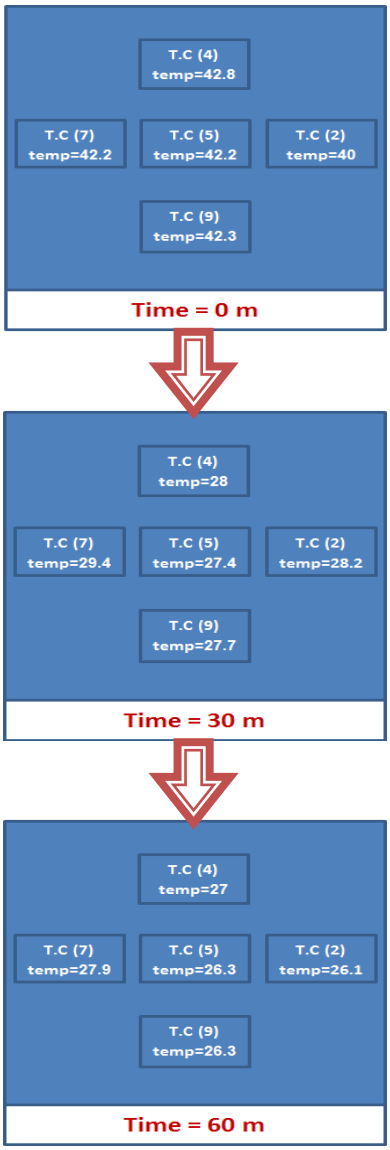

Figure 4.22 Thermocouple readings for jet initial test setup

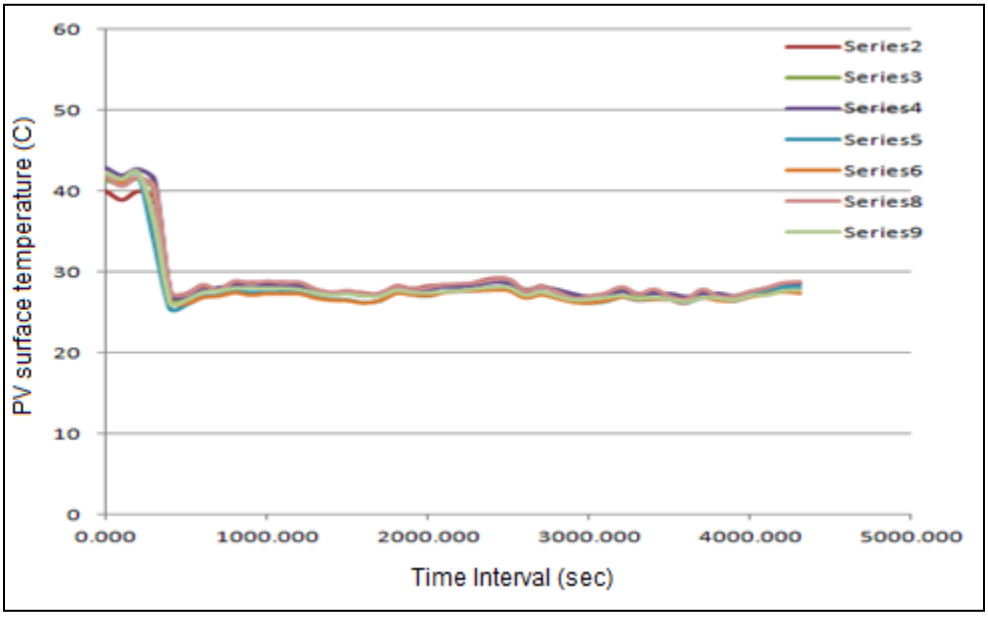

Figure 4.23 Variation of temperature on different thermocouples used on initial impingement jets test rig

After conduction of the initial tests, following parameters were decided to be fixed, as they did not affect the temperature uniformity, for the fabrication of final test rig for PV string.

Table 4.2 Fixed Parameters For Final Jet Impingemnet Setup

z/d	5.3
Jet position	Center of the cell
PV panel angle	30

After the successful results from single jet preliminary tests, fabrication of actual test rig was completed. The final test rig was exposed to the actual environmental conditions of Saudi Arabia in the month of June and December, 2014. Figure 4.24 shows the test

data for the thermocouples attached onto eight solar cells of PV string whereas Fig. 4.25 shows the location of thermocouple series. Thermocouple series 4 and 7 were at nozzle outlet and series 1 was used for inlet water temperature.

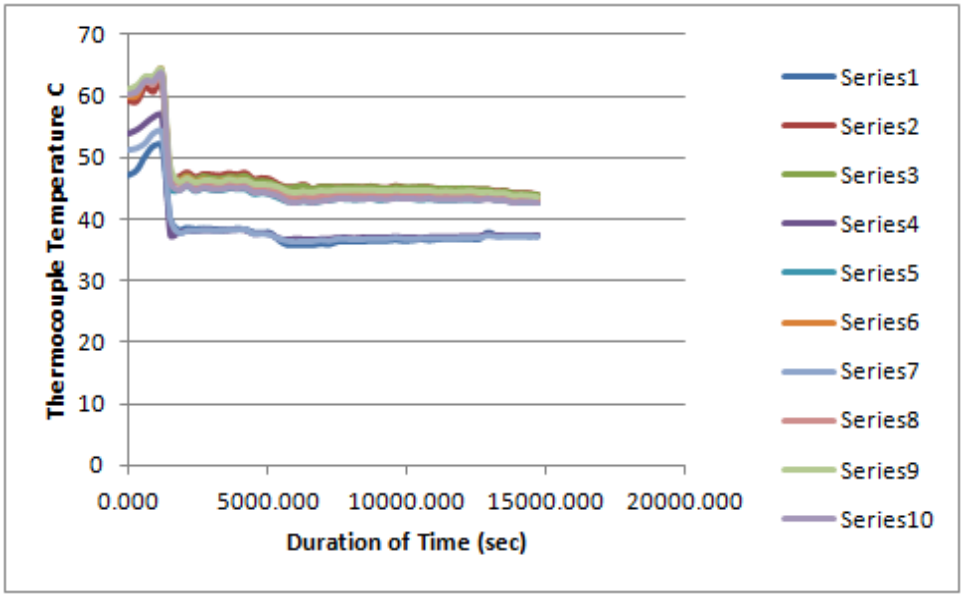

Figure 4.24 Variation of temperature on different thermocouples used on final impingement jets test rig

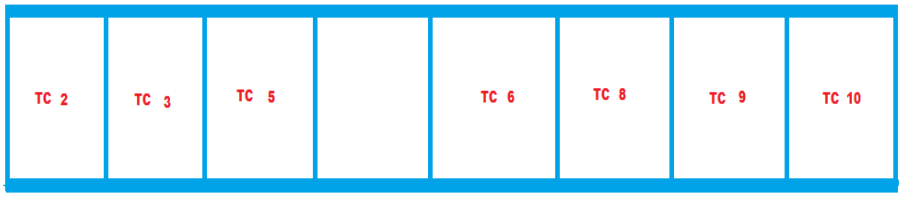

Figure 4.25 Thermocouple location and number on PV string

Figure 4.26 shows the effect of using 1.5l/ min flow rate for single nozzle. The overall flow rate for this test was 12 lit/min and the contours for each cell were uniform showing satisfactory results. In this test the initial temperature was relatively low because of clouds blocking sun radiation. Flow rate for this test was setup at 1.5 l/min for single nozzle.

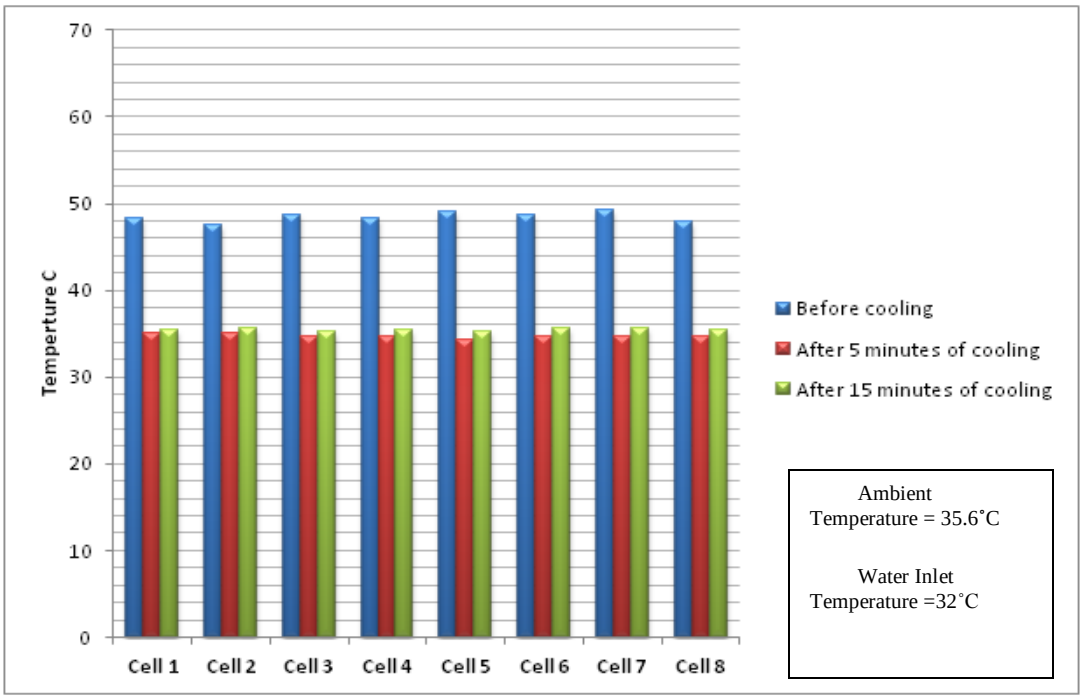

Figure 4.26 Temperature profile for each cell with 12 l/min

Also for the test purpose, in another trial 16 lit/min was utilized. The results obtained are shown in Fig 4.27. Manual measurements were carried out for each cell using thermocouples. It was later found that even using 1 lit/min would yield the similar results. Hence for future experiments 1 lit/min is suggested.

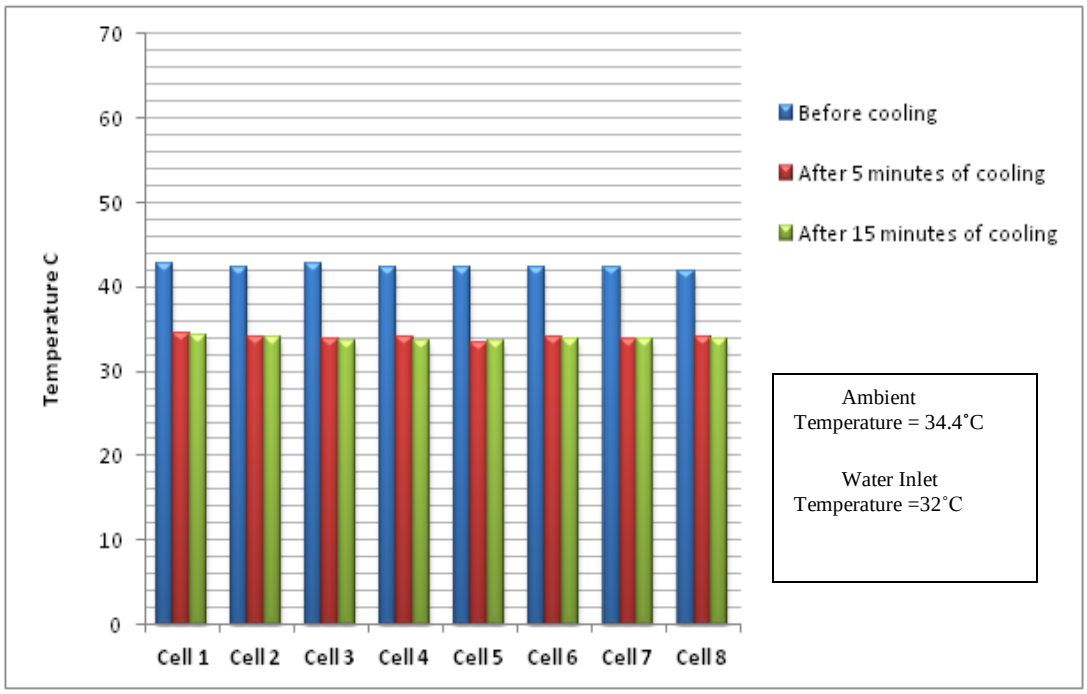

Figure 4.27 Temperature profile for each cell with jet cooling at 16 l/min

4.1.3.2 Final Jet Impingement System Description

After the initial test experiments, optimum jet parameters were found and final stand alone jet impingement test rig design was proposed and fabricated. Water is preferred as coolant because of its high specific heat and thermal conductivity than other coolant fluids. Suitable range for z/d between 2 to 14 ratio is chosen based on literature. Although the optimum is 5.3 based on Martin [85], however this range will allow the flexibility to change the nozzle to plate spacing to obtain desired output experimentally. The nozzle diameter is selected to be 5 mm with manageable jet exit velocity (near 3 m/s). Z dimension is chosen such that it can be adjusted between 10 mm and 70 mm. Figure 4.28 shows the optimum dimensions for cooling scheme. The fabrication system has been designed in such a way that the main jet parameters except diameter of nozzle can be varied. The choice of thermocouples and their location is paramount in obtaining accurate experimental data.

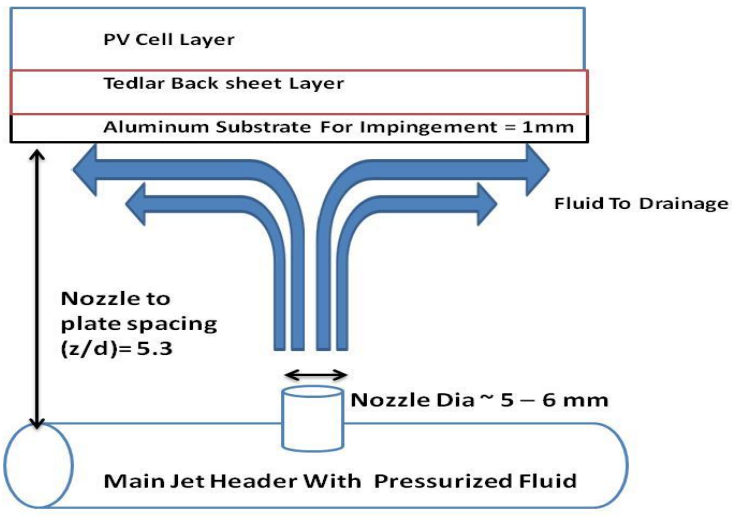

Figure 4.28 Optimum dimensions for cooling jet

Final design with the following features were designed and fabricated:

- Adjustable flow rate: By using flow meters the flow were adjusted in order to insure that each pipe will have the same flow.
- Adjustable height: It means that the jet to plate spacing was controllable in order to determine the best required height for having a uniform cooling system.
- Adjustable position: jets can be focused on several locations.
- Adjustable angle: So that cells locations could be changed in order to expose it to the sun.

Figure 4.29 illustrates the main components of the final design of the system.

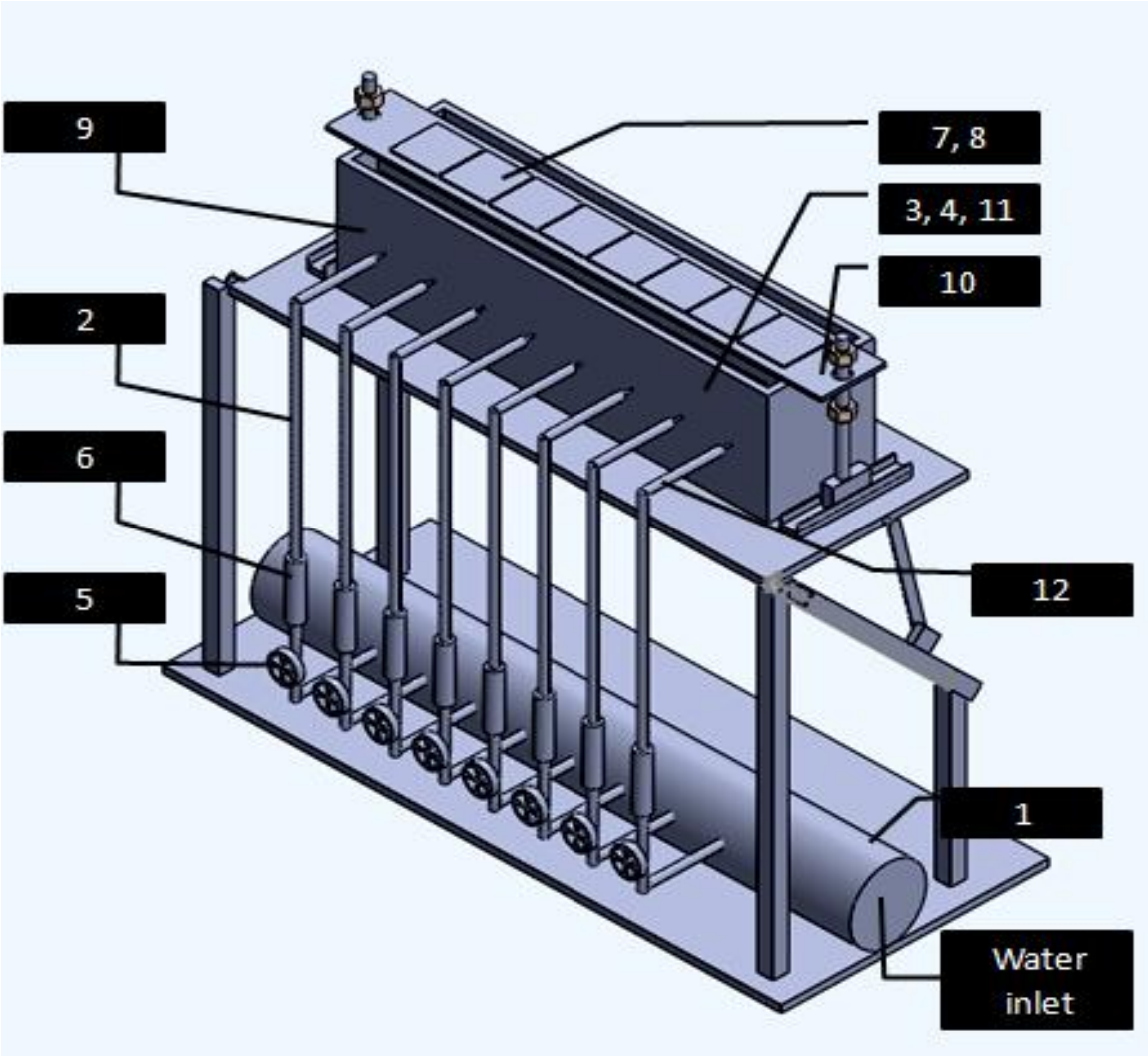

Figure 4.29 Final design of the jet impingement system

Table 4.3 Nomenclature of components used in final jet cooling system

#	**Component**
1	Main Pipe
2	PVC Pipes
3	S.S Pipes
4	Pipe Nozzles
5	Valves
6	Flow Meters
7	Aluminum Sheet
8	PV Panel
9	Main Frame
10	Adjustable Frame
11	Brass Fittings, Couplings, And Elbows.
12	Hose

The orthographic projections for the final design proposed are shown in Fig 4.30 whereas Figs. 4.31-4.35 show the manufacturing of final jet impingement test rig.

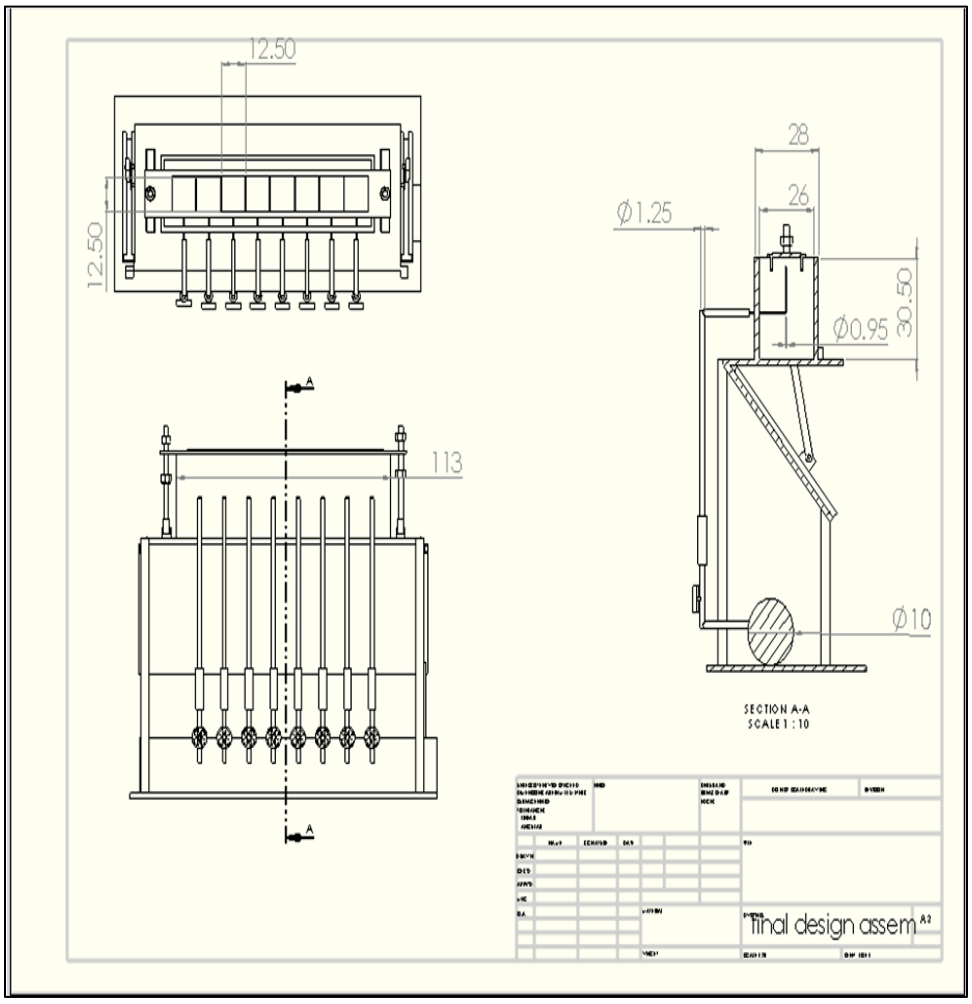

Figure 4.30 Projection diagram of jet cooling test rig

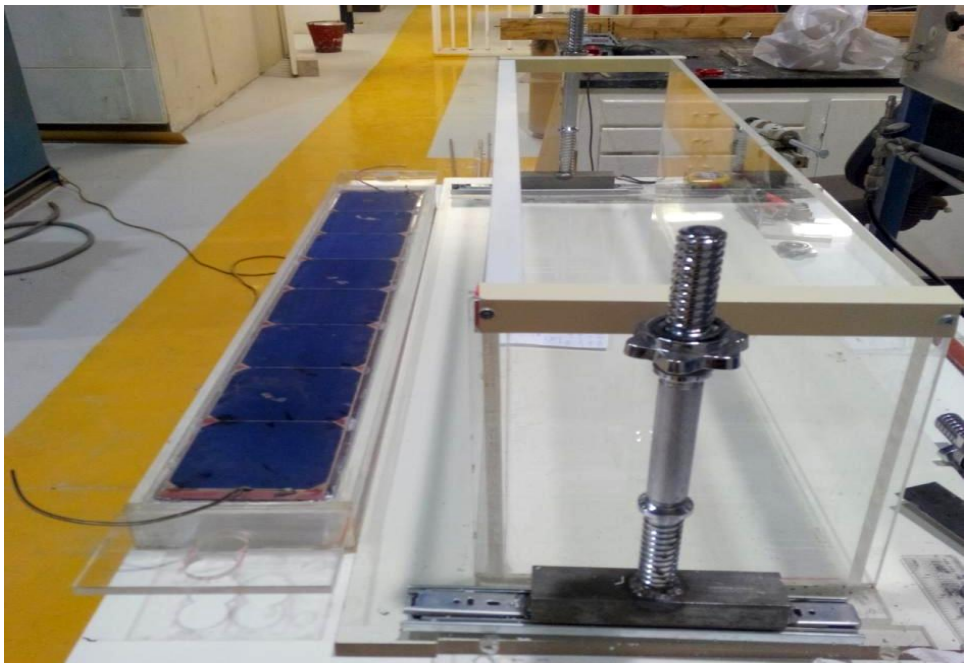

Figure 4.31 Side view of pv string assembly and jet test rig during manufacturing

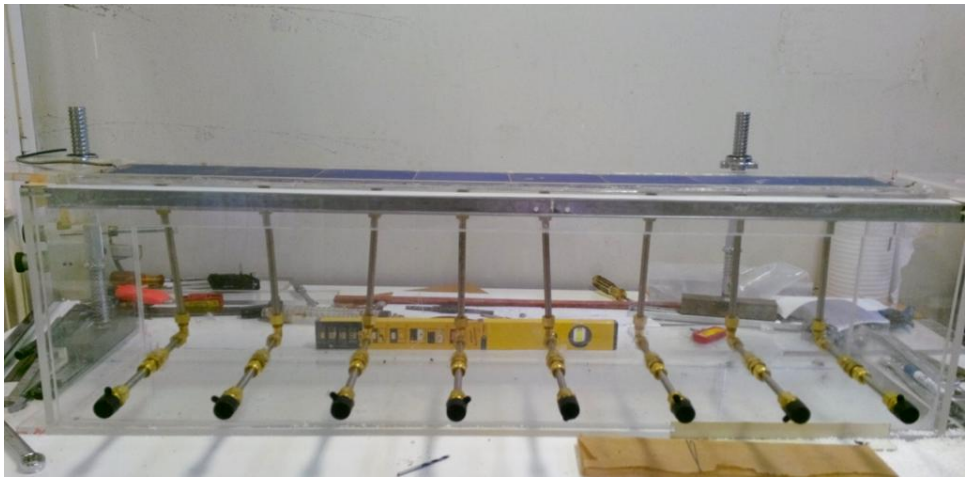

Figure 4.32 Plexi glass assembly and nozzle arrangement for the 8 cells in the PV string

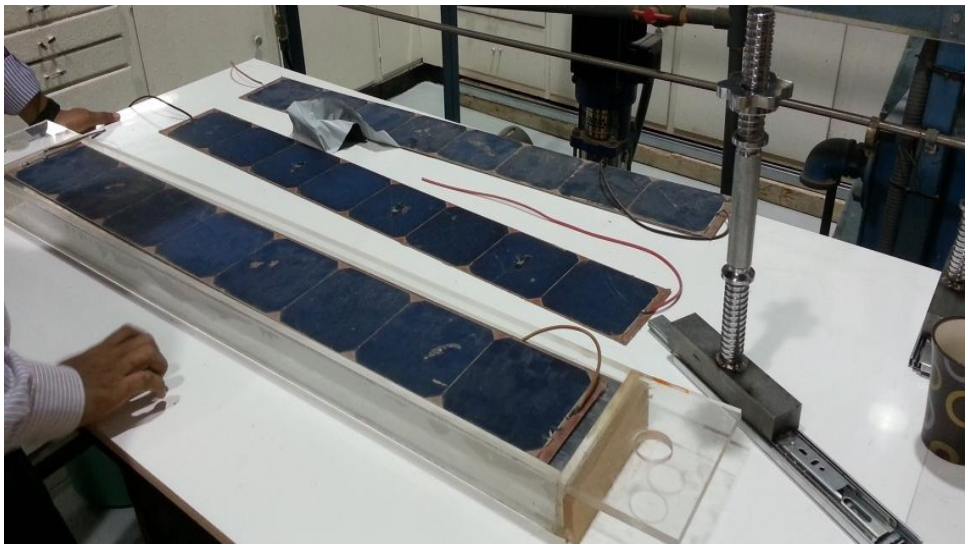

Figure 4.33 PV strings assembly along with jet nozzle position altering mechanism at right

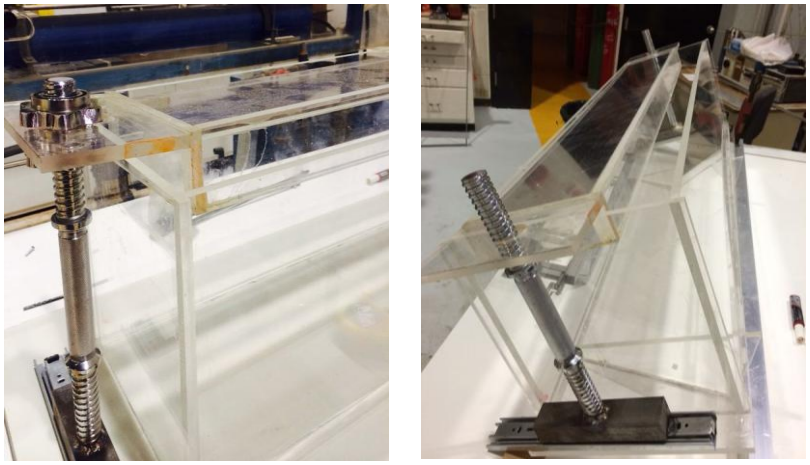

Figure 4.34 Jet impingement plexi glass assembly with nozzle position changing mechanism

Figure 4.35 Jet impingement test rig with movable angle position along with nozzles

4.2 EXPERIMENTAL SETUP /TESTING

Experimental setup has been designed and fabricated to investigate the thermal and electrical performance of PV system. This setup has been built on the open space of building 26 at King Fahad University of Petroleum and Minerals. The present setup is designed to investigate the performance of electrical efficiency and power output from the PV strings during operation.

The layout and dimensions of the string is shown in Figure 4.36. It consists of eight (8) solar cells connected in series of length about 1025 mm and the size of the single cell is 125 × 125 mm^2. The string layout is trimmed to have a rate of cells per area ratio of about 99%. The weight is about 1050 – 1400 g/m^2 and the thickness of about 600 – 700 µm. The string is bonded on to the fabricated absorber with high thermal conductivity bonding material namely silicon rubber. The power output is about 210 W/m^2.

Figure 4.36 Layout of the PV string with eight cells

The P_{max} voltage per cell is up to 0.51 V under standard conditions (light spectrum: Air Mass = 1.5; intensity = 1 kW/m^2; temperature = 25°C). The voltage in power maximum point is 0.56 V per cell. The current under standard test conditions is up to 6.0

A with an efficiency up to 22.6%. The closer view of a single cell is shown in Figs. 4.37 and 4.38.

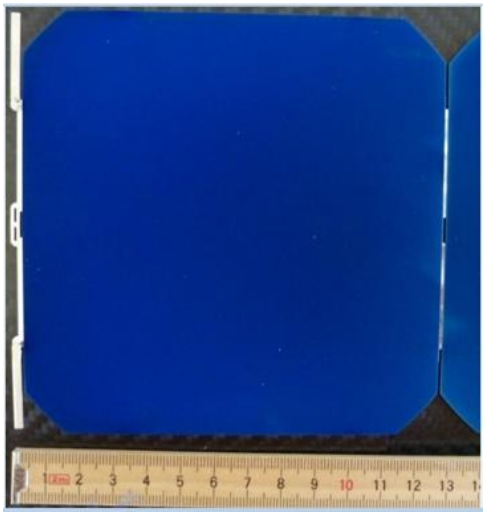

Figure 4.37 Closer view of top surface of single cell

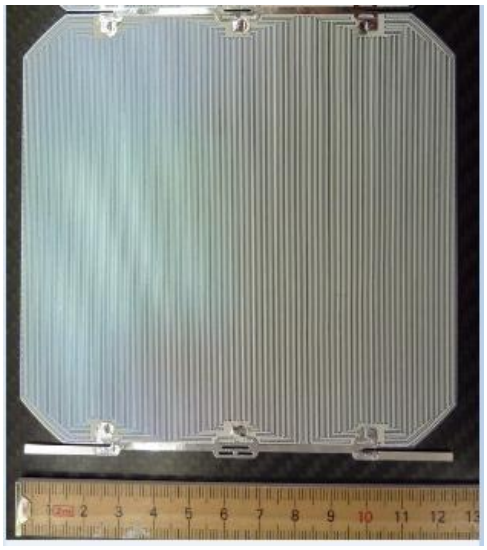

Figure 4.38 Closer view of back surface of single cell

4.2.1 PV String with Rectangular Channel Cooling and Without Cooling

All the panels are aligned along east west direction and facing due south. Inclinations of the panels are adjustable for optimization of the collectible solar radiation in different seasons. Figure 4.39 shows the actual arrangement of the rectangular channel heat exchanger cooled PV string (top) and uncooled PV string (bottom) fabricated and installed at the outside of Bldg. 26 in KFUPM Dhahran. They are manufactured using the guidelines described in the modeling section.

Figure 4.39 On site installation of rectangular channel heat exchanger and uncooled PV string

Figure 4.40 shows the PV with and without heat exchanger cooling during manufacturing steps. A storage tank with controlled inlet temperature was used to supply

cooling water to the system. For lowering the operating temperature of the module, a rectangular channel heat exchanger is placed at the bottom of the cells.

Maximum power point tracker (MPPT) has been used to extract maximum power point from the IV curve. The load has been attached after MPPT to ensure proper extraction of current and voltage from the system. The charges are then stored in the battery.

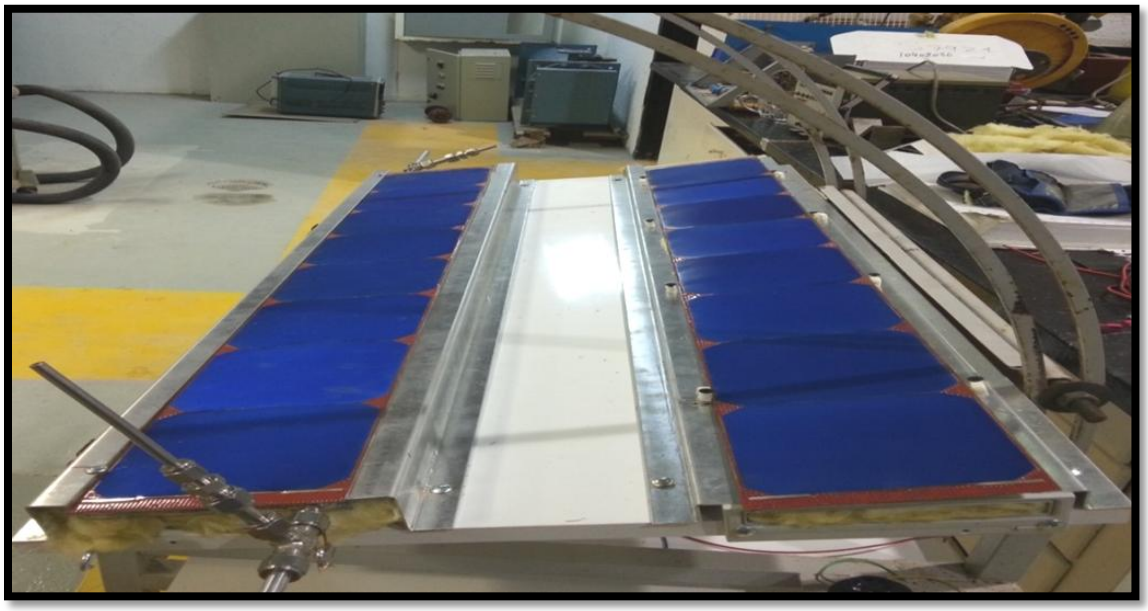

Figure 4.40 Fabricated rectangular channel heat exchanger and uncooled PV string

Thermocouples of type K has been used in this research to measure temperature on the surface of PV strings which can be directly monitored on Data Acquisition System (DAQ).The DAQ system installed for this research is capable of monitoring and storing calculations of voltage, current, wind speed, ambient temperature, wind direction , light intensity, temperature and maximum power.

4.2.2 PV String with Converging Channel Cooling

For uniform cooling of PV strings, converging channel was designed and fabricated as shown in Fig. 4.41. Based on the CFD calculations, converging channel was designed with an angle of 2˚. CFD results showed that with this optimum angle PV top surface will provide almost uniform cooling with the converging channel.

Figure 4.41 On Site installation of converging channel with Pyranometer

For lowering the operating temperature of the module, the converging channel heat exchanger is placed at the bottom of the cells. A storage tank with controlled inlet

temperature and pump is used to supply cooling water to the converging channel system. Thermocouples of type K has been used in this research to measure temperature on the surface of PV strings which can be directly monitored on DAQ. Maximum power point tracker (MPPT) has been used to extract maximum power point from the IV curve. Data is recorded in DAQ and is then used for analysis. Figure 4.42 shows the final arrangement of converging channel with pyranometer installed on site.

Figure 4.42 Converging channel installed with Pyranometer and anemometer

4.2.3 PV String with Impingement Jet Cooling

The aim of the jet cooling is to design and build a completely self-contained impingement test rig for the uniform cooling of PV string. This will be achieved by single jet exposed to each cell such that the average temperature of each cell remains constant and adjustable stand. The system for jet should allow the user to manipulate the key test parameters: the z/d ratio i.e dimensionless nozzle to plate spacing and the mass flow rate. The main design consideration is the nozzle diameter, nozzle shape, flow rate, nozzle to plate spacing, pressure drop across nozzle and the tilt angle of the jet to obtain approximately uniform temperature profile through the cell.

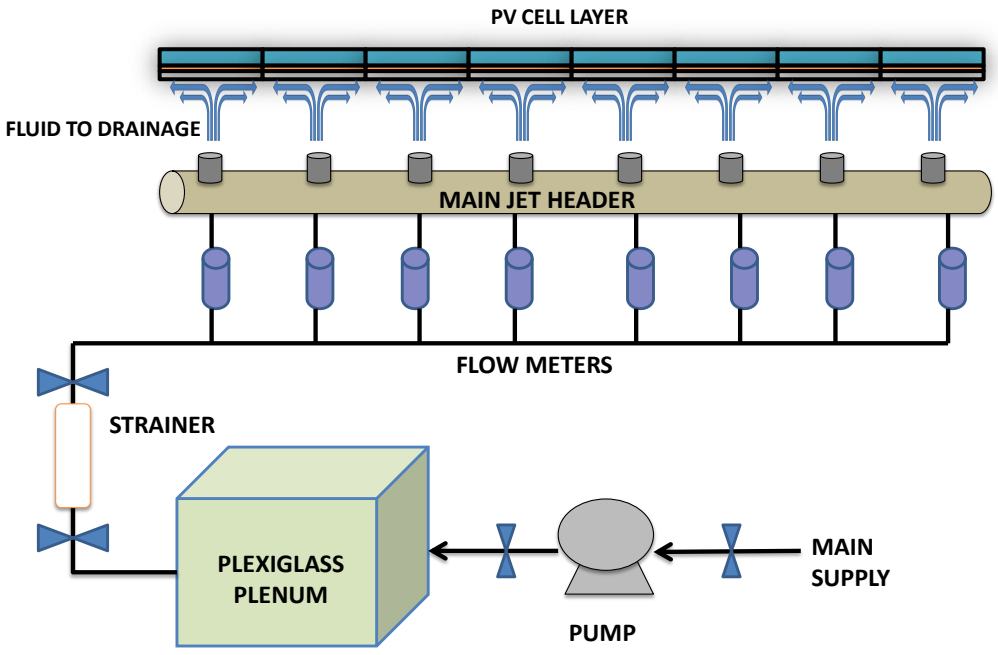

Figure 4.43 Schematic layout of jet impingement cooling for PV string

Figure 4.43 shows the schematic layout of jet cooling system for PV string. The main design issue is the main header. This was manufactured using plexiglass so that the physics of jet impingement can be monitored and if needed visuals can be captured through camera. Strainer was used before nozzle to ensure that no clogging takes place. A pump and bypass system was used in order to maintain the pressure of water supplied to the plenum. The electricity which is generated by the solar panels is stored in batteries of 12 V.

For the plenum or pressurize chamber the important parameters are the size, the material, the water inlets, the instrumentation, and the manufacturing of the plenum parts. For the material, Plexiglass has been chosen. The size of the main jet header was designed such that a rectangular array 8 nozzles for 8 cells in a string can be incorporated.

For impingement of jet aluminum sheet of 1 mm was chosen based on high thermal conductivity. Also it should be self adjusted so that the spacing between nozzle and plate can be altered for the experiment. In this research thermocouple type K will be used at multiple locations to observe the temperature profile.

The initial setup for the optimum jet parameters consists of a plexi-glass frame that contains the nozzle. Water flows upwards from the nozzle and splashes vertically on the back of the aluminum plate.

Following materials were used:

a. Plexi-glass.
b. Type K thermocouples
c. Stainless steel tube (3/8 in).
d. Plastic tube (5 mm).
e. Aluminum plate (14×14 cm).
f. Steel coupling.

Based on the literature, modeling simulations, and initial impingement jet test rig optimum parameters has been chosen for the manufacturing of jet impingement design for the experimental purpose. Establishing a water jet impingement facility generally consists of determining a jet diameter, jet-to-plate distance, jet diameter-to-radial distance, flow rate of the water and design of peripheral mechanisms such as thermocouples installation. Entire design must be performed with leak proofing in mind.

Figures 4.44-4.49 shows the installation of final impingement test system with sliding mechanism at the test site along with the position of nozzles.

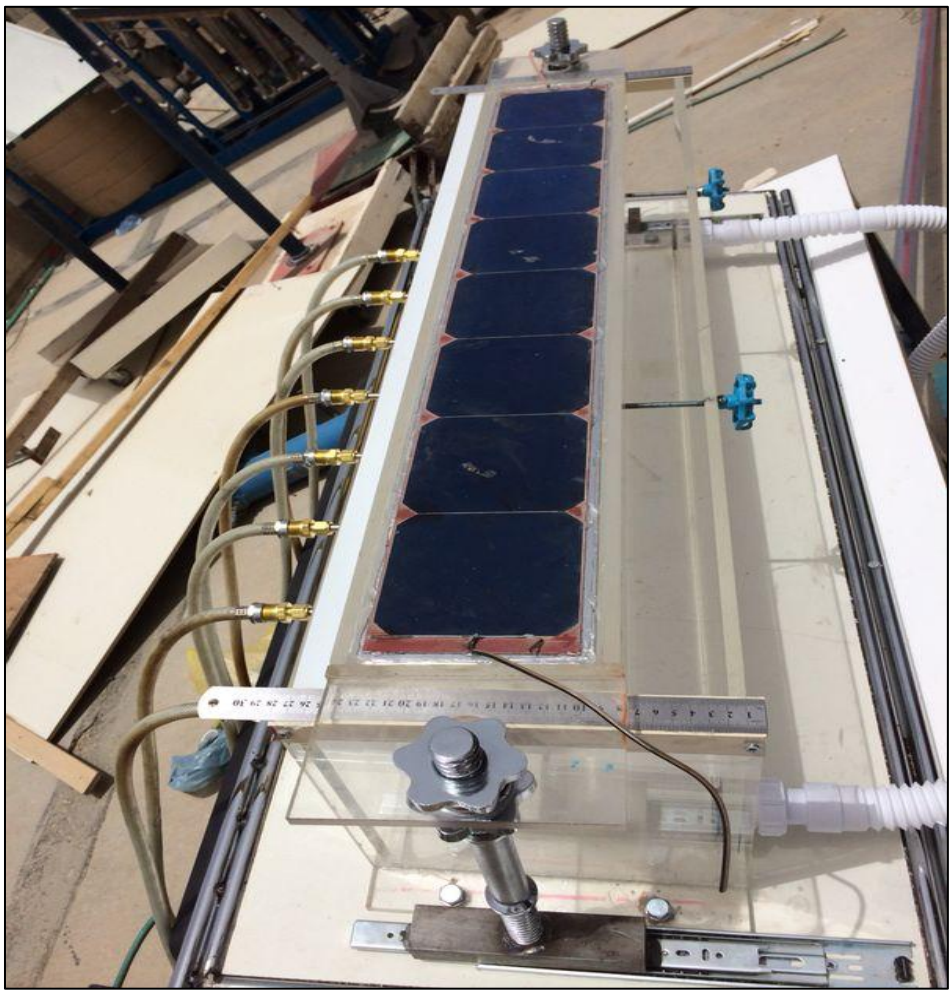

Figure 4.44 On site installation of final impingement test system with sliding mechanism

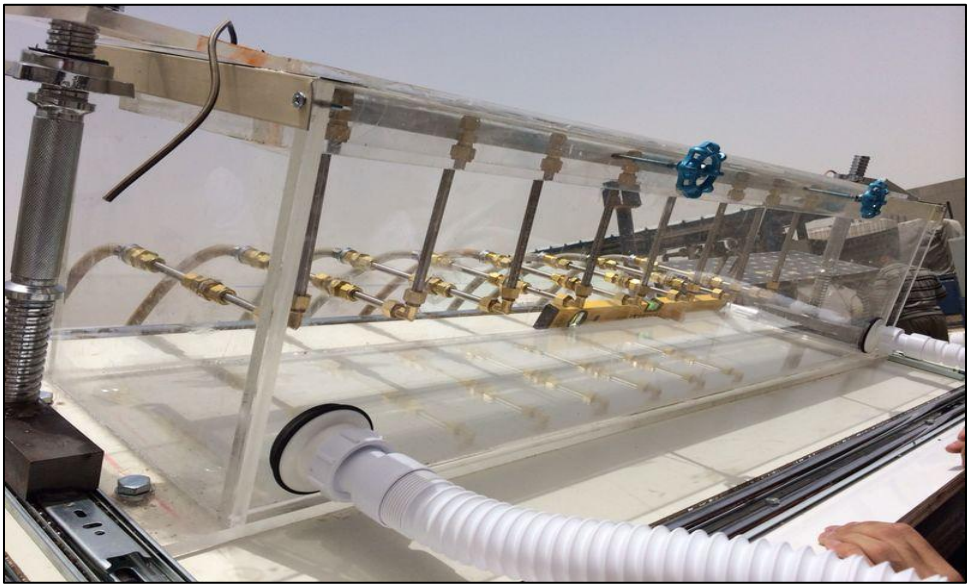

Figure 4.45 Nozzle arrangements and drainage mechanism for jet rig shown

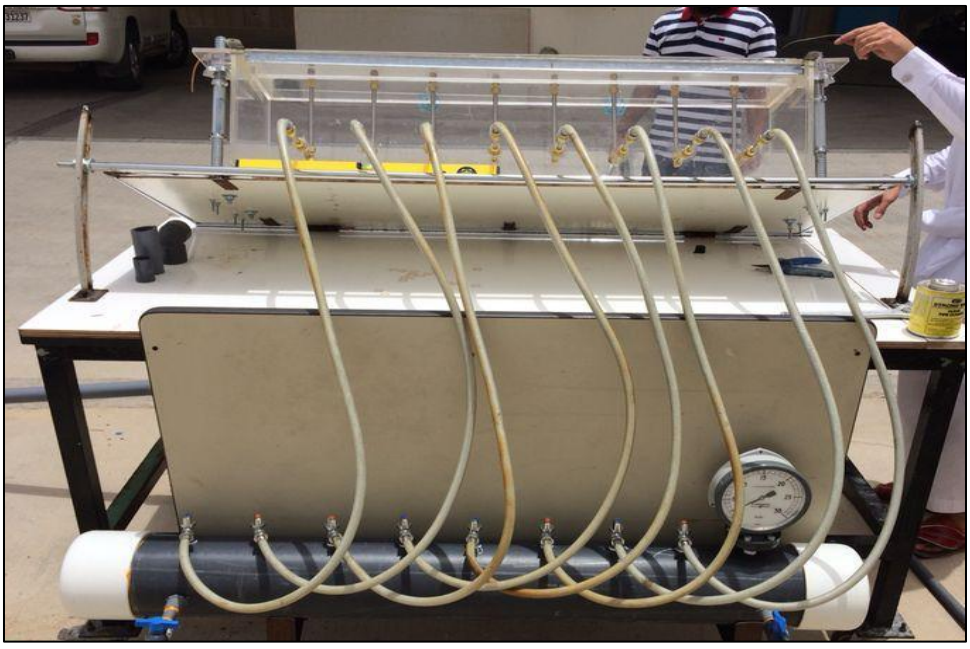

Figure 4.46 Rear view of jet cooling mechanism showing main jet header

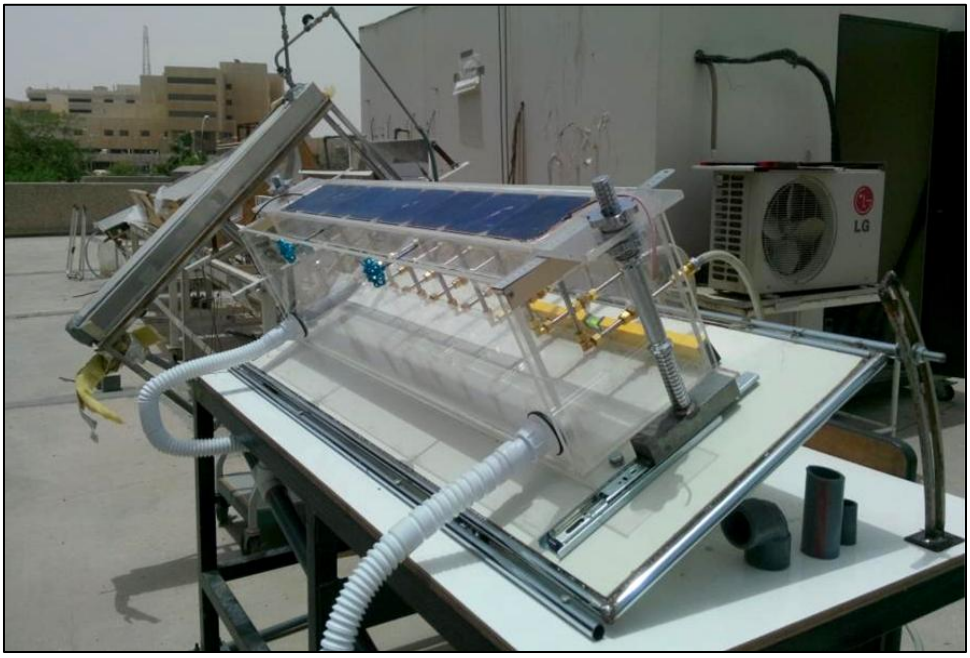

Figure 4.47 On site installation of jet impingement test setup for uniform cooling

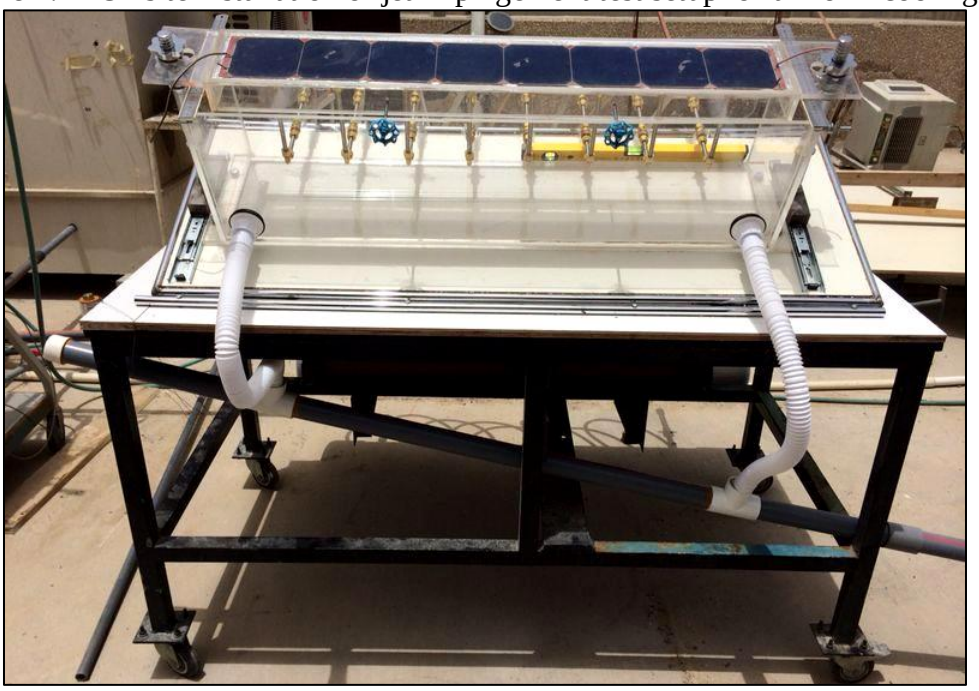

Figure 4.48 Front view of final assembly of jet impingement test system

Figure 4.49 Nozzle arrangement for uniform cooling

4.3 DATA COLLECTION AND ANALYSIS

Figure 4.50 shows the schematic for data collection of all the cooling systems with the necessary equipments required for data measurements. Data collection from the experimental setup was carried out to investigate the performance of electrical efficiency and power output from the PV strings during operation under normal concentration for uniform and non uniform cooling. Maximum power point tracker (MPPT) has been used to extract maximum power point from the IV curve. The load has been attached after MPPT to ensure proper extraction of current and voltage from the system. The charges

are then stored in the battery. Thermocouples of type K has been used in this research to measure temperature on the surface of PV strings which can be directly monitored on Data Acquisition System (DAQ). The DAQ system installed for this research is capable of monitoring and storing calculations of voltage, current, wind speed, ambient temperature, wind direction, light intensity, temperature and maximum power.

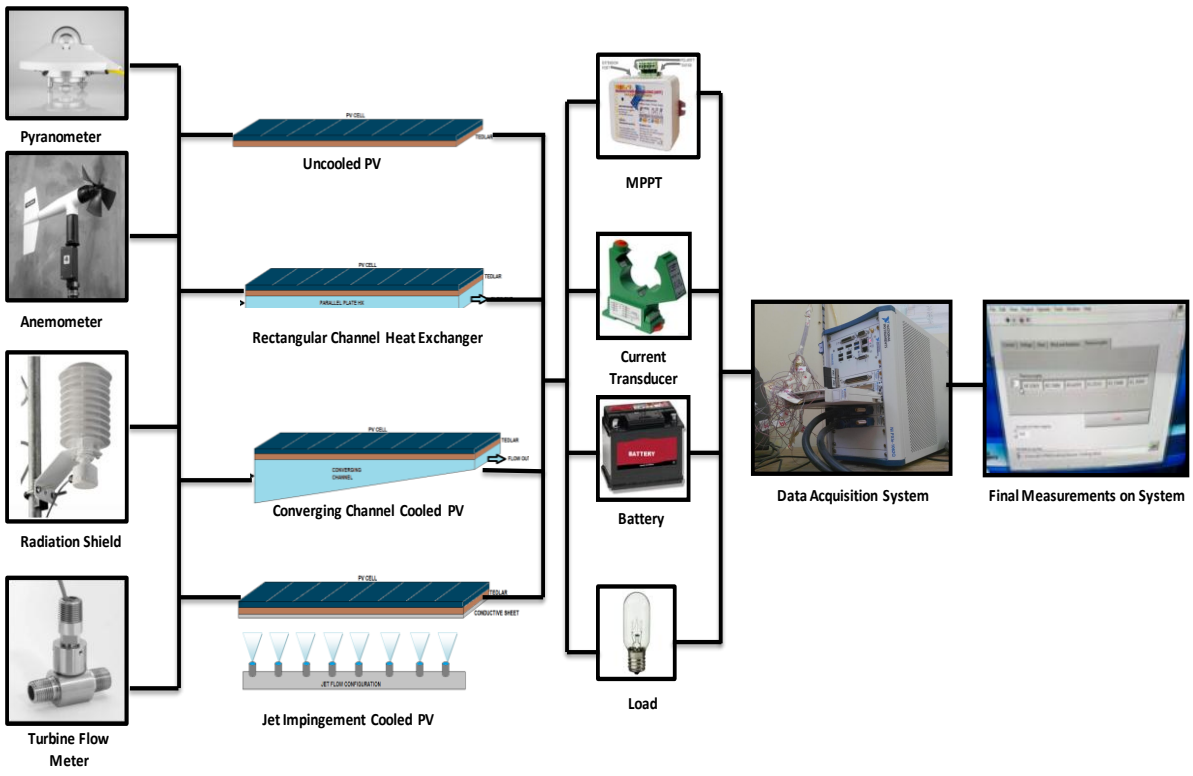

Figure 4.50 Layout of the system for four configurations

Figure 4.51 shows the layout of the system along with DAQ installed on site at Dhahran.

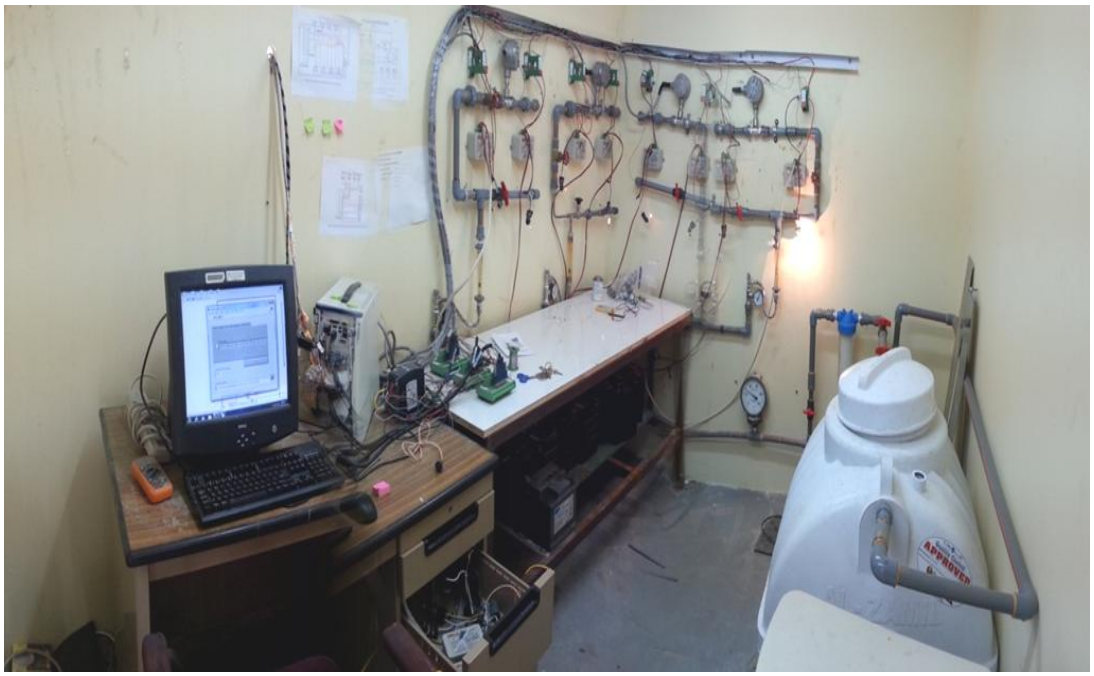

Figure 4.51 Inside View of the PV Uniform Cooling Investigation Experimental Setup

4.3.1 DAQ (Data Acquisition) System

The in-situ performance of photovoltaic strings and setup can be characterized by measuring the relationship between panel voltage, current, and power output under variable environmental situations and panel orientation. The data for the temperature of the different components was recorded by K type thermocouples. A card for measuring readings from thermocouple was inserted into DAQ as shown in Fig 4.52 and the readings were recorded automatically after specified interval of time.

Thermocouple card contains 32 input channels for analogue input. Lab View software is installed on National Instruments DAQ system and program is developed to record the experimental measurements as shown in Figs 4.52 and 4.53. Table 4.4 summarises the parameters and equipment considered.

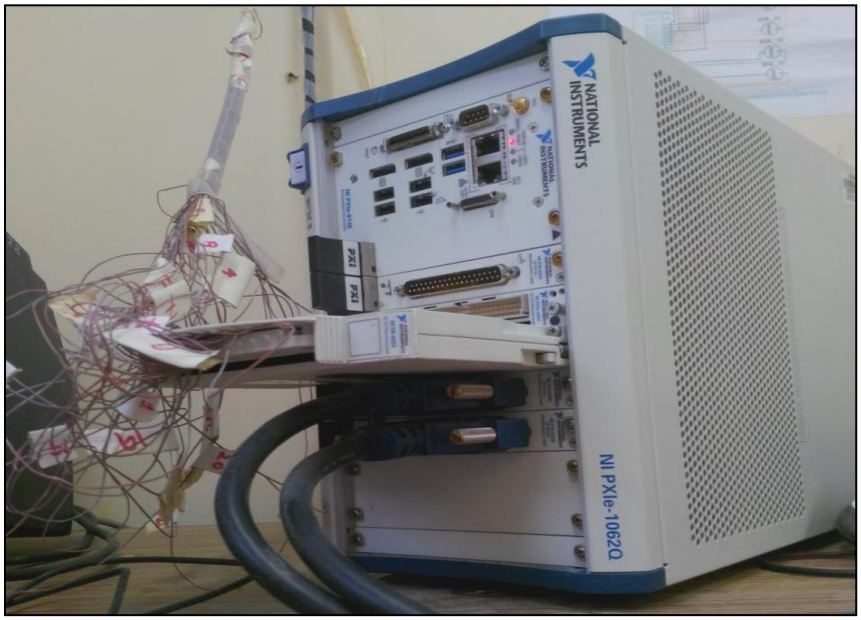

Figure 4.52 NI DAQ system showing thermocouple channel

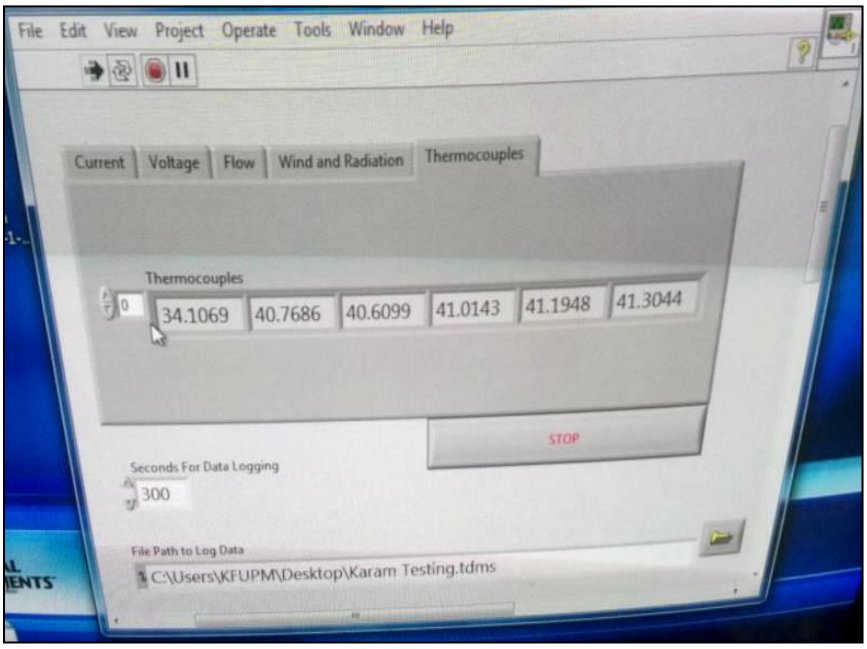

Figure 4.53 Lab view interface of experimental setup for recording measurements

Table 4.4 Main parameters and technical details considered in the study

PV Cell Specifications at Standard Test Conditions	Model	Sun Power C60
	Type	Monocrsytalline
	Geometry	125mm × 125mm
	Open Circuit Voltage (Voc)	0.680 V
	Short Circuit Current (Isc)	6.28 A
	Voltage at Maximum Power(Vmp)	0.575 V
	Current at Maximum Power (Pmp)	5.92 A
	Rated Power (Wp)	3.40 W
	Number of cells in string	8
Pyranometer	Model	CMP 22
	Voltage	0-20 mV
	Operational temperature range	-40˚C to 80˚C
Anemometer	Model	05103L Wind Monitor
Radiation Shield	Model	41382LC2 Temperature Probe
Thermocouples	Type	K
	Temperature Range	–200°Cto 1250°C
Flow Meter	Model	F-400 Series
Maximum PowerPoint Tracker	Model	SOL-1

CHAPTER 5

UNCERTAINTY ANALYSIS

An uncertainty analysis for all the test equipment involved in the measurements of the data was performed. Accuracies and ranges of the equipment were utilized to investigate the propagation of uncertainty on variable to another. The experiments were performed outside in the actual environment and bias errors were taken into account when formulating the analysis for uncertainties. When measuring the uncertainty of a measurement, bias and precision errors must be accounted for. The bias error is related to the accuracy of the measurement as well as the calibration. The precision error relates to the repeatability of the measurements. As this experiment was performed outdoors, it was very difficult to get measurements at different times with the exact same conditions. Therefore, only the bias error will be taken into consideration in the uncertainty analysis. These uncertainty values takes into consideration the maximum errors and worst case scenarios for the PV system.

Kline and McClintock [122] developed a method to calculate the bias error of calculated variables. For a calculated variable *R*, which is a function of *n* variables v_i , the uncertainty of *R*, δ_R can be found using

$$\delta_R = \left[\left(\frac{\partial R}{\partial v_1} \delta v_1 \right)^2 + \left(\frac{\partial R}{\partial v_2} \delta v_2 \right)^2 + \ldots + \left(\frac{\partial R}{\partial v_n} \delta v_n \right)^2 \right. \tag{5.1}$$

A PV string used in the research is fabricated by connecting eight C60 monocrystalline silicon solar cells in series with bottom contacts. The actual electrical specifications provided by the supplier for single C60 monocrystalline solar cell used in this research are shown below in Table 5.1.

Table 5.1Electrical parameters at standard test conditions

Open Circuit Voltage	0.680 V
Short Circuit Current	6.28 A
Maximum Power Voltage	0.575 V
Maximum Power Current	5.92 A
Rated Power	3.40 W

5.1 MEASURED VALUES

5.1.1Thermocouple Readings

The thermocouples used are type K thermocouples. They were calibrated with boiling water and repeated measurements were taken. The calibration yielded an accuracy of ±0.5 °C.

5.1.2 Voltage and Current Measurements from PV Array

The DAQ's user manual reports an accuracy of 0.01% of reading + 0.002% of range. For the voltage measurements, the range was set to -10V to 10V. The maximum expected voltage for 8 cells is around 4.6 V. The uncertainty for this particular voltage can be calculated with

$$\delta_V = (0.0001 \times reading + 0.00002 \times range) \tag{5.2}$$

$$\delta_V = (0.0001 \times 4.6V + 0.00002 \times 20V)$$

$$\delta_V = 0.00086\ V$$

To measure the current, a voltage reading is taken across a known resistance. The current is calculated from I=V/R. R is 1 ± 0.01 Ω. A maximum voltage measurement by the DAQ of 5.92 V is expected (equivalent to 5.92A current across the resistor). The measurement range is set to -10V to 10V. Using equation (5.2), the voltage measurement has an uncertainty of ±0.00046 V.

$$\delta_I = \left[\left(\frac{\partial I}{\partial V} \delta V \right)^2 + \left(\frac{\partial I}{\partial R} \delta R \right)^2 \right]^{\frac{1}{2}} \tag{5.3}$$

$$\delta_I = \left[\left(\frac{1}{R} \delta V \right)^2 + \left(-\frac{V}{R^2} \delta R \right)^2 \right]^{\frac{1}{2}}$$

$$\delta_I = \left[\left(\frac{1}{1\Omega} 0.00046V \right)^2 + \left(-\frac{5.92V}{(1\Omega)^2} 0.01 \right)^2 \right]^{\frac{1}{2}} = 0.059\ \text{A}$$

5.1.3 Irradiance

Kipp & Zonen pyranometers were used to measure the total and diffuse incident radiation. The output of voltage is proportional to the incident radiation with 7.0 μV/Wm^2 and 14.0 μV/Wm^2. For the 14.0 μV/Wm^2 pyranometer, the maximum expected output is 14.0 mV (for 1000 W/m^2).

For a range of -31 to 31mV, this gives a DAQ error of 0.946 μV. It is calculated by using the digital to analog converting relation. The resolution is calculated by dividing full scale voltage range with number of voltage intervals (2^M) where m shows the number of bits used in the system.

The pyranometer has a 1% error. The total measurement error is

$$\frac{\delta_G}{G} = \left[\left(\frac{\delta V}{V} \right)^2 + \left(\frac{\delta V_{DAQ}}{V_{DAQ}} \right)^2 \right]^{\frac{1}{2}} = \left[(0.01)^2 + \left(\frac{0.946 \times 10^{-3}}{14.0} \right)^2 \right]^{\frac{1}{2}} = 0.01 \tag{5.4}$$

Therefore, the pyranometer uncertainty is $\delta_G = 1000\,W/m^2 \times 0.01 = 10\,W/m^2$

5.1.4 Wind Speed

The anemometer has an accuracy of 0.3m/s or 1% of reading. The anemometer gave a 0-5V signal for a 0-1000m/s wind speed. For a typical value of 4m/s, the signal is 0.08V.

$$\frac{\delta_{V_{wind}}}{V_{wind}} = \left[\left(\frac{\delta V}{V}\right)^2 + \left(\frac{\delta V_{DAQ}}{V_{DAQ}}\right)^2\right]^{\frac{1}{2}} = \left[\left(\frac{0.3}{4}\right)^2 + \left(\frac{0.076\times10^{-3}}{80}\right)^2\right]^{\frac{1}{2}} = 0.07 \tag{5.5}$$

Therefore, the maximum wind speed uncertainty $\delta_{V_{wind}} = 0.07 \times 4m/s = 0.28\,m/s$

5.1.5 Ambient Temperature

The thermistor used for the ambient air temperature measurements has an accuracy of 0.3°C.

The accuracy including the DAQ is:

$$\delta_{Tamb} = 100\frac{^\circ C}{V} \times \left[\left(\delta_V\right)^2 + \left(\delta_{V_{DAQ}}\right)^2\right]^{\frac{1}{2}} = 100\frac{^\circ C}{V}\left[\left(0.003\right)^2 + \left(15.2\times10^{-6}\right)^2\right]^{\frac{1}{2}} = 0.1^\circ C \tag{5.6}$$

5.1.6 PV Power Output

The power from all the PV cells is taken as:

$$P_{elec} = VI \tag{5.7}$$

As mentioned earlier, the maximum expected current is 5.92A, and the maximum expected voltage is 4.6 V. The power will therefore be 27 W. Taking the errors for current and voltage calculated earlier, the maximum uncertainty or power for worst case scenario can be calculated with:

$$\begin{aligned} \delta_{P_{elec}} &= \left[\left(\frac{\partial P_{elec}}{\partial V} \delta V \right)^2 + \left(\frac{\partial P_{elec}}{\partial I} \delta I \right)^2 \right]^{\frac{1}{2}} \\ &= \left[\left(I \times \delta V \right)^2 + \left(V \times \delta I \right)^2 \right]^{\frac{1}{2}} \\ &= \left[\left(5.92 \times 0.00086 \right)^2 + \left(4.6 \times 0.059 \right)^2 \right]^{\frac{1}{2}} = 0.27\,W \end{aligned} \tag{5.8}$$

CHAPTER 6

RESULTS AND DISCUSSION

In this section the experimental and numerical results will be discussed for various parameters which determine the overall performance of the uniform and non uniform cooling of photovoltaic systems under normal concentration subjected to the meteorological conditions measured at Dhahran, Saudi Arabia In the first half of the chapter several numerical and experimental results of different cooling techniques of PV system will be highlighted and discussed in detail. Then in the second half comparative study between these cooling configurations will be discussed.

6.1 EXPERIMENTAL RESULTS OF INPUT PARAMETERS

The main input parameters for the models are the meteorological data in the form of ambient temperature, wind speed, incident radiation, flow rate of coolant, inlet temperature of fluid and solar cell parameters. From these data the system model is capable of evaluating the performance characteristic of PV panel. The result from thermal model is given input to the electrical model to calculate the conversion efficiency and power output. All these input variables have been collected at Dhahran, latitude 26.5°, for the months of June and December 2014. The ambient temperature for the test days is shown in Figure 6.1 . The variation of incident solar radiation received by the panel surface during the test days is shown in Figure 6.2. As the day progresses the incident radiation on the panel increases with an increase in the zenith angle and position of sun. Figure 6.3 and Figure 6.4 show wind speed and absorbed radiation calculated from optical and radiation model.

Experimental measurements and analysis for the days of June and December has been presented. For the purpose of comparison of results from modeling and experiments, a root mean square percentage deviation (RMS %) has been evaluated by the following equation [11,123]

$$RMS\% = \sqrt{\frac{\sum[100 \times (X_{sim,i} - X_{\exp,i}) / X_{sim,i}}{n}} \tag{6.1}$$

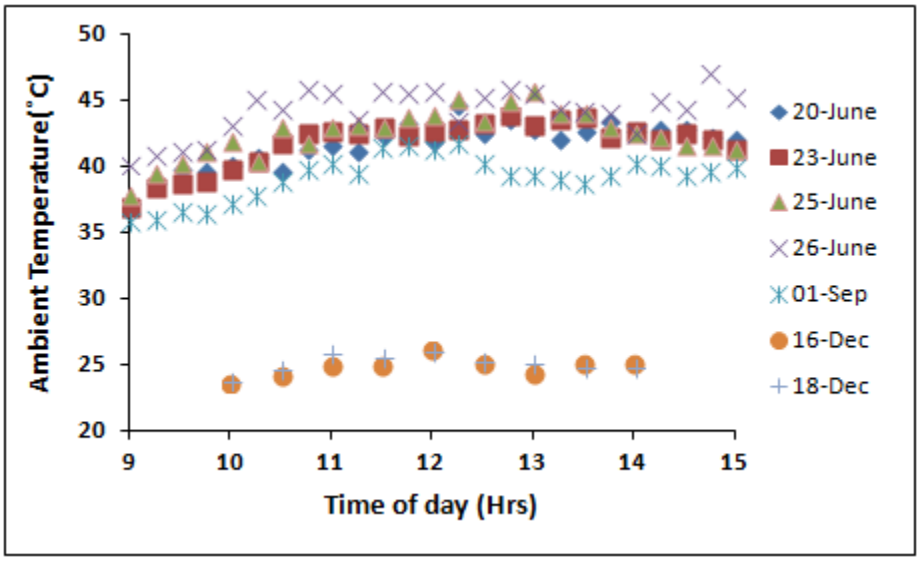

Figure 6.1 Variation of ambient temperature during test days

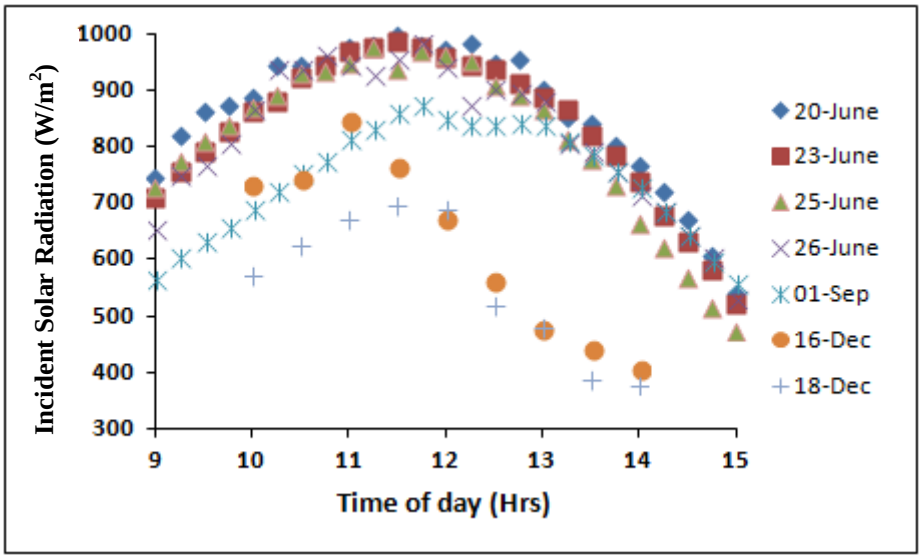

Figure 6.2 Variation of incident solar radiation during test days

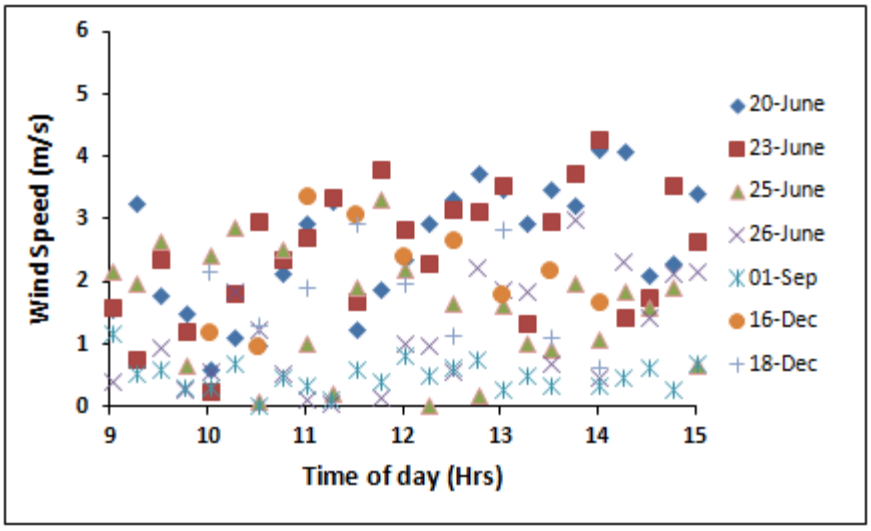

Figure 6.3 Variation of wind speed during test days

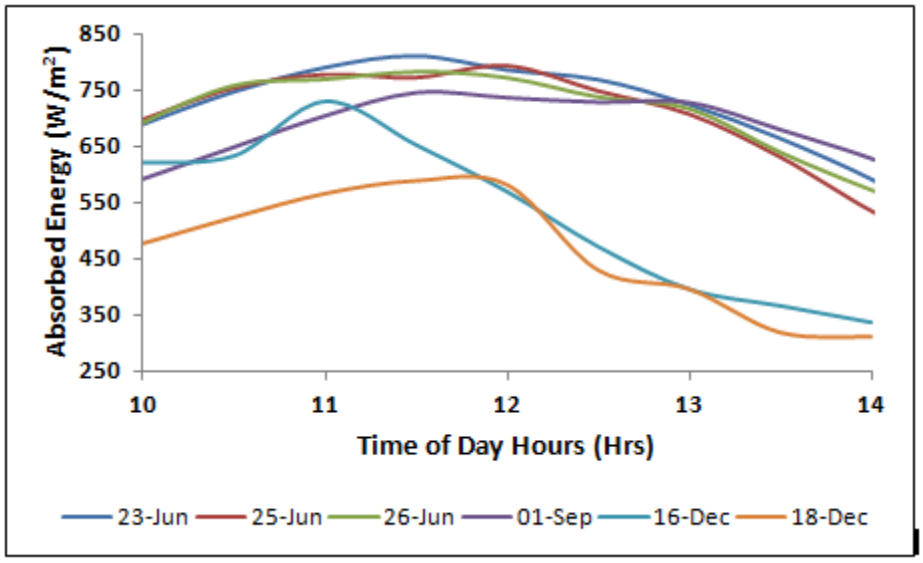

Figure 6.4 Absorbed radiation modeled during test days

6.2 UNCOOLED PV STRING RESULTS

For the purpose of comparison and as a base case, an uncooled PV string was modeled and experimental investigation was carried out in the climate of Dhahran. Experimental and simulation studies were carried out for the month of June and December. Figure 6.5 shows the variation of average PV surface temperature by an uncooled PV string. It is evident that not cooling the string has shown significant reduction in results. For uncooled PV string, maximum temperature of 71˚C was reported for 23rd June whereas the maximum cell temperature of 76˚C was recorded for 25th June. In the absence of uniform cooling, the operating cell temperature range of PV string is above the safe limit of operation. Therefore it is very critical to the life and safety of the PV cell to operate with uniform cooling. Modeling and experimental data shows fair agreement with root mean square percent deviation not exceeding 4 % for both days and total experiments for measurements in June.

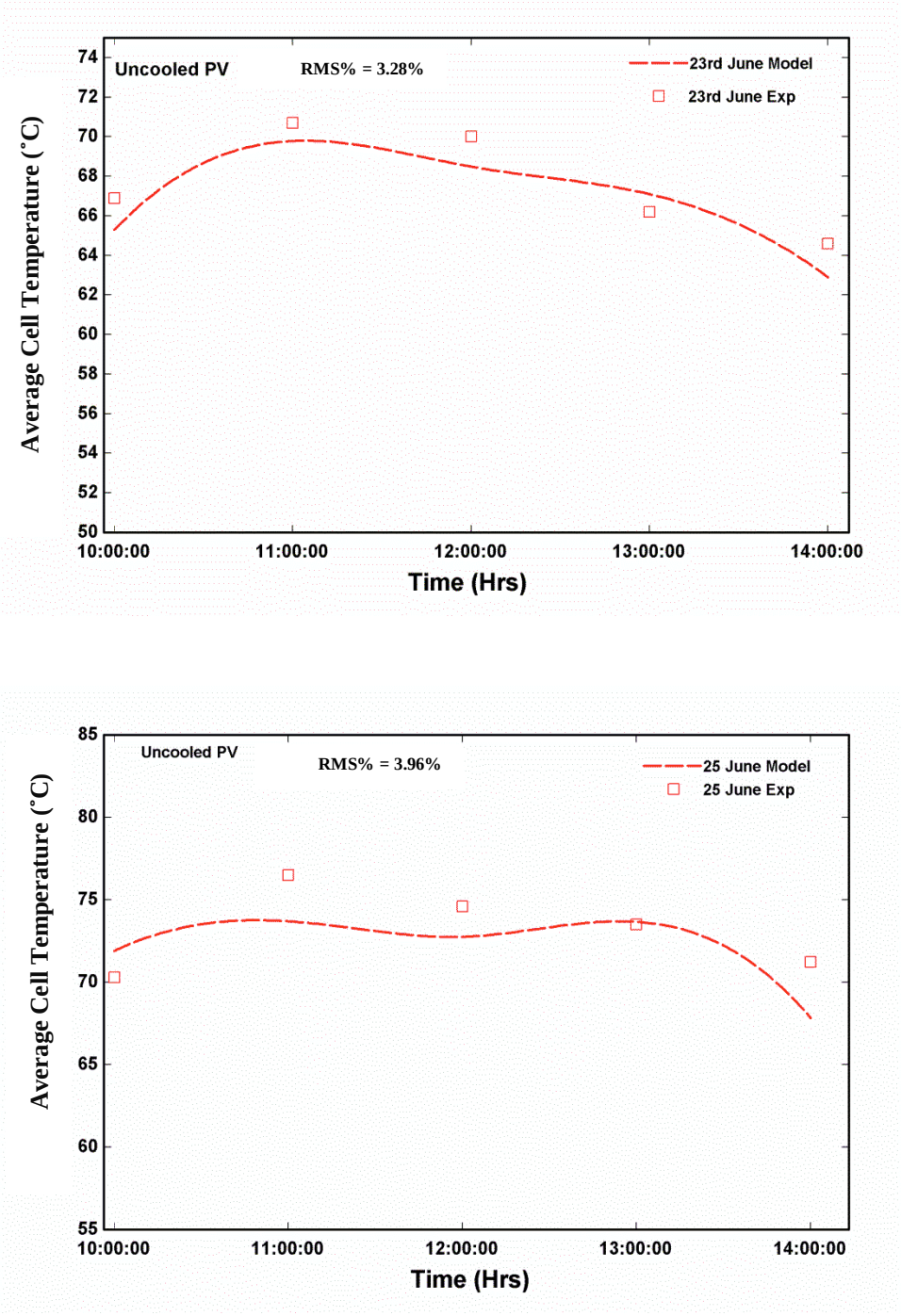

Figure 6.5 Variation of average cell temperature for uncooled PV during test days

In order to analyze the electrical performance of the photovoltaic cells, seven parameters model is used in the current study. After the estimation of seven parameters the electrical performance of the PV system can be analyzed by giving absorbed radiation and the cell temperature as the input parameters. Electrical power output for two test days for the data of June is shown in Figure 6.6. Experimentally, the power output was reported as low as 9.4W for the case of 25th June. For 23rd June, the minimum power output resulted was 8.1W. The maximum power reported were 11.2W for 25th June and 12.3 W for 23rd June. The power results show good agreement between experimental and modeling results with maximum root means square deviation of 3.6% for the case of uncooled PV system. Figure 6.7 shows the comparison between the model and experimental conversion efficiency. The maximum experimental efficiency was 9.8 % for the case of 23rd June. For 25th June, the experimental efficiency was 9.2 %. The results show good agreement between experimental and modeling results with maximum root means square deviation of 3.71 % for the case of uncooled PV system.

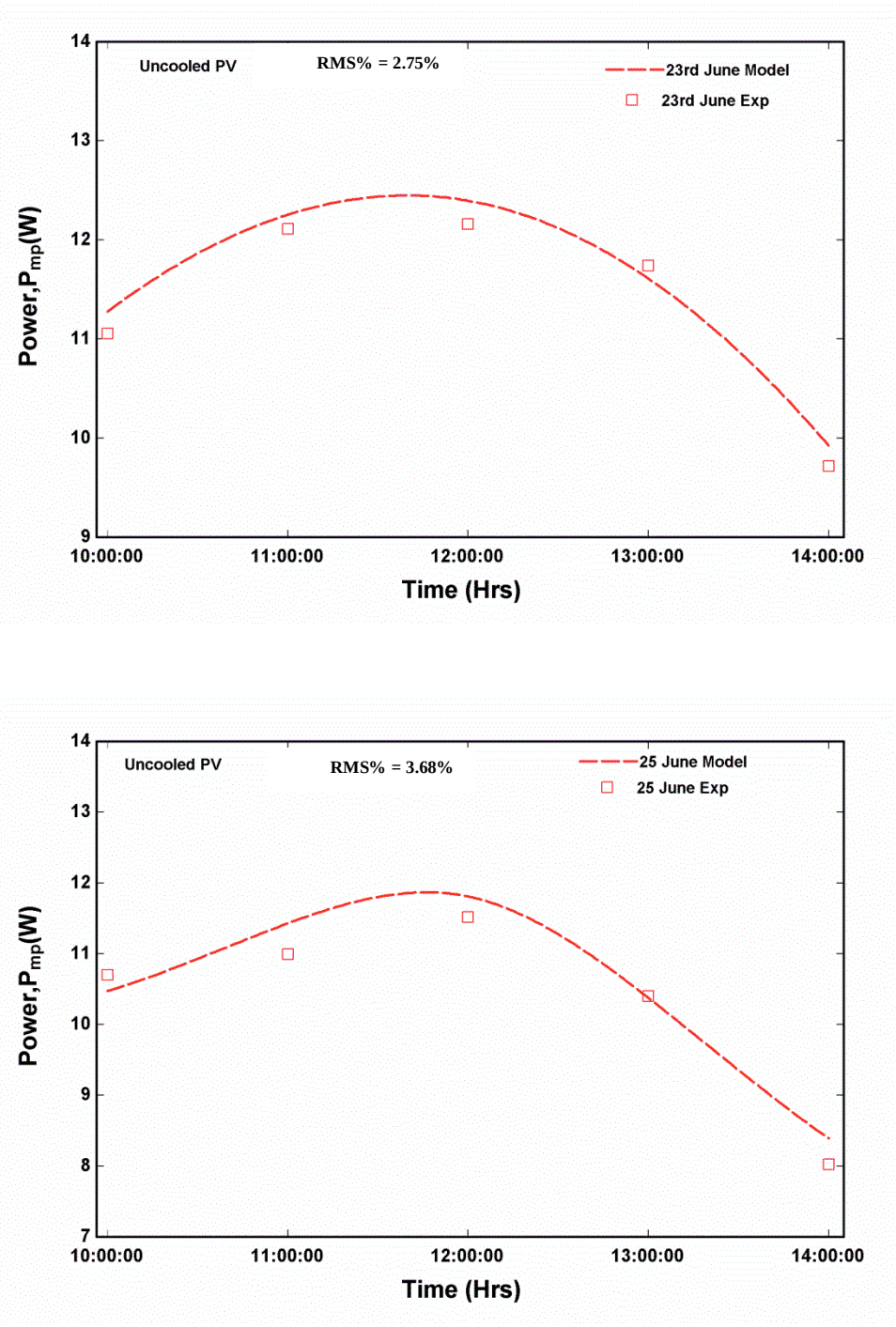

Figure 6.6 Variation of power for uncooled PV during test days

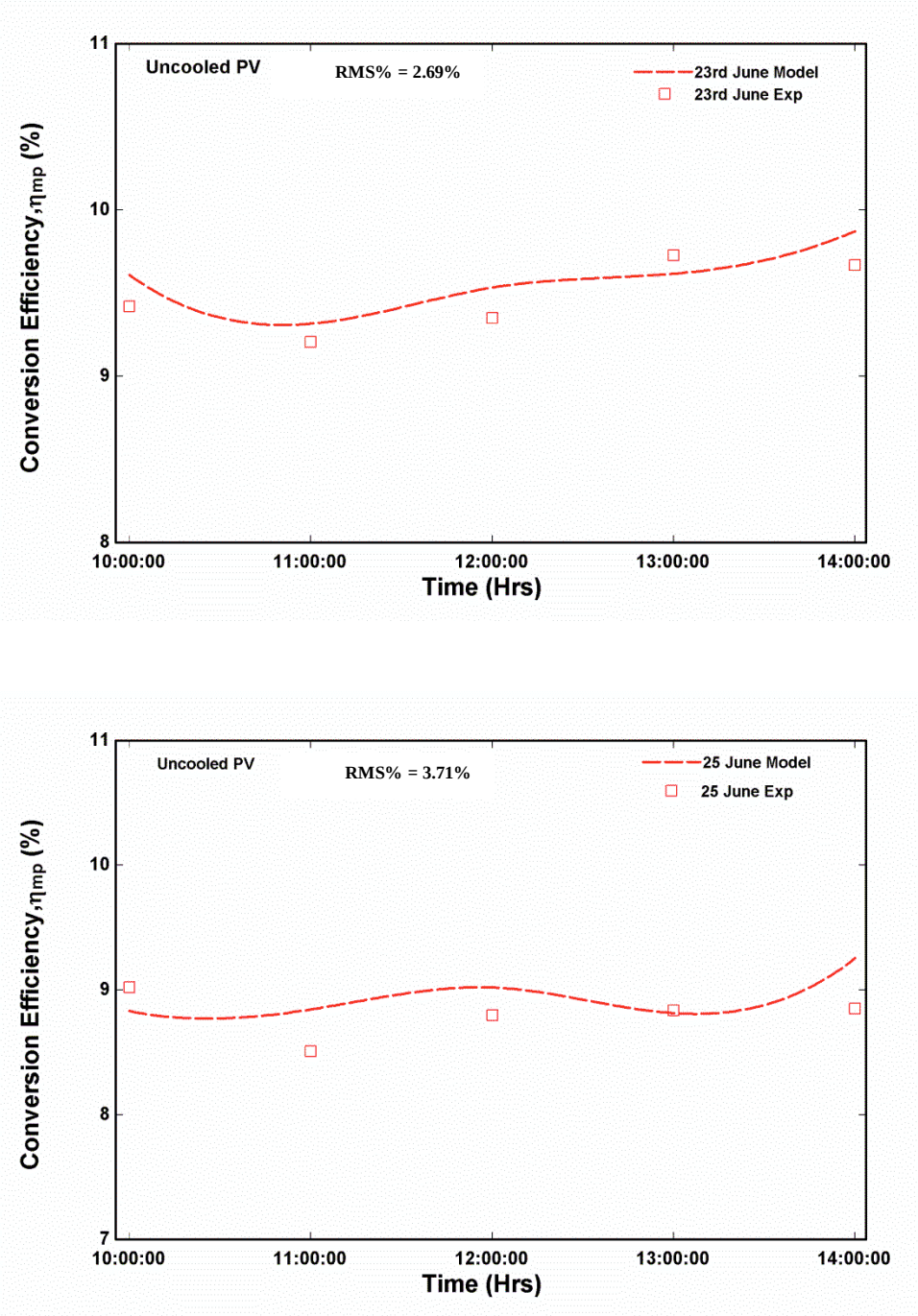

Figure 6.7 Variation of conversion efficiency for uncooled PV during test days

Figure 6.8 and Figure 6.9 shows the modeling and experimental measurements for the month of December. Figure 6.8 shows the average cell temperature for an uncooled PV for December data. In addition ,validation of modeling and experimental data shows the maximum RMS value of 4.7 which shows a fair agreement between readings. The maximum value of average cell temperature for winter season day is 45˚C which is still high than the standard operating temperature of PV system of 25˚C. Figure 6.9 shows the graphs for the power measurements for an uncooled PV system. The maximum value of power experiments is approximately 12.8 W. The maximum RMS value of the power curves is 4.8% showing a fair agreement between model and experiments.

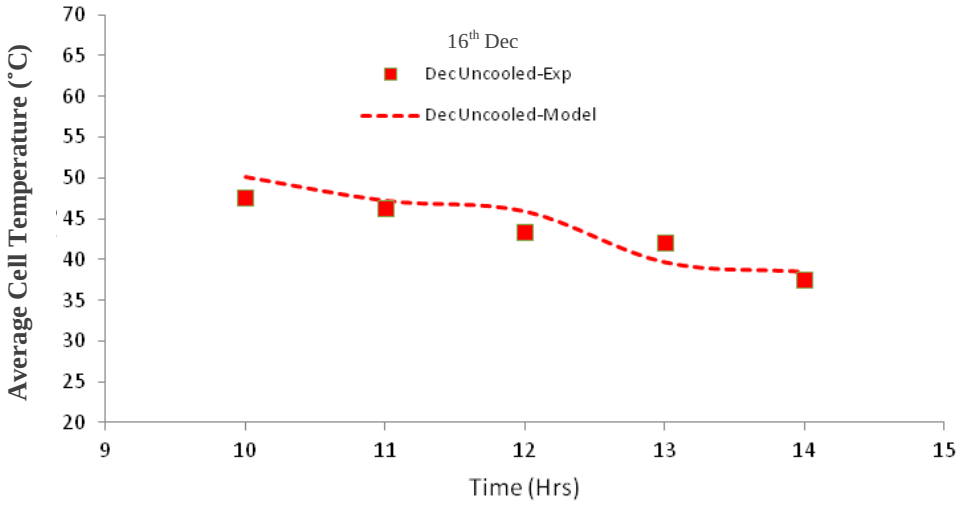

Figure 6.8 Variation of average cell temperature for uncooled PV for December

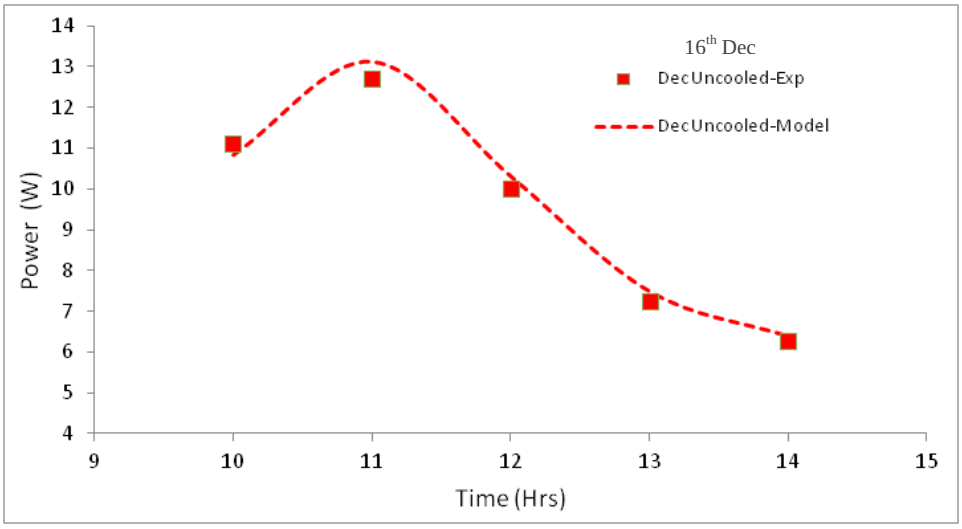

Figure 6.9 Variation of power output for uncooled PV for December

6.3 RECTANGULAR CHANNEL COOLING RESULTS

Rectangular channel heat exchanger was selected for non-uniform cooling of PV string .This is due to temperature variations present on the surface as the fluid has to pass through the back of the solar cell along the length of heat exchanger thereby resulting in non-uniform distribution of temperature. Figure 6.10 shows the variation of average PV surface temperature by rectangular channel heat exchanger (RHX) cooled PV string for the month of June. It is evident that the application of cooling has shown significant results for the conditions of Saudi Arabia. Cooling the PV string by rectangular channel resulted in temperature as high as 47 ˚C for 23rd June and 46.1˚C for 25th June. Modeling and experimental data shows fair agreement with root mean square percent deviation not exceeding 3.9 % for both days and total experiments for June. By using

rectangular channel cooling, PV string has been cooled by reducing the cell temperatures but at the expense of non-uniform temperature distribution.

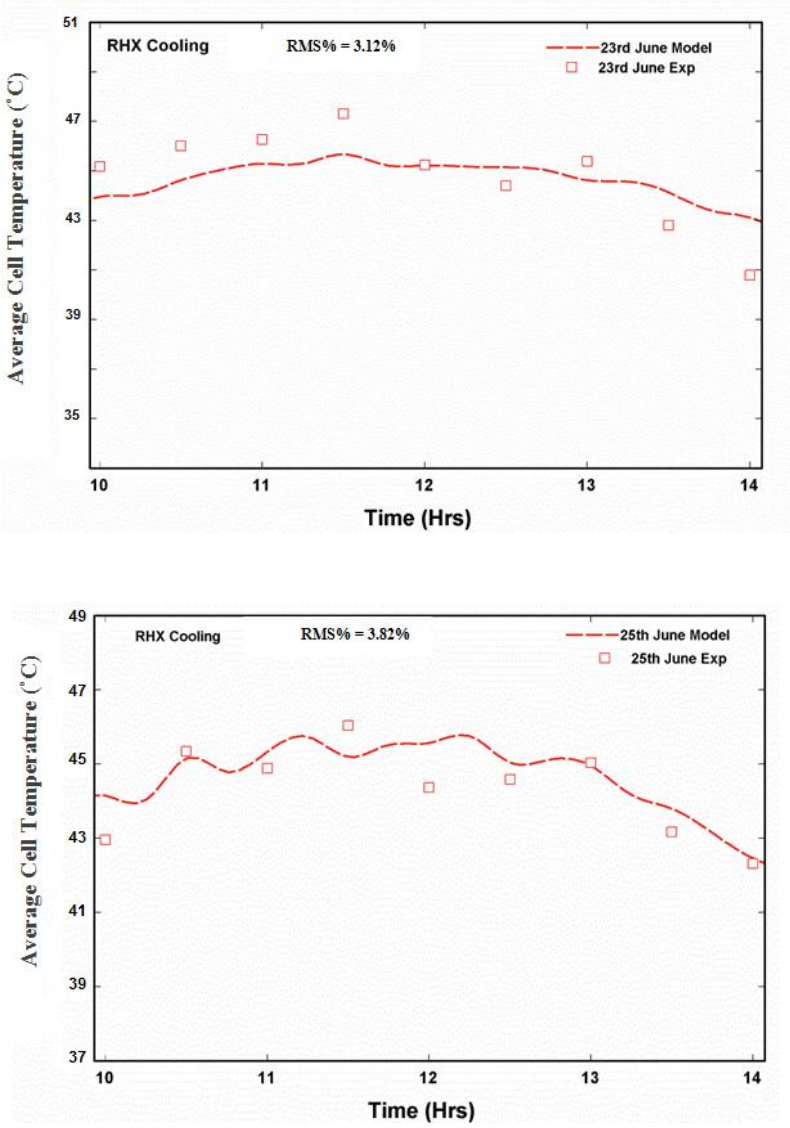

Figure 6.10 Variation of average cell temperature for rectangular channel cooled PV during test days

After the estimation of seven parameters the electrical performance of the PV system can be analyzed by giving absorbed radiation and the cell temperature as the input parameters. Electrical power output for two test days is shown in Figure 6.11. Experimentally, the maximum power output achieved was 16.7W for the case of 25th June. For 23rd June, the maximum power output resulted was 17.0W experimentally. The results show good agreement between experimental and modeling results with maximum root means square deviation of 3.07%. Figure 6.12 shows the comparison between the model and experimental conversion efficiency. The maximum experimental efficiency was 13.1 % for the case of 23rd June. For 25th June, the experimental efficiency was 12.4 %. The results show good agreement between experimental and modeling results with maximum root means square deviation of 2.61 %.

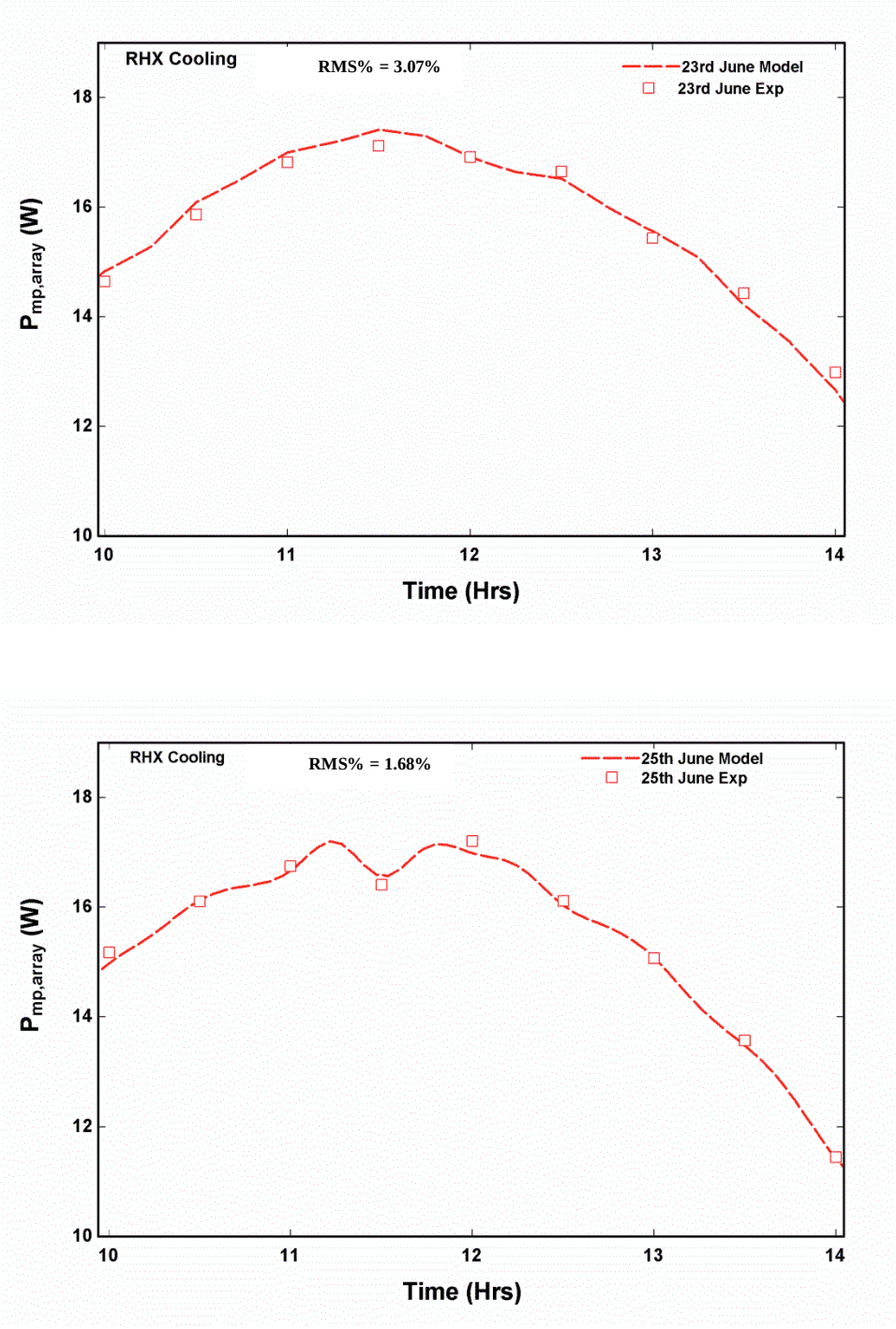

Figure 6.11 Variation of power for rectangular channel cooled PV during test days

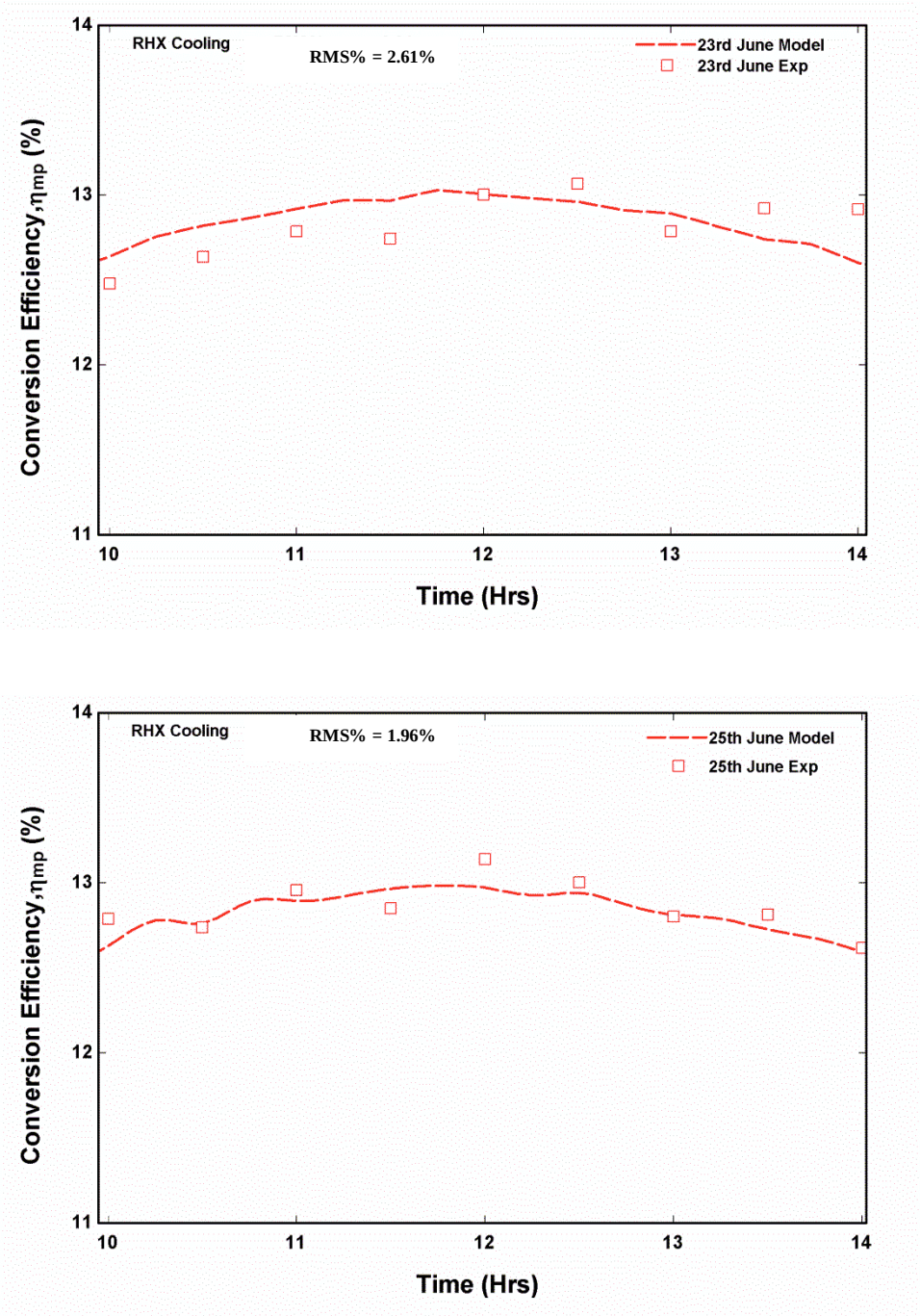

Figure 6.12 Variation of conversion efficiency for rectangular channel cooled PV during test days

6.4 CONVERGING CHANNEL COOLING RESULTS

6.4.1 Converging Channel Modeling Results

The effect of converging angle on the thermal performance of PV is studied using CFD. The objective is to achieve uniform cell temperature and to cool the cells as much as possible. An analysis was performed to obtain the optimum geometry at which there is a lesser variation of temperature resulting in almost constant temperature profile. The temperature characteristics of non-uniformity were considered in the evaluation of the model. Seven different geometries based on selected converging angles, from 0˚-10˚ were selected and simulated using the boundary conditions. For the modeling, the inlet cross sectional area of heat exchanger is varied while keeping the exit section and length constant. As the converging angle increases, the cross sectional area increases and the inlet velocity decreases, since flow rate has been kept constant for this simulation.

Standard deviation and variance was calculated for all the temperature profiles to evaluate the uniformity across the PV string. Figure 6.13 shows the effect of changing the converging angle on the surface temperature of PV cells whereas Figure 6.14 highlights the standard deviation and variance of the temperature non uniformity on the PV string. One degree angle has the second best performance. Ten degree angle has the highest temperature difference, which increases most rapidly with the converging angle.

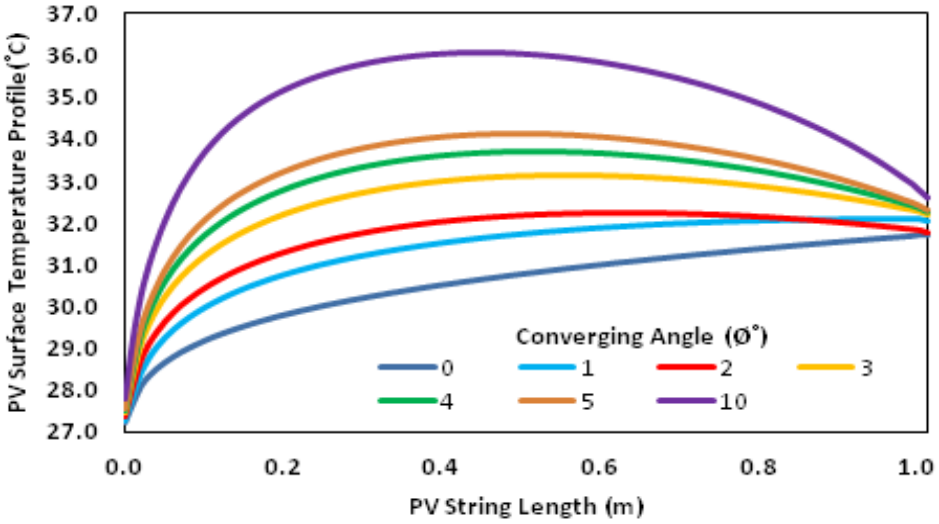

Figure 6.13 Effect of converging angle on PV surface temperature

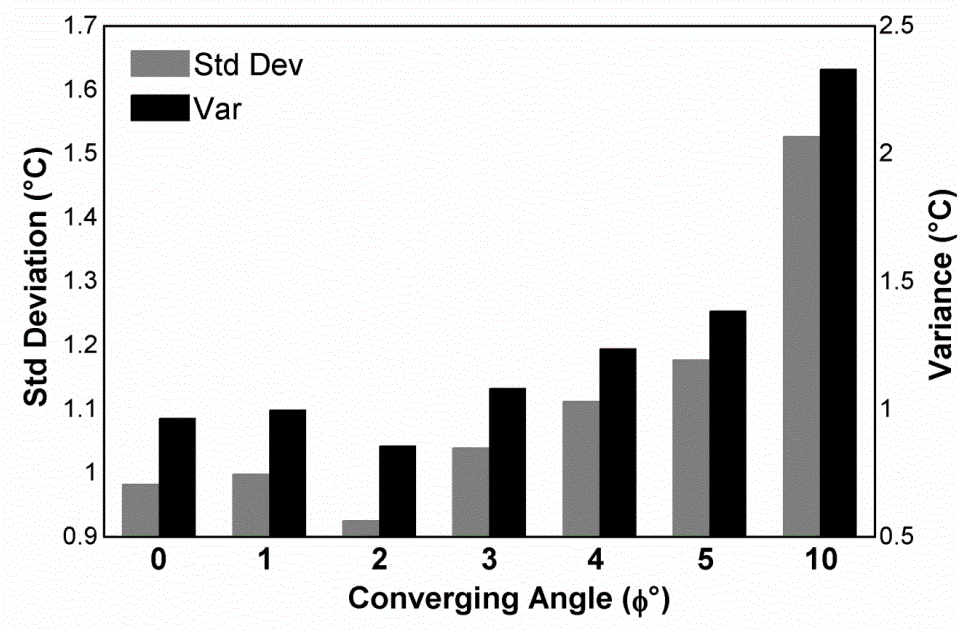

Figure 6.14 Standard deviation and Variance on PV surface temperature for converging

It can be observed from Figure 6.14, that the variance and standard deviation increases with an increase in converging angle. Also it should be noted that the best case temperature uniformity is for the case of two degree with low average cell temperature. The minimum amount of standard deviation and variance for PV surface temperature has been achieved for the case of two degree angle with one degree at second rank. The worst thermal performance in terms of temperature distribution is of a ten degree angle with the highest average cell temperature.

Temperature at the top wall has been compared for all the cases and contours are shown on Figure 6.15. At zero degree, the temperature of the fluid keeps on increasing till it leaves the heat exchanger. This is due to the fact that the velocity profile remains constant when becomes fully developed hence it takes the same amount of heat from the top plate and temperature rises with constant rate as shown by Figure 6.13 and Figure 6.15.As the angle increases, the velocity decreases and ten degree case has the lowest velocity at the inlet. With lower velocity, the amount of heat absorbed by the fluid wall becomes low which increases the temperature of the cell. Moreover, as the fluid moves towards exit, its cross sectional area decreases resulting in higher velocity and higher heat transfer coefficient. This results in decrease of wall temperature after attaining the maximum temperature at the localized regions as shown by Figure 6.13 and Figure 6.15. The ten degree has the maximum average cell temperature and non-uniformity whereas

the two degree case was found to yield higher temperature uniformity and lower average cell temperature.

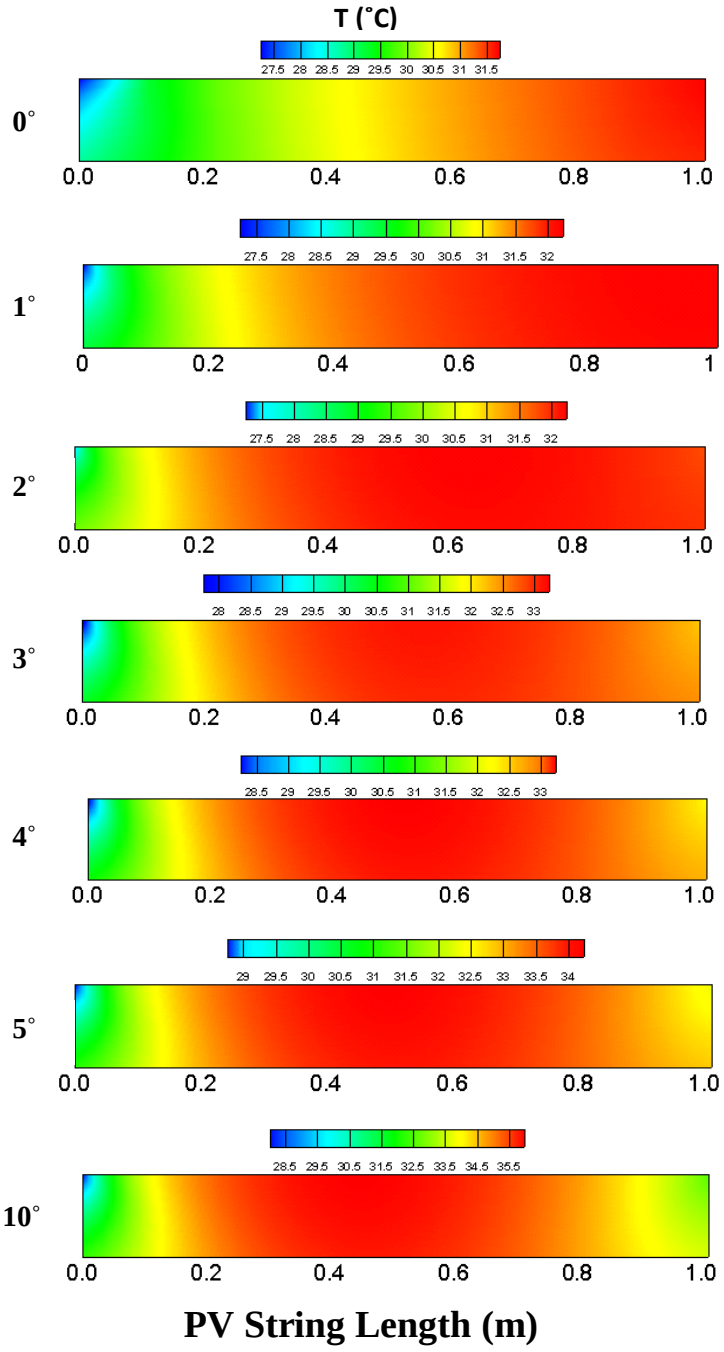

Figure 6.15 Contour plot of top surface of PV string showing temperature distribution

6.4.2 Converging Channel Experimental and Modeling Comparison

Figure 6.16 shows the variation of PV surface temperature by converging channel heat exchanger cooled PV string. It shows that by employing the converging channel, PV surface temperature is approximately uniform at the times of data collection. This figure shows the variation of the PV surface temperature by converging channel heat exchanger cooled PV string and the readings from eight thermocouples installed onto each cell. By employing the converging channel, the PV surface temperature is approximately uniform at the five hourly instants of data collection from 10:00 AM to 2:00 PM as shown by the modeling and experimental values in Fig 15. For the month of June, PV surface temperature profile showed higher readings varying in the range of 40˚C-45˚C whereas these values were reduced down to the range of 31˚C-36˚C for the month of December. This reduction in cell temperature of cooled system is due to the reduction of ambient temperature and incident radiation in the month of December. There is a fair agreement between modeling and experimental results with maximum RMS error of 6.08%.

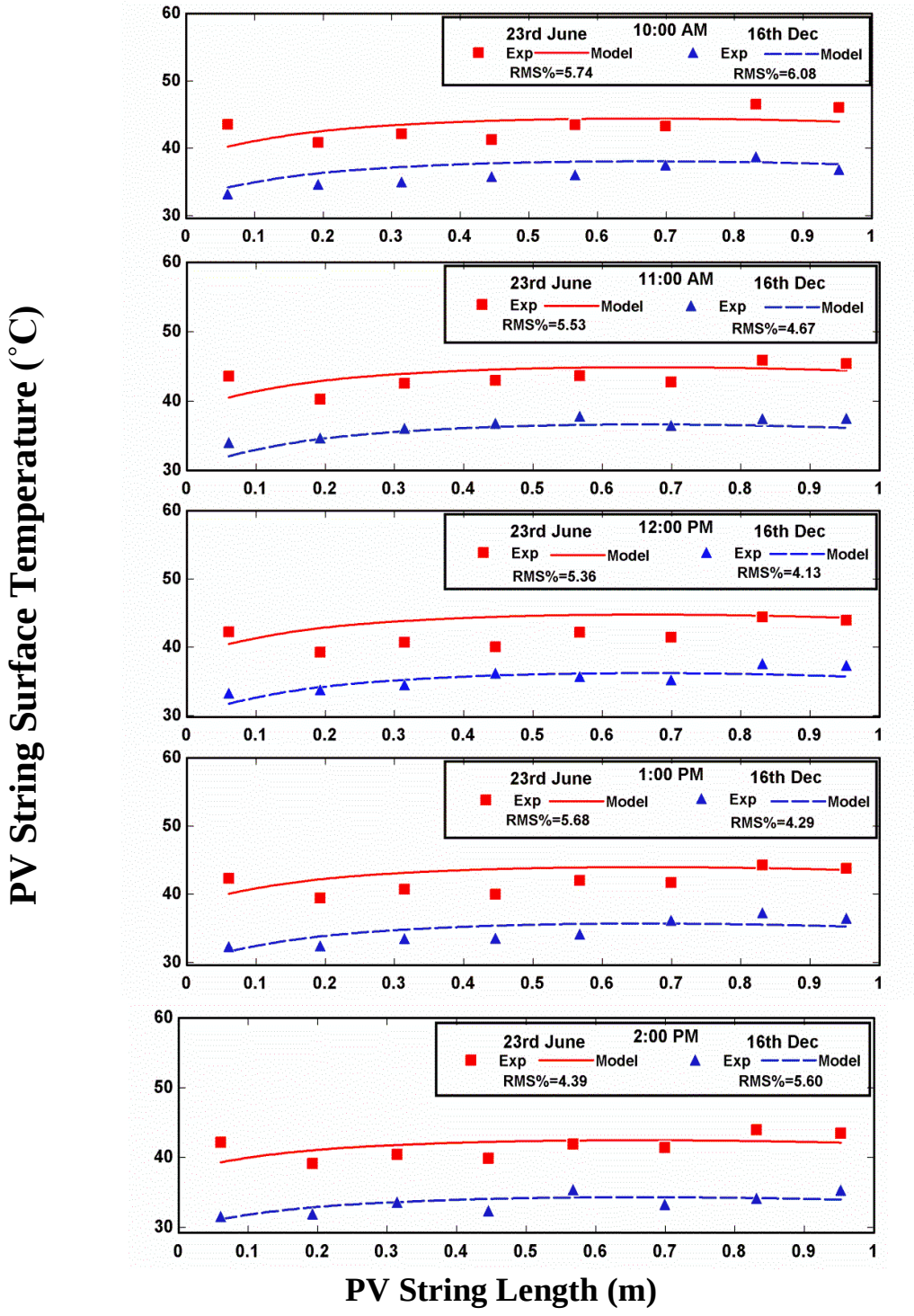

Figure 6.16 PV surface temperature profile comparison for converging PV string.

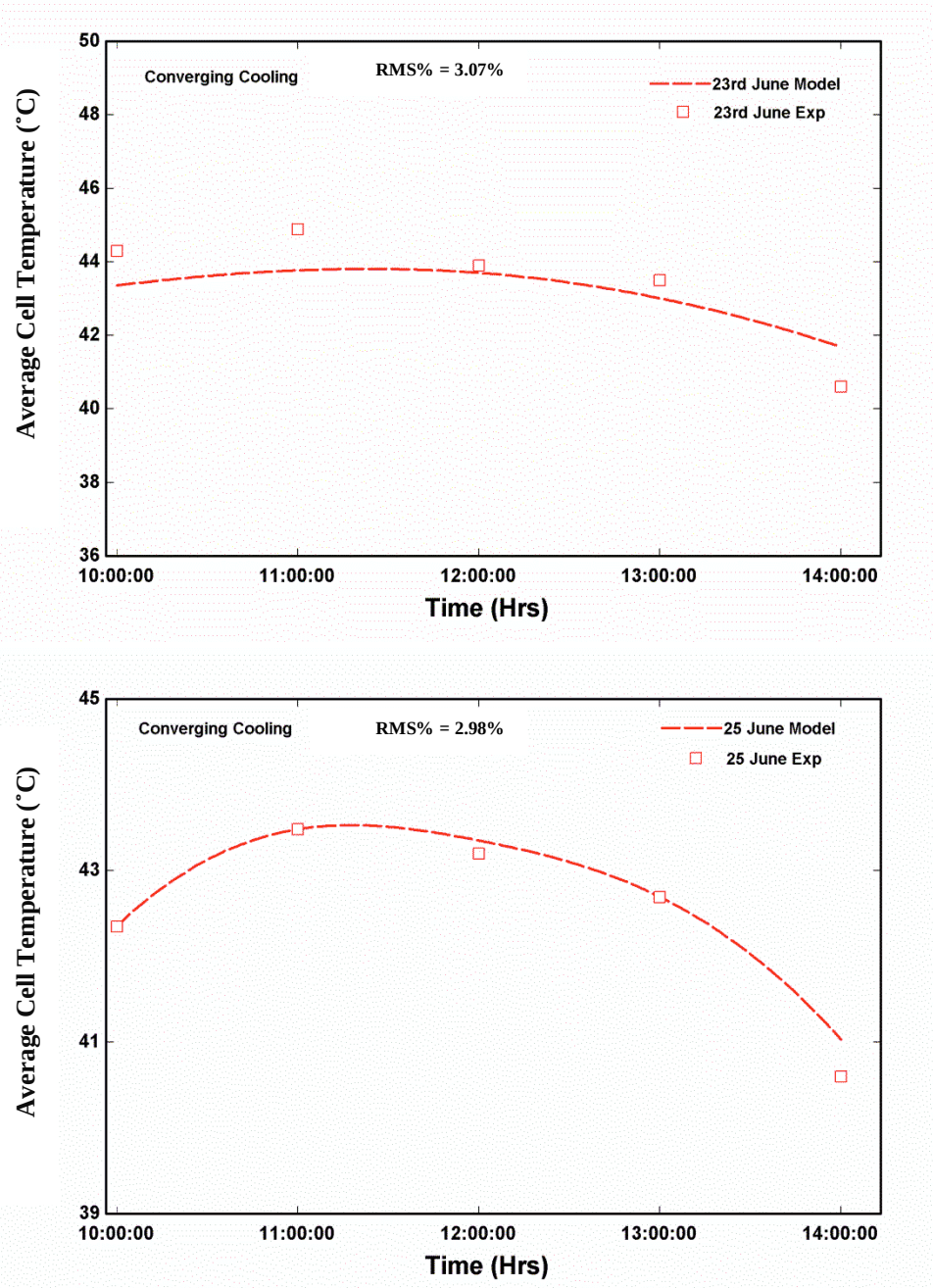

Figure 6.17 Variation of average cell temperature for converging PV string during test days

Figure 6.17 shows the variation of average cell temperature during the test days for the month of June. Cooling of PV string by converging channel resulted in temperature as low as 41˚C for 23rd June and 40.5 ˚C for 25 June. Modeling and experimental data shows fair agreement with root mean square percent deviation not exceeding 4 % for both days and total experiments. Figure 6.18 shows the temperature non-uniformity arising on the surface of PV panel. Non-uniformity from modeling resulted in 4.1˚C as an average whereas experimental results result an average of 5.3˚C.

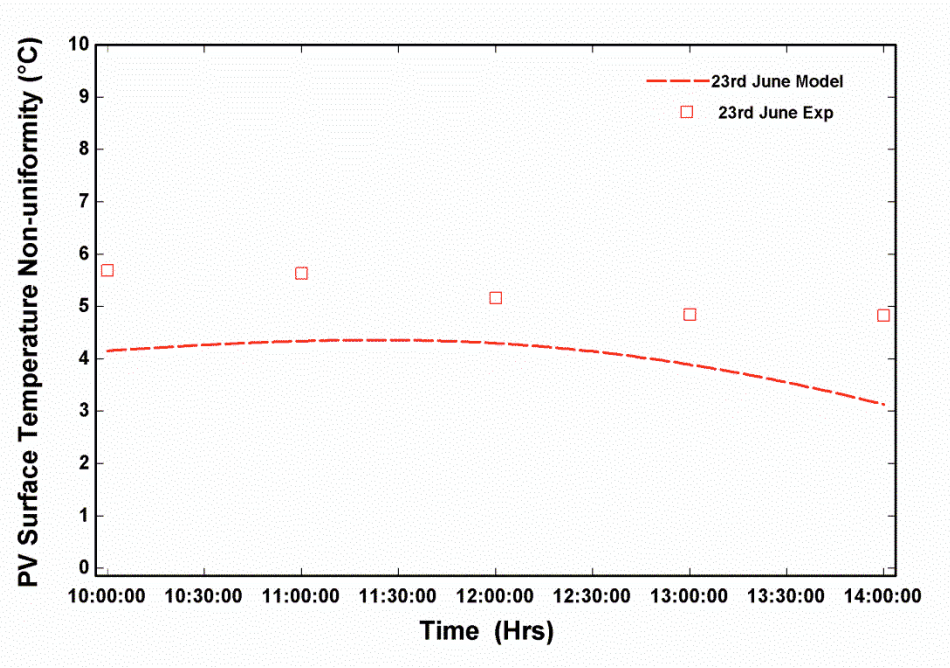

Figure 6.18 Non-uniformity on PV surface for converging cooling during test days

Electrical power output and numerical validation for two test days in June is shown in Figure 6.19. The maximum power output achieved was 16.6W for the case of 25th June. For 23rd June, the maximum power output resulted was 16.2W. The results show good agreement between experimental and modeling results with maximum root means square deviation of 1.26%. Figure 6.20 shows the comparison between the model and experimental conversion efficiency. The maximum experimental efficiency was 12.6 % for the case of 25th June. For 23rd June, the experimental efficiency was 12.5 %. The results show good agreement between experimental and modeling results with maximum root means square deviation of 1.25 %.

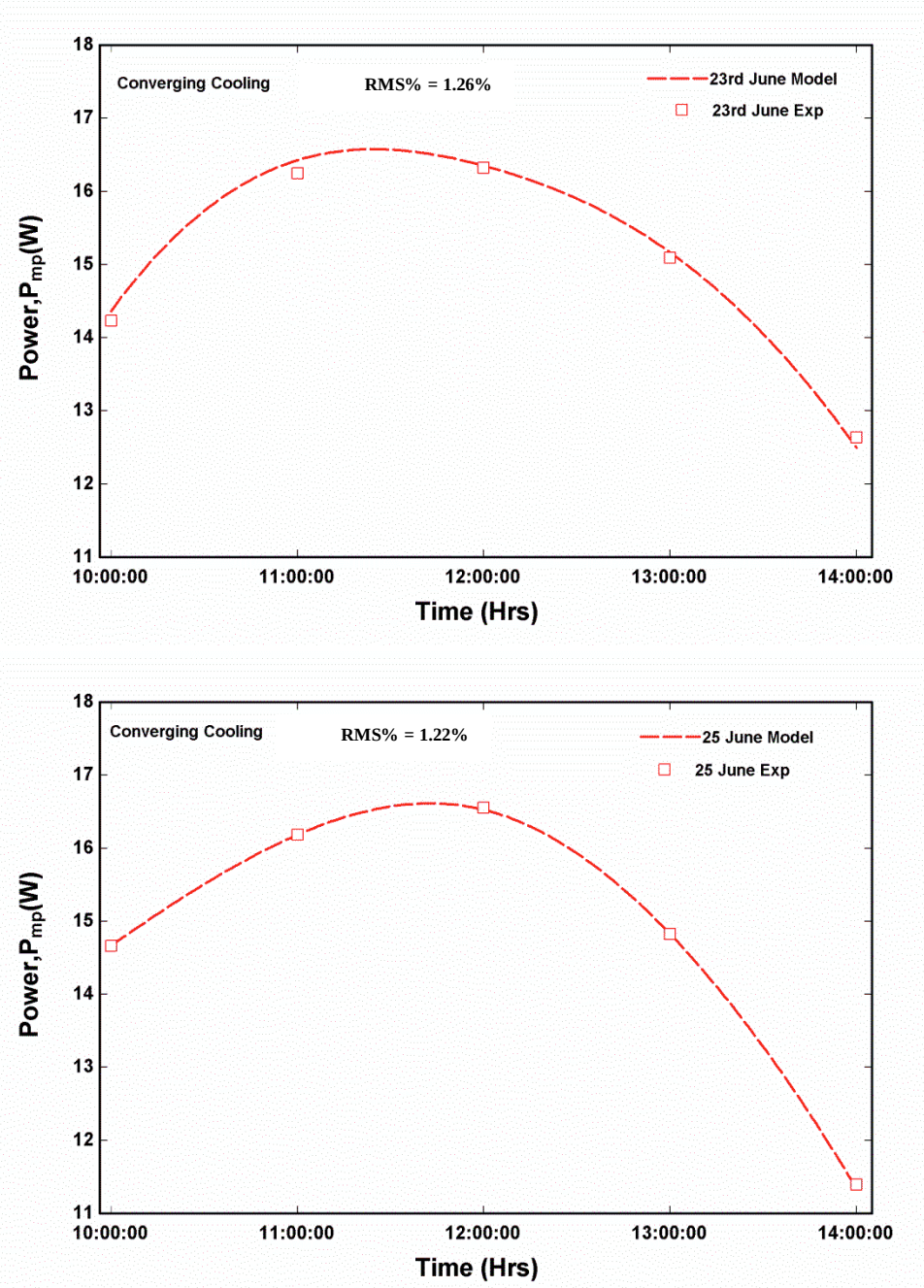

Figure 6.19 Variation of power produced for converging cooling of PV during test days

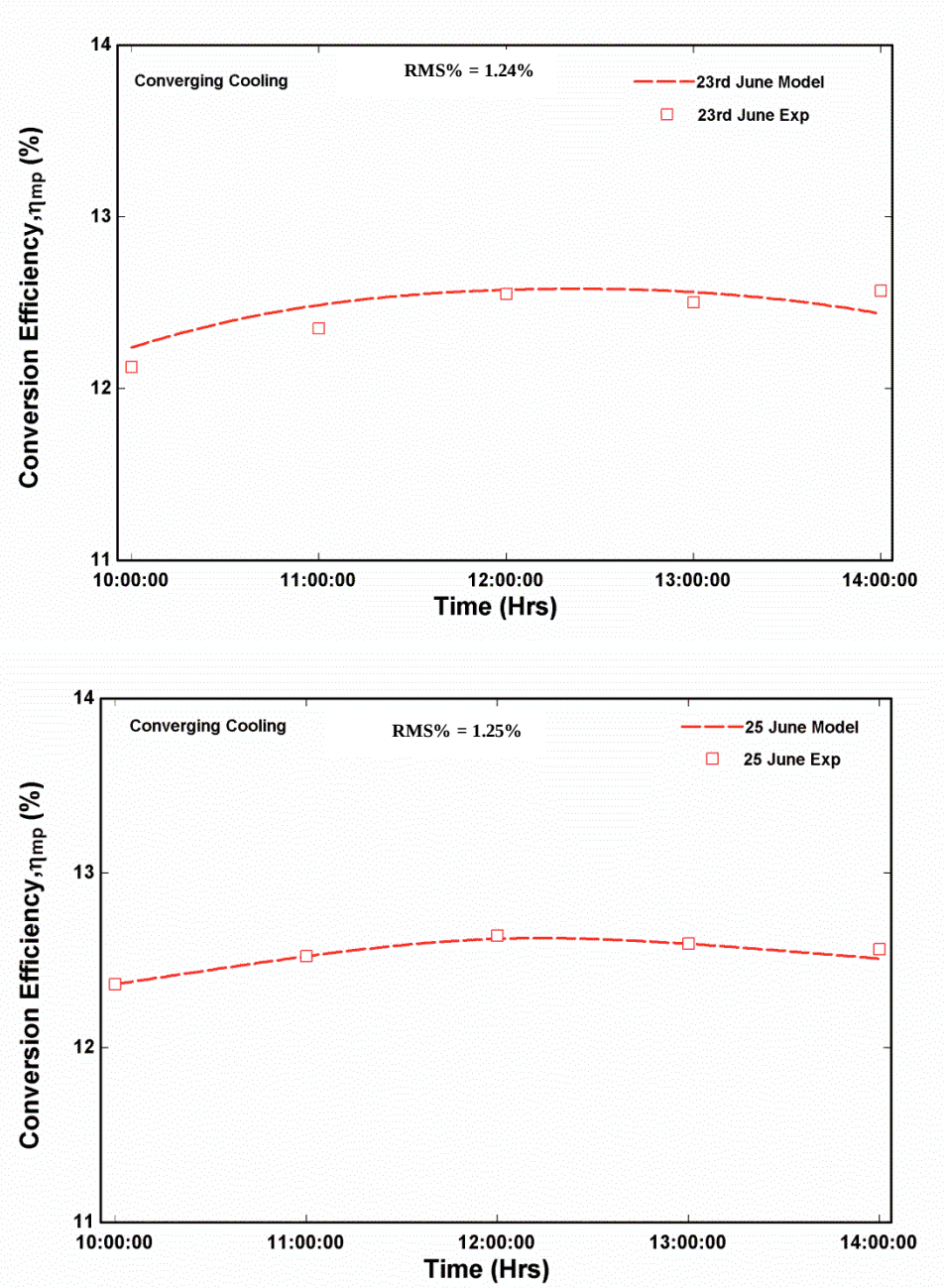

Figure 6.20 Variation of conversion efficiency for converging cooling of PV during test days

6.5 JET IMPINGEMENT COOLING RESULTS

6.5.1 Jet modeling results

Jet modeling simulations are first performed for the optimum parameters to be selected for impingement cooling of PV panels. Figure 6.21 shows the effect of cooling on the performance of cell temperature and power produced by PV string. It is evident that there exists a "knee point" in these curves, after which there would be insignificant improvement in the jet cooling model. Based on this result, average heat transfer coefficient of 1000 W/m^2.K for jet is used in the modeling of this study for jet.

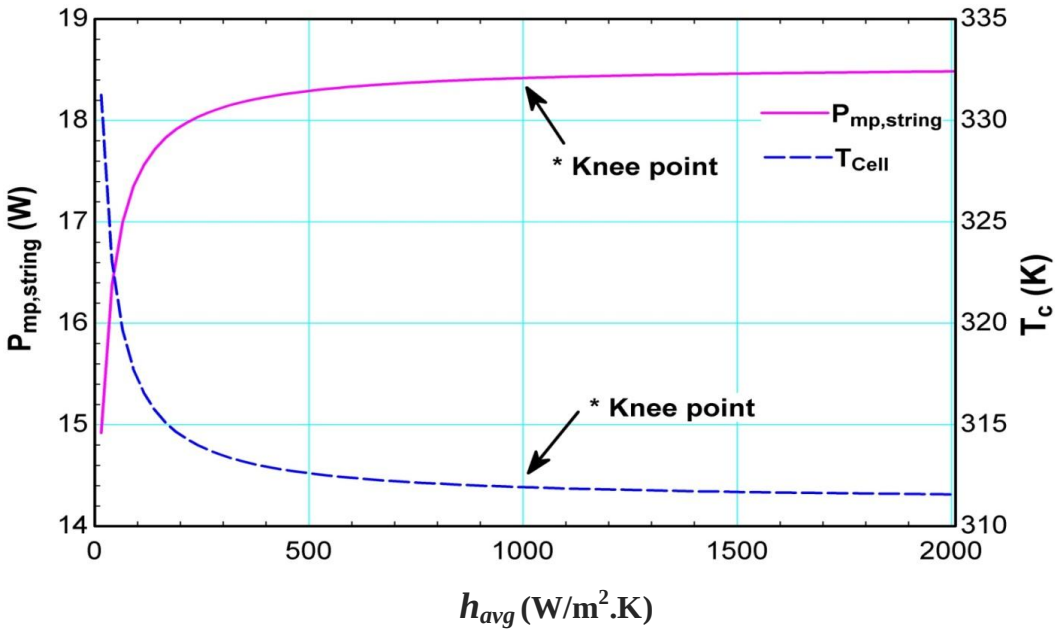

Figure 6.21 Optimization w.r.t power produced by PV string (same for all nozzles)

* $h_{avg} \cong 1000 W/m^2.K$ **(to be used for Jet Cooling)** → $\Delta P_{mp,string}(n, n-1) \cong 0.01W$

Dimensionless jet to jet spacing (s/d) in multiple nozzles determines the performance of multiple nozzles. As the number of jets increase, the pitch decreases resulting in increased stagnation zones and average heat transfer but this effect is counteracted by the interaction of jets. Hence there is a need for an optimum $(s/d)_{ratio}$ at which there will be a maximum heat transfer coefficient.

Using Lindeman[107], the optimum $(s/d)_{ratio}$ are shown in Figure 6.22 and Figure 6.23:

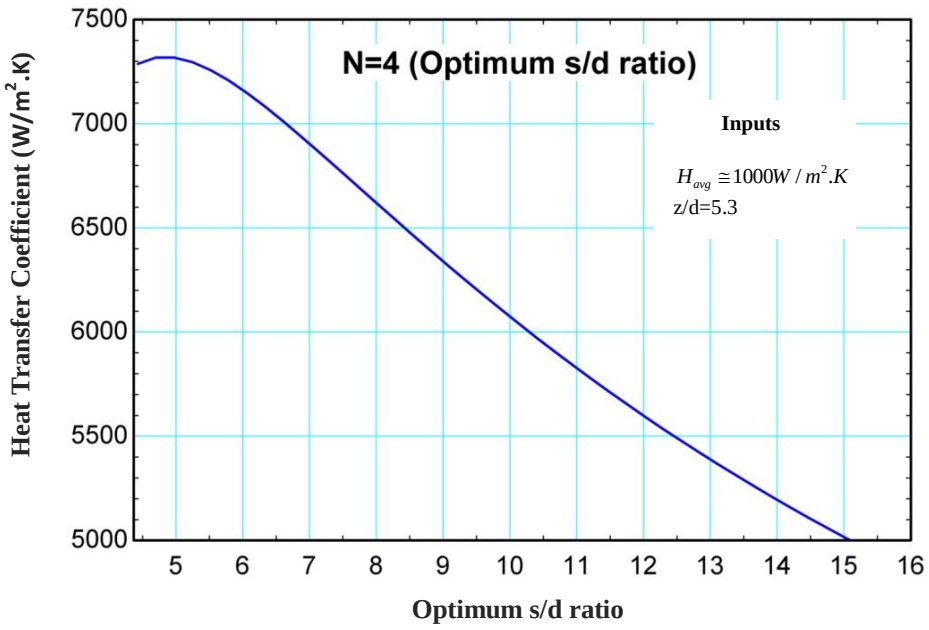

Figure 6.22 Variation of heat transfer coefficient w.r.t optimum (s/d) ratio for N=4

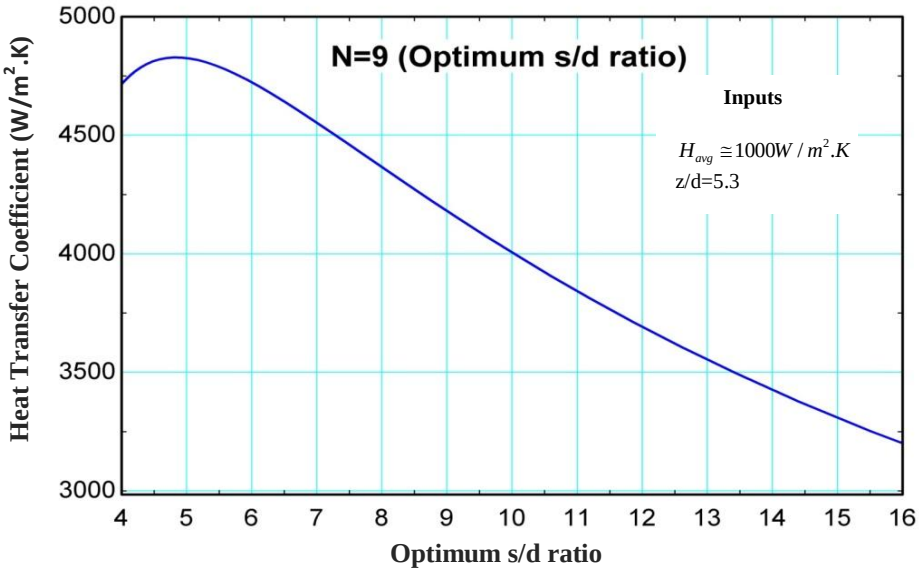

Figure 6.23 Variation of average heat transfer coefficient w.r.t optimum (s/d) ratio for N=9

Hence the maximum optimum $(s/d)_{ratio}$ lies in the range of 4-5 which agrees well with the results from Brevet et al [124].To decrease the jet to jet spacing below this range would not be efficient as it would only increase the heat transfer slightly on the expense of larger flow rate. Huber and Viskanta [86] substantiated this result and found that the heat transfer for multiple jets is considerably lower (14 – 21%) than that in an equivalent single impingement jet. This behavior was due to the interaction of adjacent jets in an array.

It should be noted that this optimum correlation gives maximum local heat transfer coefficient but if the surface is large, increasing the diameter will result in increasing the

average heat transfer. This will cause the local heat transfer to reduce gradually from the stagnation region causing lesser variation in temperature.

Tie et al [125] found an optimum of value of dimensionless nozzle to plate spacing z/d = 5 by incorporating the correlation into their model. Martin [85] in optimizing the work by Krotzsch [126] , showed an optimum z/d of 5.43. Jeffers et al. [127] showed that there exists an optimum value of z/d since there is a decrease in heat transfer with the reduction in nozzle to plate spacing. In water jets, it was showed that nusselt numbers increases to a maximum at z/d = 5 to 6 [128,129]. This behavior was attributed to an increase in turbulence and the mixing of the jet with its environment. Hoogendoorn [130] found that the in free jets the length of the potential, where the heat transfer is highest, remains undisturbed approximately to the z/d value of 5. Brevet et al [124] in their study found that the span wise distribution of nusselt number was approximately same for z/d = 2 and z/d = 5. Webb and Ma [82] found that the stagnation point heat transfer reached a maximum at z/d ~ 5.

Based on literature and the fabrication issues, dimensionless nozzle to plate spacing was selected to be 5.3. Since the knee point curve showed that $h_{avg} \cong 1000 W/m^2.K$ is the feasible and optimum solution, this will be used for thermal resistance in jet model. All the jet parameters for nozzles can be estimated by using Jet Models and values stated above.

PV impingement cooling simulation, PV heat exchanger cooling i.e: Sarhaddi Model [118] and PV panel without cooling is carried out using meteorological data at Dhahran

with monocrystalline Si Solar Cell. Comparative analysis is then made between the three cooling cases mentioned above with $h_{avg} \cong 1000 W/m^2.K$

Pumping power based on pressure drop in nozzle decreases with increasing nozzle number which in turn increases net power of system. Hence based on the requirement and design consideration diameter of the system should be selected. It should be noted that pumping power is based on the pressure drop across nozzle as explained in the modeling.

$$P_{net} = P_{mp,string} - P_{pump}$$

Figure 6.24,Figure 6.25 and Figure 6.26 show the effect of different parameters on the performance of jet nozzles. The fixed parameters are z/d =5.3, V=5 m/s while s/d is calculated using Lindeman model [107]. It should be noted that pumping power is based on the pressure drop across nozzle as explained in the modeling.

Figure 6.27 shows the effect of changing diameter of single and multiple nozzles on the net power developed by system. It can be seen that there is a significant effect of changing nozzle diameter.

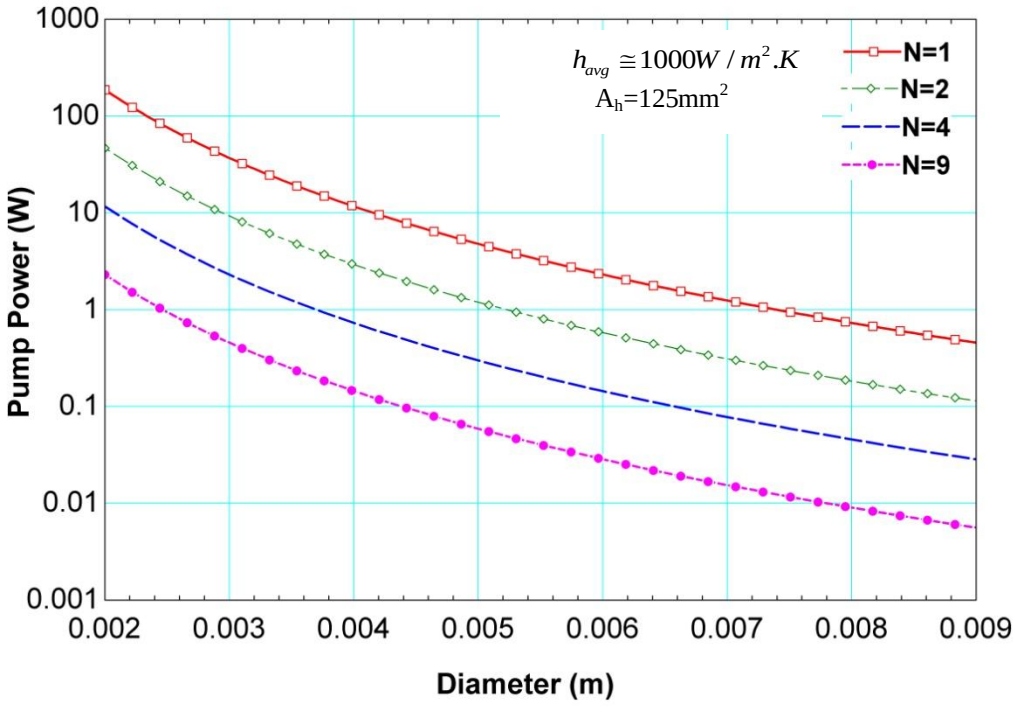

Figure 6.24 Variation of pumping power w.r.t diameter of single and multiple nozzles

From Figure 6.24 we can conclude that the maximum pump power will be in the case of single nozzle and it decreases as the number of nozzles increase. Also it should be noted that the pressure drop reduces with multiple nozzles. Figure 6.25 and Figure 6.26 show the effect of increasing number of nozzles and inlet velocity on the heat transfer coefficient. It is clear as the number of nozzle increases, the area of contact and stagnation region increases leading to an increased heat transfer coefficient. Also with the increase in velocity, heat transfer coefficient increase because of high heat extraction and thin thermal boundary layer development.

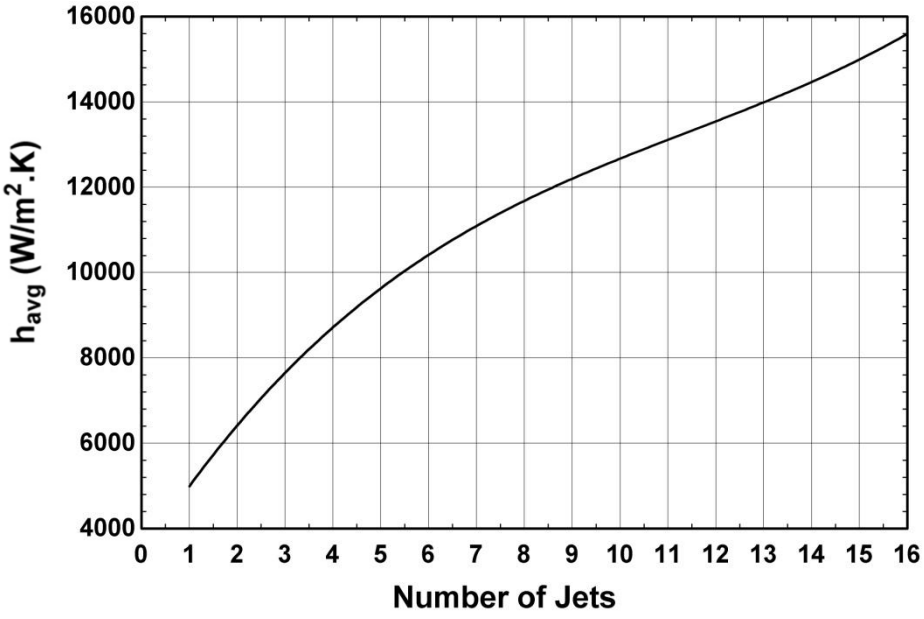

Figure 6.25 Average heat transfer coefficient variation with number of nozzles

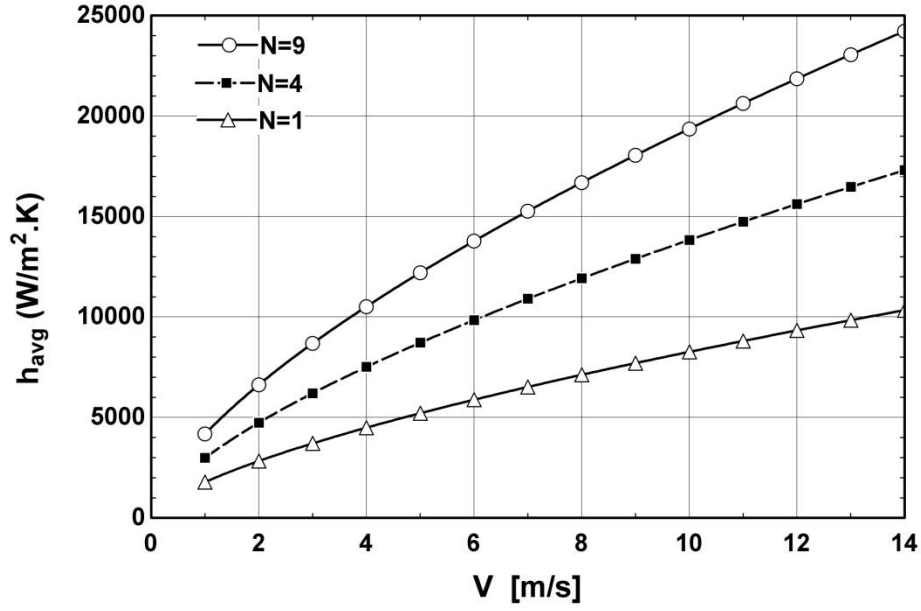

Figure 6.26 Average heat transfer coefficient variation with inlet velocity

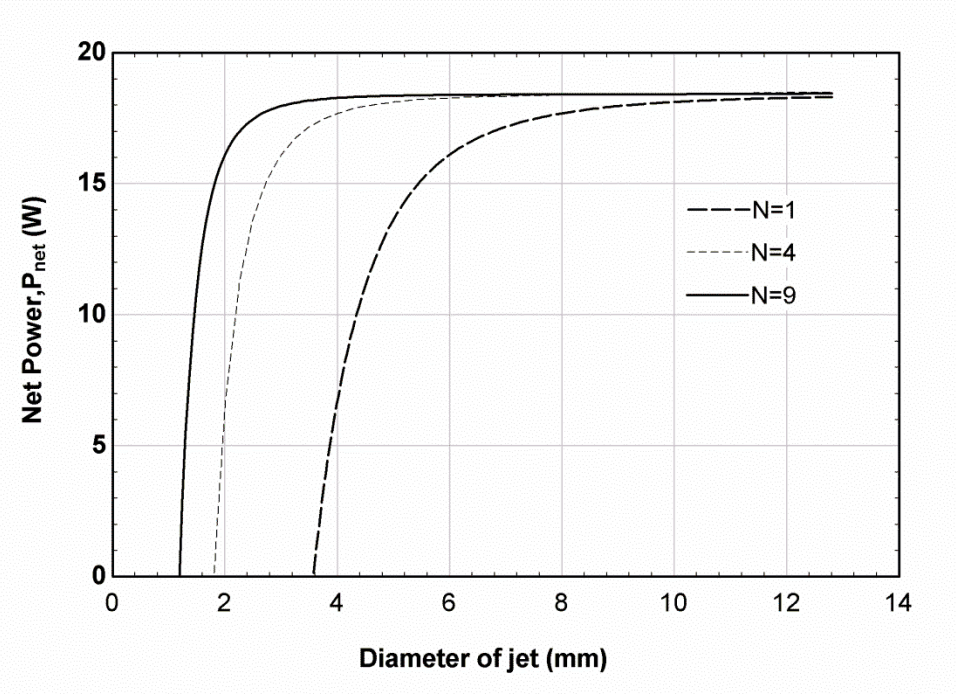

Figure 6.27 Results for net power w.r.t diameter of nozzles

Figure 6.28 shows the simulated results for PV string subjected to jet cooling. The maximum value for incident radiation (I_T) is 874.6 W/m^2 whereas the maximum absorbed radiation (S_{pv}) is 758.1 W/m^2.

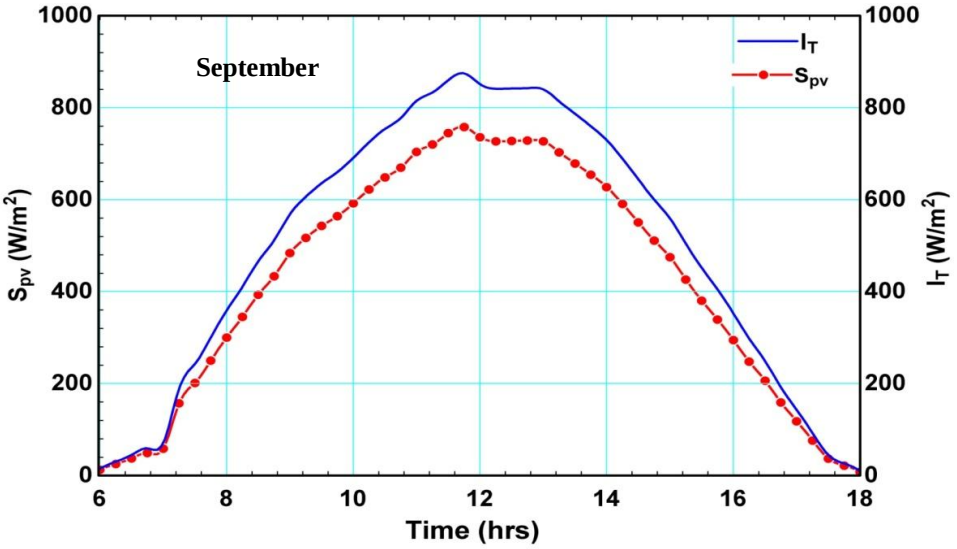

Figure 6.28 Variation of absorbed radiation and incident radiation with time.

Figure 6.29 shows the temperature variation across the entire day. It can be observed that the selection of $h_{avg} \cong 1000 W/m^2.K$ for jet Cooling has given uniform results when compared with the T_{cell} without (WO) cooling and with heat exchanger (HX). As the amount of energy absorbed increases, the cell temperature also increases along with the production of electrical energy. It was shown that the selection of jet cooling has given uniform results with approximately 0.9˚C cell temperature difference throughout the day when compared with the cell temperature without cooling and with rectangular channel heat exchanger. The temperature uniformity for the case of impingement cooling results

from the fact that a single nozzle was used to cool single cell making it uniform whereas for the case of conventional channel ,temperature variations are present as the fluid has to pass through the back of the solar cell along the length of heat exchanger thereby resulting in non-uniform distribution of temperature.

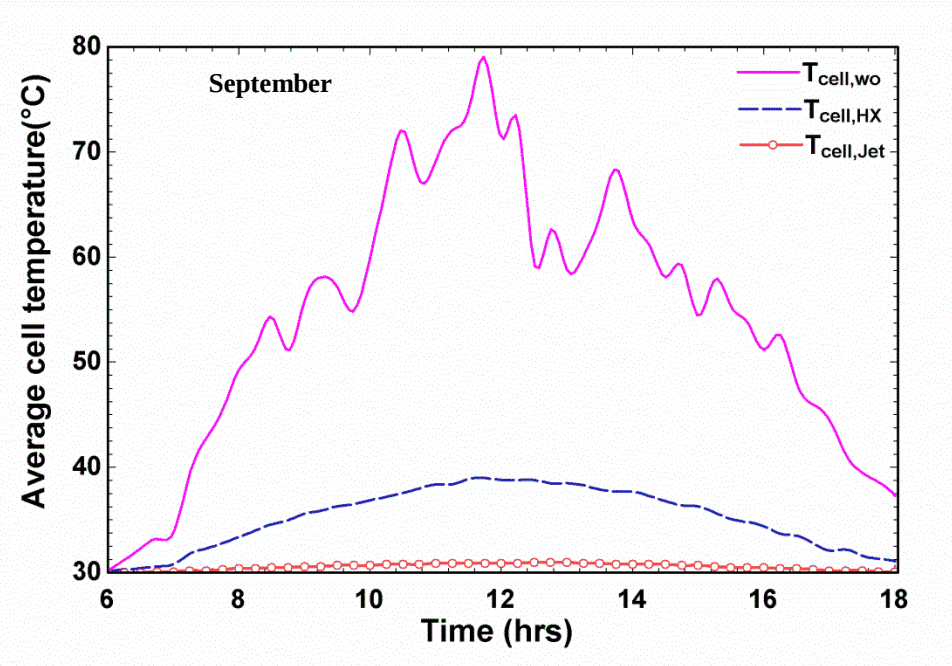

Figure 6.29 Variation of Cell Temperature for Uncooled PV Panel (wo), RHX Cooled PV panel and Uniform Jet Cooled PV panel.

This clearly reflects that the jet cooling would result in a lower minimum and maximum cell temperature when compared with other techniques mentioned which will result in increased efficiency. Moreover the cell temperature non-uniformity temperature shows the temperature is almost uniform throughout the day.

Figure 6.30 shows the comparison of power produced by a string for different cases. The power output of jet cooling, as expected, is highest at 18.8 W followed by heat exchanger at 17.3W and then PV without cooling at 10.7W. It should be noted without cooling the power is reduced during peak hours because of high cell temperature.

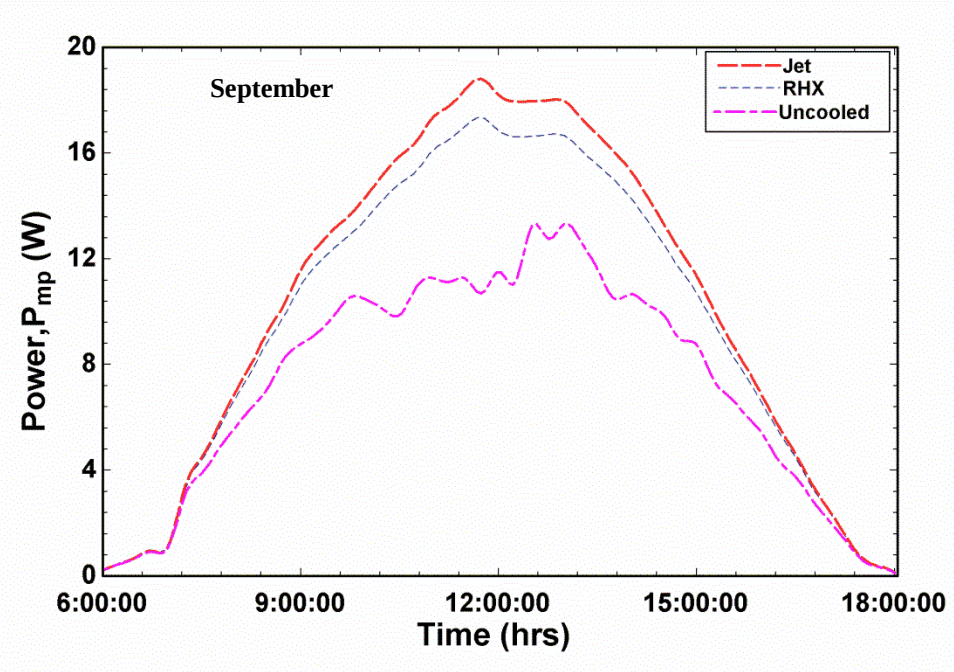

Figure 6.30 Variation of Power Produced for Uncooled (wo), HX Cooled and Uniform Jet Cooled PV panel.

Efficiency curves of different configurations are shown in Figure 6.31. Jet cooling with its high heat removal capability gives the highest value of cell efficiency of 17.2%. Heat exchanger with rectangular channel cooling shows the efficiency of 14.6% while the PV string without cooling shows negative behavior during peak hours with an efficiency of 8.2 % because of high cell temperature. This shows that implementing jet nozzle for

the purpose of uniform cooling would result in higher cell efficiency and lower cell temperature as the cooling fluid would not heat more in comparison to conventional rectangular channel heat exchanger. It should be noted that both of these cooling techniques are inherently different because of which the comparison is made based on the optimum settings for each mechanism. Based on the simulation results, it can be deduced that the effect of non-uniform and uniform cooling on solar cell performance cannot be disregarded. Also for higher concentrations, this effect will be more pronounced resulting in a greater damage to overall performance of PV system in terms of efficiency and thermal stresses. It is clear that cooling system has enhanced the performance of PV string.

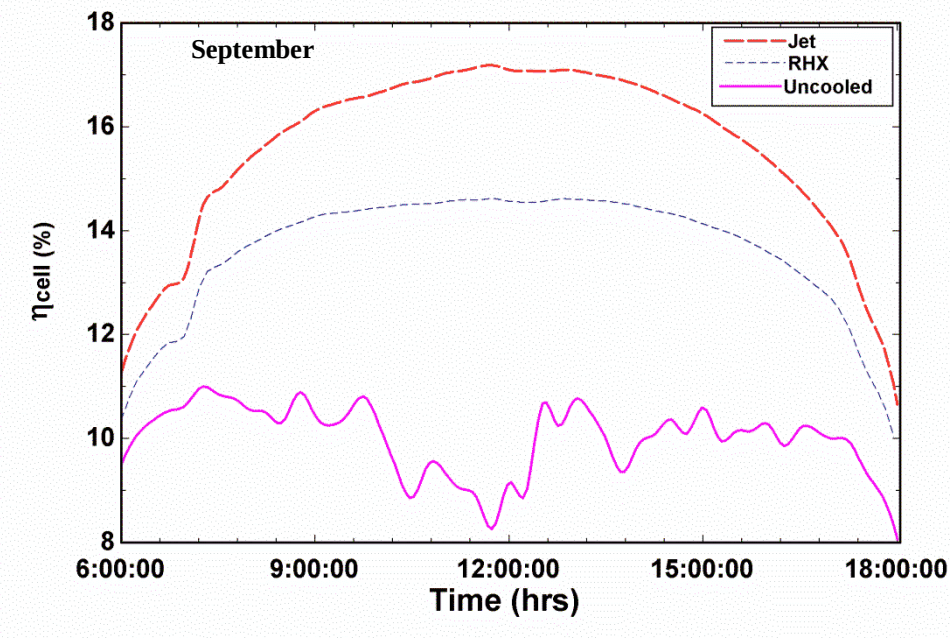

Figure 6.31 Variation of Cell Efficiency for Uncooled PV Panel (wo), HX Cooled PV panel and Jet Cooled PV panel for Dhahran, Sept 1st 2013

6.5.2 Jet Cooling Experimental and Modeling Comparison

Experimental measurements for temperature were performed in order to analyze the performance of the uncooled and uniformly cooled PV system practically. Data for the two extreme months of June and December were analyzed, both experimentally and numerically. PV surface temperature variation, average cell temperature, power output and conversion efficiency values were plotted for days of June and December and validation was carried out. Flow rate of water based on the analysis of the effect of flow rate shown in Figs 4.26-4.27 was chosen to be 1.8 lpm. Figure 6.32-Figure 6.35 shows the effect of jet cooling on the PV surface temperature profile from experimental measurements. Figure 6.32 depicts the PV surface temperature variation along the length of PV string for five hours. It is clear from the graph that jet cooling yielded uniform cooling as the temperature profile is almost linear with little variations. These variations can be attributed to the uncertainty of thermocouples and DAQ systems. The temperature on top of the surface shows reading in the range of 35.0-38.5˚C which actually depends upon the ambient temperature and temperature of water from nozzles. Similar trend is followed for the 25th June temperature profile in Figure 6.33. Figure 6.34 and Figure 6.35 show the PV surface temperature profile for the month of December where the ambient and water temperature are relatively low. This resulted in lower cell temperature as shown. In addition, by employing jet cooling uniform temperature profile is achieved with temperature non-uniformity in the range of 0.9-1.5˚C.

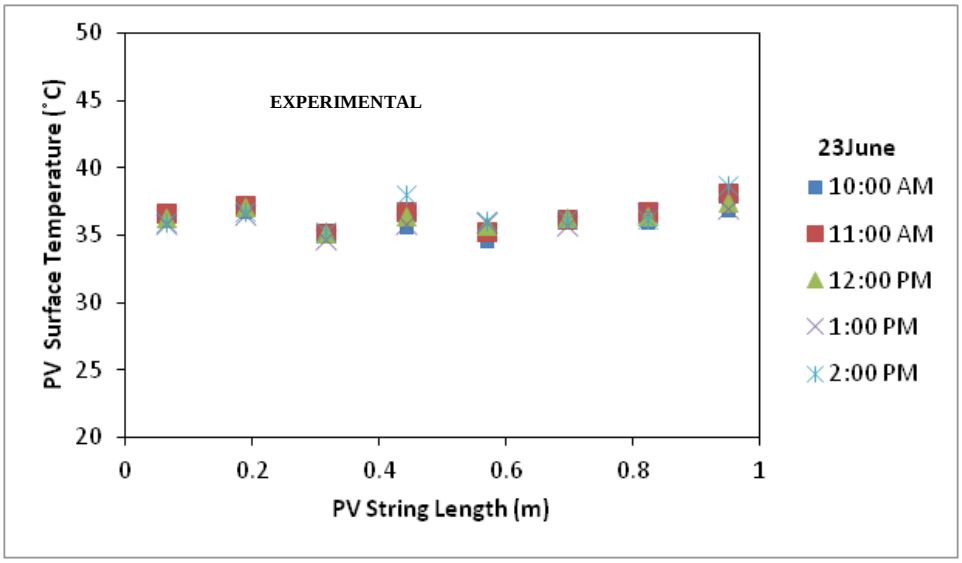

Figure 6.32 PV surface temperature profile on 23rd June

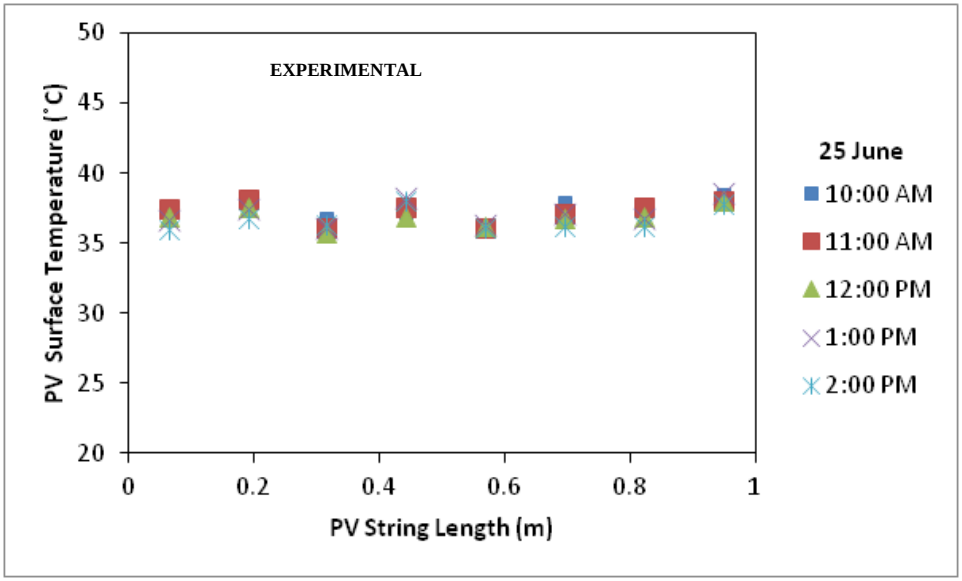

Figure 6.33 PV surface temperature profile on 25th June

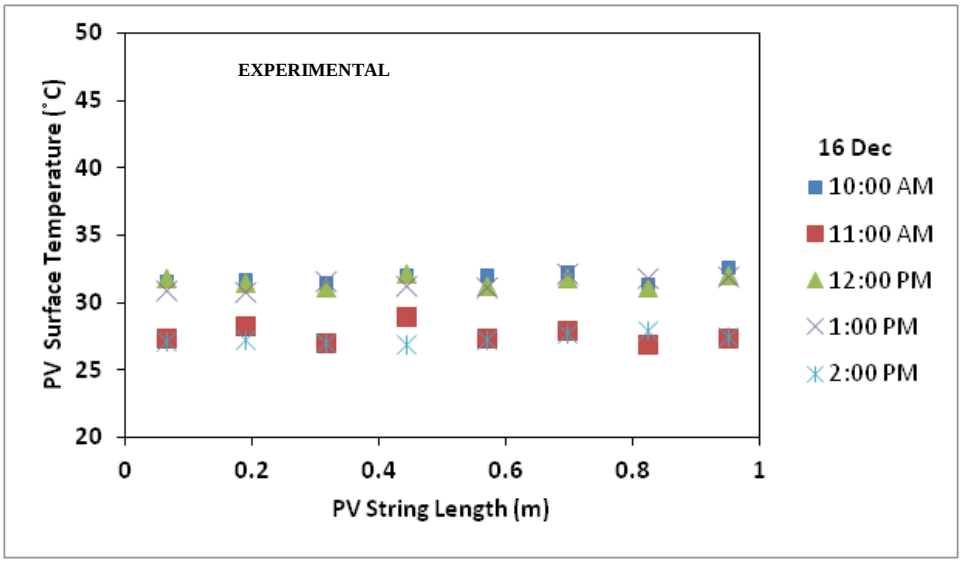

Figure 6.34 PV surface temperature profile on 16th December

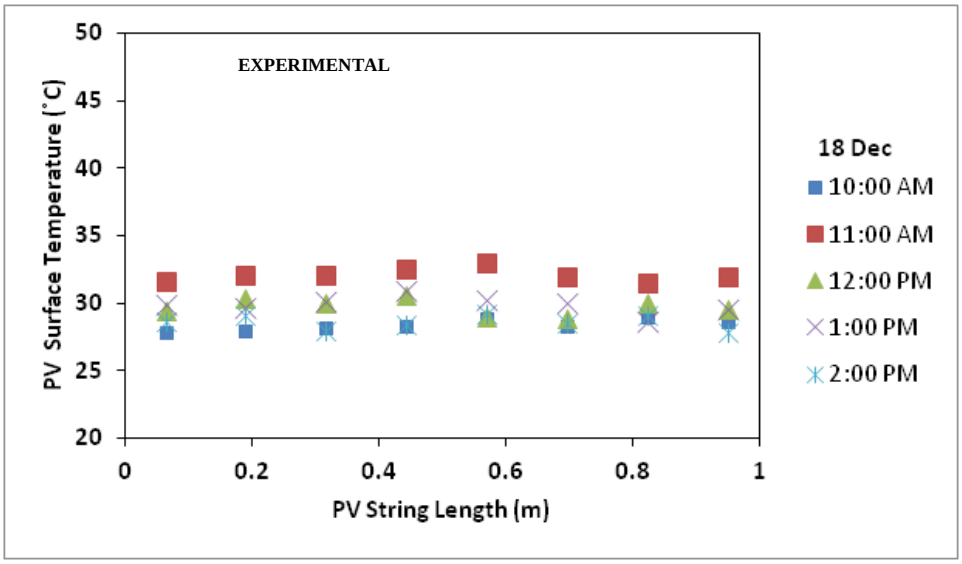

Figure 6.35 PV surface temperature profile on 18th December

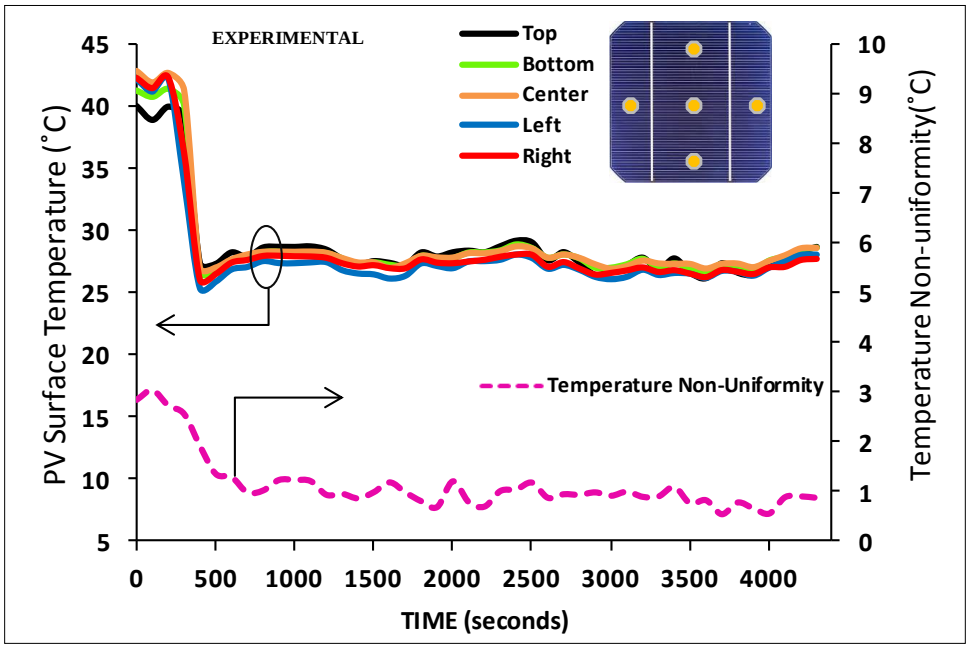

Figure 6.36 Single cell surface temperature profile variation with temperature non-uniformity

Figure 6.36 shows the effect of jet cooling on the thermal characteristics of single cell. Five thermocouples were installed on the surface of PV cell and jet cooling was applied for approximately a period of 4000 seconds. Temperature non-uniformity is shown on the right axis of the Figure 6.36 where it can be seen that after attaining steady state it lies around 1˚C. Also the PV surface temperature profile shows that PV by applying jet cooling, temperature has dropped from 46˚C to 26˚C within 500 seconds i.e transient state. In the steady state, it is noteworthy that the temperature of PV surface for all the thermocouples give uniform temperature profile with little variations from the experimental DAQ systems.

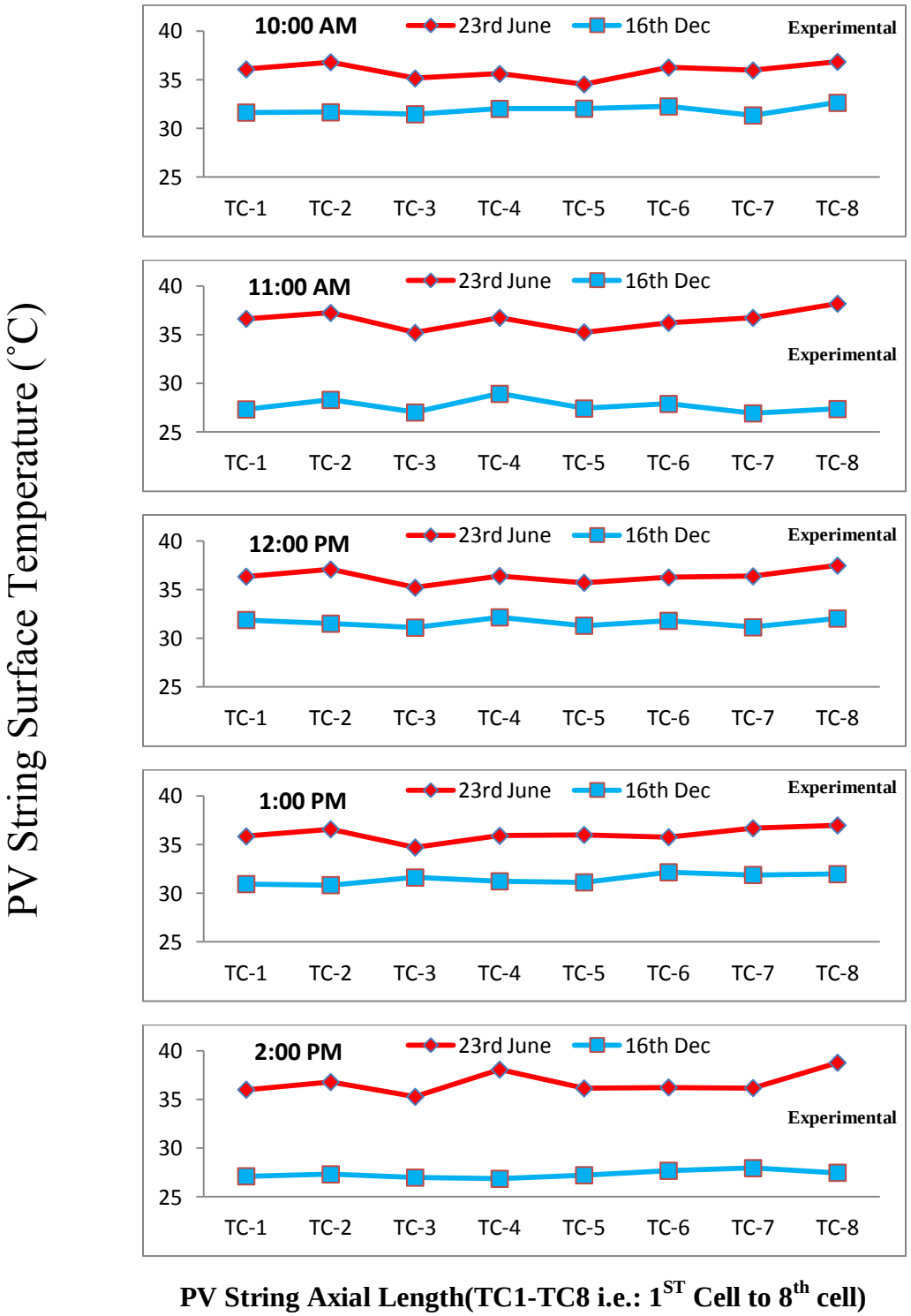

Figure 6.37 Experimental PV surface temperature variation for June and December

Figure 6.37 shows the experimental PV surface temperature along the length of PV string with each thermocouple installed at center of single PV cell. Comparison between PV surface temperature profile for June and December is shown. It is clear the effect of jet cooling in the month of December yielded lower PV surface temperature than June. This behavior is due to the lower ambient and water temperature in the winter month. It should be noted that for the seasons, the temperature profile is uniform which shows that jet cooling in extreme climatic conditions can perform better than other cooling mechanisms. Figure 6.38 shows average cell temperature variation for 23rd June and 16th December with numerical and experimental readings. Validation was performed and results showed good agreement with maximum RMS value of 4.5% for the month of December and 1.8% for the month of June. For June, by employing jet cooling PV surface temperature was reduced to 36˚C whereas for December it was reduced to around 30˚C. This decrease of average cell temperature is due to the high extraction capability of jet impingement cooling. The decrease in power for the month of December relative to June is due to less incident solar radiation and wind speed.

Figure 6.39 shows the variation of maximum power produced by jet cooling obtained through numerical model and experiments. Analysis was performed for the month of June for 23rd June and 16th December. By applying jet cooling power output for June has increase to 18.4 W whereas for December maximum power output was 18.1 W. Validation results showed good agreement with maximum RMS value of 4.4% for the month of December and 1.3% for the month of June.

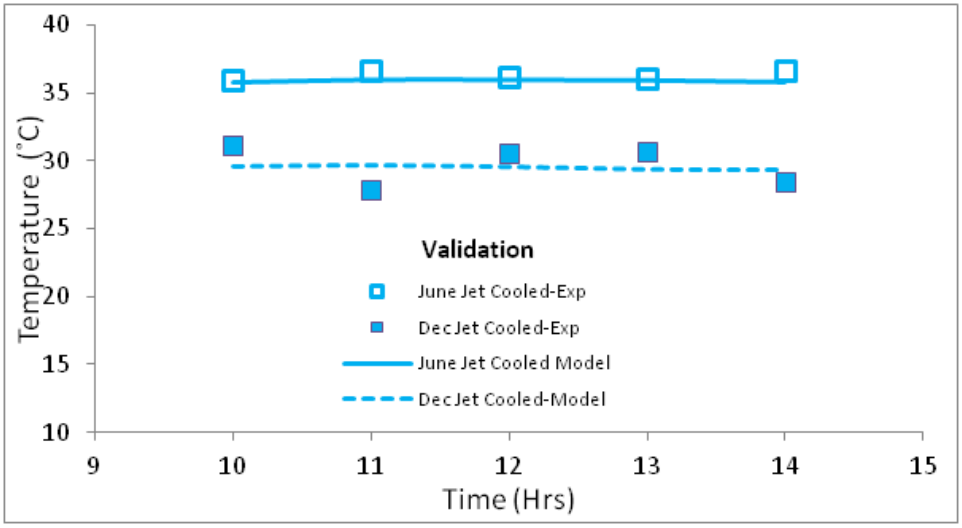

Figure 6.38 Average cell temperature variation for December and June for jet cooling

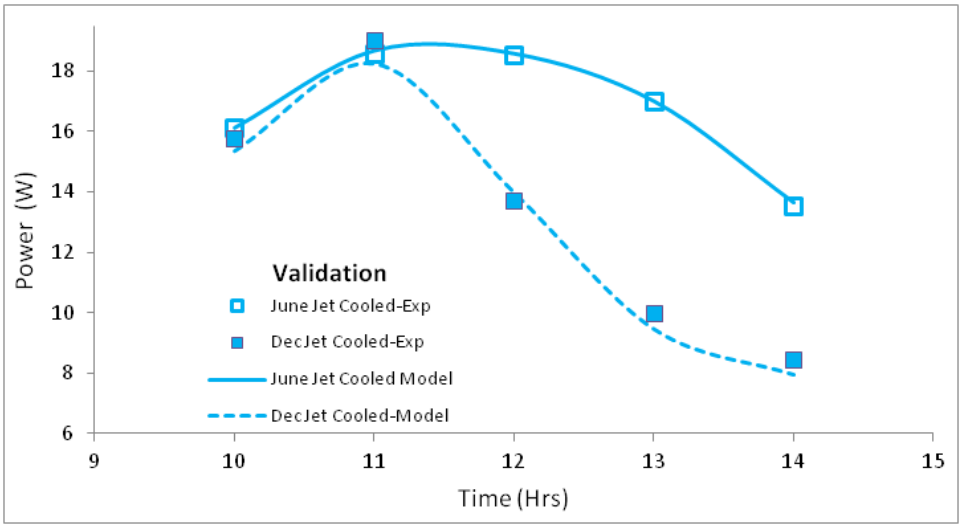

Figure 6.39 Power variation for December and June for jet cooling

Figure 6.40 shows the variation of average PV surface temperature by jet impingement cooled PV string. It is evident that the application of cooling has shown significant results for the conditions of Saudi Arabia. Cooling the PV string by jet impingement resulted in temperature as low as 35.7˚C for 25th June. Modeling and experimental data shows fair agreement with root mean square percent deviation not exceeding 4.1 %. By using jet cooling, PV string has been cooled effectively by reducing the cell temperatures while keeping the uniform distribution of temperature.

Figure 6.41 shows the temperature non-uniformity on the surface of PV string. It is measured experimentally and the data points for both days are compared. This figure shows that by employing the jet mechanism, PV surface temperature is approximately uniform at the times of data collection. For 23rd June, temperature non-uniformity is 2˚C averaged for the entire testing hours whereas for 25th June its value is 1.5˚C

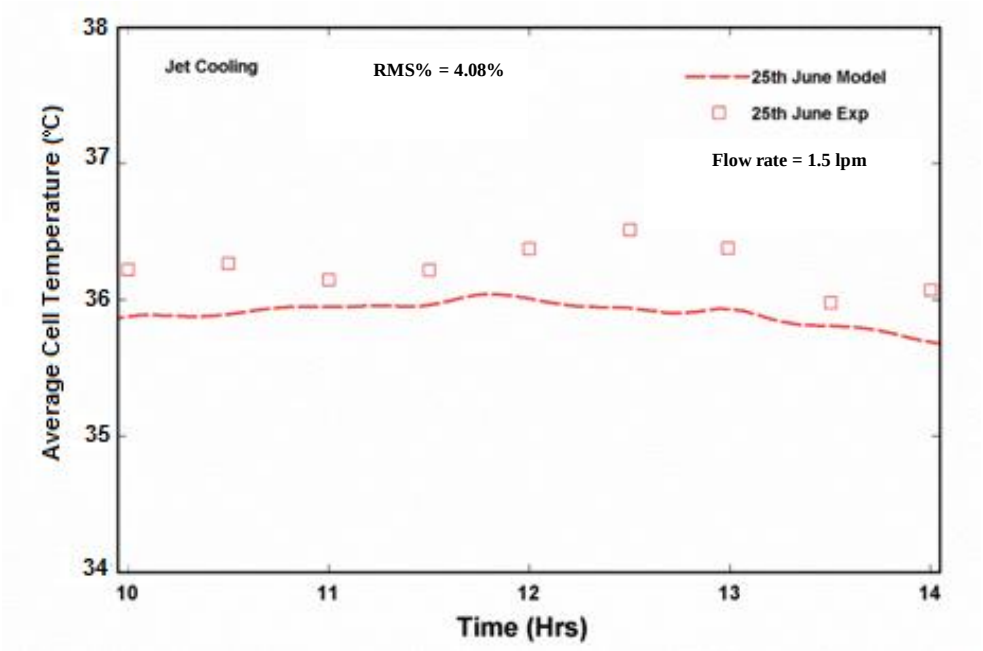

Figure 6.40 Variation of average cell temperature for jet cooled PV on 25th June

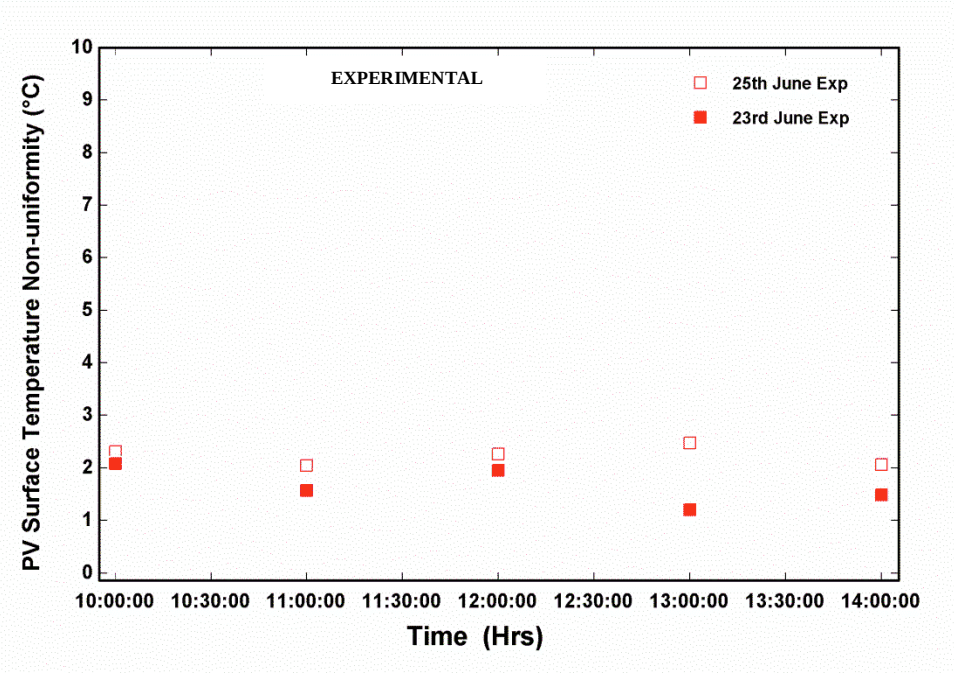

Figure 6.41 PV surface temperature non-uniformity for jet cooled PV during test days

Electrical power output for 25th June is shown in Figure 6.42. Experimentally, the maximum power output achieved was 19.4W for the case of 25th June. The results showed good agreement between experimental and modeling results with maximum root means square deviation of 1.54%. Figure 6.43 shows the comparison between the model and experimental conversion efficiency. For 25th June, the maximum experimental efficiency was 15.4 %. The results show good agreement between experimental and modeling results with maximum root means square deviation of 2.91 %.

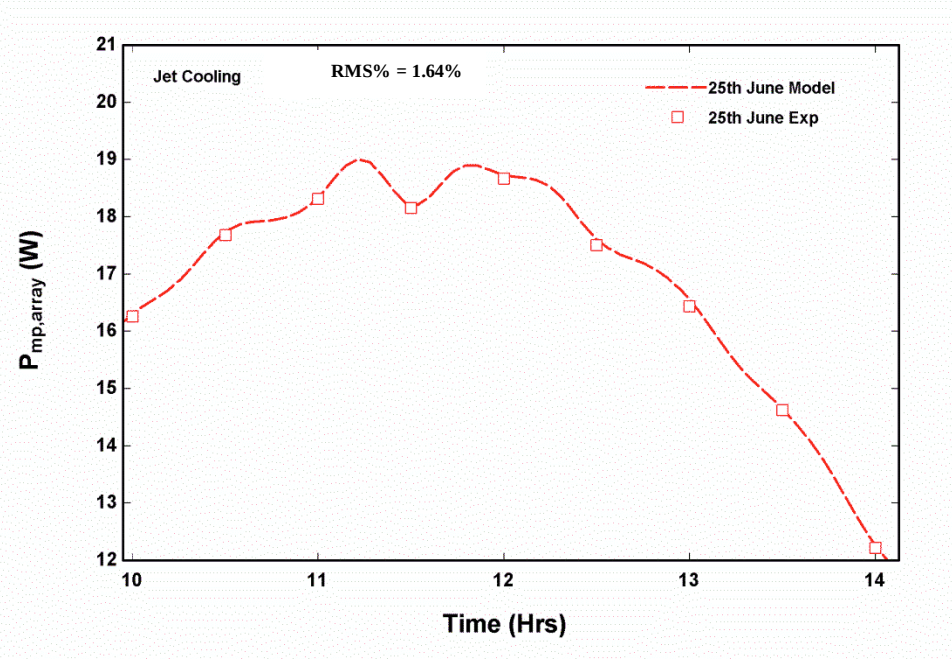

Figure 6.42 Variation of power for jet cooled PV on 25th June

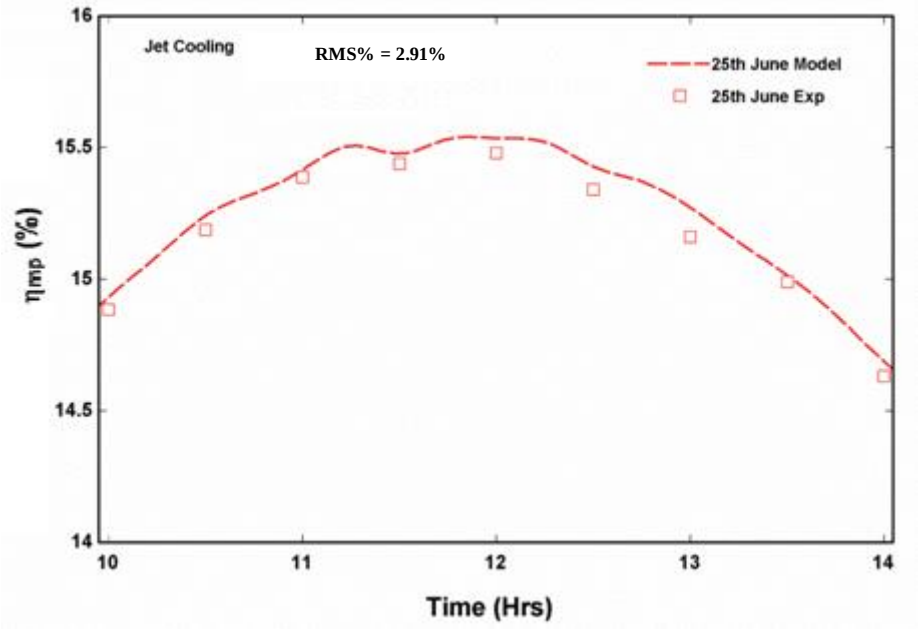

Figure 6.43 Variation of conversion efficiency for jet cooled PV on 25th June

6.6 COMPARATIVE RESULTS BETWEEN CONFIGURATIONS

6.6.1 Comparison between converging channel and uncooled PV string

In this section the comparison of experimental and numerical results will be discussed for various parameters which determine the overall performance of an uncooled and converging channel cooled PV systems. The main input parameters for the models are the meteorological data in the form of ambient temperature, wind speed, incident radiation, flow rate of coolant, inlet temperature of fluid and solar cell parameters. Figure 6.44 shows the variation of average cell temperature during the test days. Comparison between an uncooled PV and converging channel cooled PV is shown for the two extreme seasonal months selected. It is evident that the application of cooling has shown significant results for the conditions of Saudi Arabia. For an uncooled PV string, maximum temperature of 71.2˚C was reported for June whereas the maximum cell temperature of 48.3˚C was recorded for December. In comparison to this, cooling the PV string by converging channel resulted in temperature as high as 45.1˚C for June and 36.4˚C for December. A temperature reduction of 26.1˚C and 11.9˚C was observed for summer and winter months, respectively. Modeling and experimental data shows fair agreement with root mean square percent deviation not exceeding 5.76 % for both days and total experiments. By using converging channel, PV string has been cooled effectively by reducing the cell temperatures while keeping the uniform distribution of the temperature. The variation of temperature readings from modeling and experimental

can be attributed to the developed flow characteristics and steady state conditions from the CFD model, and to the uncertainty of thermocouples and DAQ system.

For the month of June, where the effects of high cell temperature is more pronounced, cell temperature reduced by 57.8 % . In addition, employing cooling in cold weather of December resulted in cell temperature reduction of 32.7 %

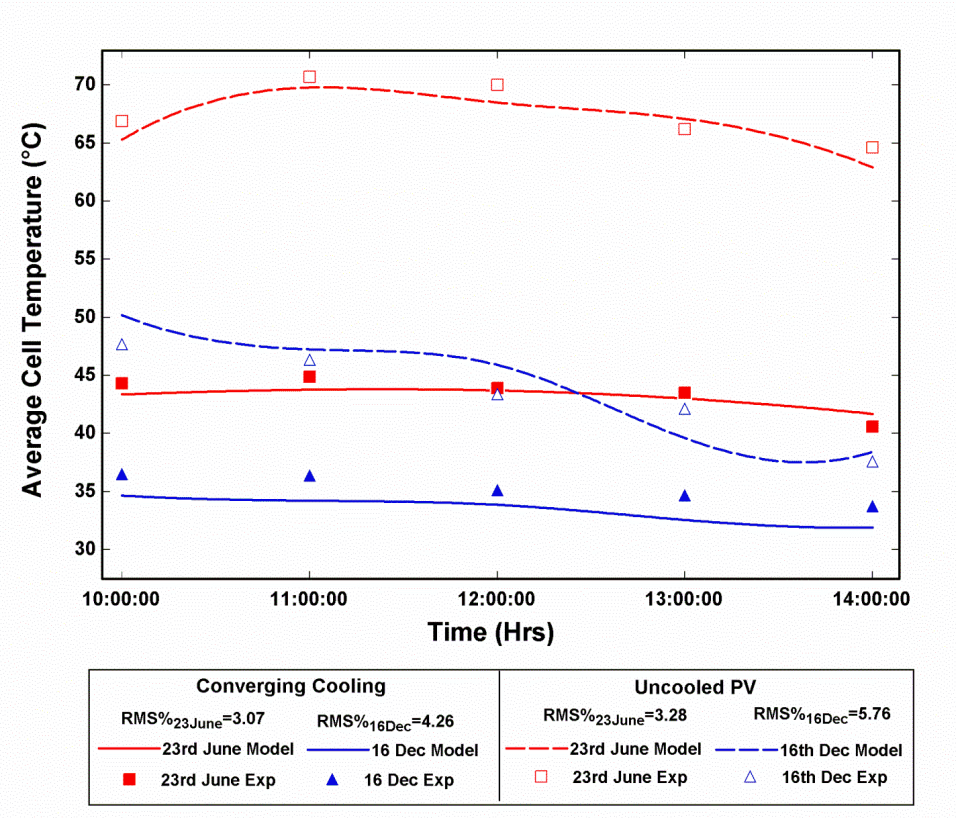

Figure 6.44 Average cell temperature comparison for converging cooling and uncooled PV

Electrical power output for two test days is shown in Figure 6.45. It is evident that the use of cooling enhances the performance of PV string. The maximum power output increases from 12.1W to 16.4W for the case of June while for December, the maximum power output increases from 12.3 W to 15.5W. The results show good agreement between experimental and modeling results with maximum root means square deviation of 3.28% for the case of uncooled PV system. An uncertainty bar of 0.27 W is also embedded in the Figure 6.45 to show the certainty of experimental results. For the month of June, PV power output was enhanced by 35.5% whereas the performance improvement for December was 26.1%. It is important to note here that the PV power output, in addition to cell temperature, is also affected from incident radiation, solar energy absorbed by PV and wind speed.

Figure 6.46 shows the comparison between conversion efficiency of the two systems considered. It is clear by employing converging cooling that the performance of PV has significantly improved. The experimental efficiency increases from 9.8% to 12.5% for the case of June. For December, the experimental efficiency increases from 10.8% to 14.7 %.Percentage improvement in the performance was 27.55% and 36.1% for June and December, respectively.

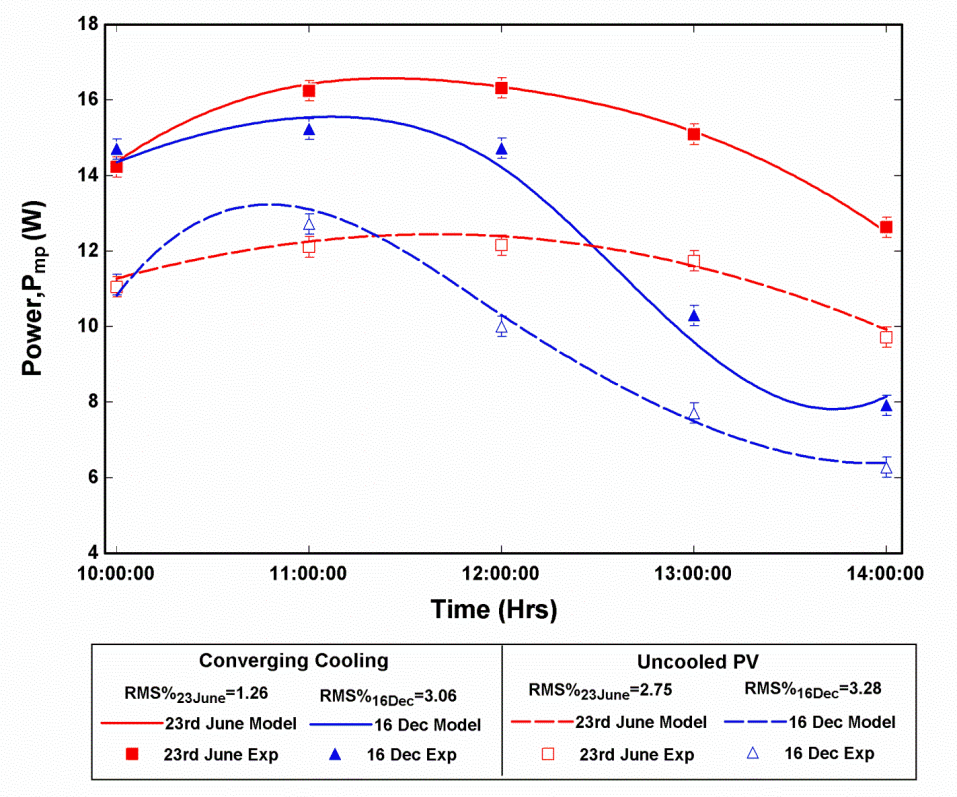

Figure 6.45 Power output comparison for converging cooling and uncooled PV

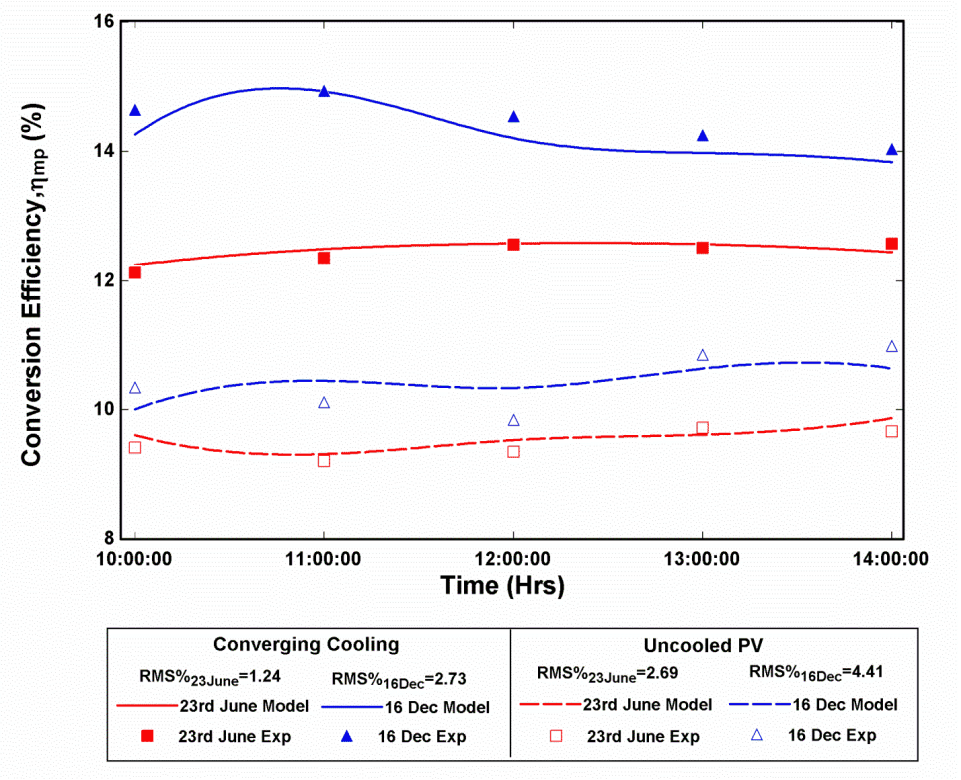

Figure 6.46 Conversion efficiency comparison for converging cooling and uncooled PV

6.6.2 Comparison among jet impingement, converging channel, rectangular heat exchanger and uncooled PV string

For the global analysis, a comparison was carried out using the ambient data of Dhahran to observe the behavior of different cooling techniques for the extreme months of June and December. The complete model developed is used to analyze the effect of ambient conditions and cooling mechanism on the overall performance of the PV system. Experiments were performed for all the configurations simultaneously for test days in order to analyze the performance of the uniform and non-uniform cooling on PV system.

Temperature gradients develop in PV modules that are being cooled due to non-uniform flow within the heat exchanger. These temperatures gradients can lead to degradation of electrical performance due to current mismatching problem. Mismatched cells that are connected together in series do not perform at their individual maximum power point simultaneously; instead, the cells perform at a lesser, collective maximum, which is limited as a result of the mismatch within the module [131]. The temperature gradients also translate into stress gradients being developed in the module which may lead to reliability issues. To solve the problem of high temperature gradients, the design of uniform cooling techniques for cooling PV modules was carried out to reduce the temperature gradient. The comparative results of all the configurations modeled and tested experimentally are presented in this section.

Figure 6.47 shows the variation of average cell temperature for all configurations during the test day in June. It is evident that the application of uniform cooling has shown significant results for the conditions of Saudi Arabia. For uncooled PV string, maximum temperature of 83˚C was recorded. In comparison to this, cooling the PV string by converging channel resulted in maximum temperature of 47˚C and 47.5 ˚C for rectangular channel heat exchanger. For jet cooled PV string, maximum temperature of 35.8 ˚C was recorded. Modeling and experimental data shows fair agreement with root mean square percent deviation not exceeding 4 % for jet, converging and rectangular channel. By using uniform jet cooling, PV string has been cooled effectively by reducing the cell temperatures to 55.4 % whereas for rectangular channel non-uniform cooling , percentage reduction in temperature was 43.1%.

Figure 6.48 shows the variation of PV surface temperature by all the cooling configurations for PV string recorded by the experiments in June. This figure shows that by employing the jet cooling, PV surface temperature is approximately uniform with a maximum variation of approximately 2.3˚C. In comparison to this, cooling the PV string by converging channel resulted in maximum temperature variation of 4.9˚C and for rectangular channel heat exchanger the variation was 4.5 ˚C.

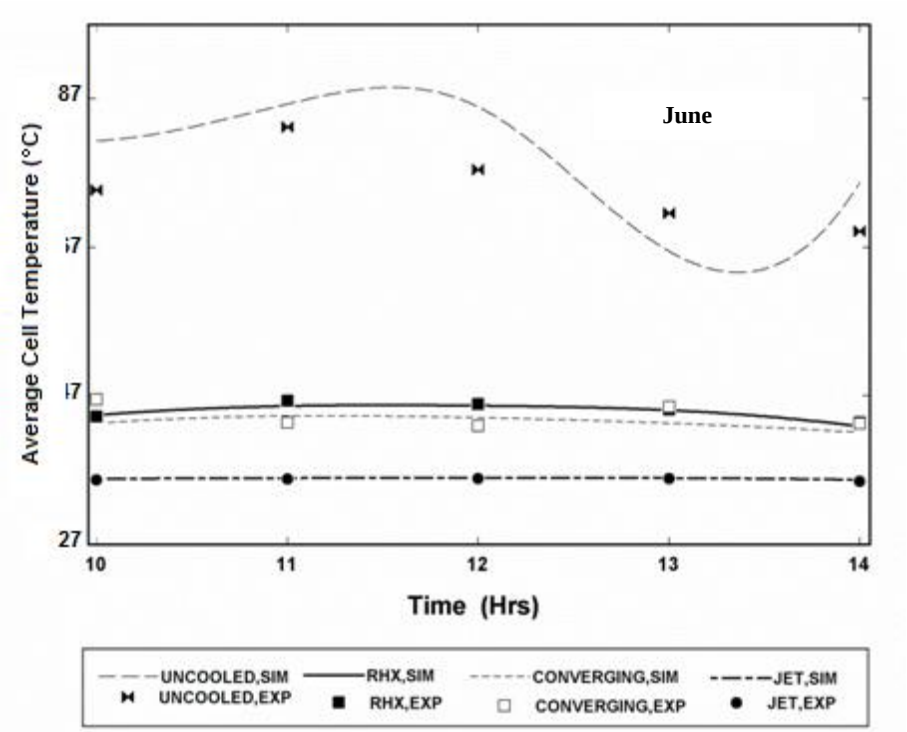

Figure 6.47 Average cell temperature comparison for 26th June for all configurations

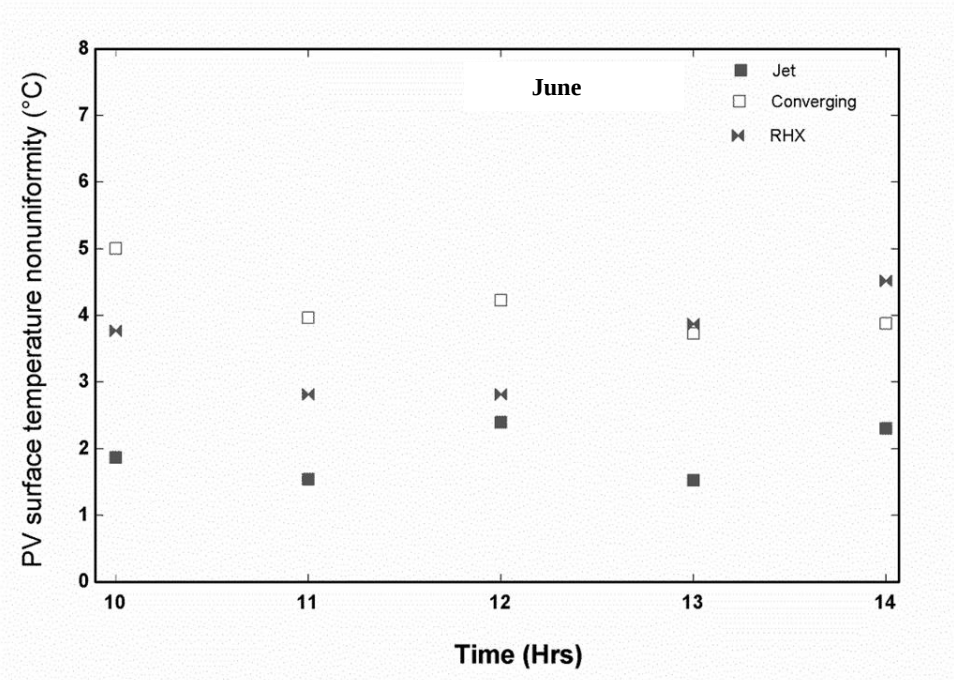

Figure 6.48 PV surface temperature non-uniformity comparison for 26th June for all configurations

Power output for jet cooled, converging cooling, rectangular heat exchanger, uncooled PV system has been shown and compared in Figure 6.49 for the data of June. It can be seen that the PV system with uniform cooling produced more power than the non-uniform cooled and uncooled PV. This increase in power is a result of low and uniform cell temperature in the case of cooling. For uncooled PV string, maximum power of 10.0W was recorded. In comparison to this, cooling the PV string by converging channel resulted in maximum power of 15.7W and 16.0W for rectangular channel heat exchanger. For jet cooled PV string, maximum power of 18.1W was recorded. Modeling and experimental data shows fair agreement with root mean square percent deviation not exceeding 3.87 % for jet, converging and rectangular channel. By using jet, PV string has been cooled effectively and power produced has increased by 81% whereas for converging and rectangular channel, percentage improvement in power was 57% and 60 %, respectively.

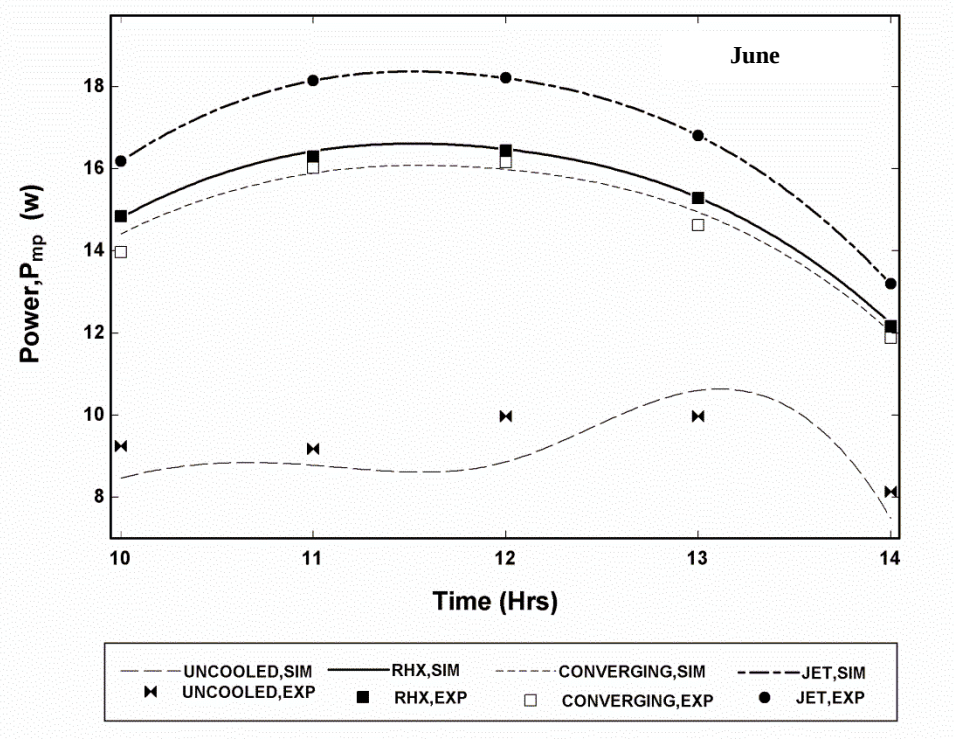

Figure 6.49 Power comparisons for 26th June for all configurations

Figure 6.50 shows the comparison between conversion efficiency of the four systems considered for hot day of June. For uncooled PV string, maximum efficiency of 7.9% was recorded. In comparison to this, cooling the PV string by converging channel resulted in maximum efficiency of 12.5% and 12.7% for rectangular channel heat exchanger. For jet cooled PV string, maximum efficiency of 15.7% was recorded. Modeling and experimental data shows fair agreement with root mean square percent deviation not exceeding 4.5% for jet, converging and rectangular channel. Figure 6.51 shows the improvement in performance parameters by applying cooling systems. By using jet, PV string has been cooled effectively and efficiency has increased by 98.4%.

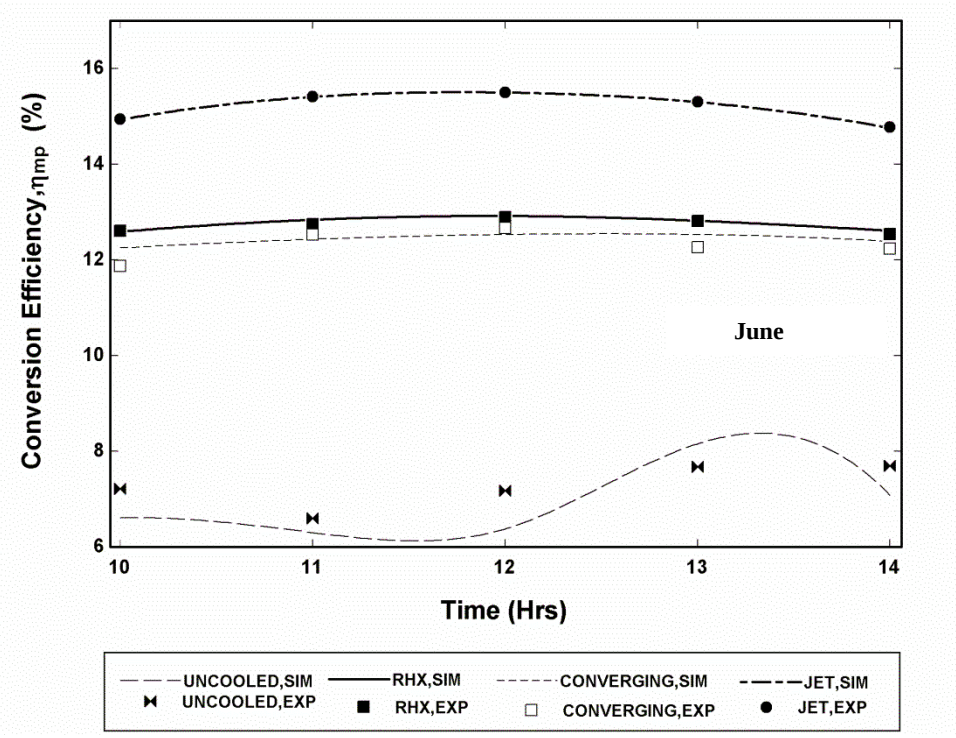

Figure 6.50 Conversion efficiency comparisons for 26th June for all configurations

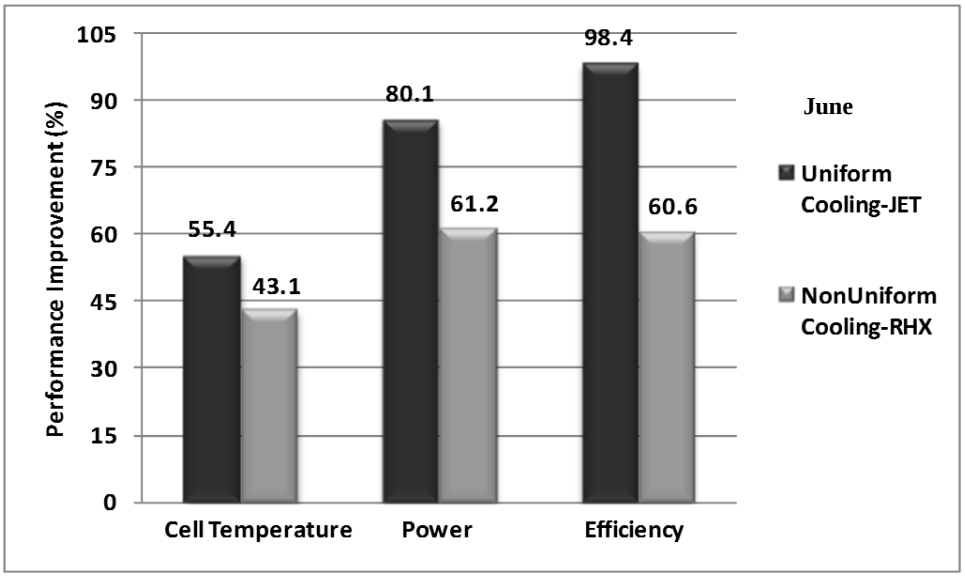

Figure 6.51 Percentage improvement comparisons for 26th June with uncooled system.

Figure 6.52 highlights the average cell temperature variation from experimental measurements and numerical results for the cold day of 16th December. For December PV without cooling showed maximum cell temperature of 48˚C. In comparison to this, cooling the PV string by converging channel resulted in maximum temperature of 37.5˚C and 38˚C for rectangular channel heat exchanger depicted by RHX in graph. By cooling the PV from uniform cooling mechanism of jet cooling, maximum cell temperature measured was 31˚C.Modeling and experimental data shows fair agreement with root mean square percent deviation not exceeding 5.6 % for jet, converging and rectangular channel. Cooling in uniform way by jet has decreased the cell temperature significantly by 54.8% whereas cooling the PV in non-uniform way resulted in temperature reduction percentage of 26.3%.

Figure 6.53 shows the variation of PV surface temperature non-uniformity by all the cooling configurations for PV string for the month of December. This figure shows that by employing the jet cooling, PV surface temperature is approximately uniform with a maximum variation of approximately 1.7˚C.The temperature non-uniformity variation of 1.7˚C can be attributed to accuracy of thermocouples and the data acquisition system signal processing capabilities. In comparison to this, cooling the PV string by converging channel resulted in maximum temperature variation of 4.8˚C and for rectangular channel heat exchanger the variation was 4.4 ˚C.

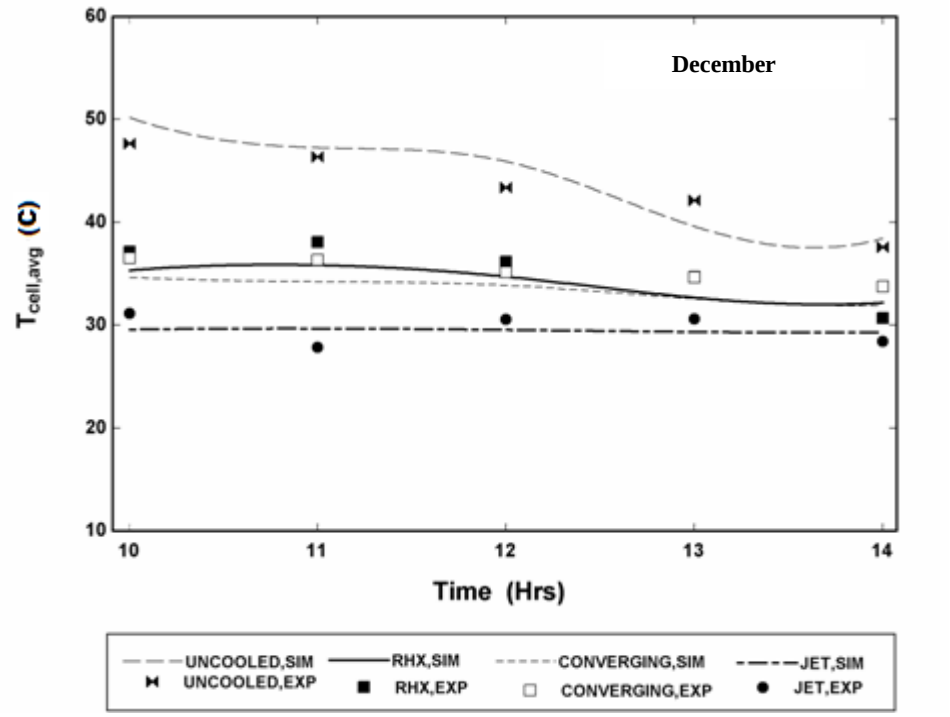

Figure 6.52 Cell temperature comparisons for 16th Dec for all configurations

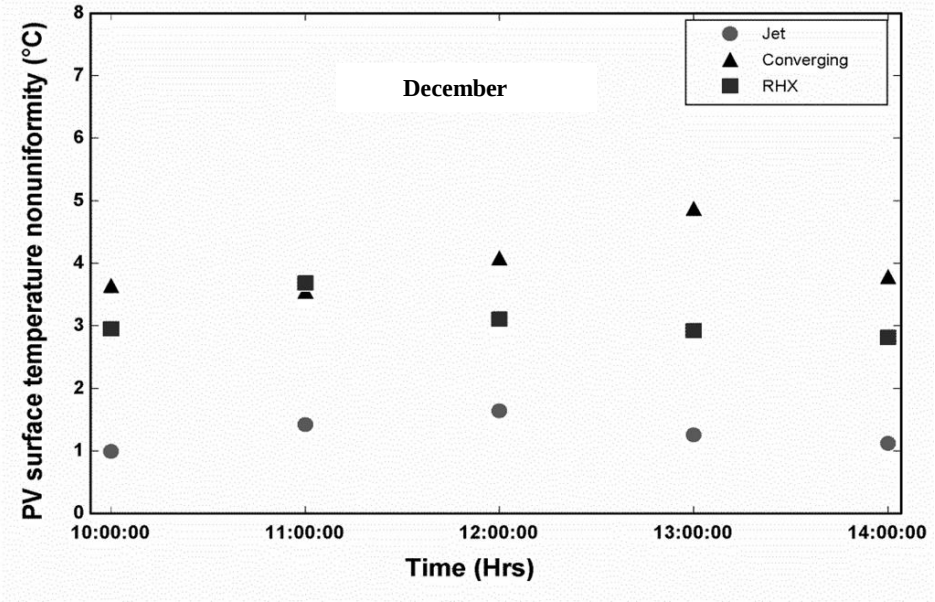

Figure 6.53 PV surface temperature non- uniformity for 16th Dec for all configurations

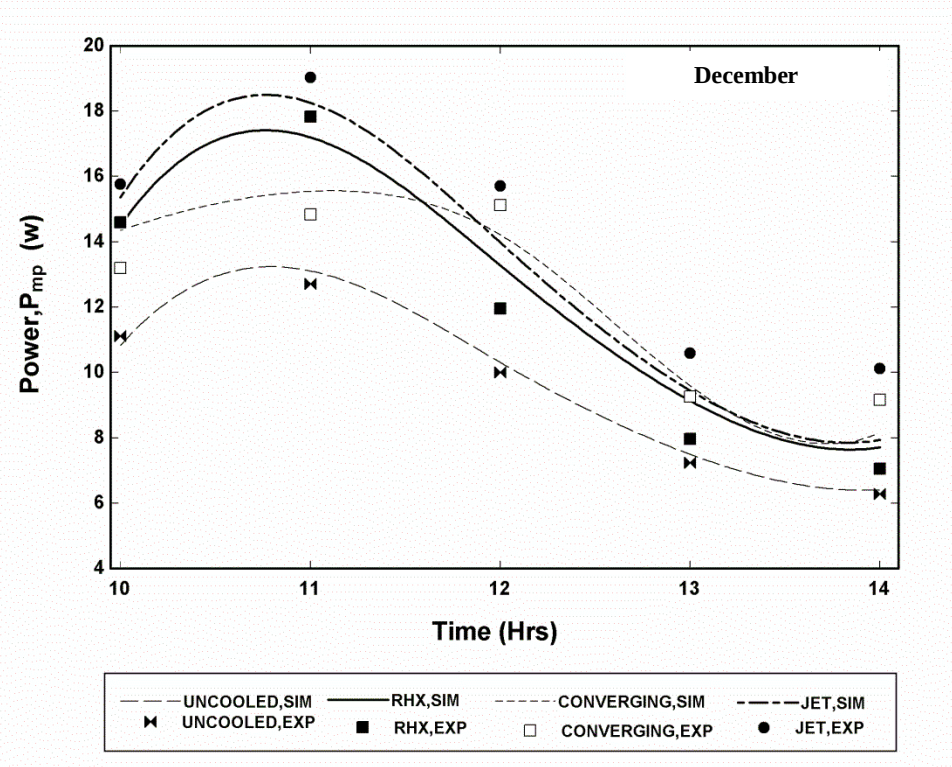

Figure 6.54 Power output comparisons for 16th Dec for all configurations

Figure 6.54 shows the comparative analysis of power output for jet cooled, converging cooling, rectangular heat exchanger and uncooled PV system for the month of December. It is evident that the application of uniform cooling by jet for PV produced more power than the non-uniform cooled and uncooled PV. This increase in power is a result of low and uniform cell temperature in the case of jet cooling. For uncooled PV string, maximum power of 12.3W was recorded. In comparison to this, cooling the PV string by converging channel resulted in maximum power of 15.4W and 17.5W for rectangular channel heat exchanger. For jet cooled PV string, maximum power of 19.2W was recorded. Modeling and experimental data shows fair agreement with root

mean square percent deviation not exceeding 6.17 % for jet, converging and rectangular channel. By using jet cooling in uniform way, PV string has been cooled effectively and power produced has increased by 56.1% whereas for non-uniform cooling from rectangular channel resulted in percentage improvement in power of 42.2 %.

Figure 6.55 shows the comparison between conversion efficiency of the four systems considered for December data. Maximum efficiency of 10.8% was recorded for PV without cooling. In comparison to this, cooling the PV string by converging channel resulted in maximum efficiency of 14.8% and 14.7% for rectangular channel heat exchanger. For uniform cooling by jet, maximum efficiency of 17.8% was recorded experimentally. Modeling and experimental data shows fair agreement with root mean square percent deviation not exceeding 6.5% for jet, converging and rectangular channel. Figure 6.56 shows the improvement in performance parameters by applying cooling systems from uniform cooling of jet and non-uniform cooling mechanism of rectangular channel heat exchanger . By using uniform cooling by jet, PV string has been cooled effectively and efficiency has increased by 64.8 % whereas non-uniform cooling increased the efficiency by 36.1 %.Hence uniform cooling has resulted in approximately doubled the output from PV string.

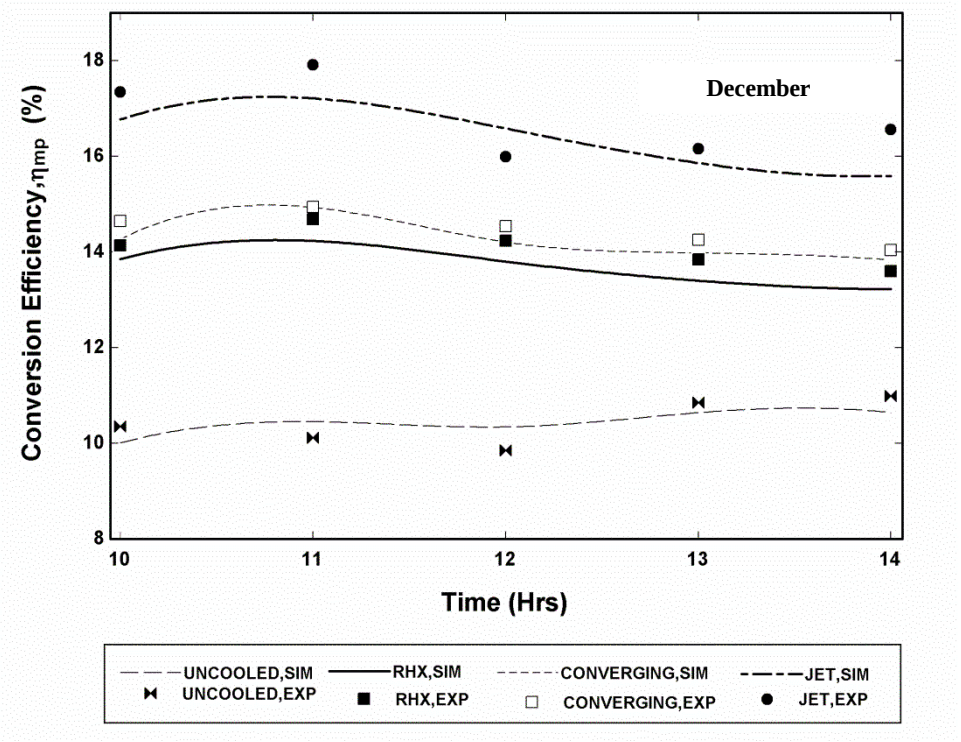

Figure 6.55 Conversion efficiency comparisons for 16th Dec for all configurations

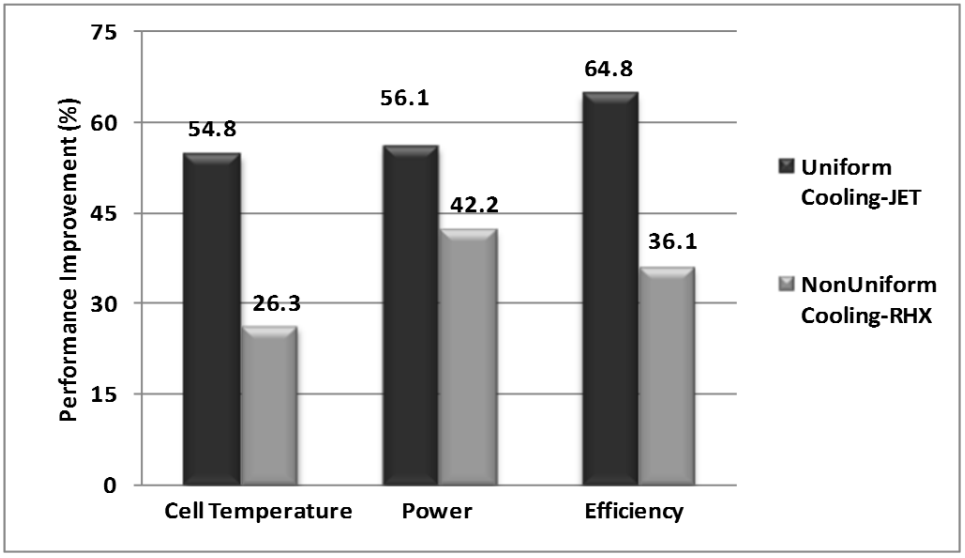

Figure 6.56 Comparison between non-uniform and uniform cooling for December

CHAPTER 7

CONCLUSIONS AND RECOMMENDATIONS

For the investigation of PV panels subjected to uniform cooling, following configurations were compared with meteorological data of Dhahran, both experimentally and numerically for June and December. Experimental setup for each configuration was developed and comparisons with modeling results were carried out.

- Configuration 1. PV string without Cooling
- Configuration 2. PV string with Rectangular Channel Cooling
- Configuration 3. PV string with Converging Channel Cooling
- Configuration 4. PV string with Jet Impingement Cooling

7.1 CONCLUSIONS

A detailed PV system model to predict the performance of photovoltaic modules was developed in this work. Optical, radiation, thermal, CFD, and electrical models were coupled together to form a complete system model. Various studies were conducted during this thesis from which the following conclusions are drawn:

7.1.1 PV String without cooling

For the purpose of comparison and as a base case, an uncooled PV string was modeled and experimental investigation was carried out in the climate of Saudi Arabia. For uncooled PV string, maximum temperature of 76˚C was reported for June whereas the maximum cell temperature of 45˚C was recorded for December. In the absence of uniform cooling, the operating cell temperature range of PV string is above the safe limit of operation. Experimentally, the power output reported was as high as 12.3W for the case of 25th June. For December, the maximum power output resulted was 12.8W experimentally.

7.1.2 PV string with Rectangular Channel Cooling

Rectangular channel heat exchanger was selected for non-uniform cooling of PV string. Cooling the PV string by rectangular channel resulted in temperature as high as 47˚C for 23rd June and 46.1˚C for 25 June. By using rectangular channel cooling, PV string was cooled by reducing the cell temperatures but at the expense of non-uniform temperature distribution. Experimentally, the maximum power output achieved was 16.7W for the case of 25th June. For 23rd June, the maximum power output resulted was 17.0W experimentally. The maximum experimental efficiency was 13.1 % for the case of 23rd June whereas for 25th June, the experimental efficiency was 12.4 %.

7.1.3 PV string with Converging Channel Cooling

Seven different geometries based on converging angles, from 0˚-10˚ were selected and simulated using the boundary conditions. A two degrees angle was found to yield best thermal performance in terms of temperature distribution and average cell temperature. Standard deviation for the top surface of PV string for the case of 2 degree was found to be 0.91˚C. The worst thermal performance in terms of temperature distribution was found from ten degree angle with the highest average cell temperature. For an uncooled PV string, maximum temperature of 71.2˚C was reported for June whereas the maximum cell temperature of 48.3˚C was recorded for December. In comparison to this, cooling the PV string by converging channel resulted in temperature as high as 45.1˚C for June and 36.4˚C for December. For the month of June, PV power output was enhanced by 35.5 % whereas the performance improvement for December was 26.1 %. The experimental efficiency increased from 9.8 %to 12.5 % for the case of June. For December, the experimental efficiency increased from 10.8 % to 14.7 % showing improvement in the performance.

7.1.4 PV string with Jet Impingement Cooling

It was found that the maximum pump power was in the case of single nozzle and it decreases as the number of nozzles increase. Also it should be noted that the pressure drop reduces with multiple nozzles. It was observed that the selection of average heat transfer coefficient of 1000W/m^2.K for jet cooling has given uniform results For June, by employing jet cooling, PV surface temperature was reduced to 36˚C whereas for December it was reduced to around 30˚C.This decrease of average cell temperature is due

to the high extraction capability of jet impingement cooling and uniform cooling. For 23rd June, temperature non-uniformity is 2.0˚C averaged for the entire testing hours whereas for December its value is 1.2˚C. By applying jet cooling power output for June was increased to 18.4 W whereas for December maximum power output was 18.1 W.

7.1.5 Comparison among four configurations

For the global analysis, a comparison was carried out using the ambient data of Dhahran to observe the behavior of different cooling techniques. For an uncooled PV string, maximum temperature of 83˚C was recorded. In comparison to this, cooling the PV string by converging channel resulted in maximum temperature of 47˚C and 47.5˚C for rectangular channel heat exchanger for June. For jet cooled PV string, maximum temperature of 35.8˚C was recorded. By employing the jet cooling, PV surface temperature is approximately uniform with a averaged variation of approximately 2.0˚C which is due to thermocouple uncertainty errors. In comparison to this, cooling the PV string by converging channel resulted in maximum temperature variation of 4.9˚C and for rectangular channel heat exchanger the variation was 4.5 ˚C. For uncooled PV string, maximum power of 10.0W was recorded. In comparison to this, cooling the PV string by converging channel resulted in maximum power of 15.7W and 16.0W for rectangular channel heat exchanger. For jet cooled PV string, maximum power of 18.1W was recorded. For uncooled PV string, maximum efficiency of 7.9% was recorded. By using jet, PV string was cooled effectively and power produced was increased by 81% whereas for converging and rectangular channel, percentage improvement in power was 57% and 60 %, respectively. In comparison to this, cooling the PV string by converging channel

resulted in maximum efficiency of 12.5% and 12.7% for rectangular channel heat exchanger. For jet cooled PV string, maximum efficiency of 15.7% was recorded. By using jet, PV string has been cooled effectively and efficiency has increased by 98.4%.It is clear that uniform cooling by jet system has enhanced the performance of PV string. It is found that the jet cooling has higher efficiency, minimum cell temperature and temperature uniformity when compared with the performance of other non-uniform cooling systems.

It should be noted that although converging channel cooling performed better as a cooling system and showed significant performance improvement however due to relatively high average cell temperature than jet cooling, it could not outperformed jet PV system. In addition, converging channel cooling and rectangular channel cooling showed similar results for the current configurations and conditions analyzed but since converging channel can result in a better thermal profile over PV surface ,it is suggested for employment for PV cooling and future research for CPV cells. Overall the main hypothesis that uniform cooling is better than non-uniform cooling was substantiated by the numerical and experimental results. It was concluded that uniform cooling performs better in terms of thermal and electrical results for PV systems and should be adopted for concentrated systems where the effect of non-uniformity is much pronounced.

7.2 FUTURE RECOMMENDATIONS

The extension of the current work can be focused on cooling systems for different systems to lower the operating temperature of the device. This research may lead to further investigation of different cooling mechanisms for low and higher concentration PV, where the effect of non-uniformity is much profound.

Impingement cooling and converging channel cooling should be employed to CPV systems to check the effect on concentrated systems.

Based on literature, micro channels and heat pipes with similar arrangement could be used for pilot study to remove non-uniform cooling from the surface of PV systems.

There is a prospect to use the model presented in this thesis for making simple correlations for the correct cooling operating conditions as a function of solar intensity, cell temperature, wind speed, etc.

Uniform cooling is an important aspect for cooling of electronics. Considering the need for cooling, the model could be extended to electronic devices by jet impingement or micro jets.

NOMENCLATURE

a	Modified diode ideality factor (V)
A	Diode ideality factor
A_c	Area of PV string (m^2)
A_h	Area of heated/cooled plate ((m^2)
C_d	Discharge coefficient of nozzle
CFD	Computational Fluid Dynamics
C_p	Specific heat capacity (J/kg.K)
CPV	Concentrated Photovoltaic
d	Diameter of nozzle
F	Reynolds number parameter in jet model
G	Total horizontal radiation (W/m^2)
G_o	Extraterrestrial radiation (W/m^2)
G_b	Horizontal beam radiation (W/m^2)
G_d	Horizontal diffuse radiation (W/m^2)
G_{ref}	Reference condition (STC) incident radiation (W/m^2)
h	Heat transfer coefficient ($W/m^2.K$)
h_w	Wind heat transfer coefficient ($W/m^2.K$)
I_T	Tilted Incident Radiation (W/m^2)
I	PV module output current (A)
I_L	Light current (A)
I_o	Diode reverse saturation current (A)
k	Boltzmann's constant, 1.38066E-23 (J/K)
K_f	Thermal conductivity of fluid (W/m.K)
K_w	Thermal conductivity of solid wall (W/m.K)
K	Extinction coefficient
$K_{\tau\alpha,b}$	Incidence angle modifier for beam radiation
$K_{\tau\alpha,d}$	Incidence angle modifier for diffuse radiation

$K_{\tau\alpha,g}$	Incidence angle modifier for ground reflected radiation
L_{glass}	Thickness of front glass layer (m)
m	Irradiance dependence parameter for I_L
M	Air mass modifier
N	Number of nozzles
n	Temperature dependence parameter for ideality factor
Nu	Nusselt Number
P	Electrical power (W)
ΔP	Pressure drop (Pa)
$\dot{q}$	Heat transfer (W)
q	Elementary charge, 1.60218×10^{-19} (coulomb)
Q	Flow rate (m^3/s)
r	Equivalent radius of cooled plate
R_{beam}	Geometric factor for beam radiation
R_s	Series resistance (Ω)
R_{sh}	Shunt resistance (Ω)
$RMS\ \%$	Root mean square percent deviation (%)
R	Thermal resistance (K/W)
Re	Reynolds number
s	Jet to jet spacing for multiple nozzles
S	Absorbed solar radiation (W/m^2)
T	Temperature (K)
V	Voltage (V)
$V_{f,in}$	Inlet water velocity (m/s)
$V_{pv,cell}$	Volume of PV cells inside the module (m^3)
V_w	Wind speed (m/s)
z	Nozzle to plate spacing

Greek Symbols

α	Coefficient of thermal expansion (K^{-1})
β	Slope of PV string
$\emptyset$	Converging Angle
δw	Uncertainty of variable "W"
η_{mp}	Electrical efficiency of PV at maximum power point
ρ_g	Reflectivity of ground
ρ	Density (kg/m^3)
θ	Incidence angle of solar radiation
θ_r	Refracted angle of solar radiation
σ	Stefen-Boltzmann's constant
$(\tau\alpha)$	Transmitivity-Absorptivity product
μ	Viscosity (Pa.s)

Subscripts

0	Reference cell
al	Aluminum
amb	Ambient
avg	Average
b	Beam radiation
bottom	Bottom loss
bs	Back sheet
c, cell	PV cell
conv	Convection losses
d	Diffuse radiation
exp	Experimental
eq'	Equivalent
f,in	Fluid Inlet Temperature
g	Glass
mod	Modeled
martin	Martin model
mp	Maximum power point
n	Normal
net	Net Power
o	Extraterrestrial
oc	Open circuit point
opt	Optimum condition
pump	Pumping Power
pv	Photovoltaic
ref	Reference cell condition
rad	Radiation losses
sc	Short circuit point

string	Parameter for PV string
top	Top loss
tot	Total
uniform	Uniform temperature distribution

REFERENCES

[1] IPCC, *Climate Change: The physical science basis.*, 7th ed., no. January 2014. Cambridge University Press, 2013.

[2] KAUST Industry Collaboration Program (KICP), "SAUDI ARABIA SOLAR ENERGY Manufacturing and Technology Assessment," 2009.

[3] B. Lawson, "Electropaedia, Solar Power (Technology and Economics)," *Woodbank Communications Ltd*, 2012. [Online]. Available: http://www.mpoweruk.com/solar_power.htm.

[4] T. Solmetric, "Guide To Interpreting I-V Curve Measurements of PV Array," 2011. [Online]. Available: http://www.solmetric.com.

[5] H. G. Teo, P. S. Lee, and M. N. A. Hawlader, "An active cooling system for photovoltaic modules," *Appl. Energy*, vol. 90, no. 1, pp. 309–315, Feb. 2012.

[6] N. Amin, C. W. Lung, and K. Sopian, "A practical field study of various solar cells on their performance in Malaysia," *Renew. Energy*, vol. 34, no. 8, pp. 1939–1946, Aug. 2009.

[7] R. Kumar and M. A. Rosen, "A critical review of photovoltaic–thermal solar collectors for air heating," *Appl. Energy*, vol. 88, no. 11, pp. 3603–3614, Nov. 2011.

[8] E. Erdil, M. Ilkan, and F. Egelioglu, "An experimental study on energy generation with a photovoltaic (PV)–solar thermal hybrid system," *Energy*, vol. 33, no. 8, pp. 1241–1245, Aug. 2008.

[9] Z. Ling, Z. Zhang, G. Shi, X. Fang, L. Wang, X. Gao, Y. Fang, T. Xu, S. Wang, and X. Liu, "Review on thermal management systems using phase change materials for electronic components, Li-ion batteries and photovoltaic modules," *Renew. Sustain. Energy Rev.*, vol. 31, pp. 427–438, Mar. 2014.

[10] D. Du, J. Darkwa, and G. Kokogiannakis, "Thermal management systems for Photovoltaics (PV) installations: A critical review," *Sol. Energy*, vol. 97, pp. 238–254, Nov. 2013.

[11] H. Bahaidarah, A. Subhan, P. Gandhidasan, and S. Rehman, "Performance evaluation of a PV (photovoltaic) module by back surface water cooling for hot climatic conditions," *Energy*, vol. 59, pp. 445–453, 2013.

[12] P. Yadav, B. Tripathi, S. Rathod, and M. Kumar, "Real-time analysis of low-concentration photovoltaic systems: A review towards development of sustainable energy technology," *Renew. Sustain. Energy Rev.*, vol. 28, pp. 812–823, Dec. 2013.

[13] L. Micheli, N. Sarmah, X. Luo, K. S. S. Reddy, and T. K. Mallick, "Opportunities and challenges in micro- and nano-technologies for concentrating photovoltaic cooling: A review," *Renew. Sustain. Energy Rev.*, vol. 20, pp. 595–610, Apr. 2013.

[14] E. Radziemska, "The effect of temperature on the power drop in crystalline silicon solar cells," *Renew. Energy*, vol. 28, no. 1, pp. 1–12, Jan. 2003.

[15] E. Radziemska and E. Klugmann, "Thermally affected parameters of the current–voltage characteristics of silicon photocell," *Energy Convers. Manag.*, vol. 43, no. 14, pp. 1889–1900, Sep. 2002.

[16] A. Luque, G. Sala, and J. C. Arboiro, "Electric and thermal model for non-uniformly illuminated concentration cells," *Sol. Energy Mater. Sol. Cells*, vol. 51, no. 3–4, pp. 269–290, Feb. 1998.

[17] A Royne, C. Dey, and D. Mills, "Cooling of photovoltaic cells under concentrated illumination: a critical review," *Sol. Energy Mater. Sol. Cells*, vol. 86, no. 4, pp. 451–483, Apr. 2005.

[18] R. K. Mathur, D. R. Mehrotra, S. Mittal, and S. R. Dhariwal, "Thermal non-uniformities in concentrator solar cells," *Sol. Cells*, vol. 11, no. 2, pp. 175–188, Mar. 1984.

[19] R. W. Sanderson, D. T. Odonnel, and C. E. Backus, "The effects of nonuniform illumination and temperature profiles on silicon solar cells under concentrated sunlight," in *14th Photovoltaic Specialists Conference*, 1980, pp. 431–436.

[20] F. Chenlo and M. Cid, "A linear concentrator photovoltaic module: analysis of non-uniform illumination and temperature effects on efficiency," *Sol. Cells*, vol. 20, no. 1, pp. 27–39, Feb. 1987.

[21] H. Baig, K. C. Heasman, and T. K. Mallick, "Non-uniform illumination in concentrating solar cells," *Renew. Sustain. Energy Rev.*, vol. 16, no. 8, pp. 5890–5909, Oct. 2012.

[22] M. W. Edenburn and J. R. Burns, "Shading analysis of a photovoltaic-cell string illuminated by a parabolic-trough concentrator," *NASA STI/Recon Tech. Rep. N*, vol. 83, p. 21537, Sep. 1982.

[23] G. N. Tiwari, R. K. Mishra, and S. C. Solanki, “Photovoltaic modules and their applications: A review on thermal modelling,” *Appl. Energy*, vol. 88, no. 7, pp. 2287–2304, Jul. 2011.

[24] J. S. Coventry, “Performance of a concentrating photovoltaic/thermal solar collector,” *Sol. Energy*, vol. 78, no. 2, pp. 211–222, Feb. 2005.

[25] H. Cotal, C. Fetzer, J. Boisvert, G. Kinsey, R. King, P. Hebert, H. Yoon, and N. Karam, “III–V multijunction solar cells for concentrating photovoltaics,” *Energy Environ. Sci.*, vol. 2, no. 2, p. 174, 2009.

[26] R. D. Nasby and R. W. Sanderson, “Performance measurement techniques for concentrator photovoltaic cells,” *Sol. Cells*, vol. 6, no. 1, pp. 39–47, Jun. 1982.

[27] N. Sarmah, B. S. Richards, and T. K. Mallick, “Evaluation and optimization of the optical performance of low-concentrating dielectric compound parabolic concentrator using ray-tracing methods.,” *Appl. Opt.*, vol. 50, no. 19, pp. 3303–10, Jul. 2011.

[28] K. A. Kerschen and P. A. Basore, “A performance model for nonuniformity illuminated front-gridded concentrator cells,” in *Conference Record of the Twentieth IEEE Photovoltaic Specialists Conference*, pp. 1129–1137.

[29] A. B. J. S. Coventry, E. Franklin, “Thermal and electrical performance of a concentrating PV/thermal collectors: results from the ANU CHAPS collector,” in *ANZSES Solar Energy Conference Newcastle*, 2002.

[30] H. Pfeiffer and M. Bihler, “The effects of non-uniform illumination of solar cells with concentrated light,” *Sol. Cells*, vol. 5, no. 3, pp. 293–299, Mar. 1982.

[31] A. Williams, *The Handbook of Photovoltaic Application*. The Fairmont Press Inc., 1986.

[32] R. B. A. Fahrenbruch, *Fundamentals of solar cells*. New York: Academic Press, 1983.

[33] T. Markvart, *Solar electricity*, 2nd ed. New York., 2000.

[34] Y. Zhangbo, L. Qifen, Z. Qunzhi, and P. Weiguo, “The cooling Technology of Solar Cells under Concentrated system,” vol. 3, pp. 2193–2197.

[35] A. Cuevas and S. López-Romero, "The combined effect of non-uniform illumination and series resistance on the open-circuit voltage of solar cells," *Sol. Cells*, vol. 11, no. 2, pp. 163–173, Mar. 1984.

[36] K. Nishioka, T. Takamoto, T. Agui, M. Kaneiwa, Y. Uraoka, and T. Fuyuki, "Annual output estimation of concentrator photovoltaic systems using high-efficiency InGaP/InGaAs/Ge triple-junction solar cells based on experimental solar cell's characteristics and field-test meteorological data," *Sol. Energy Mater. Sol. Cells*, vol. 90, no. 1, pp. 57–67, Jan. 2006.

[37] D. Meneses-Rodríguez, P. P. Horley, J. González-Hernández, Y. V Vorobiev, and P. N. Gorley, "Photovoltaic solar cells performance at elevated temperatures," *Sol. Energy*, vol. 78, no. 2, pp. 243–250, Feb. 2005.

[38] D. P. I. Anton, G. Sala, "Correction of the Voc vs. temperature dependence under non-uniform concentrated illumination," in *17th European Photovoltaic Solar Energy Conference, Munich, Germany*, 2001, pp. 156–159.

[39] G. Sala, R. Solar, and D. P. I. Antón , "IV Testing of Concentration Modules and Cells with Non-Uniform Light Patterns," in *Proceedings of the 17th European Photovoltaic Solar Energy Conference and Exhibition*, 2001, pp. 611–614.

[40] R. Boukhanouf, A. Haddad, M. T. North, and C. Buffone, "Experimental investigation of a flat plate heat pipe performance using IR thermal imaging camera," *Appl. Therm. Eng.*, vol. 26, no. 17–18, pp. 2148–2156, Dec. 2006.

[41] P. Naphon, P. Assadamongkol, and T. Borirak, "Experimental investigation of titanium nanofluids on the heat pipe thermal efficiency," *Int. Commun. Heat Mass Transf.*, vol. 35, no. 10, pp. 1316–1319, Dec. 2008.

[42] S. V Garimella and C. B. Sobhan, "Recent advances in the modeling and applications of nonconventional heat pipes," *Adv. Heat Transf.*, vol. 35, pp. 249–308, 2001.

[43] Y. Xuan, Y. Hong, and Q. Li, "Investigation on transient behaviors of flat plate heat pipes," *Exp. Therm. Fluid Sci.*, vol. 28, no. 2–3, pp. 249–255, Jan. 2004.

[44] X. Y. Huang and C. Y. Liu, "The pressure and velocity fields in the wick structure of a localized heated flat plate heat pipe," *Int. J. Heat Mass Transf.*, vol. 39, no. 6, pp. 1325–1330, Apr. 1996.

[45] B. Xiao and A. Faghri, "A three-dimensional thermal-fluid analysis of flat heat pipes," *Int. J. Heat Mass Transf.*, vol. 51, no. 11–12, pp. 3113–3126, Jun. 2008.

[46] A. Al Tarabsheh, S. Voutetakis, and A. I. Papadopoulos, “Investigation of Temperature Effects in Efficiency Improvement of Non-Uniformly Cooled Photovoltaic Cells,” vol. 35, no. 2009, pp. 1387–1392, 2013.

[47] S. Odeh and M. Behnia, “Improving Photovoltaic Module,” *Heat Transf. Eng.*, vol. 30, no. 6, pp. 499–505, 2009.

[48] C. R. Russell, “Conversion of solar radiation to electrical energy,” 1977.

[49] A. Akbarzadeh and T. Wadowski, “Heat pipe-based cooling systems for photovoltaic cells under concentrated solar radiation,” *Appl. Therm. Eng.*, vol. 16, no. 1, pp. 81–87, Jan. 1996.

[50] W. G. Anderson, P. M. Dussinger, D. B. Sarraf, and S. Tamanna, “Heat pipe cooling of concentrating photovoltaic cells,” in *2008 33rd IEEE Photovolatic Specialists Conference*, 2008, pp. 1–6.

[51] H.J. Huang, S.C. Shen, and H.J. Shaw, “Design and Fabrication of a Novel Hybrid-Structure Heat Pipe for a Concentrator Photovoltaic,” *Energies*, vol. 5, no. 12, pp. 4340–4349, Oct. 2012.

[52] L. Qifen, L. Tao, P. Cuicui, Z. Zhitian, and S. Weidong, “Design and Calculation of Cooling System to Eliminate Non-uniform Heat Transfer on Voncentration PV System (CPV),” vol. 609, pp. 143–150, 2013.

[53] S. V Garimella and C. B. Sobhan, “Transport in microchannels-a critical review,” *Annu. Rev. heat Transf.*, vol. 13, no. 13, 2003.

[54] R. J. Phillips, L. R. Glicksman, and R. Larson, “Forced-Convection, Liquid Cooled; Microchannel Heat Sinks for High Power-Density Microelectronics,” in *Int. Symp. on Cooling Technology for Electronic Equipment*, 1987, pp. 295–316.

[55] B. H. H. Salman, H. a. A. Mohammed, K. M. M. Munisamy, and a. S. Kherbeet, “Characteristics of heat transfer and fluid flow in microtube and microchannel using conventional fluids and nanofluids: A review,” *Renew. Sustain. Energy Rev.*, vol. 28, no. 0, pp. 848–880, Dec. 2013.

[56] A. Mohammed Adham, N. Mohd-Ghazali, and R. Ahmad, “Thermal and hydrodynamic analysis of microchannel heat sinks: A review,” *Renew. Sustain. Energy Rev.*, vol. 21, pp. 614–622, May 2013.

[57] J. L. L. Xu, Y. H. H. Gan, D. C. C. Zhang, and X. H. H. Li, "Microscale heat transfer enhancement using thermal boundary layer redeveloping concept," *Int. J. Heat Mass Transf.*, vol. 48, no. 9, pp. 1662–1674, Apr. 2005.

[58] Y. Wang and G.-F. Ding, "Experimental investigation of heat transfer performance for a novel microchannel heat sink," *J. Micromechanics Microengineering*, vol. 18, no. 3, p. 035021, Mar. 2008.

[59] S. F. Y. Wang, GF. Ding, "Highly efficient manifold microchannel heat sink," *Electron. Lett.*, vol. 43, no. 18, 2007.

[60] L. J. Missaggia and J. N. Walpole, "Microchannel heat sink with alternating directions of water flow in adjacent channels (Invited Paper)," 1992, vol. 1582, pp. 106–111.

[61] K. Vafai and L. Zhu, "Analysis of two-layered micro-channel heat sink concept in electronic cooling," *Int. J. Heat Mass Transf.*, vol. 42, no. 12, pp. 2287–2297, Jun. 1999.

[62] J. H. Ryu, D. H. Choi, and S. J. Kim, "Three-dimensional numerical optimization of a manifold microchannel heat sink," vol. 46, pp. 1553–1562, 2003.

[63] C. Russell, "Optical concentrator and cooling system for photovoltaic cells," 1981.

[64] L. Liu, L. Zhu, Y. Wang, Q. Huang, Y. Sun, and Z. Yin, "Heat dissipation performance of silicon solar cells by direct dielectric liquid immersion under intensified illuminations," *Sol. Energy*, vol. 85, no. 5, pp. 922–930, May 2011.

[65] H. C.Koehler, "Cooling photovoltaic (PV) cells during concentrated solar radiation in specified arrangement in coolant with as low electric conductivity as possible," DE199047172000.

[66] L. Zhu, R. F.Boehm, Y. Wang, C. Halford, and Y. Sun, "Water immersion cooling of PV cells in a high concentration system," *Sol. Energy Mater. Sol. Cells*, vol. 95, no. 2, pp. 538–545, Feb. 2011.

[67] X. Han, Y.Wang, and L. Zhu, "The performance and long-term stability of silicon concentrator solar cells immersed in dielectric liquids," *Energy Convers. Manag.*, vol. 66, pp. 189–198, Feb. 2013.

[68] X. Han, Y. Wang, and L. Zhu, "Electrical and thermal performance of silicon concentrator solar cells immersed in dielectric liquids," *Appl. Energy*, vol. 88, no. 12, pp. 4481–4489, 2011.

[69] H. Xiang, Y. Wang, L. Zhu, X. Han, Y. Sun, and Z. Zhao, "3D numerical simulation on heat transfer performance of a cylindrical liquid immersion solar receiver," *Energy Convers. Manag.*, vol. 64, pp. 97–105, Dec. 2012.

[70] Y. Sun, Y. Wang, L. Zhu, B. Yin, H. Xiang, and Q. Huang, "Direct liquid-immersion cooling of concentrator silicon solar cells in a linear concentrating photovoltaic receiver," *Energy*, vol. 65, pp. 264–271, Feb. 2014.

[71] Y.Abrahamyan, V.Serago, V.Aroutiounian, I. . Anisimova, V.Stafeev, G. Karamian, G.Martoyan, and Mouradyan, "The efficiency of solar cells immersed in liquid dielectrics," *Sol. Energy Mater. Sol. Cells*, vol. 73, no. 4, pp. 367–375, Aug. 2002.

[72] K. Tanaka, "Solar energy converter using a solar cell in a shallow liquid layer," US 65833492007.

[73] S. M. Baek, S. H. Yu, J. H. Nam, and C.-J. Kim, "A numerical study on uniform cooling of large-scale PEMFCs with different coolant flow field designs," *Appl. Therm. Eng.*, vol. 31, no. 8–9, pp. 1427–1434, Jun. 2011.

[74] J. B. Lasich, "Cooling circuit for receiver of solar radiation," WO020802862002.

[75] D. Faiman, "Large-area concentrators," in *Second Workshop on The Path to Ultrahigh Efficiency Photovoltaics*, 2002.

[76] G. Hetsroni, "A uniform temperature heat sink for cooling of electronic devices," vol. 45, pp. 3275–3286, 2002.

[77] M. Araki, K., Uozumi, H., Yamaguchi, "A simple passive cooling structure and its heat analysis for 500X concentrator PV module," in *29th IEEE PVSC*, 2002, pp. 1568–1571.

[78] C. Min, C. Nuofu, Y. Xiaoli, W. Yu, B. Yiming, and Z. Xingwang, "Thermal analysis and test for single concentrator solar cells," *J. Semicond.*, vol. 30, no. 4, p. 044011, Apr. 2009.

[79] O. Marios Theristis, Nabin Sarmah, Tapas K Mallick, Tadhg S, "Design and numerical analysis of enhanced cooling techniues for a high concentration photovoltaic (HCPV) system," in *27th EU PVSEC*, 2012, pp. 260 – 265.

[80] Y. I. C. W.M. Rohsenow, J.P. Harnett, *Handbook of Heat Transfer*, 3rd ed. Mc-Graw Hill, 1998.

[81] D.-Y. Lee and K. Vafai, “Comparative analysis of jet impingement and microchannel cooling for high heat flux applications,” *Int. J. Heat Mass Transf.*, vol. 42, no. 9, pp. 1555–1568, May 1999.

[82] B. W. Webb and C. F. Ma, “Single-phase liquid jet impingement heat transfer,” *Adv. heat Transf.*, vol. 26, no. 2, pp. 105–217, 1995.

[83] D. J. Womac, F. P. Incropera, and S. Ramadhyani, “Correlating Equations for Impingement Cooling of Small Heat Sources With Multiple Circular Liquid Jets,” *J. Heat Transfer*, vol. 116, no. 2, pp. 482–486, May 1994.

[84] A. Royne and C. J. Dey, “Effect of nozzle geometry on pressure drop and heat transfer in submerged jet arrays,” *Int. J. Heat Mass Transf.*, vol. 49, no. 3–4, pp. 800–804, Feb. 2006.

[85] H. Martin, “Heat and Mass Transfer between Impinging Gas Jets and Solid Surfaces,” *Adv. heat Transf.*, vol. 13, pp. 1–60, 1977.

[86] A. M. Huber and R. Viskanta, “Effect of jet-jet spacing on convective heat transfer to confined, impinging arrays of axisymmetric air jets,” *Int. J. Heat Mass Transf.*, vol. 37, no. 18, pp. 2859–2869, Dec. 1994.

[87] S.D. Jeong, H.Q. Ping, K. Kim, Y.H. Kim,and Y.W. Sim, “The Study on the Jet Nozzle Specified for Solar PV Power Enhancement,” *Research Center of HILEBEN Co. Ltd Report*. [Online]. Available: http://www.hileben.com/boad/bd_news/2/egofiledown.php?bd=2&ftype=0&fseq=80&key=20121023112031570015 8.

[88] J. Barrau, M. Omri, D. Chemisana, J. Rosell, M. Ibañez, and L. Tadrist, “Numerical study of a hybrid jet impingement/micro-channel cooling scheme,” *Appl. Therm. Eng.*, vol. 33–34, pp. 237–245, Feb. 2012.

[89] J. Barrau, J. Rosell, D. Chemisana, L. Tadrist, and M. Ibañez, “Effect of a hybrid jet impingement/micro-channel cooling device on the performance of densely packed PV cells under high concentration,” *Sol. Energy*, vol. 85, no. 11, pp. 2655–2665, Nov. 2011.

[90] A. Hasan, S. J. J. McCormack, M. J. J. Huang, and B. Norton, “Evaluation of phase change materials for thermal regulation enhancement of building integrated photovoltaics,” *Sol. Energy*, vol. 84, no. 9, pp. 1601–1612, Sep. 2010.

[91] M. J. Huang, P. C. Eames, and B. Norton, “Thermal regulation of building-integrated photovoltaics using phase change materials,” *Int. J. Heat Mass Transf.*, vol. 47, no. 12–13, pp. 2715–2733, Jun. 2004.

[92] P. H. Biwole, P. Eclache, and F. Kuznik, “Phase-change materials to improve solar panel’s performance,” *Energy Build.*, vol. 62, no. 0, pp. 59–67, Jul. 2013.

[93] S. Maiti, S. Banerjee, K. Vyas, P. Patel, and P. K. Ghosh, “Self regulation of photovoltaic module temperature in V-trough using a metal–wax composite phase change matrix,” *Sol. Energy*, vol. 85, no. 9, pp. 1805–1816, Sep. 2011.

[94] A. Tanuwijava, C. Ho, C.-M. Lai, and C.-Y. Huang, “Numerical Investigation of the Thermal Management Performance of MEPCM Modules for PV Applications,” *Energies*, vol. 6, no. 8, pp. 3922–3936, Aug. 2013.

[95] M. J. Huang, P. C. Eames, and B. Norton, “Phase change materials for limiting temperature rise in building integrated photovoltaics,” *Sol. Energy*, vol. 80, no. 9, pp. 1121–1130, Sep. 2006.

[96] K. Jambunathan, E. Lai, M. A. Moss, and B. L. Button, “A review of heat transfer data for single circular jet impingement,” *Int. J. Heat Fluid Flow*, vol. 13, no. 2, pp. 106–115, Jun. 1992.

[97] S. V Garimella and R. A. Rice, “Confined and Submerged Liquid Jet Impingement Heat Transfer,” *J. Heat Transfer*, vol. 117, no. 4, pp. 871–877, Nov. 1995.

[98] A. A. Tawfek, “Heat transfer and pressure distributions of an impinging jet on a flat surface,” *Heat Mass Transf.*, vol. 32, no. 1–2, pp. 49–54, 1996.

[99] S. V Garimella and B. Nenaydykh, “Nozzle-geometry effects in liquid jet impingement heat transfer,” *Int. J. Heat Mass Transf.*, vol. 39, no. 14, pp. 2915–2923, Sep. 1996.

[100] J. Gardon, R. and Carbonpue, “Heat transfer between a flat plate and jets of air impinging on it." , *Int. Developments in Heat Transfer, Int. Heat Transfer Conf.*, 1962, pp. 454–460.

[101] D. J. Womac, F. P. Incropera, S. Ramadhyani, and F. P. Incropera, “Correlating Equations for Impingement Cooling of Small Heat Sources With Multiple Circular Liquid Jets,” *J. Heat Transfer*, vol. 115, no. 1, pp. 106–115, May 1993.

[102] L. A. Brignoni and S. V Garimella, “Effects of nozzle-inlet chamfering on pressure drop and heat transfer in confined air jet impingement,” *Int. J. Heat Mass Transf.*, vol. 43, no. 7, pp. 1133–1139, Apr. 2000.

[103] J. Lee and S.J. Lee, “The effect of nozzle configuration on stagnation region heat transfer enhancement of axisymmetric jet impingement,” *Int. J. Heat Mass Transf.*, vol. 43, no. 18, pp. 3497–3509, Sep. 2000.

[104] D. H. Lee, J. Song, and M. C. Jo, “The Effects of Nozzle Diameter on Impinging Jet Heat Transfer and Fluid Flow,” *J. Heat Transfer*, vol. 126, no. 4, pp. 554–557, Dec. 2003.

[105] C.Y. Li and S. V Garimella, “Prandtl-number effects and generalized correlations for confined and submerged jet impingement,” *Int. J. Heat Mass Transf.*, vol. 44, no. 18, pp. 3471–3480, Sep. 2001.

[106] A. Royne and C. J. Dey, “Design of a jet impingement cooling device for densely packed PV cells under high concentration,” *Sol. Energy*, vol. 81, no. 8, pp. 1014–1024, Aug. 2007.

[107] B. A. Lindeman, J. M. Anderson, and T. A. Shedd, “International Journal of Heat and Mass Transfer Predictive model for heat transfer performance of oblique and normally impinging jet arrays,” *Int. J. Heat Mass Transf.*, vol. 62, pp. 612–619, 2013.

[108] B. Y. H. Liu and R. C. Jordan, “Daily insolation on surfaces tilted towards the equator,” *ASHRAE journal.*, vol. 3, pp. 53–59., 1961.

[109] D. T. Reindl, W. A. Beckman, and J. A. Duffie, “Evaluation of hourly tilted surface radiation models,” *Sol. Energy*, vol. 45, no. 1, pp. 9–17, 1990.

[110] R. Perez, R. Stewart, C. Arbogast, R. Seals, and J. Scott, “An anisotropic hourly diffuse radiation model for sloping surfaces: Description, performance validation, site dependency evaluation,” *Sol. Energy*, vol. 36, no. 6, pp. 481–497, 1986.

[111] Hay J. E. and J. A. Davies, “Calculation of solar radiation incident on an inclined surface,” in *First Canadian solar radiation data workshop*, 1980, p. 59.

[112] J. A. Duffie and W. A. Beckman, *Solar Engineering of thermal processes*, 6th ed. Hoboken, New Jersey: John Wiley & Sons, Inc., 2013.

[113] J. D. Mondol, Y. G. Yohanis, and B. Norton, "Solar radiation modelling for the simulation of photovoltaic systems," *Renew. Energy*, vol. 33, no. 5, pp. 1109–1120, May 2008.

[114] E. Skoplaki and J. a. Palyvos, "On the temperature dependence of photovoltaic module electrical performance: A review of efficiency/power correlations," *Sol. Energy*, vol. 83, no. 5, pp. 614–624, May 2009.

[115] A. D. Jones and C. P. Underwood, "A thermal model for photovoltaic systems," *Sol. Energy*, vol. 70, no. 4, pp. 349–359, Jan. 2001.

[116] F. Sarhaddi, S. Farahat, H. Ajam, and A. Behzadmehr, "Exergetic performance assessment of a solar photovoltaic thermal (PV / T) air collector," *Energy Build.*, vol. 42, no. 11, pp. 2184–2199, 2010.

[117] A. Tiwari, M. S. Sodha, A. Chandra, and J. C. Joshi, "Performance evaluation of photovoltaic thermal solar air collector for composite climate of India," *Sol. Energy Mater. Sol. Cells*, vol. 90, no. 2, pp. 175–189, Jan. 2006.

[118] F. A. Sarhaddi, S. Farahat, H. Ajam, and A. Behzadmehr, "Exergetic optimization of a solar photovoltaic thermal (PV / T) air collector," no. June 2010, pp. 813–827, 2011.

[119] M. Usama Siddiqui, A. F. M. Arif, L. Kelley, and S. Dubowsky, "Three-dimensional thermal modeling of a photovoltaic module under varying conditions," *Sol. Energy*, vol. 86, no. 9, pp. 2620–2631, Sep. 2012.

[120] W. McAdams, *Heat Transmission*, 3rd ed. New York: McGraw Hill, 1954.

[121] M. U. Siddiqui and M. Abido, "Parameter estimation for five- and seven-parameter photovoltaic electrical models using evolutionary algorithms," *Appl. Soft Comput.*, vol. 13, no. 12, pp. 4608–4621, Dec. 2013.

[122] S. J. Klein and F. A. McClintock., "Describing Uncertainties in Single-Sample Experiments," *Mech. Eng.*, vol. 75, no. 1, pp. 3–8, 1953.

[123] A. S. Joshi, A. Tiwari, G. N. Tiwari, I. Dincer, and B. V Reddy, "Performance evaluation of a hybrid photovoltaic thermal (PV/T) (glass-to-glass) system," *Int. J. Therm. Sci.*, vol. 48, no. 1, pp. 154–164, Jan. 2009.

[124] P. Brevet, C. Dejeu, E. Dorignac, M. Jolly, and J. J. Vullierme, "Heat transfer to a row of impinging jets in consideration of optimization," *Int. J. Heat Mass Transf.*, vol. 45, pp. 4191–4200, 2002.

[125] P. Tie, Q. Li, and Y. Xuan, “Investigation on the submerged liquid jet arrays impingement cooling,” *Appl. Therm. Eng.*, vol. 31, no. 14–15, pp. 2757–2763, Oct. 2011.

[126] P. Krotzsch, “Wiirme- und Stoffubergang bei PrallstrBmung aus Dusen- und Blendenfeldern,” *Chemie Ing. Tech.*, vol. 40, no. 7, pp. 339–344, 1968.

[127] N. M. R. Jeffers, J. Punch, E. J. Walsh, and M. McLean, “Heat Transfer From Novel Target Surface Structures to a 3×3 Array of Normally Impinging Water Jets,” *Journal of Thermal Science and Engineering Applications*, vol. 2. p. 041004, 2010.

[128] C. H. Oh, “Liquid Jet-Array Cooling Modules for High Heat Fluxes,” *AIChE J.*, vol. 44, no. 4, pp. 769–779, 1998.

[129] H. Sun, C. F. Ma, and W. Nakayama, “Local Characteristics of Convective Heat Transfer From Simulated Microelectronic Chips to Impinging Submerged Round Water Jets,” *Journal of Electronic Packaging*, vol. 115. p. 71, 1993.

[130] C. J. Hoogendoorn, “The effect of turbulence on heat transfer at a stagnation point,” *Int. J. Heat Mass Transf.*, vol. 20, no. 2, pp. 1333–1338, 1977.

[131] K. Wilson, D. De Ceuster, and R. A. Sinton, “Measuring the effect of cell mismatch on module output,” in *Photovoltaic Energy Conversion, Conference Record of the 2006 IEEE 4th World Conference on*, 2006, vol. 1, pp. 916–919.

VITAE

Name: Ahmer Ali Bozdar Baloch

Date of Birth: July 12, 1988

Present Address: 208/810,KFUPM Student Housing, Dhahran, Saudi Arabia

Permanent Address: A-3,Al-Shams Plaza, Block 6,Gulshan Iqbal, Karachi, Pakistan

Email Address: g201202120@kfupm.edu.sa

ahmer.ali@live.com

Educational Qualification:

M.S (Mechanical Engineering)

December, 2014

King Fahd University of Petroleum & Minerals,

Dhahran, Saudi Arabia.

B.E. (Mechanical Engineering)

December, 2010

NED University of Engineering and Technology,

Karachi, Pakistan.

Publications:

Ahmer AB Baloch and Haitham MS Bahaidarah, "Experimental Performance Evaluation of Uniform Cooling Technique for Photovoltaic Panels" ,6th Saudi Students Conference,2015.

Haitham MS Bahaidarah, **Ahmer AB Baloch** and P. Gandhidasan, " Modeling and Comparative Analysis of Jet Impingement Cooling and Conventional Channel Cooling for Photovoltaic Strings " 40th IEEE Photovoltaic Specialists Conference, Denver, Colorado, USA, 2014.

Haitham MS Bahaidarah, **Ahmer AB Baloch** and P. Gandhidasan, "Uniform Cooling of Photovoltaic panels : A review" (under review- Renewable and Sustainable Energy Reviews).

Ahmer AB Baloch, Haitham MS Bahaidarah, P. Gandhidasan and Fahad A. Al-Sulaiman, "Experimental and Numerical Performance Analysis of Converging Channel Heat Exchanger for PV Cooling". (under review-Energy Conversion and Management).

Haitham MS Bahaidarah, **Ahmer AB Baloch** and P. Gandhidasan, "Experimental and numerical performance investigation of jet impingement system for uniform cooling of PV string". (under review-Solar Energy).